Aptamer Biosensors

Kittichan Kanokphandharangkul

Imperial College London

Department of Chemistry

April 2015

Thesis submitted for the degree of Doctor of Philosophy of Imperial College London

The author declares that the work contained within this thesis is his own, and that all referenced works have been duly cited, to the best of his knowledge.

Kittichan Kanok

Acknowledgement

I would like to express my heartfelt appreciations to my supervisor, Prof Tony Cass, for many years of support, advice, and mentorship, without whom this thesis would not have been possible.

Most of all, I would like to thank my supervisor for never giving up on me, even in times when I have long given up on myself.

I would like to thank Dr Bhusana Premanode for his sage advice and guidance.

I would like to thank all the friends I have made at Imperial College, both within Cass Group and beyond, for their encouragement and in providing such a pleasant environment in which to work.

I would like to thank all the guys at AMR Asia for lending me their CNC milling machine, as well as my initial training in its use.

Finally, and most of all, I would like to thank my parents and family, for their continual love and support, and for tolerating my long absence from our home country.

Aptamer Biosensors

Abstract

Aptamers are single stranded nucleic acids, typically composed of between twenty to eighty nucleotides in length, capable of binding selectively to non-nucleic acid ligands. Aptamers are selected through a combinatorial chemistry process called Systematic Evolution of Ligands by Exponential enrichment (SELEX), which is composed of successive cycles of selection based on target affinity, followed by amplification. This results in the Darwinian evolution of the nucleic acid library resulting in increasing library homogeneity and target affinity over time.

Aptamers have been extensively investigated for potential application as sensing molecules, with roles similar to those traditionally occupied by antibodies. Aptamers and monoclonal antibodies have similar sensitivity in the pico to micro molar range. However aptamers have a number of advantages over protein antibodies, such as greater thermal stability, ease of chemical amplification, and amenability to modification, especially at the 5' and 3' prime ends.

The work performed in this Thesis is divided into three categories.

The first section describes the development of voltammetric Kanamycin and Tetracycline biosensors based on electrode immobilized, redox label bioconjugated nucleotide molecular beacons. These sensors relies on the target-aptamer binding induced spatial displacement of the redox label towards or away from the electrode surface as a means of signal generation. Further study was conducted to test the feasibility of this sensor design under likely field operation environments such as in soil sample analysis for microbial product discovery and in agricultural effluence for regulatory purposes. The biosensor was also enhanced by gel encapsulation for defense against nuclease degradation. Negative control was performed against structurally similar antibiotics of the same family in order to prove the specificity of the biosensor. Lastly, the sensor was moved onto an automated platform in a multichannel format in order to improve the utility of the sensor.

The second section describes the development of a voltammetric biosensor based on Enzyme-Linked Oligonucleotide Assay (ELONA) technology. Two sub-types of ELONA-like biosensors were originally envisioned, based respectively on direct and indirect ELONA. Both sub-types depend on the mass of redox label rich Gold Nanoparticles (GNP) at the electrode surface as a means of signal generation. Negative controls was performed against globular proteins Bovine Serum Albumin and Lysozyme, the

former since it is the most ubiquitous protein component of serum (the most likely biosensor operational environment), the latter as a worst case scenario for non-specific false positive results due to its positive charge.

The last section describes an attempt to develop an automated SELEX device based on mesofluidic flow channels. It was hoped that by using flow channels of a millimeter scale it would be possible to retain both the advantages of the conventional auto sampler based SELEX protocols (large library and sequence variation), while also gaining the primary advantages of microfluidic SELEX (reduced contamination risk, low initial cost and maintenance). Essential components of the SELEX device, such as thermal cycler, liquid handling, electronics infrastructure, and software control were designed, tested and integrated. Lastly an attempt was made to perform automated SELEX against Lysozyme targets using the device, though no nucleic acid with high affinity to target had yet been successfully isolated by the end of this study.

Table of Contents

List of Figures

List of Tables

List of Equations

List of Abbreviations

A	Area of Electrode
ASD	Automated SELEX Device
C	Concentration
CCA	Conformation Change Aptasensor
CV	Cyclic Voltammetry
D	Diffusion Coefficient
DAELAB	Direct Adsorption ELONA-Like Aptamer Biosensor
E	Potential
ELONA	Enzyme Linked Oligonucleotide Assay
EO	Standard Electrode Potential
ESS	Electromagnetic Seperation System
F	Faraday's Constant
GDE	Gold Disc Electrode
GNP	Gold Nanoparticle
HD22	Thrombin Aptamer HD22
HOMO	Highest Occupied Molecular Orbital
i	Current
IAELAB	Indirect Adsorption ELONA-Like Aptamer Biosensor
ID	Inner Diameter
J	Flux
Kd	Dissociation Constant
ko	Standard Rate Constant
LEDC	Less Economically Developed Country
LHS	Liquid Handling System
LSV	Linear Sweep Voltammetry
LUMO	Lowest Unoccupied Molecular Orbital
MEDC	More Economically Developed Country
MW	Molecular Weight
n	Number of electrons Transferred
OD	Outer Diameter

PCR	Polymerase Chain Reaction
r	Distance between Donor and Acceptor
R	Universal Gas Constant
SAB	Sandwich Aptamer Biosensor
SELEX	Systematic Evolution of Ligands by Exponential Enrichment
SPE	Screen Printed Electrode
SWV	Square Wave Voltammetry
T	Temperature in Kelvin
TBA	Thrombin Aptamer A
TCS	Temperature Control System
V	Hydrodynamic Velocity
V	Net Rate of Electron Transfer
z	Charge
α	A Constant
ΔG	Gibbs Free Energy of Activation
λ	Reorganisation Energy

Chapter 1: Introduction

1.01 Overview of Biosensors

A biosensor is an analytical device which converts a biological reaction into a measurable electronic signal [1]. While there is a large variety of biosensors, they all involve three basic components:

A) A biorecognition element, which is the biological element with target binding capabilities.

B) A transducer which transforms the change in the sensor molecule as a result of the sensor molecule-target binding event into a signal measurable by the platform.

C) The platform, typically the electronic components which amplifies and processes signals relayed by the transducer into a form that can be easily understood, and displays it.

The combination of different molecular recognition and transduce components lead to a matrix of biosensor types as illustrated in figure 1.01.

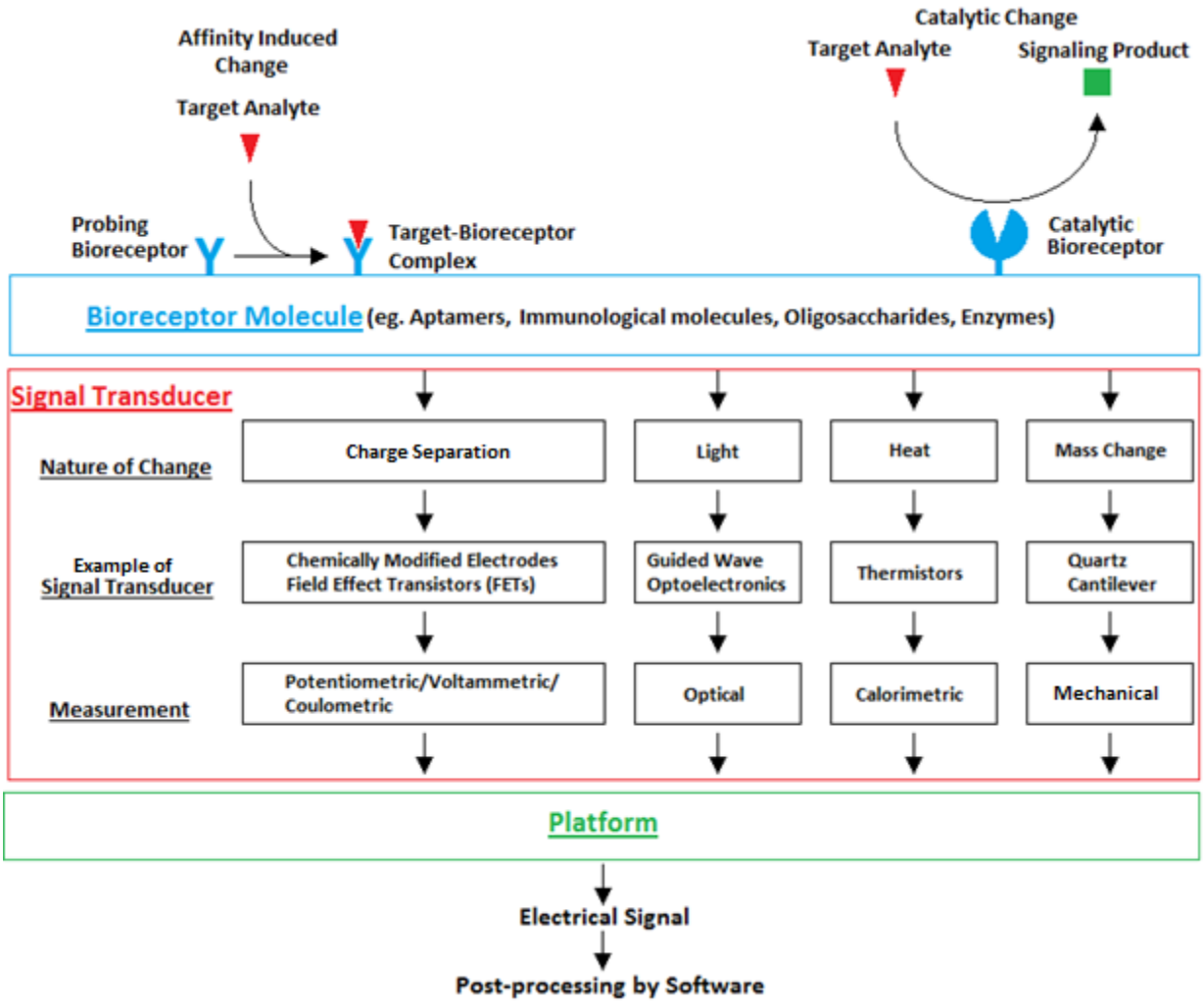

Fig 1.01 Basic principle of biosensors. Bioreceptor molecules recognizes and binds target analyte, transducer converts this change into a signal compatible with the platform, which in turn converts the signal into a measurable format, and displays it.

1.02 Operating Characteristics of Biosensors

The success of any biosensor hinges on it having sufficient sensitivity and specificity.

Specificity represents the range of targets which give rise to a signal from the biosensor. A good biosensor should not cross react with non-target molecules, yielding false positive signals. For practical purposes the biosensor should yield an unambiguous response, in order to reduce noise and false-positive signals as a result of cross-reaction. Poor specificity is typically the result of the response of the

biosensor to the environmental matrix. Specificity will be discussed further in the experimental result sections.

Sensitivity represents the lowest concentration of target the sensor is able to detect. This in turn strongly correlates to the ability of the biosensor to bind to the targeted analyte, and the ability of the sensor to convert this change into measurable signals. Low sensitivity results in the inability of the biosensor to detect the target molecule, resulting in a false negative signal. This is typically caused by low affinity of biosensory molecule to the target analyte or inability of transducer and platform to convert biosensory molecule-target interaction into measurable signal. Sensitivity will be discussed further in the experimental result sections.

While sensitivity and specificity form the two essential operating parameters which every biosensor must fulfil in order to be considered a functional device, the practical utility must also take into consideration secondary characteristics of a biosensor. This represents the practical desirability of a biosensor. These secondary characteristics include factors such as speed of response, dynamic range and robustness.

1.03 Categorisation of Biosensors

As shown in figure 1.01 there are many combinations of biorecognition molecules with transducer type and accordingly biosensors can be categorized in a number of ways. Perhaps the most common modes of classification is based on the nature of the bioreceptor molecule (a protein or aptamer biosensor, for example) or the nature of the transducing element (electrochemical or optical biosensors, for example).

Biosensors can also be categorized by the mechanism of the signaling process (affinity or catalytic). Affinity or probing type sensors bind to the target analyte leading to the formation of a target-bioreceptor complex, and the transducer revealing the concentration of the complex. Catalytic or reacting type biosensors convert the target analyte as substrate into a product, the concentration of which is measured by the transducer. Catalytic biosensors are more sensitive to environmental parameters that affect kinetic factors, such as pH and temperature, because of their dependence on rate rather than equilibrium processes. Affinity sensors depend on stoichiometry between bioreceptor molecules and targets for signal amplitude, whereas the magnitude of catalytic biosensor signal is dependent on the time and mass of the signaling substrate. A classic example of an affinity type

biosensor would be an affinity immunoassay [2][3] such as ELISA. The only major class of catalytic type biosensors are based on enzymatic mechanisms, a classic example being the electrochemical glucose oxidase sensor used for blood glucose monitoring [4].

Another mode of categorizing biosensors is by the presence or absence of a molecular label. A label is an exogenous molecule typically bioconjugated to the bioreceptor molecule, which is responsible for signal transduction to the platform. As such it could be viewed as a form of signal amplifier, and typically fills the role of transducer in a labeled biosensor system. Label free biosensors measure the change as a result of target-bioreceptor interaction itself, with the transducer detecting the intrinsic change at the molecular level involved in the binding event.

Examples of label free biosensing techniques include SPR based sensing technology [5], nanomechanical cantilever sensors [6] derived from AFM technology or quartz crystal microbalances [7]. The most obvious advantage of label free biosensors is that no bioconjugated label is required, which reduces the cost of sensor surface synthesis due to the absence of labelling reagents and simplification of sensor surface fabrication by eliminating the bioconjugation steps. Some bioreceptor molecules (relatively complex proteins in particular) are not amenable to modification, which could lead to loss of sensitivity or specificity. Since the target-bioreceptor induced change in label free biosensors is being transduced directly into quantitative signal, this eliminates potential influence of the label in signal transduction which could potentially distort signal.

The disadvantages of label free biosensing is that some bioreceptors do not generate sufficient change to be quantifiably measured without a label in the role of signal amplifier, thus reducing the range of potential bioreceptor molecules applicable. In addition the transducer and platform used in label free biosensing must typically be sensitive and relatively free from noise and interference.

1.04 Components and Design Consideration of Biosensors

There is a diverse range of organic molecules which could be used as biosensory molecules, including nucleic acids [8], antibodies [9] [10], enzymes [11] [12], binding proteins [13], and oligosaccharides [14]. The role of biosensory molecules is to interact with a target molecule and undergo change, which can occur in a variety of forms, including but not limited to heat generation [15], light generation [16], redox change, and mass change [7]. This change is then converted to a signal quantifiable to the platform by

the transducer, which converts these changes into measureable forms, such as calorimetric, optical, potentiometric or pietzoelectrical signals. In other words the transducer effectively bridges the organic biosensory molecule and the typically electromechanical platform.

The role of the platform is to convert the signal produced by the transducer into a form measurable in human terms, typically by converting transducer signal into an electronic signal which is processed and displayed by a software. Thus the selection of the biosensor platform is largely dependent on the specific transducer used. For some applications, the results displayed can be qualitative in the form of an on/off output. However by attributing a numerical value to the magnitude of the target-sensor binding signal, it is also possible to create a quantitative biosensor. The mode of quantification of the transducer signal is dependent on the nature of the transducer itself, for example the magnitude of an optical transducer's signal could be ascertained by using a platform measuring luminescensce, absorption, or light scattering. Signals generated by transducers that undergo electrochemical changes can be measured by methods such as measuring current change as a result of the application of potential (voltammetry and amperometry), potential difference between electrodes (potentiometry), and current consumption (coulometry). Other chemical changes which can be quantified include temperature, volumetric change and mass change.

At present, biosensing is dominated by optical and electrochemical modes of signal transduction. The most common optical mode of biosensor activity is based on fluorescence. Here the transducer is most commonly a fluorophore, which are chemical compounds that exhibit light emission upon photo excitation. There is an abundance of well-studied, robust, fluorophores available for biosensor design, with high sensitivity to environment, allowing it to transduce changes in the sensing surface [17][18]. Optical biosensors in general are characterized by high sensitivity, robust signal reliability and relatively easy integration into the multichannel sensing format, a classic example of this being a DNA microarray.

Electrochemical sensors have a number of inherent advantages [19] [20] over optical systems, including fast response, relatively low cost, and easy miniaturization (being highly compatible with microfabrication techniques and compatible with modern computer systems). Electrochemical biosensing will be further discussed in the electrochemistry section of this Chapter (see section 1.09).

While a diverse range of recognition molecules have been investigated for biosensing applications, there has been a significant increase in research during the past decade regarding biosensors that use

synthetic single stranded nucleic acids, especially when combined with electrochemical transducers. These biorecognition nucleic acids are commonly referred to as aptamers.

1.05 Overview of Aptamers

Aptamers are single stranded nucleic acids, typically composed of several tens of nucleotides in length, capable of binding selectively to non-nucleic acid ligands. RNA aptamers were first discovered independently by Ellington and Szostak [21], and Tuerk and Gold [22] in 1990, with DNA aptamers being discovered shortly thereafter [23]. The term “aptamer” was coined by Ellington from the Greek word “aptus”, meaning to fit. Their functional roles are analogous to antibodies in a protein bioreceptor system.

Aptamers have been observed to be able to bind to a diverse range of target molecule, including small organic molecules [24][25], proteins [26][27], viral particles [28][29] and whole cells [30]. This is not surprising, since nucleic acids must be able to interact with a number of non-nucleotide groups during process of gene regulation, both in the case of conventional DNA/regulatory complex interaction common to all cellular life [31][32][33] and in the role of riboswitch in the case of RNA[34].

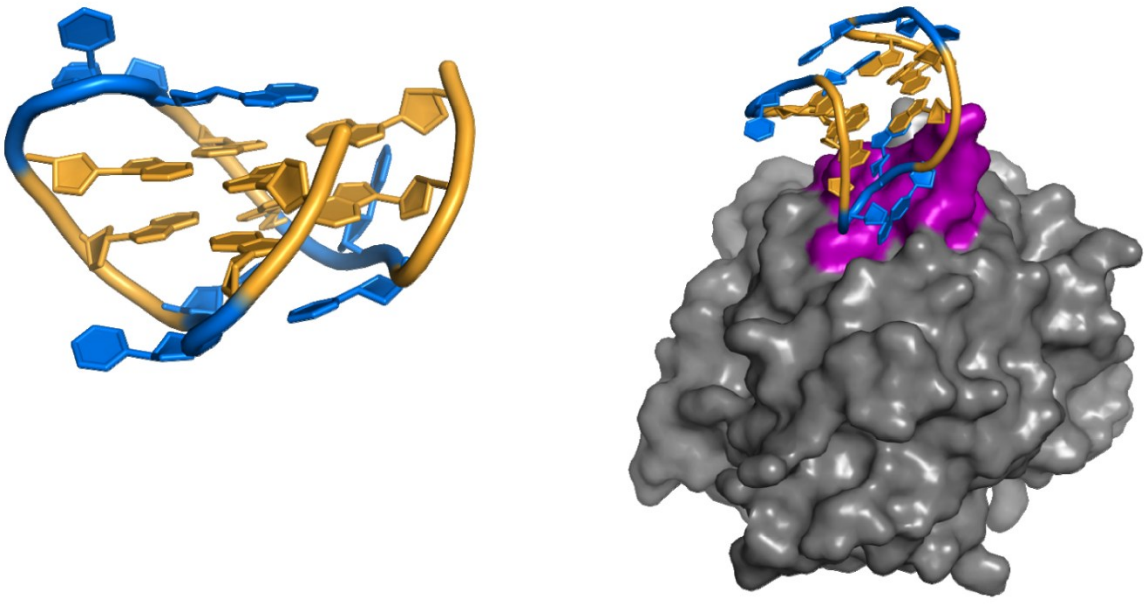

Fig 1.02 An illustration of (a) Thrombin aptamer in its resting, unbound secondary structure (b) the Thrombin aptamer complex binding of the same aptamer. Taken unmodified from [35]

1.06 Comparison of Aptamers and Antibodies

Aptamers have been extensively investigated for potential application as sensing molecules, with roles similar to those traditionally occupied by antibodies [36]. Aptamers and monoclonal antibodies have similar level of affinity in target detection (both detect at the pico to micro molar range [37] [38]). However while aptamers, particularly unmodified RNA aptamers, are susceptible to hydrolysis by ubiquitous nuclease enzymes, they do have a number of advantages over antibody based sensing assays.

This is primarily attributable to the polynucleotide structure of aptamers whereby they are much less dependent on a precise 3D structure for target binding unlike proteins, which have 3D structures assembled by a complex interaction of secondary, tertiary and quaternary structures, generally resulting in the burial of hydrophobic regions [39]. Therefore aptamer sensors are generally less susceptible to irreversible denaturation due to thermal damage than protein based sensors, allowing them to function in harsh environment. Denaturation of aptamers occurs readily in aptamers since the binding affinity is typically significantly below the primary phosphate bonds of the nucleic acid, and secondary structures spontaneously reform at low temperature, indeed the spatial arrangement of an aptamer population exist in a state of flux. Heating is therefore ideal for regenerating aptamer sensing surfaces. Heating antibodies generally results in irreversible damage [40] [41], as the protein structure reassemble in a manner different from that before heating. Antibodies with high temperature resistance are typically either specifically selected or engineered express this quality [42] [43]. This could be because a target-compatible structure may not be the most energetically stable form as a result of post translational assembly, or barriers prevent the reformation of the sensing form (such as the tendency of large globular proteins in polar solvent such as water to reassemble into a form that exposes hydrophilic element and hide hydrophobic cores after heating [44] [45]).

Another advantages of using aptamers is that they can be easily and cheaply prepared by chemical synthesis. This compares favourably to antibodies and enzymes which, being protein based, can require post translational modification, and therefore necessitate in vivo biological production [46] [47]. Additionally, because of their biological production, activity of antibody are subject to a relatively large degree of inter batch variation compared to aptamers. Typical aptamers are also much smaller than

most antibodies, and therefore less material needed for their synthesis (IgG has a MW of approximately 150kDa, while a typical 40bp long aptamer would have a MW of approximately 12kDa).

Broadly, aptamers are compatible with facilitated modification, typically of the 5' and 3' terminals of the sequence [48]. Antibodies cannot be easily redesigned without a causing damage to structure, due to the presence of complex 3D structures.

Additionally, due to the empirical nature of the aptamer selection process, it is possible to select aptamers, at least in principle, against any targets in vitro. Antibodies are based on immunological molecules, and thus are conventionally physiologically selected in vivo, which does not facilitate selection of antibody against highly toxic or otherwise growth inhibitive targets, such as heavy metals for example. However methods do exist for performing in vitro selection of protein with defined specificity and affinity, using methods analogous to SELEX based aptamer selection (e.g. phage display).

1.07 Aptamer Isolation and the SELEX Process

Aptamers are selected by a combinatorial chemistry process composed of iterative cycles of affinity selection and amplification steps known as Systematic Evolution of Ligands by EXponential enrichment (SELEX) [21][22].

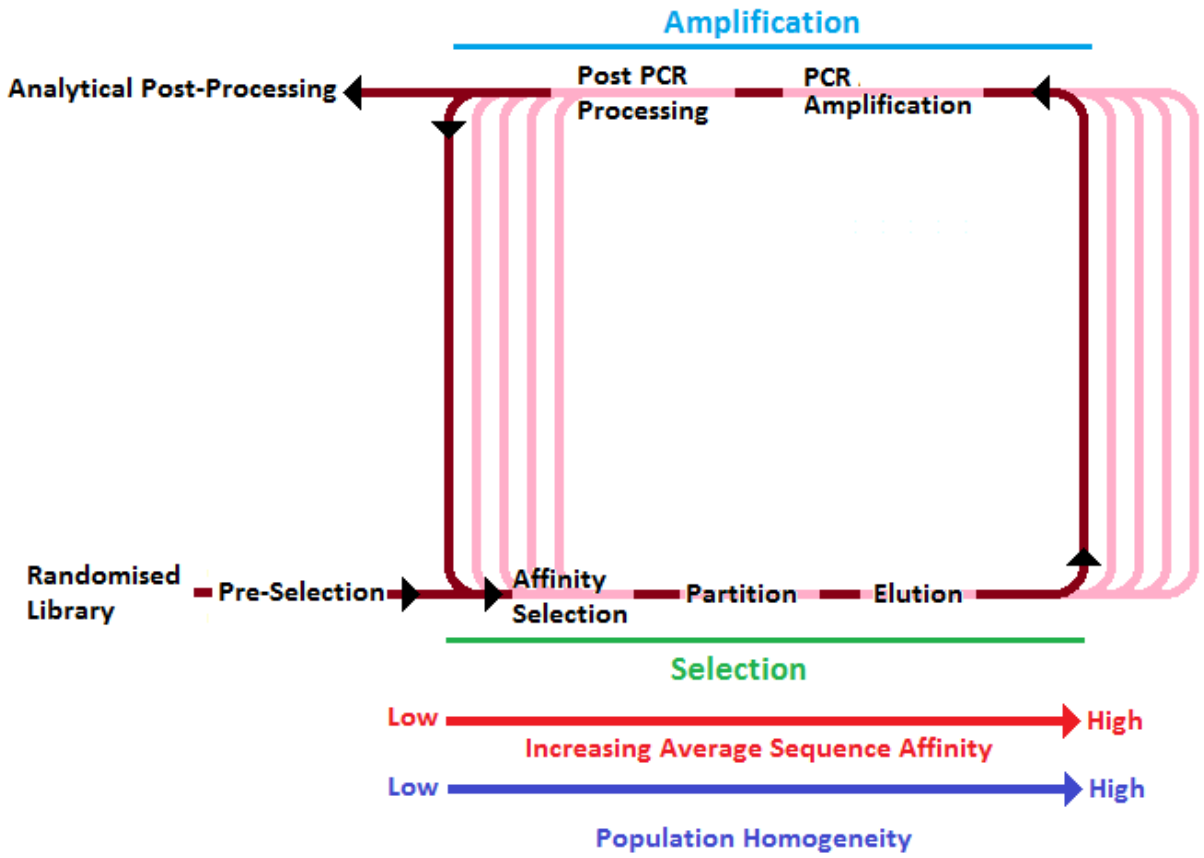

Fig 1.03 An overview of the SELEX process

The SELEX process subjects a DNA library to repeating cycles of affinity selection and enrichment. Affinity selection selects sequences with high affinity to a desired target, after which these sequences are amplified to generate a new library pool for the subsequent SELEX cycle. This cycle is recursively repeated, with each round resulting in an increase in the average affinity of the DNA library while decreasing the variation in the library population. This process can be analogized to Darwinian selection, where the key survival trait is the ability to be retained in the process of partition. A review of the SELEX process and technologies developed in its optimization is provided below.

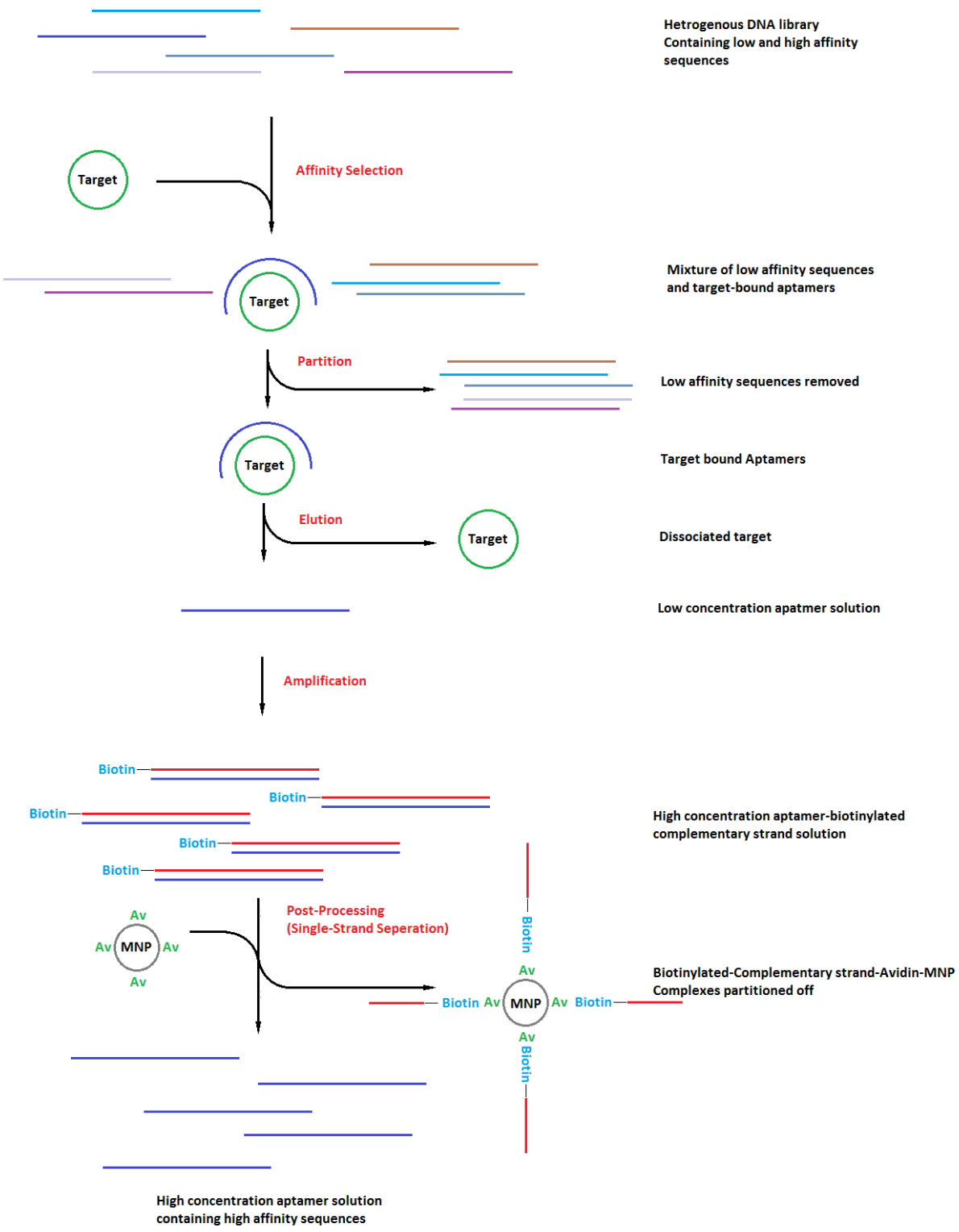

Fig 1.04 An overview of the common steps of the SELEX process. Labels in red represent essential steps of conventional SELEX, Labels in black describes the solution present in the represented step

1.07a Synthesis of DNA library

The first step of any SELEX protocol, like any other combinatorial chemistry process, starts with the synthesis of a library pool. Due to the limited variation of nucleotide monomers and the low difference in coupling efficiency of the four nucleotide variations (A, T, C and G), the synthesis of an unbiased pool of DNA is relatively simple compared to other libraries (peptide for example), as bias is relatively small and well-studied and therefore can easily be compensated for [49].

The libraries used in conventional SELEX process contain constant regions flanking the random sequences, which are used for primer binding in the amplification phase of the SELEX process. The diversity of the SELEX library depends on the length of these random sequences. Thus theoretically a library with a 30 nucleotide long random region generates a library with 4^{30} (1.153×10^{18}) variations. In such cases it is highly unlikely that all the sequences will be present in a SELEX library, since 1.152×10^{18} is equivalent to a 1.915×10^{-6} mole mass of DNA. Thus if a SELEX operation uses a starting library of 1 nanomole (this is a typical mass used), only approximately 1/2000 of possible sequences will be present in the starting pool. Thus the maximum variation of sequences present in the pool can be either a function of initial library mass or length of random sequence.

It should also be mentioned that in practice additional variants of sequences not present in the initial library will be synthesized as a byproduct of the conventional SELEX process. This is largely due to the absence of 3' to 5' exonuclease proof reading feature in Taq polymerase [50]. This means that Taq polymerase has a low fidelity resulting in the formation of a relatively large number of non-perfect replication of DNA sequences in the process of amplification. Thus the number of sequences investigated may in practice be greater than that suggested by the size and random sequence length of the initial library.

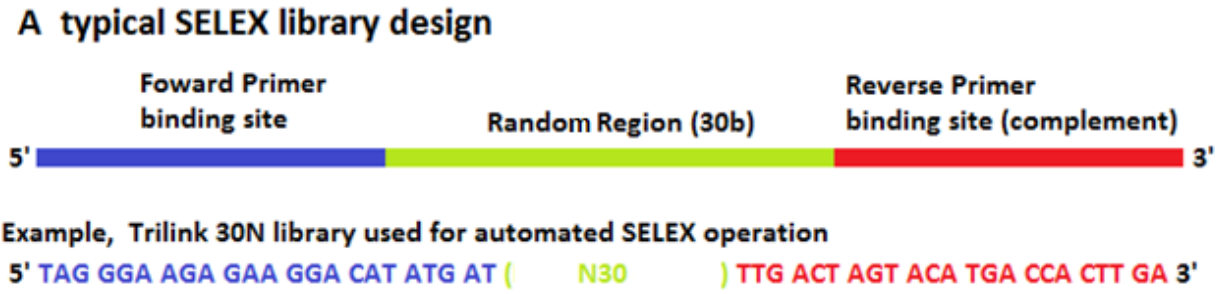

Fig 1.05 Design of a typical SELEX library, containing a random sequence flanked by primer related sequences. An example of a random 30b library sequence is shown below (sequence is a commercial Trilink design, the same library design used for Automated SELEX operation in chapter 6)

1.07b Selection

Sequences with high affinity to the desired target are selected from the DNA library. This step defines the SELEX process, in that the conditions of affinity selection drives the evolution of the DNA library population. While a diverse range of methodology for affinity selection has been studied in order to fulfil the requirements of the specific investigation, all conventional SELEX affinity selection protocol share common functional steps.

1.07c Affinity Selection

Fig 1.06 A representation of the Affinity Selection step

In conventional SELEX, the first step of affinity selection is the binding of target molecule to the oligonucleotide library. The end goal of affinity selection is to determine the sequence in the library with the greatest specific affinity to the target molecule, therefore this step typically involves the incubation of the library with a concentration of target molecules for an extended period of time. The empirical nature of the target-aptamer binding process mean that a thorough understanding of the target-aptamer molecular interaction is not necessary for the process of aptamer selection, only that the target could be bound and retained.

1.07d Partition

Fig 1.07 A representation of the Partition step

After incubation, the target-bound nucleic acid sequences are partitioned from the unbound population. This is classically achieved by passing the target-aptamer solution through a filter with high adsorption efficiency against the target molecule or with a molecular weight cutoff below the size of the target molecule. This results in the retainment of target-aptamer complex, and the removal of unbound sequences. Membrane based retainment has an obvious disadvantage, in that they cannot be used for selecting non-protein targets. Another disadvantages is that in practice the membrane retains a quantity of unbound aptamers via non-specific target-filter interaction which is eluted along with target-binding aptamers as stringency is increased in process of elution, though this problem exists in all solid phase mode of partition. Conversely membrane filter retainment is never completely efficient, and a significant portion of target-aptamer complex may be lost. Aptamers selected by filter adsorption based separation include aptamers targeting Bacteriophage T4 DNA Polymerase [22], protein ERK-2 [51], and *Escherichia coli* Rho-factor [52].

Another classical method of partition is by affinity chromatography. Here the initial DNA library is run through an affinity column with bound target molecules. This process is one of the first used for SELEX partition, having been developed from methods very commonly used for antibody isolation. Sequences with affinity to target molecule binds to the target within the column, with the highest affinity being typically at the top of the column with affinity decreasing towards the end of the column, while the unbound sequences elute via the column drain. By allowing rapid flow of material althrough the affinity column, it is possible to select sequences by speed of binding and not just by affinity. Similar to membrane filter partition, the affinity column filtration can retain a quantity of unbound aptamers via

non-specific interactions. Affinity chromatography generally requires considerable target mass, making this method unattractive for selection against expensive targets. Aptamers selected by affinity chromatography based separation include organic dyes [21], Pro-gastrin-Releasing Peptide [53], and HIV-1 Tat protein [54].

A development of the Sepharose bead based affinity chromatographic partition technique is partition using target-bound magnetic beads. In this method the SELEX library is incubated with Target-MNP particles, resulting in the formation of Aptamer-Target-MNP complexes. In most cases biotin bioconjugated target is typically bound to streptavidin coated magnetic nanoparticles. Placement of a magnet results in the separation of Aptamer-Target-MNP complexes from the solution, which can then be drained out. Separation efficiency of MNP is very high, with >95% the MNP mass being retained in the process of partition. Non-specific interaction between unbound aptamers and platform remains a problem, but is it is significantly lesser than that noted in affinity chromatography. Due to the relatively simple handling and ease of implementation and control of an electromagnet, this separation method is highly amenable to automation. Aptamers selected by MNP based separation include Human Cancer Cell Membrane Antigen [55], Domain II of Hepatitis C Virus [56] and Thyroid Transcription Factor 1 [57].

Capillary electrophoresis is another popular mode of separation. Here unbound oligonucleotides are separated from target-bound sequences by electrophoretic mobility. Free oligonucleotides have lower MW than target bound sequences, and therefore migrate at a faster rate towards a positive electrode than target bound sequences. One of the key advantages of capillary electrophoresis separation is their amenability to miniaturization, making them highly suitable for integration into microfluidic SELEX operations. Aptamers selected by capillary electrophoresis based separation include aptamers targeting IgE [58], HIV-1 RT [59], protein kinase C δ [60] and, ricin toxin [61]. It should be noted that most of these are relatively large protein targets, which would further increase the difference between rate of migration between target-bound and unbound sequences.

Other less commonly used or more recently developed modes of partition includes Electrophoretic Mobility Shift Assay [62], Surface Plasmon Resonance [63], Centrifugation [64], Flow Cytometry [65].

While SELEX can be considered a cyclical process, the conditions of the selection process do not necessarily need to remain constant throughout the cycles. The stringency (which includes temperature, number and intensity of washes, pH, ionic strength and $MgCl_2$) of the incubation and partitioning process is very commonly increased in proportion to the number of cycles performed. This allows the

earlier cycles to retain sequences with even relatively modest affinity to the target in the early round of SELEX when the population of the DNA library is largely non-specific, while allowing higher affinity sequences to be favored during the late stages of SELEX.

1.07e Elution

Fig 1.08 A representation of the Elution step

In conventional SELEX, the process of partition is followed by the process of elution where the target-aptamer complex is broken, releasing the binding sequences. There are a number of ways this could be achieved, but most of them basically result in an increase in stringency. Examples of the method of elution include heating [66], changing ionic concentration [21], and the addition of elution substances such as SDS, urea and EDTA [51]. Competitive binders could also be used as a means of elution [67].

A problem associated with all conventional SELEX affinity selection process is the selection of non-target specific sequences with high affinity to the selection platform. The selection process of conventional SELEX is an empirical process which selects sequences based solely on its ability to remain within the system in the face of increasingly stringent binding conditions. A sequence not specific to the target but which nevertheless could bind tightly to a component of the platform empirically fulfills this objective, and thus remain in the system to be amplified in the subsequent round of selection.

This problem is typically solved by the addition of pre-selection and counter-selection rounds, where the library is incubated with the platform material of the selection assay. This results in the retainment of sequences with high affinity to the platform. The remaining sequence not bound to incubation vessel

wall is drained out and used in the subsequent rounds of selection, and the sequence bound to the platform material is discarded.

1.07f Amplification

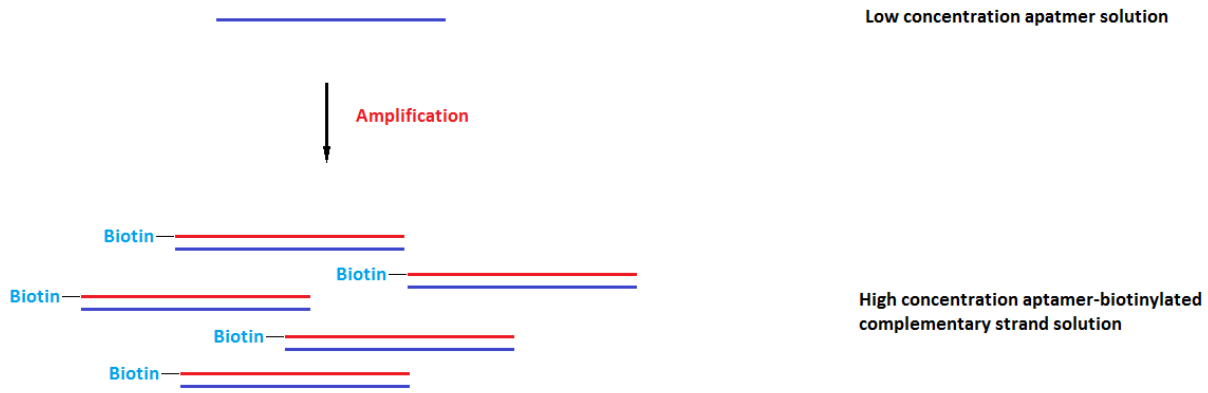

Fig 1.09 A representation of the Amplification step, the complementary sequence here has been biotinylated for post processing.

The selection steps result in the reduction from a highly diverse population in the initial library to an eluted DNA solution containing a significantly reduced population, both in terms of mass and variation. In order for further selection to take place, it is therefore essential that the eluted mass is amplified to bring DNA concentration in line with original concentration of initial library. This is achieved in conventional SELEX by using Taq Polymerase PCR. Temperature conditions are generally kept highly stringent, in order to reduce formation of non-specific amplicons which may accumulate in the SELEX cascade.

1.07g Second Strand Removal

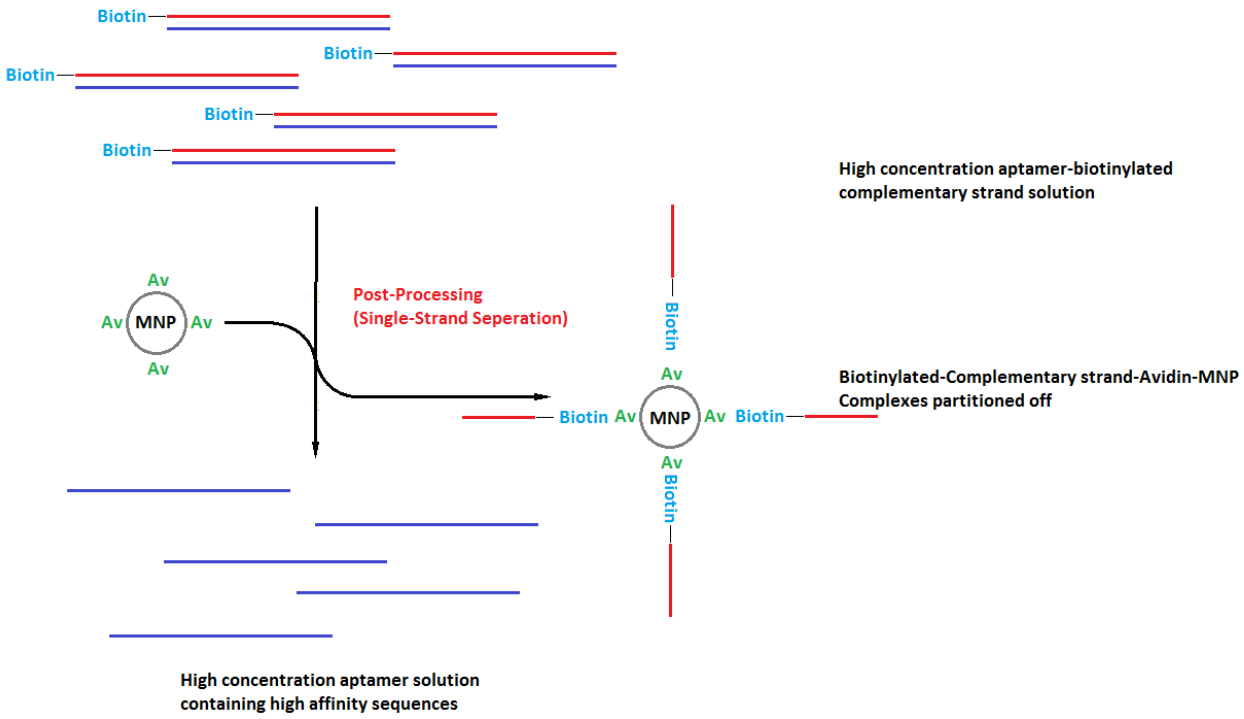

Fig 1.10 A representation of single strand separation, a common post-processing step

The PCR process involves first creating complementary sequence to the original template during the first PCR cycle. During subsequent PCR rounds both forward and backward sequences are amplified. Thus half of the products of PCR are complementary sequences which have not been selected by SELEX affinity selection. These sequences can negatively affect the SELEX process for reasons discussed in the electromagnetic separation section of the Automated SELEX Device chapter. By using biotynalated (reverse) primer for sequence amplification, it is possible to remove the complementary sequence by partitioning using magnetic nanobeads [68]. Alternatively by using biotynalated (forward) primer for selected sequence amplification, it is possible to remove the complementary sequences using Lambda nuclease [69], which specifically targets double strand molecules in the 5’ to 3’ direction, with a strong bias in favour of the substrate with exposed 5’-phosphate group, which results in decreased cleaving of biotynalated selected sequences.

Phenol/Chloroform extraction and ethanol precipitation is typically performed to purify DNA pool from detritus from the PCR and upstream post-PCR conditioning steps. The purified single stranded library can at this point be used as library for the subsequent round of SELEX.

1.08 Automated Selection

The manual SELEX procedure can be reasonably characterised as long, manually intensive, and repetitive. It can also be considered a highly skill intensive process, requiring highly qualified personnel with a good understanding of molecular biology and highly developed sterile technique. Thus automating the SELEX process could be considered highly desirable. The repetitive nature of the SELEX process mean that the range of operational tasks that need to be performed by the SELEX device is fewer than the complexity of the manual operation and length of operation would suggest.

A literature review of this topic reveals that most works have taken one of two approaches towards automating the SELEX process. These are the Manual-like automated SELEX assay, and the microfluidic automated SELEX assay.

1.08a Conventional Automation of SELEX Process

The first is to effectively replicate the human actions of a manual SELEX process entirely (we will call this the manual-like approach). In this study, the automotive process not only performs functions analogous to manual SELEX, but also largely replicates the same methodological process performed by the human hand. A good example of this mode of automation is the pioneering work performed by Cox and Ellington [70].

In this study a three axis robot with a pipette actuator was used to perform a modified manual SELEX operation. The automative machines used here are non-specialised, which makes sense in the context of a pioneering work in that most of the robotic tasks are performed by an commercial liquid handling robot (containing a three axis manifold, a liquid handling pipette head, and a carousel type tip reloader) adapted to perform the SELEX process. The heating element likewise uses a commercially available design, and a commercial recirculating chiller is adapted for enzyme preservation. The selection process is very similar to those described by the original Cox and Ellington paper [21], including the use of

nitrocellulose filter as a means of partition. This is a somewhat unusual choice, since the target is already immobilized on MNP, which would have made magnet based partition easy to implement. It should be noted that this experiment preceded the widespread usage of automated MNP based separation. Later automatic SELEX devices designed in this format typically utilizes magnetic separation, including further studies conducted by the Ellington team [71]. This would suggest that the separation method may not be based on protein-nitrocellulose adsorption but on MNP entrapment by filter.

This paper does not detail the control software infrastructure of the device. Since both the thermal cycler and automated workstation have independent control software, the devices are presumably synchronized either with an integrated virtual environment platform such as Labview or simply by synchronized timing. The latter would not be practically feasible in highly complex operations.

The manual-like approach has a number of advantages. Firstly since the process replicates human actions, it is possible to migrate already well-established SELEX protocols with minimal modification. SELEX is not the first manual work intensive activity to be automated, liquid sampling robots are already commercially available as off the shelf products. By replicating liquid handling in a conventional form, pre-existing automative components can be adapted for SELEX applications which implies that very little hardware fabrication is required, allowing the mechanical aspects of this approach to be limited to assembly and to the adaptation and integration of off-the-shelf parts to perform the SELEX process.

However there are a number of weaknesses to the human-like approach to automation.

Firstly while the use of off the shelf products allow for a fast development time, it is also relatively expensive. Off the shelf products are designed for the purpose of general use and have significant redundancies and excess features which may not be necessary in the SELEX process. This result in unnecessary high setup cost. The production of a prototype from scratch allows removal of excess features and enhancement of specialized features benefiting the SELEX process. It should be noted for example that one of the main hurdles noted by the Cox Ellington paper [70] in automating their SELEX process was the development of a filter separation process. While the prototype will take longer to build without using off the shelf material, and result in a potentially much more expensive prototype, the cost of production per unit will decrease with mass production.

Another problem which typically affects automatic sampler is the potential of contamination, particularly of the sampling tip. Most automatic sampler control contamination by rinsing the sampling

tip either in a well or through a water flow stream. This sufficiently cleans the sampling tip for most general purpose, but SELEX is particularly vulnerable to contamination due to the relatively small mass of the eluted library compared to the initial library, as well as the cascading nature of the SELEX process. This problem could be bypassed by the use of a pipette tip loader, such as the pipette tip carousel loader used in the Cox and Ellington study, which completely renews the pipette tip during operation in a manner similar to that applied in the manual technique. Contamination from outside sources is difficult to control. This mainly involves the entry of contaminants to the reaction mix.

Theoretically, most nucleotide contaminants should not be significant, as they would not be compatible with the SELEX primers and would therefore not be amplified by PCR downstream. However serious problems could arise in instances where contamination by sequences with common primers occur, such as sequences from another SELEX operation performed with another target, but utilizing the same initial library. It is important to note that for a sampling tip to access the reaction vessels and reagent vessels, it is necessary for these vessels to be open topped, creating point of entry for contaminants. Moving parts of mechanical hardware are simply not amenable to sterilization, thus causing the automatic sampler to become a reservoir of contaminants.

All in all it is certainly not impossible to minimize contamination possibility in human-like automated SELEX, but doing so requires a significant amount of work and maintenance, as well as good sterile techniques.

1.08b Microfluidic Automation of SELEX Process

An alternative approach to manual-like automated SELEX is the microfluidic SELEX approach, of which a good example is the one described by Hybarger et al [72]. In this approach, the directional flow of the liquid handling process is regulated by actuator valves, whose pattern of opening and closing determine the direction in which the liquid is being driven by the pump. This control of liquid movement allows the correct reagents to be taken up from input reservoirs and delivered to the correct reaction channel. Micropipes of uniform diameter allow accurate calculation of the movement of the solution plugs. Complex valve behaviour is made possible by the use of Labview software, which enables integration and synchronization of SELEX device components.

Decontamination protocols based on flushing with the decontaminant ELIMINASE, which eliminates nucleases, followed flushing with MilliQ. ELIMINASE is sufficiently cheap to be used in scaled up mesofluidic automated SELEX processes. Since the system is completely enclosed, the inner surface of the device is completely isolated from the external surface. Therefore the external surfaces do not need to be cleaned, which is a major potential advantage. The report does not study the possibility of dealing with contamination during extended operation. It is therefore impossible to gauge how frequently a more thorough decontamination would be required to take place, and how long the process will take when it is required.

An obvious benefit of microfluidic based selection is the reduction in scale of the SELEX process, which implies that this SELEX process is rendered highly economical. This will be useful for any SELEX process by reducing the cost of the stock reagents (primers, libraries, PCR mastermix) but particularly so for the selection of aptamer against rare targets that are difficult and expensive to produce.

A potential weakness of microfluidic based SELEX process is that the reduction in the volume of incubation solution also reduces the maximum mass of initial DNA library that can be implemented. As mentioned above, the DNA library size is directly proportional to the mass of the initial library used. Thus by reducing the volume (and therefore mass) of the initial library, the complexity of the library in terms of total sequence variety is also concurrently reduced.

The affinity-selection component of the SELEX process is achieved by driving the DNA library though microchannels by the control of valve actuators, which direct flow of liquid. To use the study by Hybarger et al as an example, for a standard segment of microchannel with the maximum gauge size used here (150um), the volume of the microchannel will only be 1.76ul. This means only relatively small amount of DNA can be used in the process of selection, and therefore relatively low library complexity. For example, a typical DNA concentration used for the process of selection is 1uM. This translates to a maximum of 1.06×10^{12} DNA sequences in a 1.76ul volume. This would mean that, for 30 random base pair library (1.2×10^{18} total variations), only 1 out of 1.1×10^{6} sequences will be present in the library.

In this thesis it is hoped that by increasing the scale of microfluidic channels from a micrometer to millimeter scale, it would be possible to gain the primary advantages of the large volume SELEX (large library and sequence variation), while also retaining the primary advantages of microfluidic SELEX (reduced contamination risk, low initial cost and maintenance). An comparison of Conventional

Automated SELEX, Microfluidic Automated SELEX and the proposed Mesofluidic Automated SELEX, can be found in the table below.

	Conventional Automated SELEX Process	**Microfluidic Automated SELEX Process**	**Mesofluidic Automated SELEX Process**
Liquid Handling	Sampling tip and (typically syringe) pump	Solenoid valve and pump	Solenoid valve and pump
Scale	ml	ul	ml
Total sequences	~10^9	~10^6	10^8 to 10^9
Contamination risk	High	Low	Low
Initial Invested Capital	High	Low	Low
Typical mode of partition/elution	Filtration (older systems)/magnetic (newer systems)	Magnetic or electrophoretic	Magnetic

Table 1.01 A comparison of typical Conventional Automated SELEX Process and Microfluidic Automated SELEX Process. Mesofluidic automated SELEX process represents the automated SELEX device described in Chapter 6 of this thesis.

1.09 Electrochemistry

Having chosen aptamers as the type biosensory molecule to be used this study, it is then necessary to select a compatible transducer to it. For this project, electrochemical transducers were selected.

Electrochemistry is the study of chemical reactions taking place between (generally) metallic or carbon electrodes and an electroactive species at the electrode/solution interface, resulting in the transfer of electrons. Electroanalytical techniques typically involve the measurement of current in response to an applied voltage.

The electroanalytical method used for this study is voltammetry, the measurement of the current as a function of electrode potential. Thus by performing a voltammetric measurement for each concentration of a titration series, it is possible to measure changes in target concentration, thus enabling quantitative analysis of the biosensor response to concentration of redox label, which in turn is correlated to the target concentration of the biosensor, or the concentration of an redox active target

itself. Since the applied potential is varied, voltammetric techniques also yield information on the electrode process taking place at the electrode solution interface.

The current response in a voltammetric experiment is controlled by two predominant factors, charge transfer and mass transport rates. Under conditions where charge transfer is fast (compared to both mass transport and the rate of change of potential) then the redox couple is in near thermodynamic equilibrium with the electrode.

Charge transfer process involving electron transfer can be represented by the following equation:

$$O + ne^- \leftrightharpoons R$$

O being the Oxidised form of a redox couple

R being the Reduced form of a redox couple

Thus the oxidised species receives n electrons in order to be converted to its reduced form. The electrons of the electrode have a maximum energy distributed around the Fermi level, and electrons can be donated or received into this level.

For the process of reduction to take place, the electrons in the electrode must have sufficient energy to transfer to the lowest unoccupied molecular orbital (LUMO) of the oxidised species. Vice versa, in order for electrons to be donated from the reduced species to the electrode, the highest occupied molecular orbital (HOMO) must have an energy level higher than the Fermi level of the electrode. This can be visualized in the diagram below:

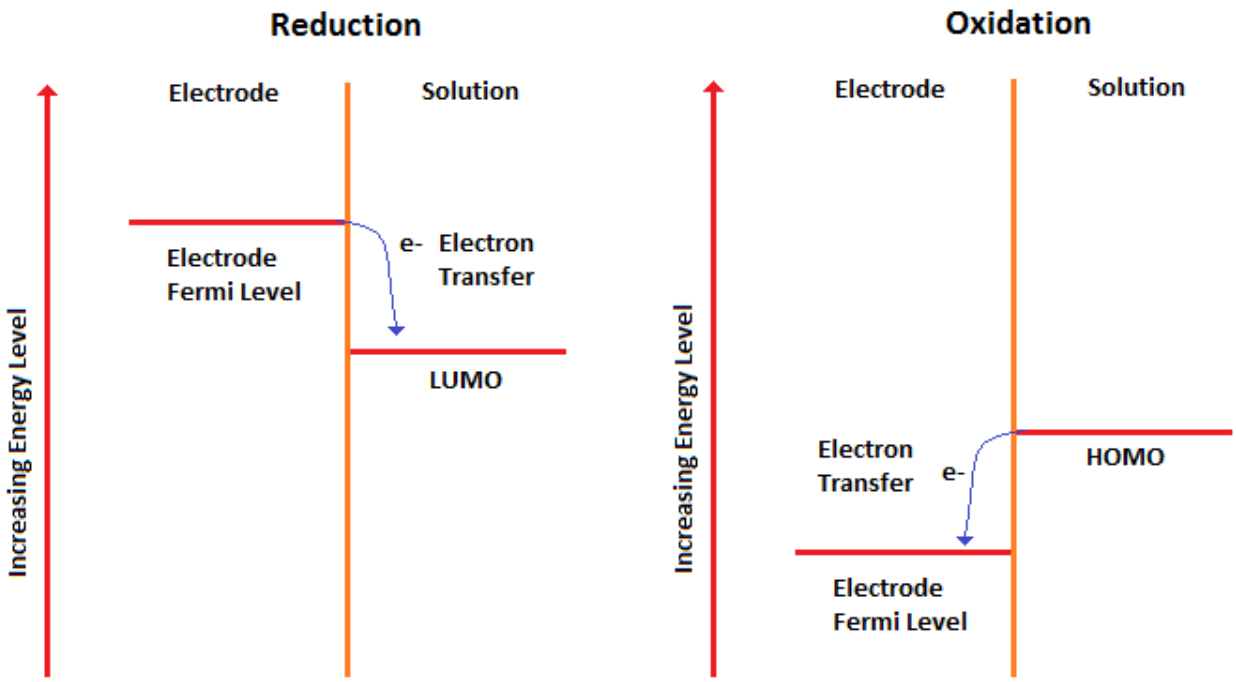

Fig 1.11 Visualisation of the electron transfer process at the electrode interface.

In electrodes the electrons of the s and p orbitals of the metal atoms are delocalized, resulting in the effect commonly referred to as a "sea of electrons". Potential applied to the electrode results in a change in the energy level of the electrode as a whole, with this energy level being known as the Fermi level. The Fermi level depends on the electrode potential as well as the material of which the electrode is made. For a system where electron transfer is fast, the current can be represented using the following equation:

$$i = nFAV$$

i is the current

n is the number of electrons transferred

F is Faraday's constant

A is area of electrode

V is net rate of electron transfer

Eq 1.01 Rate equation of an electrochemical system limited by electrode potential

The net rate of reaction is the difference between the rates of forward (anodic) and reverse (cathodic) electron transfer thus:

$$i = nFA(V_{forward} - V_{reverse})$$

The rate of the forward and reverse reactions could be represented using the rate equation:

$$V_f = k_f(C_o)$$

$$V_r = k_r(C_r)$$

k_f and k_r being forward and reverse rate constant respectively

C_O and C_R being concentration of Oxidised and Reduced species at x=0 respectively

The forward and reverse rate constant could be represented by the Butler-Volmer Equation, which describes the relationship of the current and potential for thermodynamically controlled reactions:

$$k_f = k_0 e\left[\frac{\propto_f nF(E - E^o)}{RT}\right]$$

$$k_r = k_0 e\left[\frac{(1-\propto_r)nF(E - E^o)}{RT}\right]$$

k_o is standard rate constant

E is potential

αf is forward transfer coefficient

αr is reverse transfer coefficient

E^O is the standard potential of the reaction

R is universal gas constant

T is temperature in K

Combining the above equations gives:

$$i = nFAk^o[C_o e\left[\frac{\propto_f nF(E-E^O)}{RT}\right] - C_r e\left[\frac{(-\propto_r)nF(E-E^O)}{RT}\right]$$

Eq 1.02 the Butler-Volmer Equation

At equilibrium (where *i* = 0), rearranging and using $\alpha_f + \alpha_r = 1$ yields the Nernst equation, which could be used to establish the concentration of the electrochemically active species at the electrode interface using the potential of the electrode.

$$E = E^{O} + \left(\frac{2.3RT}{nF}\right)\log\left(\frac{C_O}{C_R}\right)$$

Eq 1.03 the Nernst equation [73]

The current resulting from a change in the concentration of the reduced and oxidised states of the electrochemically active specie is referred to as the faradaic current. The faradaic current can be used as a means of quantifying of the rate of redox reaction, and therefore (since quantity of redox label at electrode interface is proportional to target concentration in affinity biosensors) of the concentration of the target analyte.

1.10 Mass Transport Controlled Reactions

Mass transport in an electrochemical cell is dependent on three factors:

1) Diffusion: Movement along a concentration gradient
2) Convection: Bulk movement of liquid
3) Migration: The migration of charged particles along an electrical field.

The rate of mass transport at a fixed point is known as the flux, described as the number of molecules arriving at a fixed surface area per unit time. In substrate depleted electrochemical systems it represents the rate at which reactant is being renewed at the electrode interface. Flux to the electrode is described using the Nernst-Planck equation.

$$J = -D\left(\frac{dC}{dx}\right) - \left(\frac{zFDC}{RT}\right)\left(\frac{d\Phi}{dx}\right) + CV$$

Eq 1.04 the Nernst-Planck equation

J is flux

D is the diffusion coefficient, which in aqueous solution is generally between 10-5 and 10-6$cm^{-2}s^{-1.}$

(dC(x,t)/dx) is the concentration gradient

z is charge

C is concentration

(dΦ /dx) is potential gradient

V is Hydrodynamic velocity

In unstirred cells (where there is no convection) with high salt concentration (no migration), the mass transport mechanism is predominantly diffusion down the concentration gradient. Thus Flux can be described using Fick's First Law:

$$J = -D\left(\frac{dC}{dx}\right)$$

Eq 1.05 Fick's First Law

1.11 Effect of distance on Transfer Kinetics

One of the underlying principles of the conformation and configuration change aptasensors discussed in the subsequent section of this chapter is that signal is dependent on the distance between redox label and the electrode surface.

The Marcus theory of electron transfer posits that the probability that an electron transfer will take place between an acceptor and donor couple during transition state decreases with increasing distance between the redox couple and electrode, and can be described using the following equation:

$$k = (e^{-\alpha r})(e^{\frac{\alpha \Delta G}{RT}})$$

Eq 1.06 Marcus' theory of electron transfer

r is the distance between donor and acceptor

α is a constant representing the medium through which electron transfer takes place

ΔG is the Gibbs free energy of activation, which determined by the standard reaction Gibbs energy and the reorganization energy. This can be described as:

$$\Delta G = \frac{(\Delta G^o + \lambda)^2}{4\lambda}$$

ΔG^o is the standard reaction Gibbs energy

λ is the reorganization energy

Thus the rate of electron transfer is dependent on the distance between the redox label and the electrode surface. Labeled electrochemical biosensors signal is not the direct result of electrochemical change of biosensor target molecule, but as a result of altered separation distance between redox label and electrode surface. How this is achieved will be further discussed in the subsequent section of this chapter.

1.12 The Charged Double Layer Theory

The electrical double layer occurs at the interface of any solution and charged surface. In electrochemistry, this phenomena is caused by the attraction of particles of the opposite charge to charged electrode surface. This results in the formation of a charged layer on the electrode surface, which attracts more particles of the opposite charge to the layer. This process is repeated, forming a charge structure that is composed of two distinct sub-structures. The inner layers closest to the electrode surface, called the compact layer, is composed solvent molecules and specifically adsorbed ions on the electrode surface, as well as solvent ions attracted to the surface by long range coulombic forces. The compact layer is strongly held in place and organized by the electrode charge. The outer layer further from the electrode surface, is called the diffuse layer, is a less organized layer which

formed of scattered ions which extend from the compact layer into the bulk solution. The structure of the diffuse layer is a compromise between the organizing force of the electric field and the disruption caused by random thermal motions. The width of the diffuse layer is influenced by the ionic concentration of the solution.

This charged double layer acts like a capacitor, storing charge when a potential is applied. This excess charge is electrostatically balanced between electrolytes and other charged molecules, in a manner similar to a parallel plate capacitor, with the total capacitance of the double layer being a combination of the capacitance of the compact layer and the capacitance of the inner layer.

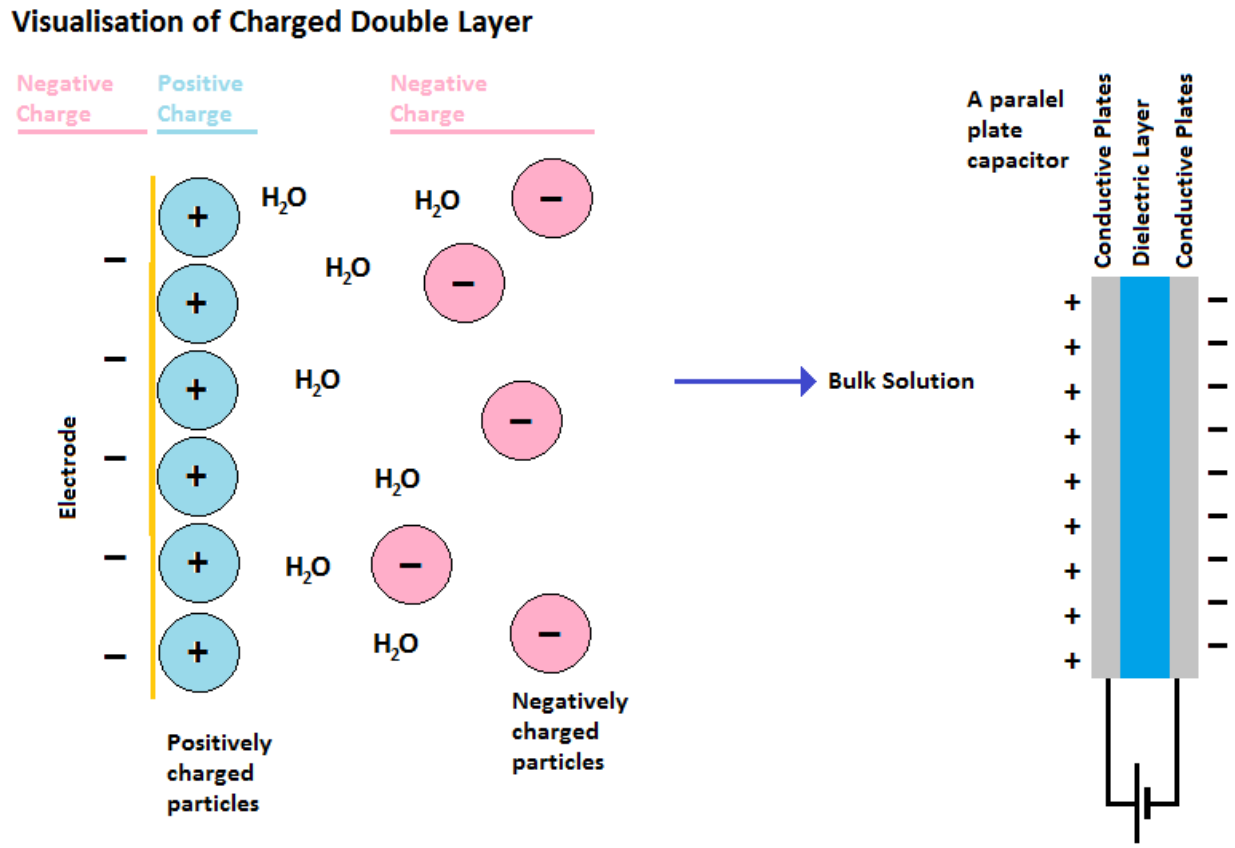

Fig 1.12 Diagram visualizing a simplified charged double layer (compact layer shown only). A conventional parallel plate capacitor is also displayed for comparison.

The double layer's capacity for charge storage is responsible for the current known is the charging current. This current is non faradaic (it does not involve the transfer of electrons) but occurs due to application of potential across the double layer, and is a significant factor in the detection limit of

controlled potential techniques. The charging current decays exponentially with time, and therefore could be minimized by the use of pulse voltammetric techniques such as DPV and SWV, which will be discussed below.

1.13 Linear Sweep Voltammetry (LSV)

Perhaps the simplest form of voltammetry is Linear Sweep Voltammetry (LSV). In linear sweep voltammetry, a potential sweep is applied as a steady ramp. Initially the applied potential at the electrode interface falls short of those necessary to drive redox reaction, and no reaction takes place, resulting in no flow of current. As the potential is swept towards the Standard Electrode Potential (see the Nernst equation above), the faradaic current begins to rise exponentially.

Faradaic current continues to increase until a point is reached at which the current is a maximum. In an unstirred system, this peak is a result of the depletion of the surface concentration of redox substrate at the electrode interface. Redox species is renewed by additional substrate diffusing in from the bulk solution, thus the rate of electron transfer becomes limited not by the potential, but by the flow of substrate to the electrode interface (see Nernst-Planck equation above), resulting in a plateau.

Unlike homogeneous chemical reactions, electrode reactions take place at a surface. This results in the formation of a concentration gradient between the solution at the electrode interface and that in the bulk solution. As the reaction exhausts the concentration of substrate at the electrode interface, the substrate concentration is replenished by diffusion from the bulk solution. As the reaction progresses this leads to an expanding thickness of the diffusion layer, and a decrease in flux. On the voltammograms this is represented by the current decreasing after the peak and ultimately reaching a plateau where the rate of the electrode reaction is balanced by the rate of diffusion.

1.14 Cyclic Voltammetry (CV)

Cyclic voltammetry is the combination of a forward and reverse linear sweep voltammetry. This results in the formation of the anodic peak as the reduced species formed in the forward sweep is oxidized back into the oxidized species. This allows the products formed from the forward reaction to be investigated in the reverse sweep. This results in cyclic voltammetric methods being able to rapidly determine

considerable information on the redox reactions, including simultaneously the kinetics of many different electron transfer reactions as well as adsorption processes, which can be exploited to transduce binding events into comprehensible electrochemical signals. The potential wave form of a CV and an example of the expected current-potential curve for a reversible redox couple undergoing a single forward/reverse cycle is shown below.

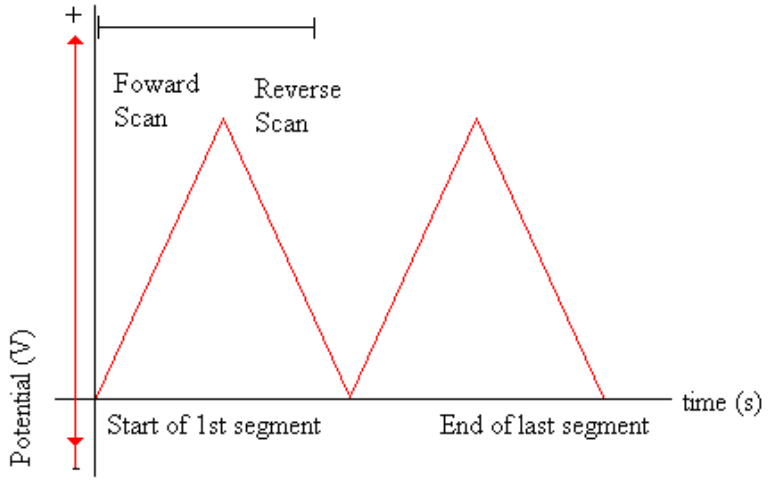

Fig 1.13 Potential diagram of a 4 segment CV

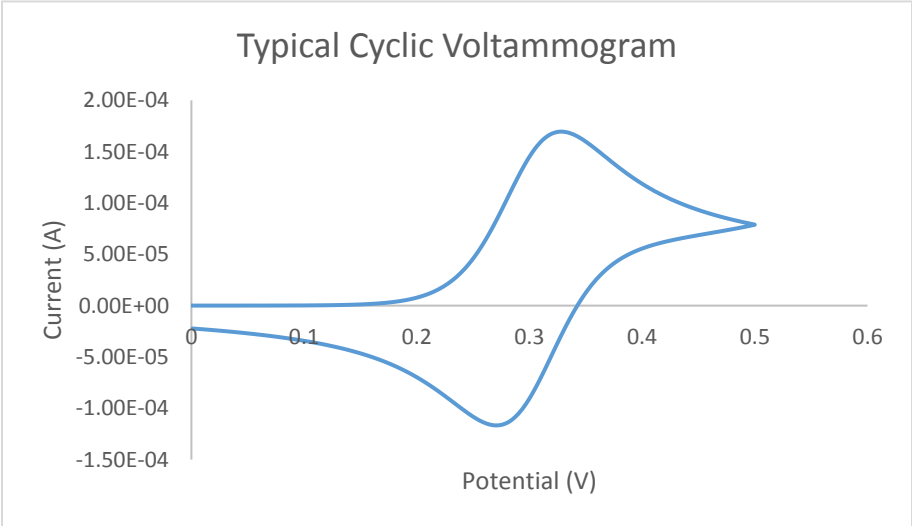

Fig 1.14 A typical cyclic voltammogram, simulated on Chi Instrument Inc, Chi 1030a potentiostat proprietary software. Peak separation is 0.056V which is indicative of a reversible system.

1.15 Square Wave Voltammetry (SWV)

A potential weakness of cyclic voltammetry and other linear sweep voltammetry derived methods is interference from charging currents. Square Wave Voltammetry (SWV) is derived from Differential Pulse Voltammetry techniques, which is in turn derived from LSV. The difference between DPV and LSV is in the potential waveform. In LSV, the waveform is in theory analogue in nature producing a smooth potential ramp in direct correlation with potential increase over time.

Since the potential is held at a steady stated between pulses, this results in the reduction of the capacitance current which decays at an exponential rate, but not the faradaic current which decays at an inverse square root of time.

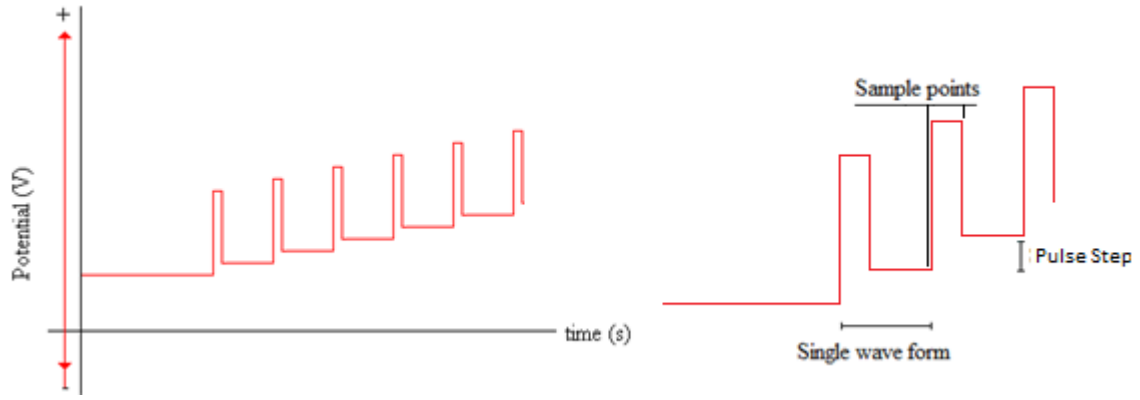

Fig 1.15 Potential diagram for Differential Pulse Voltammetry

Square Wave Voltammetry is developed as an optimization of the mechanisms of pulsed voltammetry. In SWV a waveform composed of symmetrical square waves superimposed on a base staircase potential is applied to the electrode. The current is sampled twice per wave form, first at the end of the foward pulse, and second at the end of the reverse pulse. Due to the significant modulation in amplitude of the square wave, the product of the forward step is converted back to its original form by the reverse pulse. The net difference between the two measurements per wave form are then plotted against the base staircase potential.

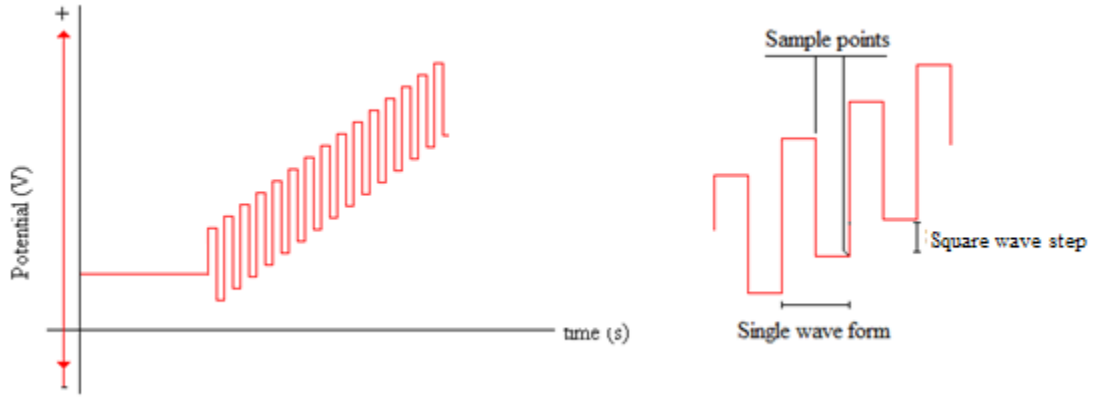

Fig 1.16 Potential diagram for Square Wave Voltammetry

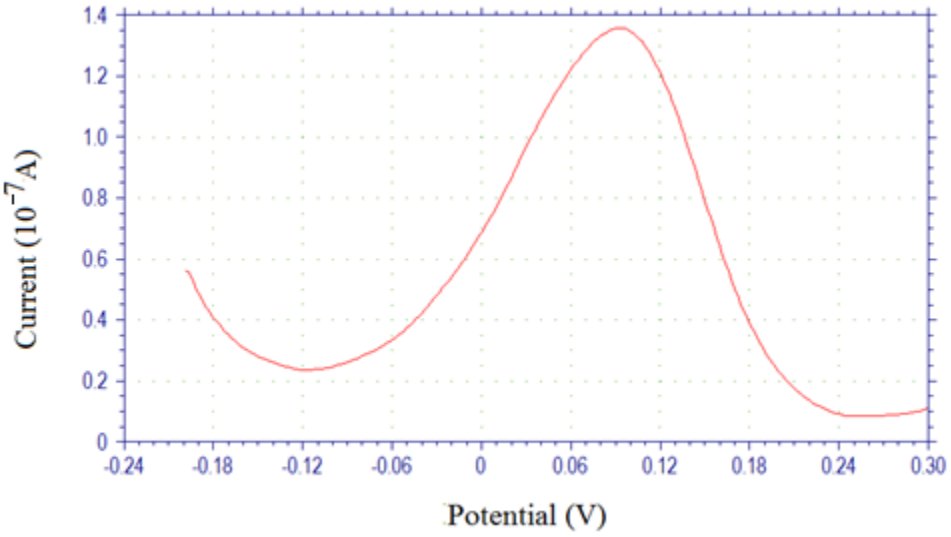

Fig 1.17 A typical square wave voltammogram

Since the net current, which is the difference between the forward and reverse pulses, is larger than both the forward or reverse component individually, this results in a sensitivity greater than that of differential pulse systems which only have a forward component, while retaining the benefit of reduced effect of capacitance, resulting in very high sensitivity, so that detection limits in the nanomolar range could be achieved.

1.16 Electrochemical Aptasensors

There are a number of different formats in which electrochemically transduced aptamer biosensors have been be implemented and studied. These can be divided into two broad categories:

1) Configurational-Change Aptasensors
2) Conformational-Change Aptasensors

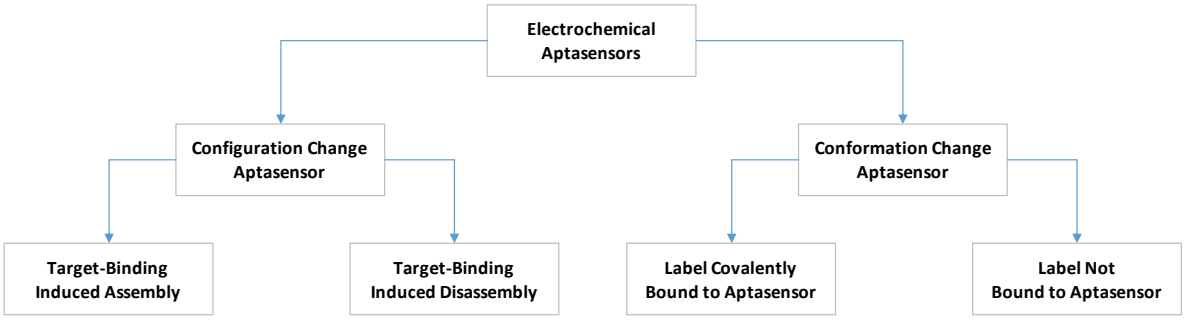

Fig 1.18 Categorisation of electrochemical aptasensors

1.16a Configurational-Change Aptasensors

These are biosensors where target binding results in the assembly or disassembly of the sensor construct resulting in a change in signal. These can be subdivided into two subgroups. The first are sensors where target binding results in assembly of the biosensing construct. These are typically “signal-on” sensors, where target-binding results in the formation of complex signal structures (sandwich structures, for example). The second are sensors where target binding results in the disassembly of the sensor construct. These are typically composed of two sequences of hybridised oligonucleotides, one of which is bound to electrode surface, where target binding results in the dissociation of Crick-Watson interaction, resulting in the release of the second strand.

A good example of an induced assembly configurational aptasensor is the thrombin aptasensor developed by Numnuam et al [74]. In that study, two aptamers were used in a sandwich format, in a manner similar to ELISA. The surface-bound aptamer, performing a role analogous to the ‘primary antibody’ in ELISA, is immobilized onto gold substrate surface by thiol-gold interaction. The second aptamer is bound to CdS quantum dot label and performs a role analogous to the ‘detection antibody’ in

ELISA. The aptamer performing both roles is the TBA aptamer originally selected by Bock et al [149], which has multiple binding sites per thrombin molecule.

The sensing mechanism involves first the incubation of thrombin on electrode surface, resulting in the binding of the thrombin target to the surface-bound aptamer. The label-bound aptamer is incubated with this structure, resulting in the formation of an aptamer-thrombin-aptamer sandwich. CdS is dissolved by hydrogen peroxide, resulting in a dilute electrolyte background suitable for the detection of released Cd^{2+} by an ion-selective microelectrode. A detection limit of 140pM of analyte was achieved.

A similar aptasensor was designed by Polsky et al [75] using a sandwich-forming mechanism similar to that described by Numnuam et al. However, in the former study, the CdS label has been replaced by platinum nanoparticles, which generate signal by electrocatalysing the reduction of H_2O_2 to H_2O. The greater the target concentration, the lower the concentration of redox active H_2O_2 which can be detected voltametrically as an intense cathodic current in the range of -0.1 to -0.6 V. Here a detection limit of 10nM was achieved.

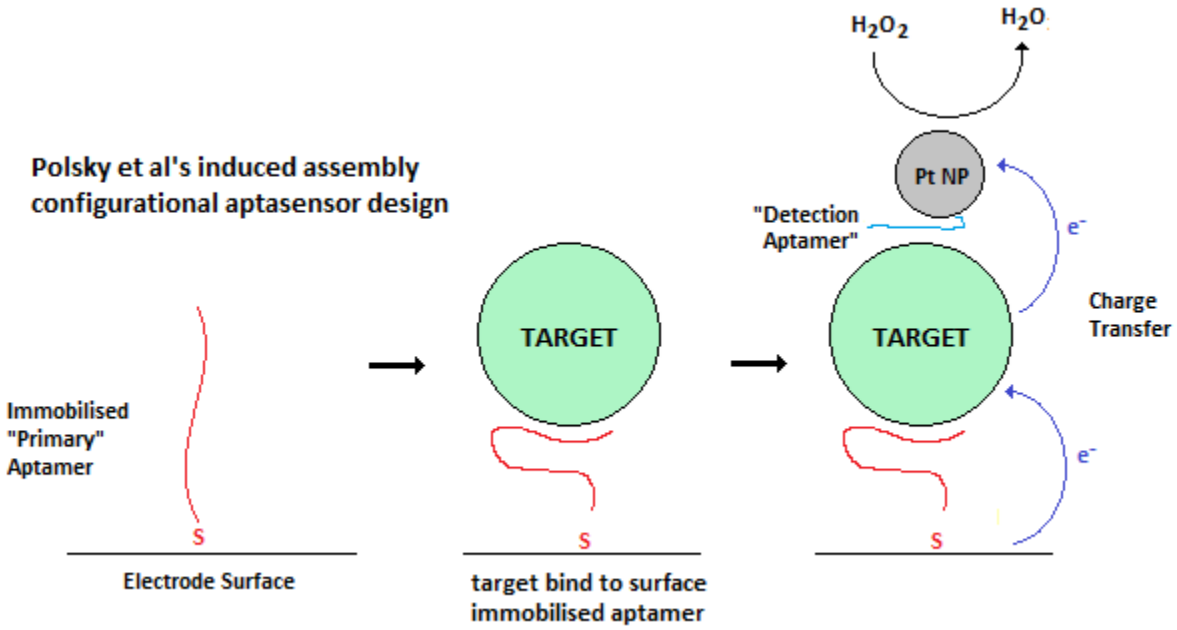

Fig 1.19 Example of an induced assembly configurational aptasensor. The aptasensor designed by Numnuam et al uses a similar binding mechanism, but with a different label method.

The aptamer biosensors based on gold nanoparticles discussed in Chapter 5 of this thesis could be considered induced assembly configurational aptasensor (see page 162)

A good example of an induced disassembly configurational aptasensor is the ATP aptasensor designed by Zuo et al [76]. The construct of this aptasensor in the absence of target molecule is composed of an aptamer sequence, bound to electrode surface by thiol-gold interaction, hybridised to a complementary oligonucleotide. The label used is ferrocene, bioconjugated at the opposite end of the aptamer to the electrode-binding thiol group. The aptamer-complement hybrid has a linear helical structure due to Crick-Watson base-pairing, resulting in the displacement of the redox label far from the electrode surface (and therefore giving a low current) in the absence of target. The presence of target results in the displacement of the complementary sequence by the target, forming a target-aptamer complex. This target-bound aptamer structure results in the ferrocene redox label being moved closer to the electrode surface than the linear aptamer-complementary oligonucleotide hybrid, resulting in an increase in current.

A similar approach was used by Lu et al [77]. Similar to Zuo et al's study, the aptasensor here is also composed of an aptamer-complement hybrid containing a ferrocene label, bound to electrode surface by thiol-gold interaction. However, in the approach used by Lu et al, the surface bound, label-bioconjugated sequence is the complementary sequence. Target binding results in the release of the target-bound aptamer into the bulk solution. The complementary sequence, in the absence of its linearising aptamer hybrid, has a hairpin loop as its most stable secondary structure. This results in the ferrocene label being relocated close to the electrode surface, resulting in high current. This sensor has a detection limit of 1 nM in undiluted environmental sample (blood serum), and 50pM in buffer diluted environmental sample.

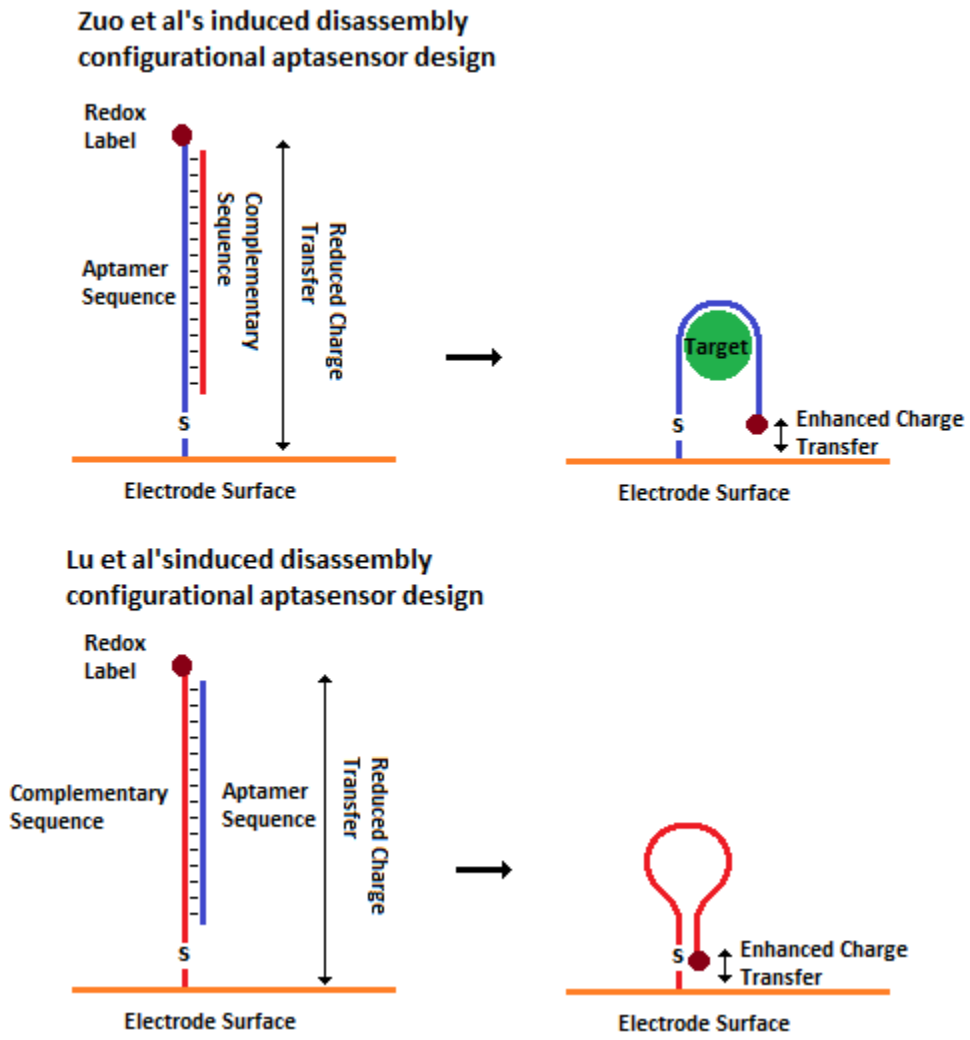

Fig 1.20 Examples of induced disassembly configurational aptasensor design

1.16b Conformation Change Aptasensor

These are biosensors where target binding results in a spatial rearrangement in the folding of aptamer construct, resulting in a change in signal. Conformation change aptamers are typically composed of oligonucleotide sequences bound to the electrode surface, usually by thiol-gold interactions. These can be subdivided into two subgroups, one in which the redox label is covalently bound to the aptamer molecule and signal is generated by the spatial rearrangement of the redox label and the other in which the label is not bound to the aptamer molecule and signal is generated by the association or dissociation of the redox label from or to the bulk solution, respectively.

A good example of a conformational-change aptasensor with covalently bound redox label is the thrombin aptasensor designed by Xiao et al [78]. Their sensor construct is composed of a single oligonucleotide sequence bound to the electrode surface by thiol-gold interaction, with a methylene blue redox label bound on the opposite end of the sequence, in a manner similar to the aptamer sequence in Zuo et al (in the absence of a complementary strand). In the absence of target molecules, the aptamer molecules exist in an equilibrium of states, some of which could bring the redox label relatively close to the electrode surface, resulting in current. In the presence of target molecules, the aptamer folds into a G-quadruplex tertiary structure, resulting in the rearrangement of the redox label away from the electrode surface and, therefore, decreased current. Xiao et al's aptamer biosensor has a detection limit of 6.4 nM.

This sensor displays one of the most noticed advantage and disadvantage of the conformation change aptasensor with covalently bound redox label. The advantage is that this sensor could be regenerated and reused, due to the chemical and temperature stability of the DNA primary structure. The disadvantage is that this sensor has relatively high background signal to bound-state signal (the amplitude of the bound signal is 20% higher than that of the unbound signal), mainly as a result of unpredictability of the unbound state (this is atypical because it is usually the bound state which cannot be predicted); the use of this aptamer has the advantage of the well-studied interaction between thrombin and its aptamer.

A similar approach was used by Lai et al's platelet-derived growth factor aptasensor [79]. However, in this case, the target-bound state results in the redox label (ferrocene in this case) being relocated closer to the electrode surface relative to the unbound equilibrium. This results in a 'signal on' system where target binding results in an increase in current.

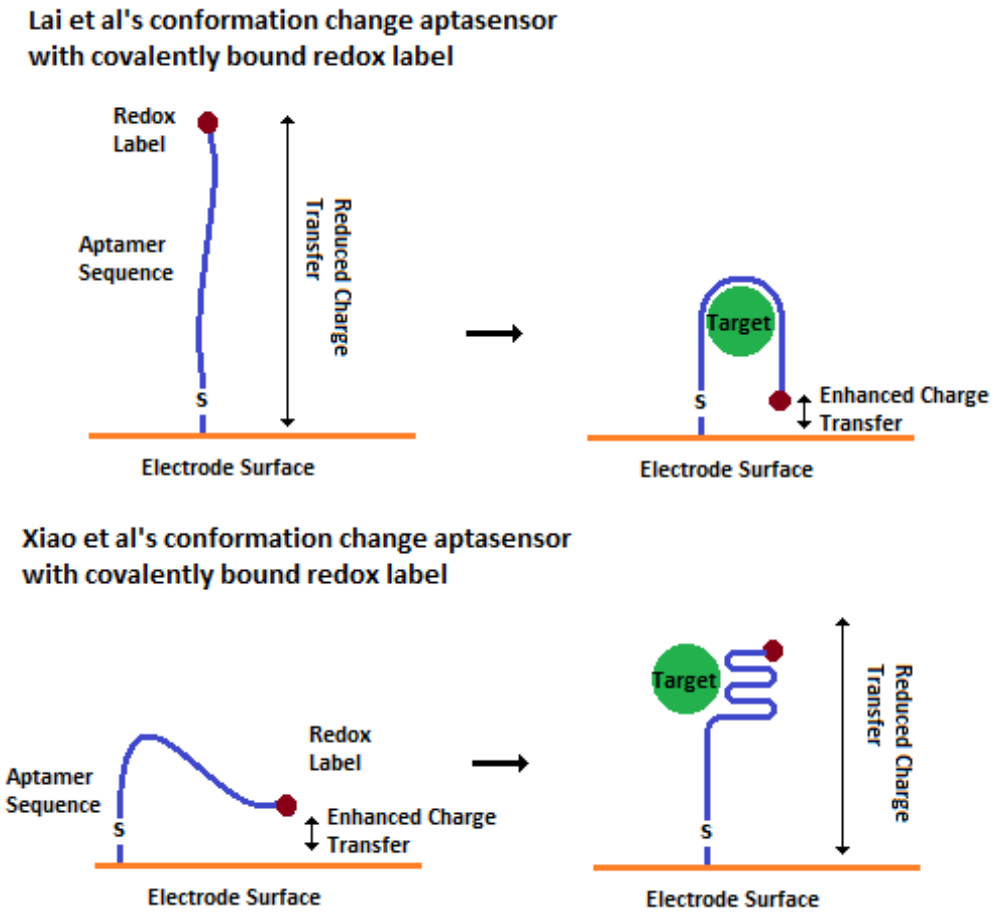

Fig 1.21 Examples of conformational-change aptasensor with covalently bound redox label. Note that unbound aptamers with non-specific structure exist as an equilibrium of both 'signal on' and 'signal off' states

The conformation-change kanamycin and tetracycline aptasensors discussed in Chapters 3 and 4 of this thesis could be considered conformational-change aptasensor with covalently bound redox label, with the 'signal off' and 'signal on' formats, respectively (see page 90).

A good example of a conformation-change aptasensor without covalently bound redox label is the lysozyme aptasensor designed by Rodriguez et al [80]. This sensor construct is composed of a single biotinylated oligonucleotide sequence bound to an indium tin oxide electrode surface via biotin-streptavidin interaction. The sensor operates in a solution containing ferricyanide/ferrocyanide ions. The negatively charged oligonucleotides immobilized on the electrode surface prevent access of the ferricyanide/ferrocyanide ions to the electrode surface by same-charge repulsion. Binding of the aptamer to positively charged lysozyme results in the reversal of the surface charge, allowing access of

the electrode surface to ferricyanide/ferrocyanide ions. This results in a decrease in impedance, which is detected using electrochemical impedance spectroscopy.

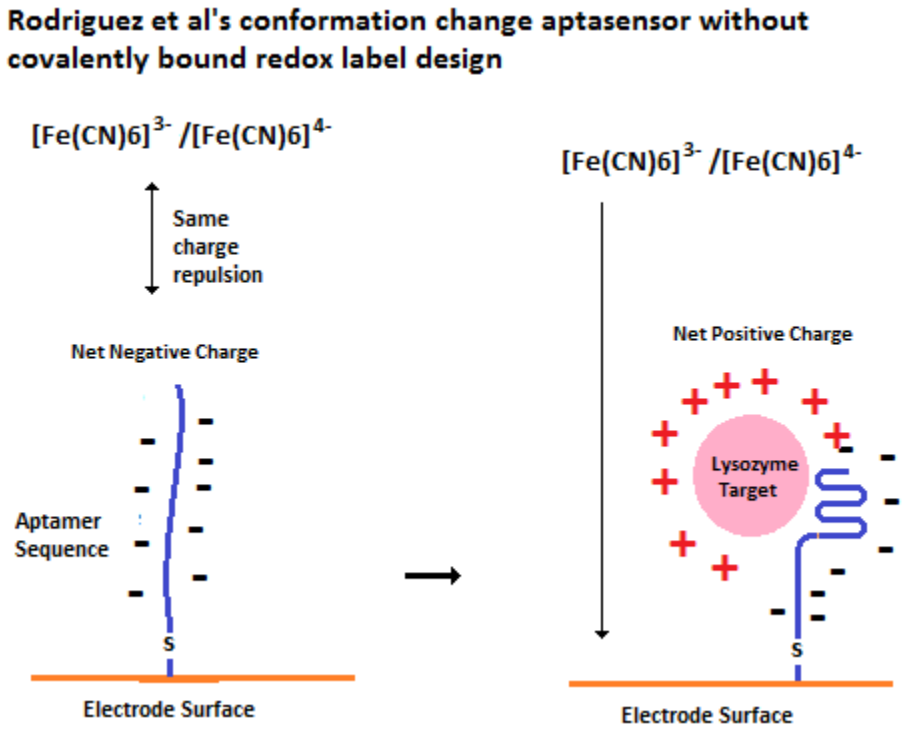

Fig 1.22 Example of conformational-change aptasensor without covalently bound redox label

1.17 Field Biosensor

At present, the primary methods of detection and quantification of trace concentrations of molecular targets, for the purpose such as regulation enforcement, are performed in centralised laboratories with sophisticated instrumentation, such as by HPLC or mass spectrometric techniques. Similarly microbial bioproduct discovery is typically performed at present in a central laboratory setting, typically by some form of spread plate based growth or inhibition assay [81]. Field operation are typically limited to sampling only [82]. Methods such as HPLC and mass spectrometry are highly sensitive and robust, but the former suffer from high initial capital investment, and the latter from labour intensiveness. Both have high operating costs and significant human resource skill requirements. The use of a centralized laboratory approach also potentially prevents, or reduces the accuracy of, detection of analytes which are not amenable to sampling, perhaps due to their short half-life.

A need therefore exists for the development of biosensors capable of operating in a real life setting under field conditions, with minimal requirement for human intervention. While the performance of a biosensor under laboratory conditions is indicative of the sensor's ability to operate under optimal conditions, it is ultimately a very simplistic environment maintained under ideal conditions, and therefore is not wholly indicative of the sensor system's efficacy in field operations.

Ultimately the environmental challenges which will reduce the effectiveness of the biosensor in field application will be defined by the specific environment under which the biosensor must operate, which in turn will be defined by the target of the biosensor. The measures that could be taken to minimize the effects of these challenges will also be defined by the nature of the environment under which the sensor is operating, the target, and the nature of the biosensor itself.

Some of the common potential environmental challenges to electrochemical biosensor operation are listed below:

1.17a Competition

A universal aspect of biosensor design is the specificity of a sensor to its target. Ideally a biosensor should not have high affinity to any species that is outside its targeted range, so that no false positive signal is generated from non-target/sensor interaction.

In practical terms, it is obviously impossible to test the sensor against all potential contaminants present in most environmental samples. However the more closely related and structurally similar the molecules is to the target the greater the chance that it will have high affinity to the biosensor molecule. Thus a negative control tests can be performed using a molecule outside of the targeted range with structural similarities to the target.

Potentially some of the most significant sources of competition are molecules with high ubiquity in the test environment matrix, since their high concentration in the environmental sample will translate into a false positive signal, even if they have modest affinity to target molecule.

1.17b Background noise

Background noise is a signal distortion, usually the result of direct interaction of the cell solution with the electrode surface unrelated to the biosensor molecule, or as a result of non-faradaic current caused by the charged double layer phenomena. The former is caused the presence in the environmental solution of another redox species active within the same potential range as the redox label, resulting in the electrochemical reaction of redox species as a result of the potential ramp. Unlike competitive interference, since there is no formation with label conjugated biosensor at electrode surface, a relatively high concentration of background redox species must be present in order to generate a noticeable peak.

Another major source of background noise is the charging current. This has been extensively discussed in the charged double layer theory section of this chapter (see page 54)

1.17c Degradation of target

Degradation of targets in environmental matrix results in a decreased sensor response to environmental samples as a result of the depletion of target molecules. This can be a significant problem for some targets, particularly proteins which typically have short unrefrigerated half-lives. Small organic molecules and inorganic targets are typically more stable.

1.17d Degradation of sensor

Degradation of sensor molecules in the environmental matrix leads to decreased sensor signal as a result of loss of signaling target-biosensor complexes. For most biosensors this is typically a factor of thermal damage and presence of degradative elements within the environmental sample. In the case of aptamer biosensors the latter is far more significant, due to the thermal stability of polynucleotides and its vulnerability to degradation by nucleases [83][84].

1.17e Fouling of Electrode Surfaces

Fouling of Electrode Surfaces as a result of non-specific accumulation of redox inert species prevents access of electrode surface (and thus biosensor molecules) to the target species. Non-specific adsorption to the electrode surface thus results in a loss of sensor sensitivity [85][86]. Fouling is typically a more significant factor in environmental samples with greater dissolved and suspended particle density than less heavily loaded environmental samples. Fouling is a more significant problem in sensors designed to operate over long periods in environmental samples than sensors designed for relatively brief sampling. Potential solutions to fouling include the use of repellant semi permeable membranes and blocks, which reduce the rate of fouling by repulsion or exclusion of the electrode surface from fouling molecules.

1.18 Optimising Biosensors

While the ability of the sensor to operate in the field could be considered the key objective of this study, an ideal sensor must not only be functional but also meet a need and to do so at a cost and convenience acceptable to the user. While a field biosensor may be able to complete its basic objectives, in practice any biosensor will face competition from alternative methods of detection. In the case of biosensors against novel targets, the desirability increases the lifespan of the sensor technology before a better method of detection is discovered. In the case of biosensors against targets with existing sensors, the novel method of detection must be superior to the existing one at least in a niche function to be of any practical utility.

1.18a Broadening Specificity

This can be approached in one of two ways with regard to an aptamer biosensor. The first is to modify the selection component of the SELEX process in order to favor sequences which bind to multiple targets. This is typically achieved either by alternating the selection target between rounds of SELEX, or by performing selection of second target immediately after selection against the first target within a round of selection. The strength of this approach is that it allows for a single sensing electrode to detect multiple targets, thus increasing economic desirability and simplicity of platform. The weakness of this approach is that it increases the complexity of the Selection process, and thereby diluting the specificity

of the selection protocol, which will possibly result in the final product having greatly reduced affinity to either target compared to a sequence specifically selected against the one.

An alternative approach is to immobilize specific one target sensors on a multi-channel electrode array. Conformational change aptamer are well suited for small volume cells in particular since in low volumes redox label released into bulk solution by configurational change aptamer could result in signal cross talk between electrodes. None of the disadvantages of the above mentioned sensor apply here. Since the sensors are based on multiple specific biosensors in array, broad specificity is not an issue as long as the specific biosensor for the target exist, and since these sensors produce independent signals quantification of specific targets is likewise not impeded.

1.18b Sampling Automation

Another potential avenue of optimization is sampling automation. Like the SELEX device, the most feasible modes of automatic sampling will probably be based on a 3 axis manual-like sampling process or a flow type assay controlled by pump and valve actuators.

Automating the sampling process is desirable as it reduced the degree of human interaction needed to operate the sensor. In LEDC this is beneficial since a pool of skilled labor may not be available or plentiful for widespread biosensor deployment, in MEDC this would be beneficial for economic reasons since it reduces the number of human hours needed for equipment operation. Automating the sensing process also eliminates human error and thus provides a more consistent and reproducible mode of testing.

Chapter 2: Materials and Methodology

2.01 Materials

2.01a Reagent

All reagents used were of analytical grade or better unless otherwise specified.

All bulk chemicals and reagents, including target molecules were purchased from Sigma-Aldrich, VWR or Thermo Fisher Scientific.

Molecular biology reagents were generally purchased from Thermo Fisher Scientific, with the exception of Taq Polymerase which is manufactured by RBC.

18.2 MΩ water derived from Millipore system was used for all experiments unless otherwise specified.

Buffer is flushed through a 0.2mm filter.

2.01b Oligonucleotide Synthesis

All oligonucleotides used in electrochemical aptasensing are synthesized by Genscript, with the exception of the 29bp Thrombin SPE side aptamer which is manufactured by Thermo.

Unless stated otherwise, the 5' ends of all the ordered oligosequences were modified with either thiol group (-SH) or dithiol group attached to hexane (-SS-C_6H_{13}). The 3' end was modified either with an amine group or pre-conjugated ferrocene group.

Early-phase energetic and structural modeling of DNA sequences were performed using Integrated DNA Technology OligoAnalyzer software. The University of Albany mFold software was then used for further analysis and confirmation.

Further analysis regarding aptamer beacon designs are provided in the respective chapters.

2.01c SELEX library

The SELEX library used in the ASM chapter of this study was designed and synthesized by Trilink. The library is composed of 76-bp-long sequences, with the original library being composed of forward

sequences only. The random region of this library is 30-bp long and is flanked with a 23-bp-long forward-primer binding-site complement with the sequence 5′ TAG GGA AGA GAA GGA CAT ATG AT 3′, and a 23-bp-long reverse-primer binding site with the sequence 5′ TTG ACT AGT ACA TGA CCA CTT GA 3′.

Thus, the forward and reverse primers were 5′ TAG GGA AGA GAA GGA CAT ATG AT 3′ and 5′ TCA AGT GGT CAT GTA CTA GTC AA 3′, respectively.

Fig 2.01 Design of the original Trilink Library

The rationale for the selection of this library can be found in the Automated SELEX operation section of this thesis (Chapter 6)

2.01d Equipment

All electrochemical experiments were performed on a Metrohm 910 PSTAT mini potentiostat. Data analysis was performed using proprietary software supplied with the potentiostat, Microsoft Excel spreadsheets, and Graphpad Prism 5 software.

The potentiostat is a compact device and can be powered from a USB cable; this fits well with the sensors' targeted role and allows it to be operated from mobile field units, without access to structural power supply.

2.02 Molecular Biology Techniques

2.02a Manual Polymerase Chain Reaction

Mastermix is composed of DNA template; 1 µM of each primer; 0.5 mM of dNTP; 10x of buffer supplied by the manufacturer of TaqPol (50nM Tris HCl pH9.0, 100mM NaCl, 0.1 mM EDTA, 1% Triton X100, 5mM DTT, 50% Glycerol Stabilisers) and 5 U of TaqPol, which was added last. No additional $MgCl_2$ was added beyond that already present in buffer. The mix was placed on ice until further use.

Heating process involves a 94°C, 2 min long, initial melting step. This is followed by cycles of:

Melting at 94°C for 30s

Annealing at 57°C for 30s

Extending at 72°C for 30s.

The melting temperature was selected for being sufficiently low to prevent boiling, while being sufficiently high to ensure efficient melting of the DNA pool. Annealing temperature was kept deliberately relatively high to prevent formation of large non-specific amplicons. Extending temperature was selected as this is the optimum temperature of Taq polymerase.

30s can be considered a relatively short step duration for annealing and extending parts of the PCR process. However short annealing time is a means of minimizing the formation of large non-specific amplicons in the annealing step. Due to the shortness of the SELEX sequence, is sufficient for the extending step.

Two scales and procedures of manual PCR were carried out, namely, trial PCR and large scale PCR. Trial PCR was performed on a 20-µl scale, while and large scale PCR was typically performed on a 2-ml scale (20 × 100 µl aliquots).

After amplification, 5 µl of the PCR product was extracted for quality control (QC) testing by gel electrophoresis. In the absence of noticeable defects, mass PCR was pooled and subjected to post-processing, typically phenol chloroform extraction, followed by ethanol precipitation.

2.02b Phenol Chloroform Extraction

Phenol Chloroform extraction is performed in order to purify nucleic acids by removing protein and lipid impurities.

Dried mass of DNA was resolubilised with MilliQ water. The same volume of chloroform was then added. The solution was well shaken and then centrifuged at 10000 g for 5 min at 4°C. The upper-phase aqueous phase was then pipetted out and the lower organic phase discarded. This process was repeated three times.

2.02c Ethanol precipitation

Ethanol precipitation is performed in order to purify and concentrate a nucleic acid solution by precipitation of nucleic acid out of solution.

Next, 10% volume of sodium acetate (3M; pH, 5.2) was added to DNA solution, and 2 volumes of ice-cold absolute ethanol was then added to the sample. The sample was incubated for a minimum of 2 hours at -20°C, although overnight incubation is preferable. This was significantly longer than the duration described in most methods, but necessary due to the relatively short length of the DNA sequences investigated. Precipitated DNA was spun down at 10000 g for 30 minutes. Supernatant was then tipped out. The pellet could then be dried under vacuum.

2.02d Gel Electrophoresis

DNA samples were mixed with 6x loading dye at a ratio of 1:5, mixed thoroughly with the pipette and then kept on ice. Next, 3% agarose gel was created by adding 2.1 g of agarose to 70 ml of TAE buffer; 1 µl of ethidium bromide was added to 10 µl per 20 ml agar to allow the sample to be viewed under UV light. This solution was then heated until fully fluid. Agarose was then poured into a tray with a comb set over.

After hardening of the gel, it was submerged in 800-ml TAE buffer on electrophoresis station. Care was taken to ensure that the buffer was barely submerged in the gel and that no bubble was present.

DNA sample and DNA ladder were then loaded. Either a 25-bp or 100-bp ladder can be used for the PCR products, while only the 25-bp can be used for the bioconjugation product. Electrophoresis was performed at a constant voltage of 120 V until the dye moved up a fair distance over the gel. After the completion of electrophoresis, the gel was viewed under UV light.

2.02e ELONA Protocol

ELONA was performed in order to determine the affinity of the selected and amplified DNA pool. Further details regarding the ELONA protocol can be found in section 6.10 of chapter 6.

The library to be analysed is amplified by PCR using biotynalated forward primers. The PCR product is purified by chloroform extraction followed by ethanol precipitation.

The purified library is resuspended and hydrolyzed using Lambda nuclease, resulting in the removal of the unbiotinylated, unselected, reverse sequence. The Lambda nuclease cleaved product is purified again by chloroform extraction followed by ethanol precipitation, after which the mass of the remaining forward library is determined by spectrophotometry using a nanodrop machine.

100ul of 1uM target solution in adsorption buffer (Carbonate/bicarbonate pH 9.6) is added to the ELONA plate per well (100pmole per well). The plate is covered in paraffin film and incubated for 12h at °C. After incubation the wells are washed by adding 100ul volume of wash buffer (PBS 7.4, 137 mM NaCl, 2.7 mM KCl, Tween 0.1%), followed by rinse. The wash is repeated twice.

200ul of 2% BSA solution in adsorption buffer is added to the ELONA plate per well. The plate is incubated for 1h at 25°C. After incubation the wells are washed by adding 200ul volume of wash buffer, followed by rinse. The wash is repeated twice.

100ul of 1nM Forward Biotinylated Aptamers (1nM) in adsorption buffer is added to the ELONA plate per well. The plate is incubated for 1h at 25°C. After incubation the wells are washed by adding 200ul volume of wash buffer, followed by rinse. The wash is repeated twice.

100ul of HRP-Avidin (1ug per ml) in adsorption buffer is added to the ELONA plate per well. The plate is incubated for 1h at 25°C. After incubation the wells are washed by adding 200ul volume of wash buffer, followed by rinse. The wash is repeated twice.

100ul of HRP substrate (TMB and hydrogen peroxide) is added to the wells. This catalytic sensing system is based on the oxidation of TMB catalyzed by HRP in presence of H2O2. The final TMB oxidation product is stable under highly acidic conditions. Therefore after 20 min of incubation 20ul of 2M H_2SO_4 is added, terminating the reaction. Final product is yellow and absorbs at 450nm.

The plate is then analysed using a microplate reader.

2.03 DNA-Label Bioconjugation

2.03a Bioconjugation of ferrocene carboxylic acid to NH2-DNA

This method derived from those of a previous study [87].

This process was only applicable for DNA sequences purchased with amine modification at the 3’ end. DNA sequences purchased pre-conjugated to redox label forego this procedure.

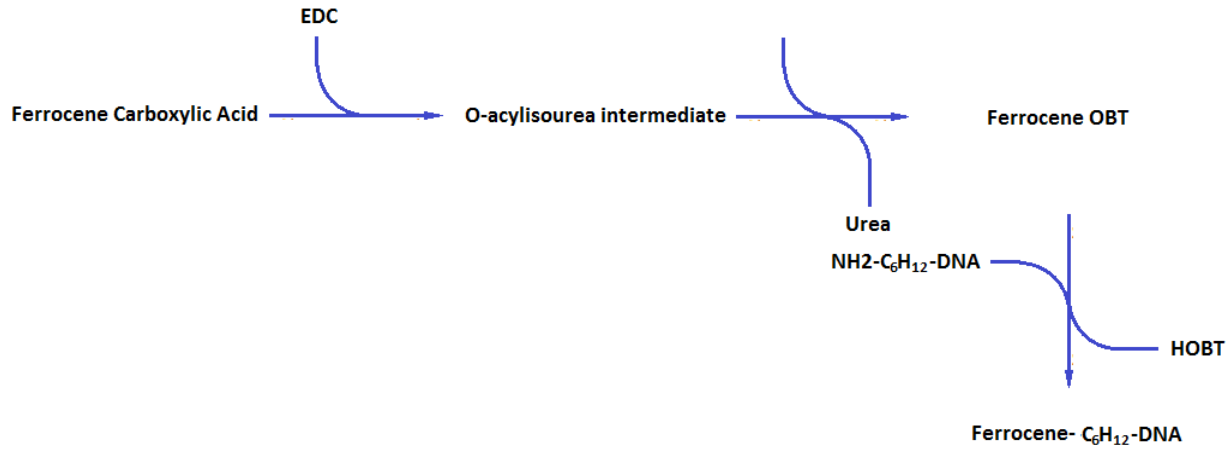

Fig 2.02 Overview of the Bioconjugation of ferrocene carboxylic acid to NH3-DNA

Ferrocene carboxylic acid (5 mmol), Anhydrous *N*-hydroxybenzotriazole (HOBt) (5 mmol) and EDC (10 mmol) 1-Ethyl-3-(3-dimethylaminopropyl)carbodiimide (EDC) (10mmol) was solubilized in 20 ml of dichloromethane, and cooled to 0°C. Aluminium foil was wrapped around the container to prevent photochemical reaction. This mixture was incubated while stirred for 1 hour.

Organic solvent is removed by evaporation with a speedvac vacuum centrifuge, yielding a solid residue of Ferrocene-OBt, Urea and Excess EDC, as well as small amounts of unreacted HOBt and Ferrocene carboxylic acid.

DNA (10 nmol) with NH_2 modification at 3' was solubilized in 0.5 ml of carbonate/bicarbonate buffer (pH 9) and added to an excess solution of Ferrocene-OBt in 0.1 ml tetrahydrofuran. The solution was stirred at 0°C overnight. Condensation reaction between the carboxyl group of the Fc-OBT and the amine group at 3' end of the DNA sequence occurs, resulting in bioconjugation via a amide coupling of the Fcn and DNA molecules and the release of HOBT catalyst. This reaction yields a solution of Fcn-DNA, unreacted Fcn-HOBT, and other reagents of the reaction.

Purification processes were carried out using phenol/chloroform extraction and ethanol precipitation.

No confirmation of stoichiometry was made, though an electrochemical comparison of conjugated and unconjugated aptamer in sensor format could be found on Section 3.07 of the third chapter of this thesis.

2.03b Dialysis

For the final steps of purification, the DNA solution is dialysed using a Harvard Apparatus 1-kDA cutoff Micro Dispodialyzer, capable of receiving sample volumes of 5 µl to 100 µl.

The membrane of the microdialyser is first wetted with MilliQ. A corner of the microdialyser slide is then attached to a floatation device. The slide is then floated on a large beaker filled with copious volumes of the desired buffer. The solution is maintained under constant stirring. The buffer is replaced every 2–3 hours. Typically, 3 changes of buffer take place. This should result in a dilution factor of 10^{11} (assuming 0.1 ml starting volume in dialyser and 1000 ml of buffer).

Concentration of DNA in sample was then analysed using a nanodrop spectrophotometer. The solution was then diluted down to 10 mM. Assuming a typical remaining DNA mass of 4 nmol after bioconjugation and purification, this would require with storage buffer or MilliQ. The DNA is typically then aliquoted into 50-µl tubes for ease of use and stored at -20°C.

2.03c Preparation of MNP-Lysozyme

Next, 10 nmol of lysozyme was solubilized in 0.98 ml of PBS buffer (0.1 M PBS, 0.15 M sodium chloride, pH 7.2). 20 µl of 10 mM sulpho-NHS-SS-biotin is then added to this solution to create a 20-fold excess of biotin according to the manufacturer's recommendations [88].

The mixture was incubated for 30 min. After incubation, excess sulpho-NHS-SS-biotin was removed by buffer dialysis using a method similar to that described above, by using a membrane with a <3000 mW cutoff.

Stock streptavidin-MNP was thoroughly agitated, after which 100 µl of streptavidin MNP was extracted (this should be equal to a 1-mg mass of MNP). The streptavidin-MNP was washed by resolubilising in 1

ml bead buffer (PBS buffer, pH 7.4), followed by precipitation and removal of supernatant. This was repeated twice, after which streptavidin was resuspended in 0.9 ml of bead buffer.

Excess biotin-lysozyme solution (100 µl) was then added to the MNP solution and left to incubate under rotation for 60 min. After incubation, target-MNP was precipitated and washed 3 times using the process described above, followed by resuspension in SELEX buffer. The binding capacity of the streptavidin-MNP was approximately 400 pmol of target for each milligram of the bead, according to the manufacturer's specifications [89].

2.04 Electrodes and Electrode Maintenance

2.04a Gold Disc Working Electrode

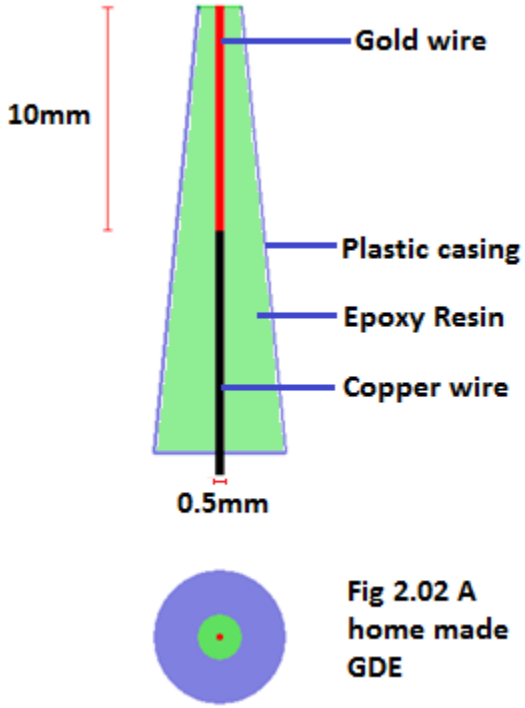

Fig 2.02 A home made GDE

Tempered hard, 99.99% purity Gold wire manufactured by Thermo was use. Typically 25-35mm length of gold wire is used. Gold wire is attached to copper wire with a small droplet of silver epoxy to provide a conductive link between the copper and gold wire. The gold wire is then encased in a mix of Araldite MY750 epoxy and Aradur hardener and heated at 50°C until solid. These will be referred to as 'homemade gold disc electrodes'.

Alternatively gold disc electrodes were purchased from ALS. Electrode is 1.6mm diameter 20mm length, encased in PEEK. Such electrodes are purchased ready for use.

Both encasement materials are of relatively similar hardness to gold, polishing abrades both encasing material and gold wire resulting in exposure of previously unexposed cross section of both material. Encasement material plays no role in electrochemistry, but is necessary in order to increase the structural strength of the electrode as well as making sure the cross sectional area of the gold disc electrode exposed is kept at a constant.

2.04b Electrodes Polishing

Electrode polishing is performed in order to produce a smooth electrode surface, essential for the creation of a uniform layer of self-assembled aptamer molecule through thiol-gold interaction.

The wire is initially cut with a sharp and hard blade, either a medical scalpel or a high grade craft knife. While medical scalpels are stronger and more resistant to breaking, some craft knife are thinner and therefore result in less deformation of electrode surface, while still being sufficiently sharp and robust. For freshly made electrodes, the surface of the electrode is first mechanically polished successively using P1000 and P2000 sand paper, average grain size 18.3 and 10.3 um respectively. The electrode was then thoroughly rinsed with MilliQ and sonicated for 5 min. Electrode must be held completely vertical throughout the polishing process to guarantee smooth surface.

The electrode was then polished successively by 0.1um, 0.3um and 0.05um alumina powder in slurry form, with a 15 min period of sonication between the polishing steps to remove alumina grain from previous polish. Pattern of polishing should resemble a figure of eight to produce a uniform surface. Electrode should be periodically inspected under a light microscope for any signs of surface defects, especially scratches. Electrode should be dry for inspections as scratches are not easy to observe while surface is wet.

In used electrodes, the initial steps of preparation are skipped, as the geometric surface area would already be relatively smooth from previous treatment. Here polishing is performed to remove the immediate gold electrode surface along with any molecules assembled onto it. For this purpose polishing starts directly at the alumina polishing step.

2.04c Electrochemical Cleaning

Electrochemical cleaning was performed in order to remove any residual impurities from the electrode surface via electrochemical oxidation and reduction of the metal.

Electrochemical cleaning is achieved by applying a positive potential of 2V on the electrode for 5s, followed by negative potential of -0.35V for 10s, followed by repeated cyclic voltammetry cycles in 0.5M H_2SO_4, with a scan rate of 50mV/s, scan range -0.3 to 1.55V.

The electrode is then rinsed with large quantities of MilliQ and blown dry with nitrogen. The electrode is typically used for Immobilisation immediately.

2.04d Reference Electrode

Silver/Silver chloride reference electrode were used as reference electrode for all experiments conducted. Reference electrodes are purchased ready made from ALS, electrode is composed of a silver wire coated with a thin layer of silver chloride. This wire is suspended in a solution of KCl, held in a long glass tube with tapering end. Tapered end is sealed with a porous plug which enable interaction between the cell environment and the Ag/AgCl electrode.

Reference electrode is tested periodically against a saturated calomel electrode to determine the quality of AgCl film. This is achieved by placing both reference electrodes in a cell containing a 3M KCl cell solution. Potential across the electrode is determined using a pH meter. 46mV difference is expected, with a tolerable variance of 10mV in both directions.

2.04e Counter Electrode

A counter electrode is either composed of a platinum mesh or platinum wire bonded to copper wire by baked conductive epoxy. Sealant material is electrical insulation tape.

2.04f Dropsens Screen Printed Electrode

The Dropsens SPE was purchased in a finished integrated state containing working, reference and counter electrode on a single slide surface. Electrode are arrange in circular pattern in order to optimize droplet cell deposition. Device is considered single use only. Best droplet cell size is 50ul. Dropsens SPE cannot be electronically cleaned by harsh treatment under 0.5M H_2SO_4, since it is noticed to strip the thin SPE surface.

2.04g Immobilisation of Biosensor Aptamer on Gold Disc Electrode

Stock DNA solution is diluted down to 5uM. 500uM TCEP is added to reduce the thiol group, and the solution is incubated for 60min at RTP. pH9 TE buffer is typically used, composed of 10mM Tris-HCl, 1mM EDTA. Prior to use solution is heated to 70°C for 5 min, in order to melt the DNA and produce a pool of disaggregated DNA molecule.

A polished and freshly electrochemically cleaned gold disc electrode is selected. The electrode is held in a 90-degree vertical position (an empty 200ul pipette tip box is ideal for this application), and a droplet of the 5uM aptamer solution is deposited onto electrode surface using a Gilson's pipette. 20ul has generally been found to be the optimal droplet size for ALS produced gold disc electrodes as this provides ample volume to cover entire electrode surface, without excess volume resulting in wastage, but this volume should be varied to fit the requirements of the specific electrode being used. The electrode is then incubated for at least 12 hours. An eppendorf cap is enclosed over the electrode tip to prevent contamination and retain humidity. Electrode was stored in a dry, dark place to prevent electrode from drying out.

The electrode is rinsed with copious quantities of MilliQ water. Electrode is then incubated with 1mM of butanethiol in absolute ethanol for 30 min. This results in the formation of a self-assembling layer of butanethiol blocker molecules on the electrode surface, bound by thiol-gold interaction. Electrode is then copiously rinsed Ethanol, followed by another rinse with MilliQ water.

2.05 Electrochemistry Methods

2.05a Electrochemical Cell Setup

The sensor electrode is characterized in a 5ml glass electrochemical cell. The electrodes are arranged spatially to allow maximum isolation of reference electrode. Special care is taken to prevent electrodes coming into contact in order to reduce risk of short circuit.

Cell solution is composed of 10mM tris-HCl, 100mM KCl and 5mM $MgCl_2$, pH is adjusted to 7.6 for all electrochemical run. This standard condition has been selected in advance so that electrodes, in particular conformation change aptamer sensor electrodes, can be modeled to operate in the same environment, making multichannel sensing feasible. pH and salt concentration is typical of electrochemical cell conditions for biosensing applications, with salt concentration being sufficient to

prevent effect of ionic migration as a relevant mass transport, while being low enough to allow flexibility in biosensor molecule design.

Mixing was achieved using a magnetic stirring bar, rotated using a magnetic stir plate located underneath the electrochemical cell. Care is taken to ensure stirring bar is arranged in middle of electrochemical cell. Mixing was carried out for approximately 60 seconds at 100rpm per dilution in the titration. Since reaction kinetics could be influenced by effective concentration change as a result of mass transportation by solution convection, electrochemical measurements are not carried out till stir plate has been off for at least 30s.

5ml volume was sufficiently large to reduce the dilution effect of added volumes as a result of titration. Cumulative increase of volume should not exceed 10% of the original cell volume (so 500ul, to 5.5ml).

2.05b Automated Multi-Channel Aptamer Biosensor Protocol (AMCAB)

The aptamer cell was set up in a manner similar to the single electrode electrochemical cell setup described above. However for AMCAB two working electrodes are present in the cell rather than just one. Due to the absence of a multichannel electrode at the time, the measurements were taken sequentially. Immediately after characterization of the first electrode the working electrode lead was detached from the working electrode and attached to the second working electrode, after which an identical scan protocol is run. Feed protocol is implemented using an automatic sampler constructed in house. Protocol is otherwise identical to those of the standard electrochemical setup above.

2.05c Square Wave Voltammetry (SWV)

SWV was performed to the following parameter Start Potential 0V, End Potential 0.7V, Potential Step 0.01V, Step Amplitude 0.05V. Frequency selected was 15 Hz. This gives each run 70 data points. Quiet time is set at 30 sec, measured manually. The scan range was narrowed down based on peak observation of SWV runs to 0.1-0.6V during later experiments.

This common electrochemical protocol was used for both conformation change and ELONA-like assays.

2.05d Soil Sample Preparation

Soil sample was extracted from a garden near the university campus. Spot selected was soft soil near a tree. Sampling point has significant decomposition of plant material, while having significant moisture. Soil was observed to have a distinctly 'earthy' odour, which indicates presence of Geosmin, which can be a product of *Actinomycetales* activity.

Soil was selected in this environment for a number of reason. Firstly these soil conditions are a classical environment for *Actinomycetales* growth. *Actinomycetales* are the mainstay of microbial bioproduct discovery, known for producing diverse secondary metabolites and with well-studied and simple growth conditions which would facilitate integration of bioproduct post-discovery. Secondly, decomposing plant material is a relatively poor nutrient medium, which is the condition under which secondary metabolites (which are non-growth products) are produced.

Soil sample was extracted using a disposable plastic spatula, and stored in a corning tube. Soil sample was added to 100ml MilliQ, and agitated thoroughly. Sample was then divided between 2 corning tube. Target spike then takes place using appropriate target concentration.

Sample was then spun down on a centrifuge briefly, resulting in the large insoluble particles being aggregated at the bottom of the corning tube. Supernatant was extracted, keeping care not to disturb the aggregate at the tube bottom. Supernatant was then filtered through a Millipore HAWP01300 filter.

Sample is mixed with 2x concentration cell buffer for SWV analysis. This gives the soil matrix solution a theoretical soluble soil mass of 10mg/ml.

2.06 Sandwich Type Aptamer Biosensor Methods

2.06a Synthesis of Gold Nanoparticle

Gold nanoparticles were synthesized using the commonly applied Frens [90] method.

50 mg of Gold(III) chloride trihydrate ($HAuCl_4.3H_2O$) was added to 5ml MilliQ water, mixed thoroughly and added to 250 ml boiling MilliQ water stirred using a magnetic bar.

125 mg trisodiumcitrate dihydrate ($C_6H_5Na_3O_7.2H_2O$) was added to 15ml MilliQ water, then added to the boiling mixture.

Once particles of the desired size are formed (based on reference timing, for 10nm gold nanoparticles this typically takes 10 min after the addition of trisodiumcitrate dihydrate), the solution was allowed to cool slowly to room temperature. The final solution should be wine red.

Due to the electrostatic nature of the dispersal mechanism of GNP, a sufficient change in the ionic strength of the dispersing medium or damage to the repelling surface of GNPs could result in the reaggregation of GNP. This results in the formation of large aggregated lumps of GNP at the bottom container. Special care was therefore taken to reduce potential contamination of GNP solution. All glassware were, at the very least, washed thoroughly, rinsed with piranha solution solution (3:1 H_2SO_4 to 30% H_2O_2), followed by thorough wash with MilliQ water. Glassware was then dried at 70°C.

The resulting solution was characterized through UV-Vis spectrophotometry for the purpose of quality control. Physical characterization of the shape and size of the nanoparticles was achieved using transmission electron microscopy.

2.06b Assembly of Aptamer onto Gold Nanoparticle (GNP)

This method was based on a previously described one [91].

Gold nanoparticle is concentrated using a centrifuge and the supernatant removed. The GNP solution was then resolubilised in TETBS buffer composed of 20mM Tris-HCl (pH 7.35), 300 mM of NaCl, 5 mM EDTA, and 0.05% tween 20.

Oligonucleotide was added to the nanoparticle solution to a final concentration of 4 µM thiolated DNA. Since the short 15-bp thrombin aptamer was composed entirely of T and G bases, it had no complementarity, and therefore, pre-heating was not required. The mixture was incubated for 24 h at room temperature in order to produce an ordered self-assembly.

The solution was centrifuged and the supernatant was pipetted out gently in order to remove unbound excess oligonucleotides. The GNP pellet was then washed, followed by at least 2 more cycles of reconcentration and resuspension.

According to data from investigations on the design of aptamer-coated gold nanoparticles, the shelf-life of aptamer-coated GNP should be no less than 2 months when stored under refrigerated conditions.

The resulting Ferrocenated-DNA-enriched GNP is then characterized by UV/Vis for the purpose of quality control. Fc-DNA-enriched GNP should have high peaks at 260 nm (as a result of DNA contribution) as well as 520 nm for particles of approx. nm in diameter. This is in contrast to bare GNP, which should have a high peak only at 520 nm, or supernatant, which has a high peak at 260 only, relative to the Fc-DNA-enriched GNP sample.

Dynamic light scattering was performed in order to determine presence of DNA on GNP surface.

2.06c Assembly of Aptamer to Screen Printed Electrode (SPE)

Immobilisation of the long 29-bp thrombin aptamer onto the SPE surface is carried out using the same protocol as that listed in the conformation-change aptamer section. It is important to note that the SPE should not be electrochemically cleaned, as this has been observed to damage the SPE gold film.

2.06d Indirect Adsorption ELONA-Like Aptamer Biosensor (IAELAB) Protocol

An SPE slide with immobilized long 29-bp thrombin aptamer was selected and placed on a flat surface. The desired titration of the target molecule in the cell buffer (Tris-HCl 7.6, 100 mM KCl, 5 mM $MgCl_2$) was pipetted onto the electrode surface at a volume of 10 µl; this was expected to create a droplet significantly larger than the working electrode, but not expansive enough to cover the reference and counter electrodes. The target was allowed exactly 120 s to immobilize, this should be sufficient to allow specific adsorption of target molecule to electrode surface, while minimising non-specific adsorption. The slide was then tilted to an approximately 20° angle and rinsed thoroughly but very gently with approximately 5 ml of water. It is advised that a 5-ml Gilson's pipette be used, with a drip mode of wash. Unlike ELONA, where the wash was carried out at least three times, the wash process was carried out only once.

The slide was then placed again on a flat surface, and 20 µl of GNP was then pipetted to form a bubble over the working electrode. The GNP was allowed to immobilize for 300 s, after which the slide was tilted and rinsed with 5-ml buffer in the manner described above. The slide was then considered ready for electrochemical analysis processing.

2.06e Direct Adsorption ELONA-Like Aptamer Biosensor (DAELAB) Protocol

DAELAB shares the same protocol as IAELAB described above, except that a clean SPE was used rather than one immobilised with the long 29-bp aptamer.

2.07 Automated Sampling Platform Design and Fabrication

Part of the process of enhancing the applicability of the conformation change aptamer biosensor includes automation of liquid handling via an automatic sampler.

The Type 2 Automated Sampling Platform (T2ASP) was developed from a RepRap 3D printer. The electronics and hardware components of the 3 axis robot was largely retained. The most significant difference between a RepRap and the T2ASP is the replacement of the extruder with a sampling head attached to a syringe pump. The syringe pump was of in-house manufacture.

The device avoids the unstable Y axis as a movement axis completely. Y axis (which has built in coded endstop) is used instead as the syringe pump motor axis. This can be considered a hardware downgrade from earlier two axis sampling model, and significantly reduces the surface available for sampling. However the device is more mechanically stable, has a practical software complexity, and still has sufficient sampling space for the task at hand. Sample tray weight is also less constrained as the sample bed no longer needs to be able to move without excessive shaking.

Electrochemical cell which sits on sampling tray is now also complete static, which should reduce data anomaly caused by spatial rearrangement of cell components. Sampling tray wall also no longer need to be as tall to prevent spilling and thus allow the device z axis faster movements to clear cell tray obstacles.

All plastic structural parts were designed on Solidworks, and converted to Gcode using sprinter software. All plastic structural components excluding timing belt were fabricated by 3D printing, settings are solid external parts with honeycomb interior (for best compromise between strength and weight). The only exception to this is the main lever, which is made of solid print only.

Timing belt is T3 type, same as those used to control RepRap X and Y axis. Stepper motor is a generic NEMA 14 type.

Pumping syringe is a standard U-100 insulin syringe. This was chosen partly due to relatively standard size of such syringe and their ubiquity. The sampler is not expected to carry large volumes of liquid for the multichannel sensor tests (50-150ul being most likely estimate), thus there is no need for a syringe pump with large volumes. Also since the volume pumped is translated from linear timing belt movement, the smaller the syringe volume/length ratio the finer the pump resolution controlled by Gcode. A relatively small volume also means reduced friction on the sampler (Y-axis) motor.

The primary weakness of the insulin syringe is relative lack of durability. This is understandable, since insulin syringes are strictly one use by original design. In practice, the syringe pumps are generally replaced after every 2-3 multichannel tests. Insulin syringes are cheap enough to be replaced frequently without excessive cost. Replacing insulin syringes at frequent intervals can also be considered to be a benefit as it reduces cross contamination as a result of retainment of residue between experiments, an important design aspect in automatic samplers.

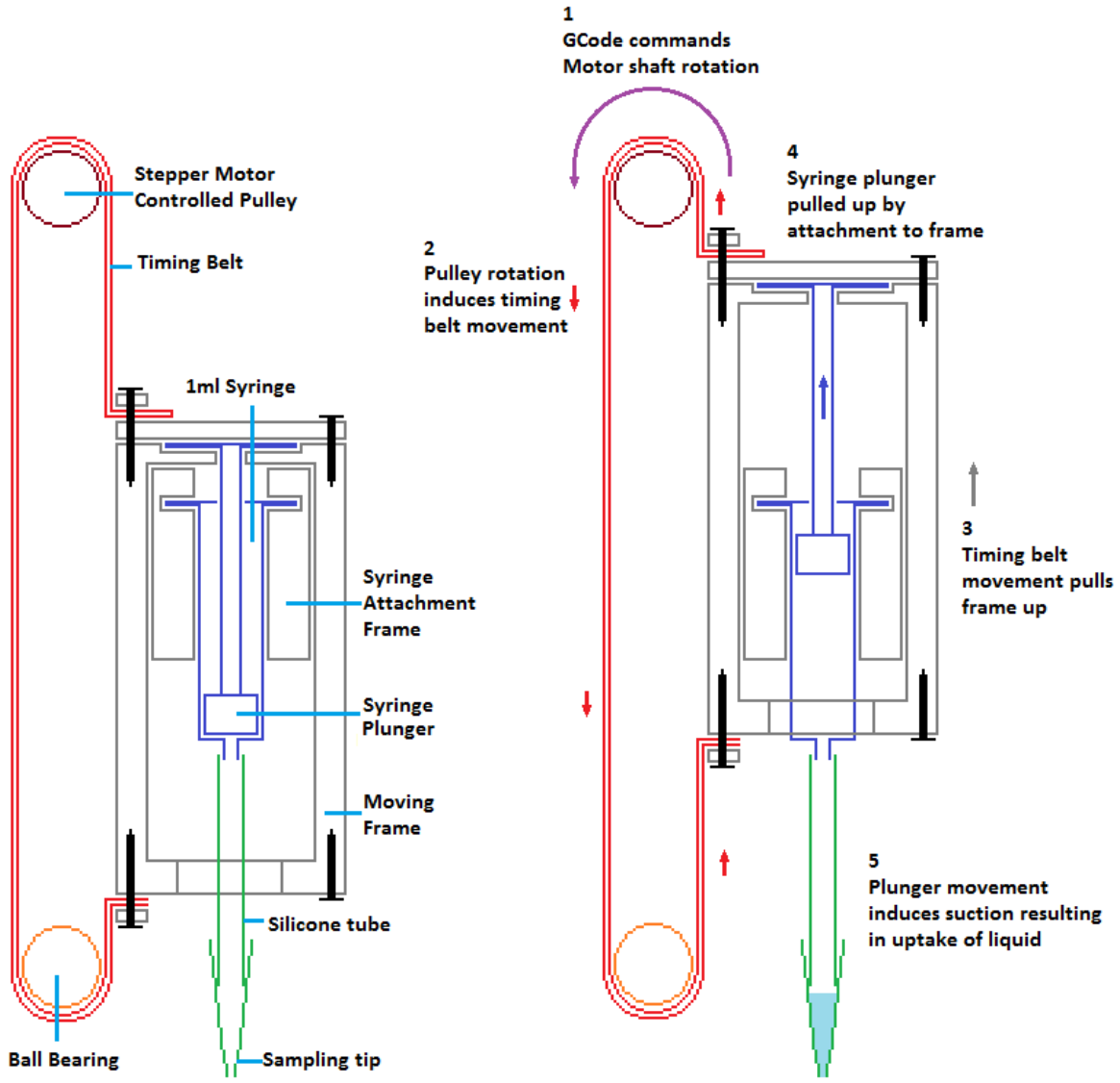

Fig 2.03 A depiction of the mechanism of the syringe pump used in the T2ASP. Command is issued in GCode format resulting in motor shaft rotation, which pulls the syringe pump connected to the timing-belt attached moving frame forwards or backwards. This results in suction, leading to liquid uptake.

10ml HPLC syringe were also considered. This would have had a significant advantage over the 1ml insulin syringe in terms of both accuracy and durability, but was ultimately rejected as the friction of the syringe exceeded the power of the stepper motor even at slow speed. Also the increase in weight caused by a more powerful motor needed to drive this new syringe (in addition to the considerable weight increase of the syringe itself) may decrease the accuracy of the X axis movement whose weight now considerably exceed the extruder head of the original Reprap design.

Sampling head is composed of friction bonded 200ul pipette tip and CNC milled PTFE connector modelled around the dimensions of a 200ul Gilson's pipette. This ensures a snug fit between the connector head and the pipette tip. 200ul pipette tip is sufficiently small to allow easy entry into smaller sampling wells, and its small aperture should reduce liquid loss in transportation process.

PTFE is a relatively low friction material, so stretched paraffin film is typically wrapped around the sampling head to prevent slippages and seal any potential air gaps. The connector head is connected to silicone tubing by elastic bonding via an overlapping segment of PTFE tubing (which in turn has been bonded into the connector head by a compression joint). Silicone tubing is connected to the syringe by elastic bonding to the syringe nozzle.

PTFE tubing was considered as a replacement for the silicone tubing. PTFE has the benefit of being a much lower friction material than silicone, potentially greatly reducing contaminant retainment. However PTFE is also a much less flexible material than silicone, which would result in considerably decreased flexibility of head placement, as well as increasing tube length, leading to an increased internal volume of the pumping system, decreasing suction. Pumping volume was expected to be between 50-150 ul, so sampled liquid is never expected to enter the connector head or tube in any case. Both material could be autoclaved prior to experiment, guaranteeing sterility at experiment start. The entire sampling head assembly (minus the paraffin film) could be sterilized via autoclave. This together with the insulin needle which are sold pre-sterilised, means that the entire fluid pathway of the sampler could be assembled from a sterile state.

Chapter 3: Conformation Change Aptasensors

3.01 Introduction

This part of the thesis describes the development of a second generation affinity biosensor based on the conformational change of single strand nucleic acid aptamers upon target-binding. Conformation Change Aptasensors (CCA) depend on the spatial rearrangement of the nucleic acid strand as a consequence of a target-aptamer binding interaction. This is in contrast to first generation configurational change aptamer biosensors which depends on the displacement of (typically label containing) sequence.

Signal generation is the result of a change in the distance between label and electrode surface as a result of this spatial rearrangement, and can be either higher or lower than the initial (target free) signal. Positive signal change, typically referred to as a "signal on" system, can be considered an analogue of a "normally off (NO)" switch and results from the bound state bringing the label closer to the sensing surface. Negative signal change, typically referred to as a "signal off" system can be considered an analogue of a "normally connected (NC)" switch and results from the bound state taking the label further from the sensing surface (the beacon designs described below would be a good example of this).

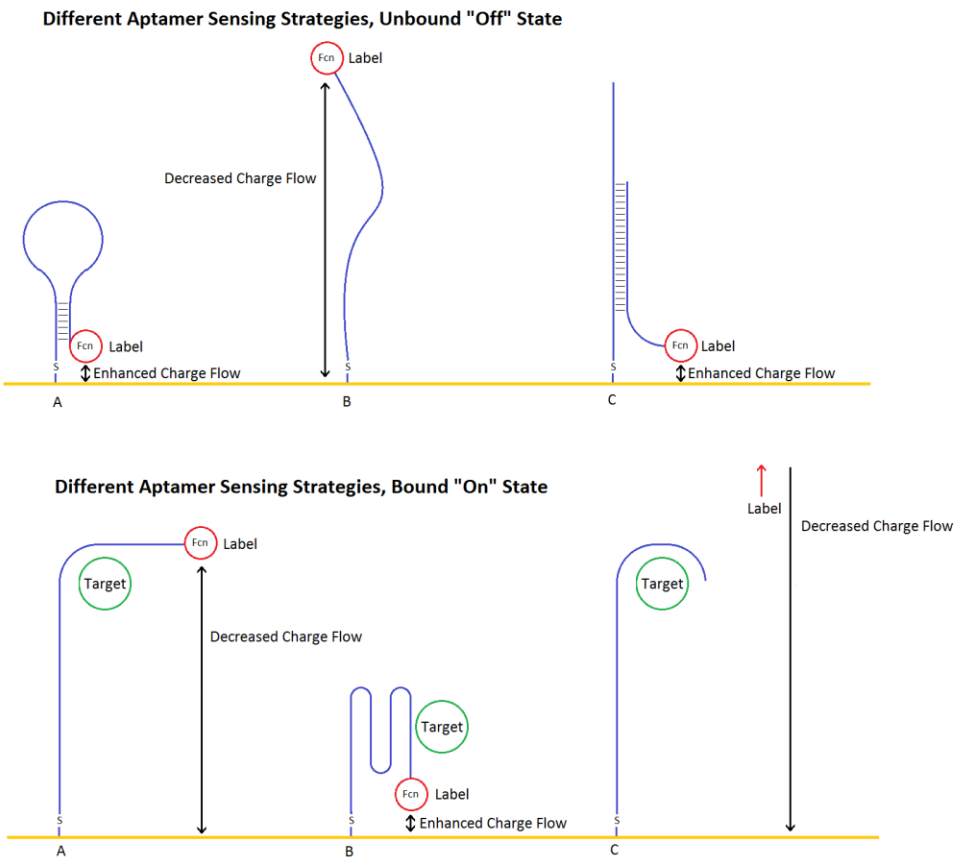

Fig 3.01 Overview of CCA Sensing Strategy. A) represents a typical beacon type “signal off” electrochemical biosensor. B) represents a sensor with a “signal on” format. C) Represents a typical configurational change aptamer sensor.

3.02 Advantages and Disadvantages of CCA

Much of the competitive advantages of second-generation aptamer sensors can be linked to their relatively greater temperature tolerance as compared to the first generation (configurational change) aptamer sensors

By attaching the redox probe to the same DNA strand as the sensing sequence, the sensing surface can be regenerated by thermal denaturation, followed by reannealing. The first generation structures are composed of hydrogen bond bound probe and sensing sequences which result in dissociation of the two hybridized structure upon heating. This represents a significant disadvantage in real-world application, since configuration change aptamer biosensors therefore may not be able to operate at all in hot

environments. This is unlikely to be a relevant issue with centralized laboratory based diagnostics, but could be a significant weakness in a sensor designed for field application.

Thermal stability also significantly benefits the reusability of the conformation change sensor. It is possible to regenerate CCA by simple heating, as the single nucleotide strand would simply return to stable secondary structures after heating. Configurational change aptamers biosensors will require, at the very least, a replacement of the unbound sequence in order to renew the sensing surface, while most protein based antibodies will permanently lose viability after extensive heating, since post translational tertiary and quaternary structures needed for sensing may not be the most energetically stable configuration, or barriers may exist preventing reformation (see section 1.06, chapter 1)

The most significant weaknesses of the CCA biosensor design is the limited distance in which the target-aptamer binding event can displace the label. Since conformational change aptamers typically have the label located on a complementary strand, the displacement of the label containing strand results in the loss of the label to the bulk solution. In the case of CCA biosensors, the displacement of the label is limited by the length of the nucleic acid strand. Thus displacement remains within molecular distance of the sensing surface. Since charge transfer is a distance dependent phenomena, the difference between target-bound signal and resting signal of CCA is likely to be relatively small compared to those of first generation aptamers.

Another weakness of the CCA vis-à-vis configuration change systems is the difficulty in designing the former. Nucleic acid-nucleic acid interaction has been well investigated, and many relatively robust modeling tools exist for the determination of nucleic acid secondary structures. In fact, it is possible to calculate the most energetically stable resting states of the nucleic acid stem loops (and therefore the location of the label in the resting state relative to the sensing surface) with a fair degree of certainty. Thus resting signal can be predicted at least qualitatively (in a “high” or “low” sense). Molecular beacons rely on this principle to create a stable background signal.

However, the current state of knowledge of molecular physics does not allow the interaction between nucleic acid aptamers and other molecules to be modelled easily or with any degree of accuracy. This issue is exacerbated by the sheer range of targets of nucleic acid aptamers, which range from ionic salts, to large globular proteins, and virus particles. As such it is impossible to predict the “on” state of an aptamers-target interaction without resources far beyond the scope of this work (if it is possible with the current state of technology at all). This problem can be ameliorated to some degree by having a very

stable resting state. This is where the equilibrium of resting state greatly favours a single energetically highly stable form, which either brings the label very close to, or very far away from, the sensing surface. This makes it statistically unlikely the bound state will result in a form that is respectively even closer to or even further from the sensing surface, resulting in the bound state current decreasing in the former and increasing in the latter case. This is the underlying strategy of molecular beacon sensors which will be discussed below.

3.03 Model for Surface Binding

In this work, it was initially hypothesized that the aptamer-target-binding event occurs as a two molecule binding process. At condition of equilibrium the thermodynamic value of the target-aptamer complex could be estimated from the designated target titration.

When using this model, several assumptions need to be made:

1) It is assumed that the gold electrode does not influence target-aptamer interaction, and that this is a largely two molecule process.
2) Concentration of target at the electrode surface is the same as that in the bulk solution.

Thus based on the above assumptions, the influence of the surface does not affect target sensing (and thus behaves like a constant), and there is no further signal changes after the formation of the target-aptamer complex. In this design aptamers are immobilized on the electrode surface. Therefore fractional occupancy of surface-bound aptamer (f) is directly related to target concentration at electrode surface. According to 2) the target concentration at the electrode surface is proportionally influenced by the concentration of the target at the bulk solution. Thus titration of the target solution into the electrochemical cell results in a correlating increase in f, which can be represented as follows:

$$f = \frac{[ST]}{[S0]}$$

Eq 3.01 Fractional Occupancy of Aptasensor

[ST] representing target bound aptamers

[S0] representing net aptamer concentration at electrode surface.

In this electrochemical analysis, change in the bound state could be determined through the observation of change in peak current. Thus, peak current measurements could be used in order to determine the fractional occupancy of surface-bound aptamer.

$$f = \frac{i - i0}{isat - i0}$$

i is peak current

i_0 is background peak current (i in absence of target)

i_{sat} is the peak current at point of titration where the curve plateaus.

Thus:

$(i - i_0)$ represents peak signal at investigated point [ST],

$(i_{sat}-i_0)$ represents total signal of aptamers present at electrode surface [S0]

The dissociation constant (Kd) can be expressed as follows:

$$Kd = \frac{[S][T]}{[ST]}$$

Eq 3.02 Expression of Dissociation Constant

[S] is unbound aptamer density

[T] is Target Concentration

[ST] is target bound aptamer density

Unbound aptamer density is the total mass of aptamer not in a bound state:

$$[S] = [S0 - ST]$$

Thus:

$$Kd = \frac{[S0 - ST][T]}{[ST]}$$

Fractional occupancy can be described as a function of dissociation:

$$\frac{1}{f} = \frac{[S0]}{[ST]}$$

Thus:

$$Kd = \left(\frac{1}{f} - 1\right)T$$

The equation can also be re-arranged to include mass balance constraint. Net aptamer mass at the electrode surface can be described as the sum of bound and unbound aptamers.

$$[S0][A] = [S][A] + [ST][A]$$

[A] represents the electrode surface area

Net mass of target can likewise be represented by the sum of the mass of aptamer bound target and the mass of target in the bulk solution.

$$[T0][V] = [T][V] + [ST][A]$$

[V] represents the volume of the bulk solution

By rearranging this equation, target concentration can be represented as:

$$T = [T0] - \frac{A}{V}[S0]f$$

Thus, Kd can be rearranged as follows:

$$Kd = \left(\frac{1}{f} - 1\right)\left([T0] - \frac{A}{V}[S0]f\right)$$

Under the abovementioned assumptions, A, V and [S0] remain constant throughout the experiment, and thus can be represented as a constant:

$$Kd = \left(\frac{1}{f} - 1\right)([T0] - [Ka]f)$$

Eq 3.03 Expression of surface binding

In practical terms, *f* could be calculated directly from the current peak provided by square wave voltammograms. The Kd can then be derived from the fit.

3.04 Molecular beacons

The molecular beacon is a sensing molecule that relies on a hairpin structure. A nucleic acid hairpin is composed of two components, a single-stranded loop and a double-stranded duplex stem. This secondary structure is commonly seen in single-stranded nucleic acids as a result of self-hybridization at the strand terminus. The self-hybridized form is designed to be energetically stable, resulting in a resting configuration which greatly favors the hairpin. Target-binding results in the opening of this hairpin, resulting in the "on" state. While some of the ss DNA of the "on" state could potentially be adsorbed onto the electrode surface, statistically the majority of the label would be displaced further than its location in the unbound state. In practical terms for electrochemical aptamers this means that the resting state of beacon-based sensors will have a higher current relative to the target bound state.

In many ways, the aptamers beacon is the logical extension of a typical sensing-strand/complimentary strand type configurational change aptamers. Here the complementary strand has simply been attached to the end of the sensing strand.

Molecular beacons originated as optically labeled nucleic acids modified by a fluorophor and quencher at the 3' and 5' terminus [92]. This mechanism is initiated by the donor group being excited by a fluorophore and then relaxing into its lowest excited state by Kasha's rule. The presence of the quencher in close proximity results in efficient non-radiative decay of the excited state. Formation of a hairpin loop result in the fluorophore and quencher couple being in van der Waal's contact to enable efficient quenching. This results in reduced luminescence. Formation of a target-aptamer complex results in the beacon "opening up", resulting in greater spatial distance between the fluorophore and quencher, resulting in luminescence. Fluorophore-Quencher couples are highly sensitive to separation distance. Thus even small changes to the spatial arrangement of the molecular beacon could result in significant changes in luminescence.

For example the original DNA molecular beacon developed by Tyagi et al [92] would result in the backbone of the complementing nucleic sequences being located at a distance of <1 angstroms from each other in the closed configuration. In the open configuration, the maximum distance between the termini would be the length of each nucleotide multiplied by the number of nucleotide. While it is almost certain the ssDNA will form secondary structures, which will decrease distance due to increased arrangement density of the nucleotide sequence relative to the linear sequence, the distance between the quencher-fluorophore couple is greater in the open than in the closed form.

For practical purposes, the design of aptamer molecular beacon takes into consideration a number of factors:

1) The sequence targeted by the complementary sequence must also bind target. Otherwise target-binding may not result in displacement of the complementary sequence.
2) Complementary sequence must have significant affinity to its matching sequence. Overall the hairpin should be significantly more thermally stable than other resting forms.
3) For obvious reasons the complementary sequence must not have a higher affinity to its matching sequence on the aptamers than the target molecule. Otherwise the target will not be able to displace the complementary sequence at all.
4) The hairpin should not have significant affinity to any other sequences in the nucleic acid strand, especially one close to the matching sequence on the aptamer. Otherwise the displaced complementary sequence will simply bind to this site, resulting in minimal signal change.
5) For obvious reason the added segment must not result in a loss of overall sequence affinity to target. However due to the difficulty in modelling target-nucleotide sequence interaction discussed above, the effect of added sequence on target affinity may not be discernable without practical experimentation.

One of the essential divergence in the design of aptamer molecular beacons and conventional molecular beacons used as complementation probes is in the position of the target-binding sequences. For the molecular beacon the target complementary region is typically located within the loop of the single-stranded hairpin secondary structure [92][93][94]. Binding of the target sequence to the molecular beacon results in the linearization of the molecular beacon-target sequence duplex as a result of Crick-Watson interaction, thus resulting in a separation of the fluorophore-quencher couple. In aptamer molecular beacons, the target-aptamer interactions cannot be reliably modeled. Therefore target-binding to a sequence located at the loop may not result in the dissociation of the stem structure of the hairpin, resulting in no separation of the 3’ and 5’ terminus. Thus the complementary sequence binding region should be the same region predicted to bind to the target molecule [95] [96], so that the target-aptamer binding event would result in the displacement of the complementary sequence, resulting in the dissociation of the stem of the hairpin structure.

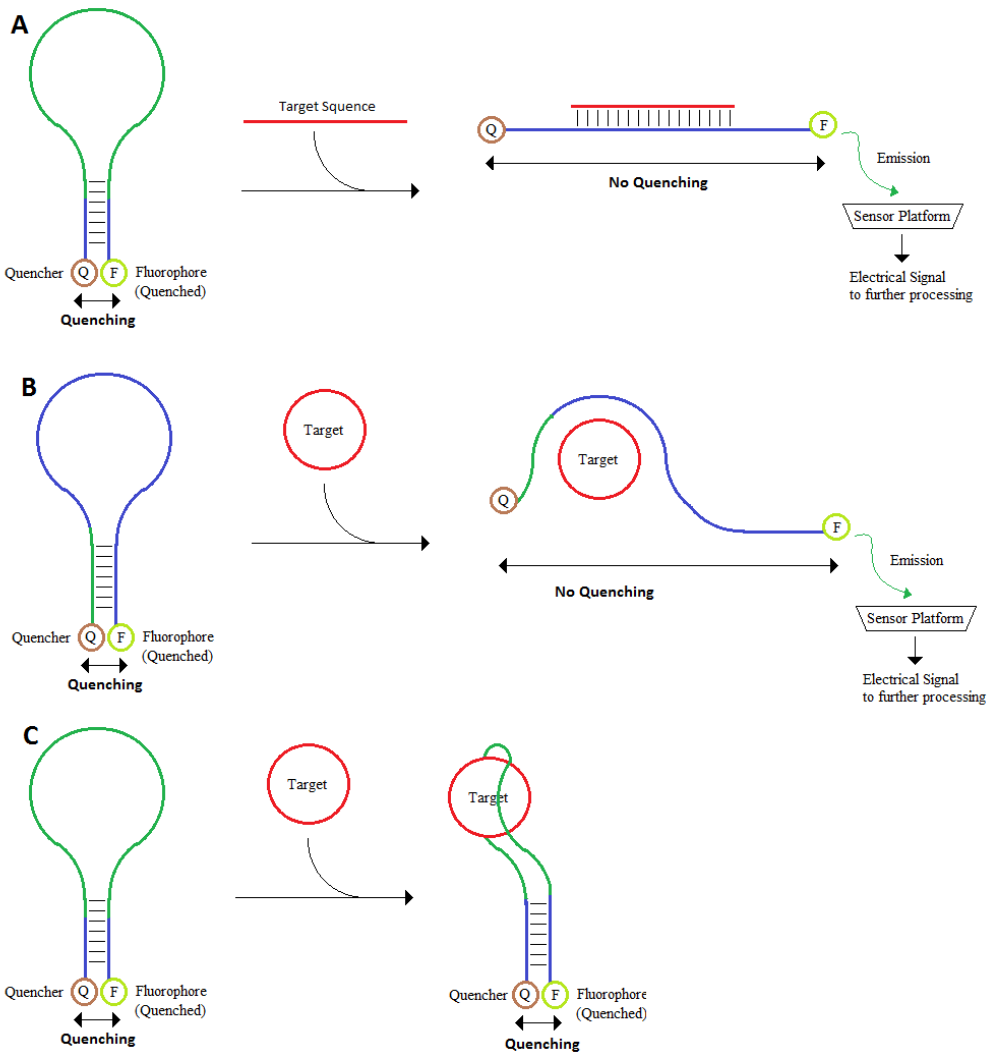

Fig 3.02 Comparison of the design aspects of conventional molecular beacon and aptamer beacons. Green represents target-binding sequence. A) Represents a well-designed molecular beacon, with target-binding event resulting in the linearization of the molecular beacon B) Represents a well designed aptamer beacon, with target-binding resulting in disaggregation of the hairpin stem C) Represents a badly designed aptamer beacon, with target-binding event failing to disaggregate the hairpin stem, resulting in no signal change.

3.05 Titration against Spiked Environmental Sample

3.05a Objectives of Sampling in Environmental Matrices

The final goal of this study is to develop, as far as possible, a viable aptamer sensor for the detection of designated targets for real-world use. The nature of the environment in which this biosensor would be used will dictated largely by the target molecules of the biosensor developed under controlled laboratory conditions. A number of criteria were used in this selection process:

1) Sensor reliability. How reproducible and reliable the sensor is under controlled conditions. Ideally there should be a single dominant electrode variation, which responds predictably to target titration.
2) Sensor signal strength. The magnitude of the sensor signal. This is likely to be particularly important in environmental samples since, unlike under controlled conditions, environmental samples can potentially contain solute substances which are electrochemically active within the applicable scan range which may result in significantly increased noise.
3) Detection limit of the sensor. Ideally (in order to have potential real world significance) the developed sensor should have a detection limit better than, or at least comparable to, conventional techniques of similar complexity. Should the sensor not have a competitive detection limit compared to presently available conventional techniques, the sensor should be sufficient for a specific commonly needed task.
4) Sensor dynamic range. A large dynamic range is desirable as it will potentially allow the sensor to not only determine the presence of target molecule, but also to quantify concentration of target molecules present.

3.05b Selection of Targeted Environment

Based on target potential and preliminary results of controlled environment experiments, the two sensors selected for use in further study were kanamycin aptamer and tetracycline aptamer.

One of the benefits of selecting kanamycin and tetracycline is that it is reasonable, from a practical/real world viewpoint, to have both biosensing tips on the same sensor array. While being structurally very different and having different mechanistic targets, Kanamycin and Tetracycline have very similar practical functions, since both are characterized as broad spectrum antibiotics.

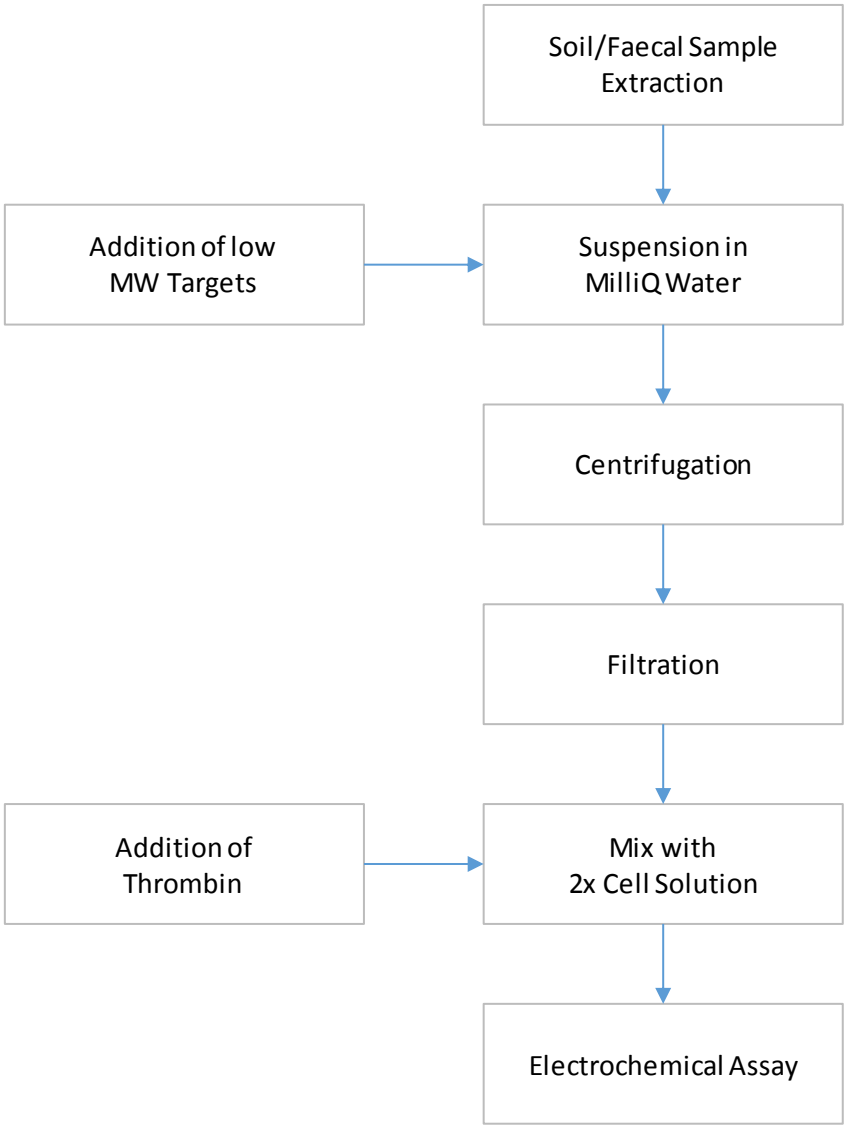

Fig 3.03 Flow chart displaying the treatment process of environmental samples

The conventional microbial product discovery process discovers products based on function rather than chemical properties. Most antibiotic selection assays involve observation of growth inhibition of a target organism on spread plates [81][97]. These tests are empirical in nature, yielding very little theoretical information about the secondary metabolite being produced by the organism beyond the fact that it can inhibit the target species. Thus having an array of biosensors specific to the products of similar function in the context of microbial product discovery fits well with current doctrine. Both secondary metabolites

are also originally the product of *Actinomycaetales* extracted from soil (similar to the vast majority of the current catalogue of secondary metabolites), which gives us an ideal matrix for environmental sampling.

Another potential area of interest for broad spectrum antibiotic sensing would be in the detection of antibiotic residues in agriculture. Antibiotics are used in livestock agriculture to increase feed conversion ratio [98] and to prevent spread of contagion among herds. Unlike in medicine where narrow spectrum antibiotics are employed for most purposes, agriculture tends to use broader spectrum antibiotics. Both aminoglycosides and polyketide antibiotics have been used in agriculture in this context [99].

Use of antibiotics for food animals are heavily regulated in most if not all More Economically Developed Countries (MEDC). Drug withdrawal periods are legally mandatory to prevent transfer of residual antibiotics to humans [100], which can result in problems such as antibiotic resistance and allergic reactions [101]. Thus there is a potential real world context for a biosensor capable of the detection of broad spectrum antibiotics in agricultural effluence. Effluence from livestock would be an ideal matrix for investigation, poultry faeces was selected since it is most easily accessed.

The base environmental matrix was extracted locally. 5 g of soil or 2g of faeces were added to 100ml of MilliQ water. The solution was thoroughly agitated. Secondary metabolite target spike was then solubilized at the concentration desired. The solution was spun down briefly to eliminate the largest insoluble particles. The solution was then extracted, while avoiding the precipitate as much as possible. The solution was then filtered through a Millipore HAWP01300 filter. The filters may need to be replaced several times due to clogging by particles not eliminated by centrifugation. The sample was then mixed with 2x buffer solution at the same concentration. Analyte spike was then applied at desired concentration. Samples were then considered ready for use in assay.

This protocol was designed specifically such that it can be feasibly carried out in the field. Filtration could be performed using a syringe through a filtration cassette. A number of portable centrifuges are commercially available powered by car battery. All reagents could be pre-autoclaved and stored for long periods without refrigeration.

It was strongly considered that instead of mixing the environmental sample with a 2x buffer to make a 50% environment solution, it may be better to add the buffer in a solid state directly into the environmental solution. This would allow the usage of a 100% environmental matrix, automatically

increasing the sensitivity of the aptamer biosensor by two fold. However to mix a buffer with the environment matrix would require a pH meter for pH adjustment and an alkaline solution, not a convenient thing to do in the field. Since the aim of this study is to produce a sensor capable of convenient field operation, this factor must be given considerable weight.

3.06 Kanamycin Sensing with a Ferrocene Modified Aptamer

The aptamer sequence around which the aptamer electrochemical biosensor is designed was previously published by Song et al. [102]. Kd of the aptamer was determined by Song et al's publication to be 78.8 nM by colorimetric analysis using 5' fluorescein amidite modification. The detection limit was determined to be 25nM by using GNP based colorimetric method. The sequence was also determined to have significant affinity to closely related aminoglycoside tobramycin (Kd 103nM).

In the original publication the sequence was hypothesized to have a beacon like structure based on mFold calculation (see section 3.07 of this chapter, page 104). After having confirmed that this is also the case under the conditions used in this study, by using mFold [103][104] and idtdna's OligoAnalyzer[105], the sequence was selected for use as biosensory receptor without further sequential modification.

Published Sequence:

5'-TGGGGGTTGAGGCTAAGCCGA-3'

The sequence selected was adapted for electrochemical conformational sensing by the addition of a C6 mixed disulphide group at the 5' end terminus of the sequence and a ferrocenyl modified base at the 3' end.

Finalised Biosensor Sequence:

5’- C_6H_{13}-S-S-TGGGGGTTGAGGCTAAGCCGA-Fcn-3’

3.07 Kanamycin Aptasensor Titration against Target Molecule

The finalised biosensor sequence was immobilized on planar gold electrode by thiol-gold interaction. Investigation of a target titration by SWV shows significant correlation between signal magnitude to target concentration. The titration plot profile is highly typical of a conventional binding curve, with the signal drop correlating to target concentration at lower concentrations before plateauing at high concentration as the sensing surface is saturated with target molecules at high concentrations.

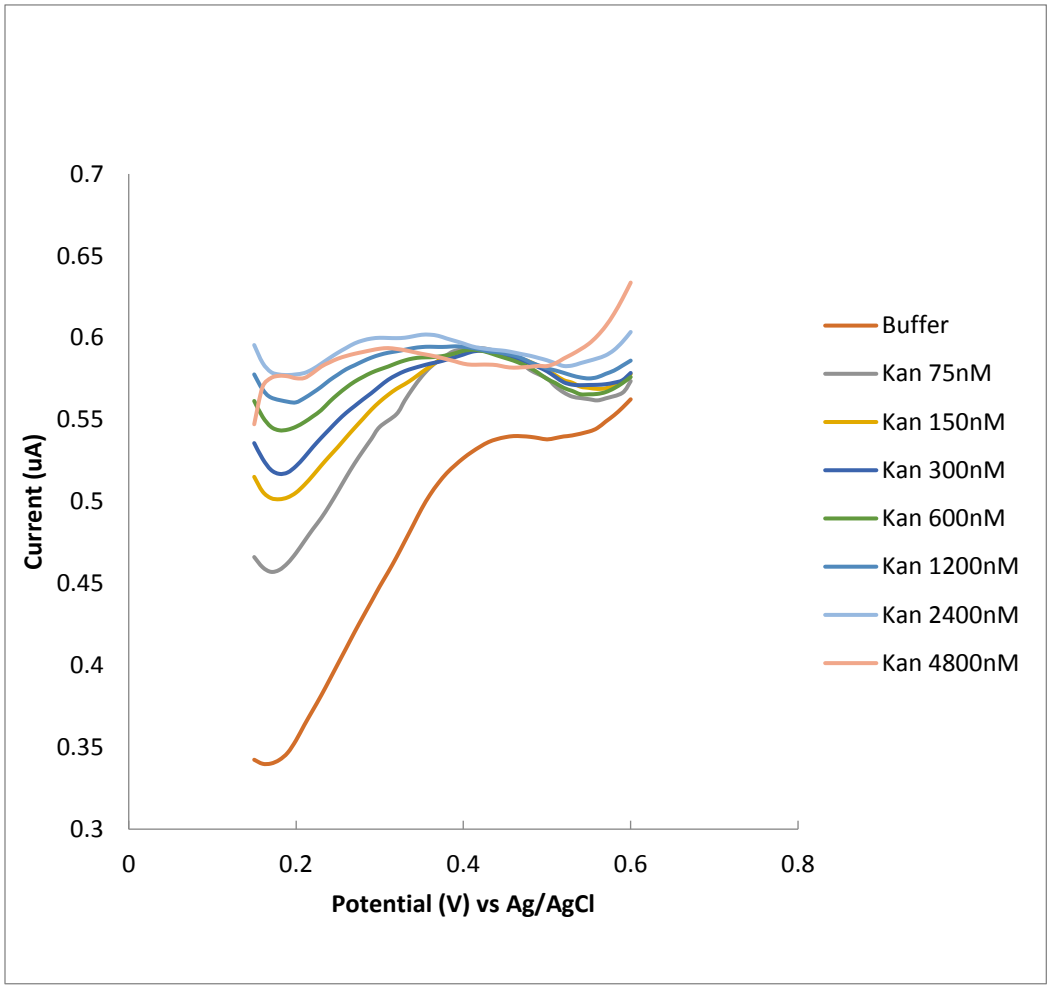

Fig 3.04 SWV of kanamycin fcn-aptamer biosensor’s response to kanamycin titration vs Ag/AgCl, performed in clean buffer

All the SW Voltammograms display a significant baseline slope and this was corrected for by linear interpolation between the minima either side of the voltammetric peak. The peak current is the maximum magnitude of difference between the SW voltammogram and the interpolated slope between the minima.

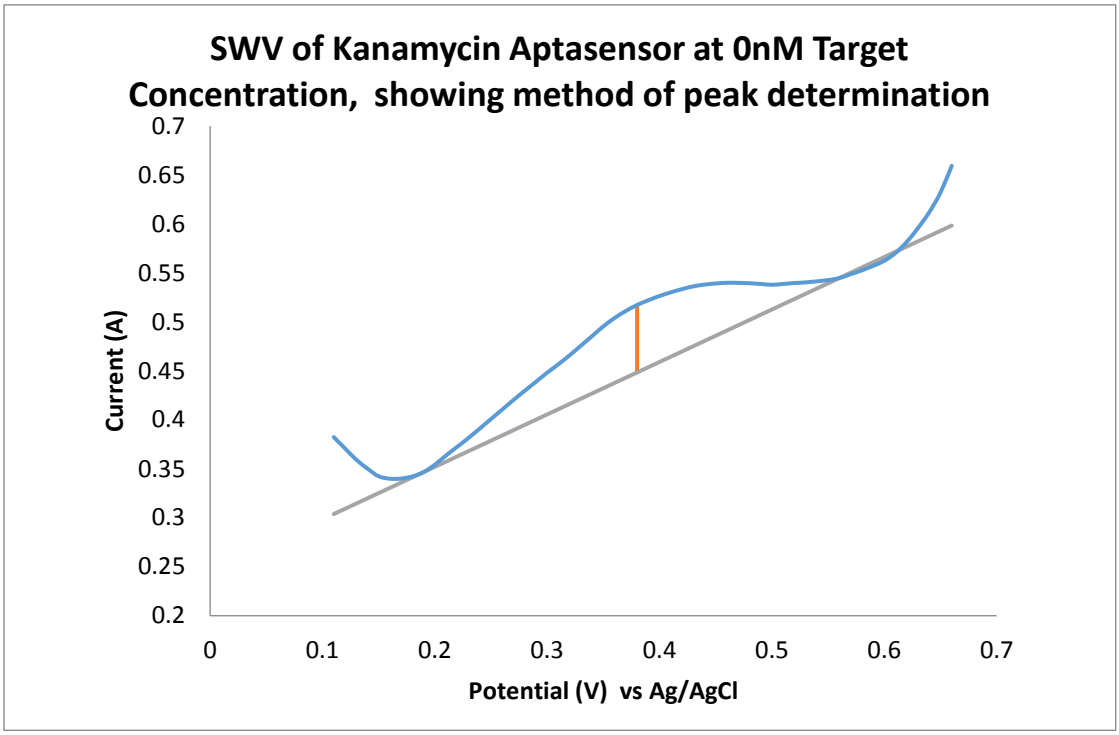

Fig 3.05 An example of peak current calculation by slope subtraction (the voltammogram is that of the buffer concentration from the titration series shown above). Blue represents the voltammogram, green represent the interpolated slope and red represents the magnitude of difference at point of greatest difference between the voltammogram and the slope.

Using the aforementioned method, peak current response from the titration could be derived.

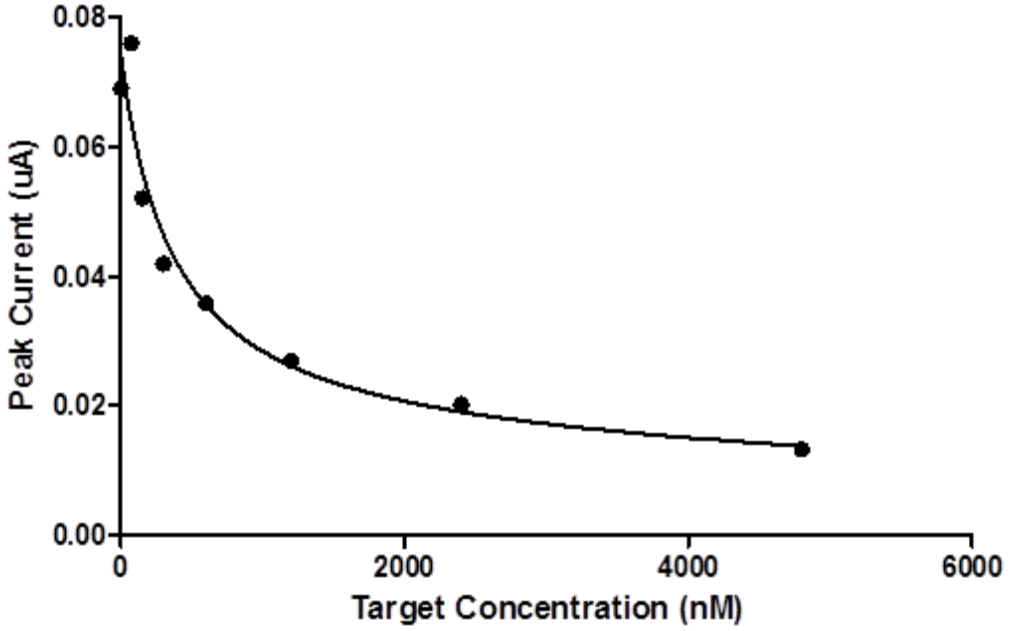

Fig 3.06 SWV derived peak current response of kanamycin Fcn-aptamer biosensor to kanamycin titration vs Ag/AgCl, performed in clean buffer

Fitting the peak currents as a function of the target molecule concentration by using a Langmuir-type fitting as discussed in the introduction section of this chapter (see page 93) yields an average Kd of 565.8 +/-232.5 nM, which is significantly higher than the literature Kd of 78.8 nM. This could be attributed to a number of factors. One of most common causes of Kd variation between experimental sets is change in experimental conditions, however it must be noted that in this particular case the method utilized to obtain Kd in the original publication by Song et al publication is similar to those utilized in this experiment (binding buffer used was composed of 20 mM Tris–HCl, 50 mM NaCl, 5 mM KCl, and 5 mM $MgCl_2$, pH 8.0, electrochemical cell solution utilized here is 10 mM Tris–HCl, 100 mM KCl, and 5 mM $MgCl_2$, pH 7.6). The main difference between this study and the original publication is that the aptamer here is immobilized on a planar gold electrode surface which may potentially interfere with target binding.

The structural and energetic modelling by the mFold software could be used to explain the change in current amplitude of the target-bound and unbound states. Based on Mfold, the majority of the kanamycin biosensor molecules exist in three stable states under electrochemical assay conditions. Form A and C greatly resembles a classical molecular beacon type hairpin. Form A has two 2 base self-

annealing segments in close proximity near the terminus of the strand and Form C has a 2 base self-annealing segment and a 3 base self-annealing segment in close proximity. dG for Form A is -7.8kJ/mol and a melting point of 41.7°C. dG for Form C is -6 kJ/mol with a melting point of 38.6 C. Form B has minimal self-annealing, with random placement of the ferrocenated terminus relative to the electrode surface. dG for Form B is -7.2 kJ/mol and melting point is 47.3°C.

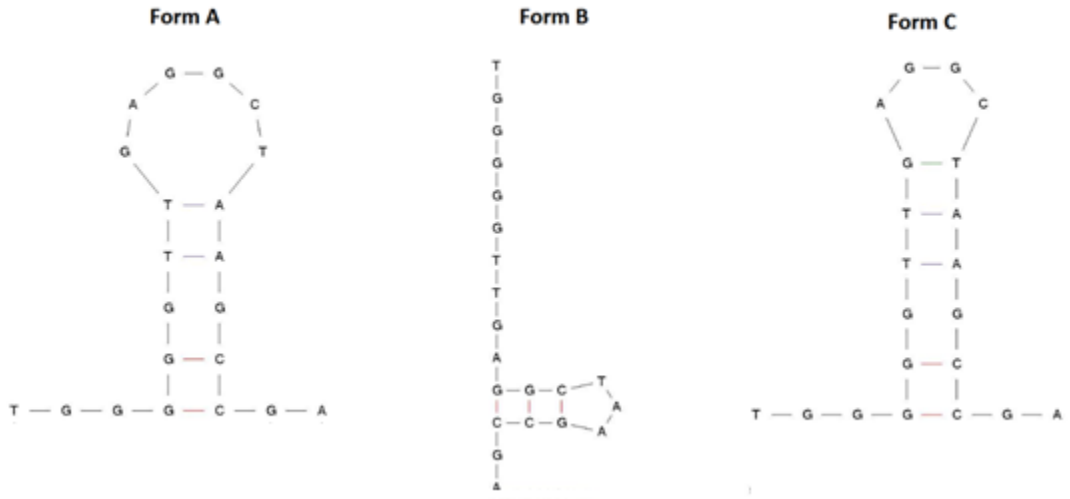

Fig 3.07 Structural diagram of the most energetically stable self-binding conformations of Kanamycin biosensor molecule as calculated using the mFold model, Form A being the most and Form C being the least stable. Modeling parameters: Temperature 25°C, Salt concentration 100mM NaCl, 5mM $MgCl_2$

It should be noted that the original Song et al paper [102] determined the melting point of this aptamer to be 71°C. Again however this could be attributed to differences in the conditions between the experiments described in this thesis and those of Song et al's. Since Song et al's melting point is determined by empirical methods based on relatively robust UV/Vis spectrometry, this difference could perhaps be attributed to the inherent inaccuracy due to the relative simplicity of mFold's mathematical model.

Based on the model, it is likely that the biosensor at the resting state would exist in equilibrium composed largely of the three stable forms (due to the relatively similar thermal stability of the forms, especially form A and B). The result would be that part of the population (composed of those in the form A and C configuration) would express strong electrochemical signal (label located close to the electrode surface, and therefore more charge transfer) while some part of the population (composed of those in form B configuration) would express a weak electrochemical signal (label located far from electrode

surface, resulting in less electron transfer). The signal direction of the bound state would depend largely on the conformation of the target-aptamer complex, with a configuration that results in spatial arrangement of the label closer to the electrode resulting in a positive signal trend (as form A and C sensor molecules are converted to a form more similar to form B), and a configuration that results in spatial arrangement of the label further from the electrode resulting in a negative signal trend (as form B molecules are converted to a form similar to A and C)

Energetically the model supports the hypothesis that the target-aptamer complex displaces the self-annealing segment of the target unbound bioreceptor molecule. The most energetically stable secondary structure calculated by mFold (Form A) has a dG = -1.86 kcal/mol or -7.8 kJ/mol

Kd of Kanamycin to this aptamer is 78.8nM based on the original publication.

Therefore using the Gibbs free energy equation [106]:

$$dG = RT\ln(Kd)$$

Eq 3.04 Gibbs free energy equation

The dG for the target-aptamer complex is -39.8 kJ/mol, which is more thermodynamically stable than the most stable resting self-dimer.

In total nine independent titrations were performed under simple matrix clean buffer conditions with separate sensors in each case. The results of these replicate titrations can be found in Appendix A (page 267). In all cases the quantitative behavior followed the same pattern, with the current falling in correlation with an increase in kanamycin concentration. However sensor to sensor variation meant that the Kd values varied from a K_{max} of 955.9 nM to a K_{min} of 291.3 nM. R squared was calculated to be greater than 0.9 in all cases, and in all but three of the titration the r squared was calculated to be greater than 0.98.

Based on the results of the target titrations, the detection limit of this sensor is at least as low as 120 nM (many 75nM results in this set show decreased signal response compared to the remaining titration data points). This compares very favorably with conventional antibiotic productivity selection based on observation of zones of growth inhibition. Growth inhibition typically involves observation of areas of clearance on a spread plate around areas of applied antibiotic. Thus detection limit of such method is directly influenced by the toxic dose the secondary metabolite to plated microbes. Since toxic dose of

kanamycin to target organism is equal to or greater than 103 nM [107][108] sensitivity of this sensor is comparable to the most optimistic detection limit of conventional detection methods.

3.08 Kanamycin Aptasensor Titration against Target molecule in Environmental Matrix

3.08a Kanamycin Aptasensor Titration against Target Molecule in Environmental Matrix, Soil Sample Matrix

Nucleases are ubiquitous in any natural environment. Much of sterile techniques developed for nucleic acid molecular biology are developed partly in response to the effect of sample degradation by nucleases as a result of contamination of sample. It was initially expected that in any environmental sample there might be signal loss over time due to nuclease activity. This was tested by preparing a soil sample as described in introduction section of this chapter (see 100). Therefore the assay protocol was conducted by SWV immediately after electrode was placed into electrolyte solution, and the experiment carried out promptly. Assay time typically takes less than 15 min, which was expected to keep nuclease influence on sensor response to a minimum.

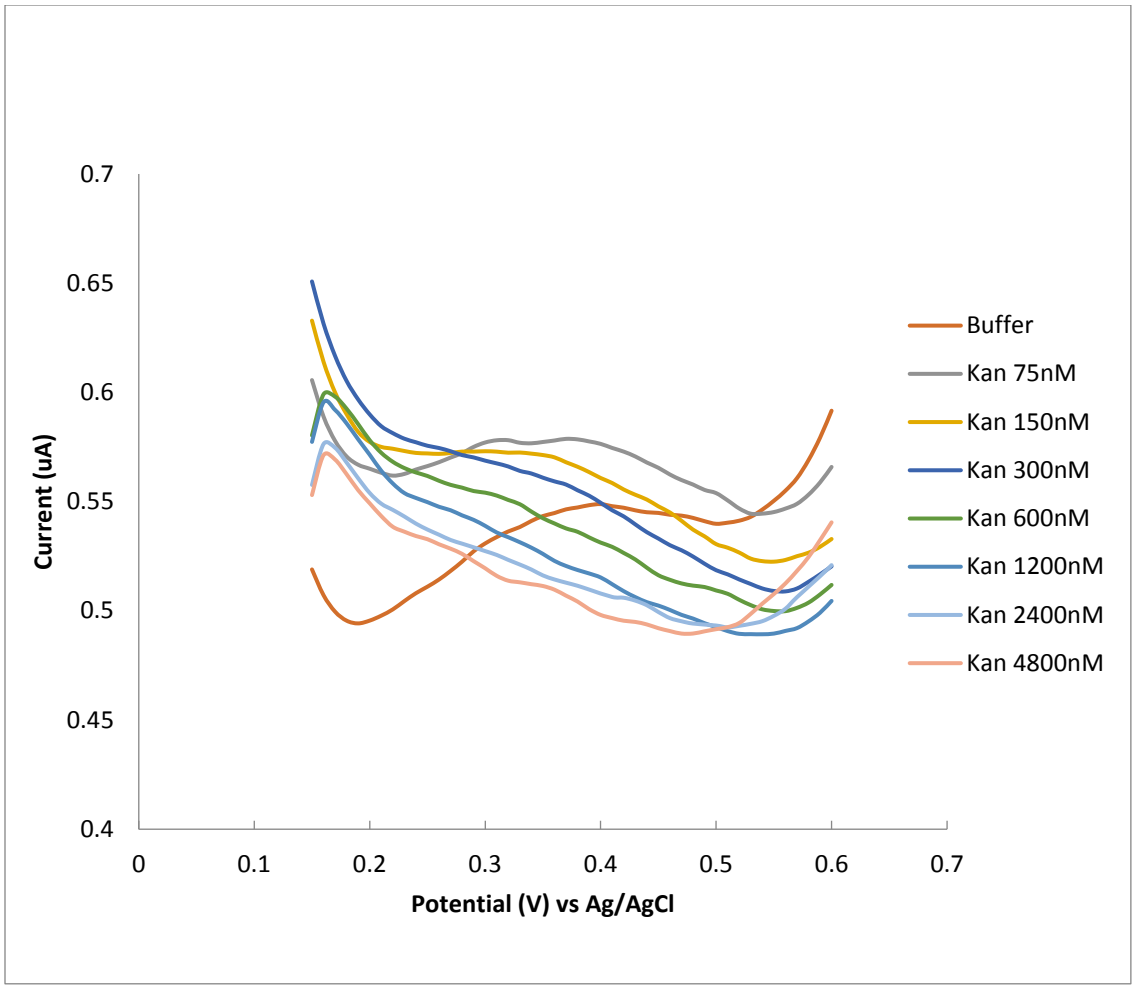

Fig 3.08 SWV of kanamycin fcn-aptamer biosensor's response to kanamycin titration vs Ag/AgCl, performed in soil sample matrix

The titration curve trend under these conditions show minimal difference in comparison to that obtained for the assay performed under clean buffer conditions. Investigation of a target titration under environmental matrix enriched the cell solution by SWV shows significant correlation between signal magnitudes to target concentration. Similar to an assay under clean buffer conditions, the titration plot profile is typical of a conventional Langmuir-type fitting (a signal drop followed by a plateauing at high concentration).

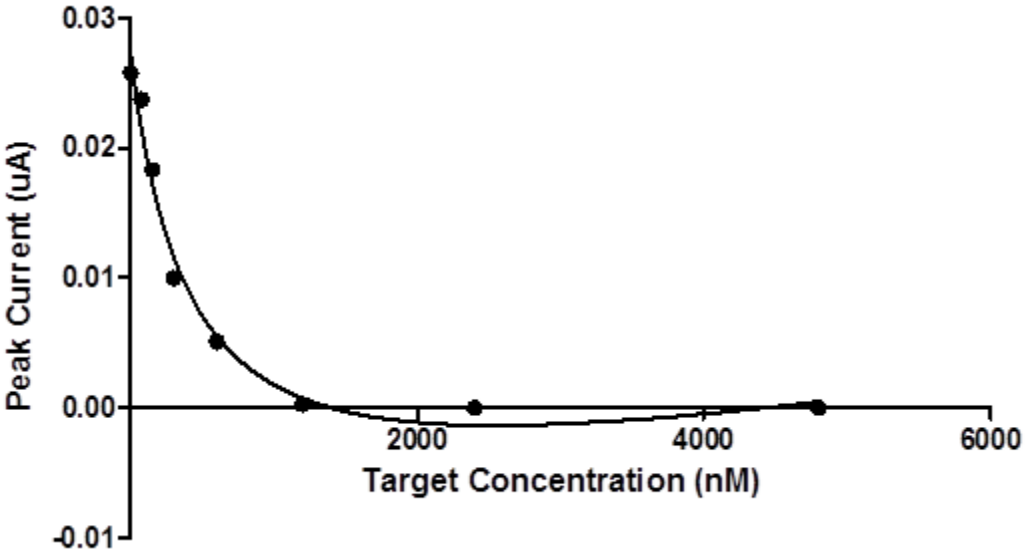

Fig 3.09 SWV derived peak current response of kanamycin Fcn-aptamer biosensor to kanamycin titration vs Ag/AgCl, performed in soil sample matrix

Based on the results of the target titrations, the detection limit of this sensor is at least 75 nM (this would suggest the 75nM data point with reduced signal on a number of clean buffer condition experiments are anomalous). This is equivalent to a 150 nM, or 72.6 ng/ul, prior to the addition of 2x cell buffer solution. Since the total mass of soil mixed with liquid was 5g, this translates to a detection limit of at least 1.452 ug/gram of soil, assuming complete solubilisation of soil based Kanamycin upon mixing with water.

In total three independent titrations were performed in soil environmental matrix buffer conditions with separate sensors in each case. The results of these replicate titrations can be found in Appendix B (page 276). In all cases the quantitative behavior followed the same pattern, with the current falling in correlation with an increase in kanamycin concentration.

Fitting the peak currents as a function of target molecule concentration using a Langmuir-type fitting yields an average Kd of 356.2 nM which compares closely to the results of the clean buffer samples described previously (average Kd of 565.8 nM), and to a lesser extent the literature Kd of 78.8 nM. That being said the trend of this result may be skewed by one of the two results having a Kd of only 108nM, the lowest Kd data for this sensor. As the Langmuir fit for that curve is less has an r squared value of less than 0.98 (though only marginally so, the r squared here is 0.979) it is quite likely the Kd may be skewed by the lack of signal at higher concentrations (3 signals for this curve was not measurable).

The measured Kd values reflect the affinity of the aptamer rather than total mass of label bearing biosensory molecules on the electrode surface. Hence the latter can be more accurately judged from the signal intensity rather than Kd. The magnitude of the buffer signal (average 21nA) was significantly reduced compared to that observed in the experiment performed under standard titration protocol with clean buffer (average 56nA). The difference was not as significant as initially expected, and does not appear to affect titration profile. To confirm that the signal reduction is caused by formation of target-aptamer complex and not nuclease activity, an assay was performed under the same conditions, with exception of a 2 hour incubation period in the environmental matrix enriched cell solution prior to experimentation. This is at least 800% greater than the time lag of the last concentration under the protocol without wait time.

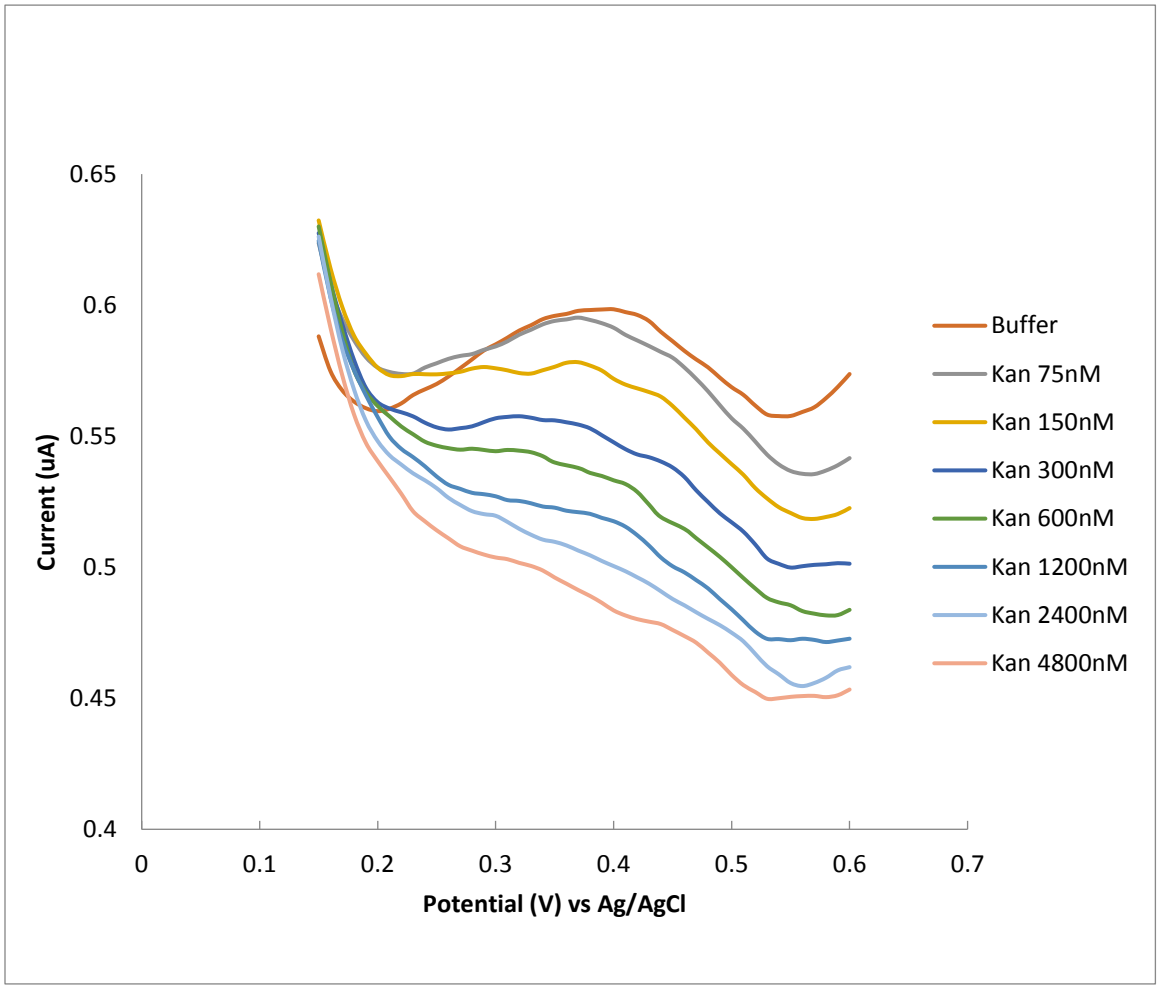

Fig 3.10 SWV of kanamycin fcn-aptamer biosensor's response to kanamycin titration vs Ag/AgCl, performed in soil sample matrix following a 2h incubation

In total two independent titrations were performed in soil environmental matrix buffer conditions following a 2h incubation period, with separate sensors being used in each case. The results of these replicate titrations can be found in Appendix B (page 276).

The results again show a profile very similar to that obtained for the titration under clean buffer conditions, with titration plot profile being typical of a conventional binding curve. Kd is 429.3 nM and 423.7nM. Average peak amplitude at buffer is 35nA which is in fact higher than the average of the soil matrix results without the lag (21 nA), but lower than the results of the clean buffer condition titrations (55 nA). This is probably the result of simple batch variation (the clean buffer conditions test, which has the largest sample population, has a signal amplitude outlier ranging from 83.8nA to 22.6nA).

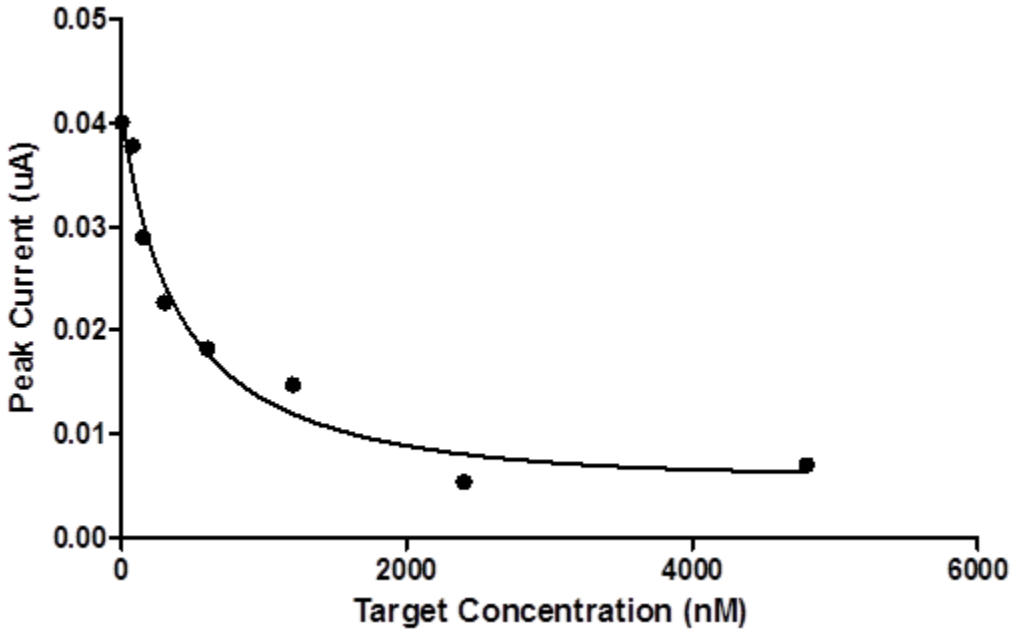

Fig 3.11 SWV derived peak current response of kanamycin Fcn-aptamer biosensor to kanamycin titration vs Ag/AgCl, performed in soil sample matrix following a 2h incubation

The magnitude of the peak signal after 2 hours under the environmental matrix enriched cell solution would indicate that the effect of nuclease degradation does not appreciably impact on performance. While the peak size was lower than that obtained for clean buffer condition, signal loss is not to a

degree that renders the sensor unworkable since the signal loss as a result of soil matrix conditions is significantly less than the signal decrease as a result of titration of target molecules. The lack of a signal loss in the incubated series of electrodes would support a conclusion that there is minimal loss of signal as a result of nuclease activity or other soil based interferences.

There are a number of potential causes for the small effect of soil in the test sample. Perhaps the most likely reason is due to the pretreatment protocol which includes filtration through a Millipore HAWP01300 filter. The ability of nitrocellulose to adsorb protein is well known [109] [110], and is a core principle of western blotting [111]. This property was exploited by Tuerk and Gold's pioneering publication [21] as a means of separation of protein target bound DNA from unbound sequences.

There is also the possibility that the immobilization of the biosensor molecule to the electrode surface results in reduced susceptibility to, for example, nuclease activity. It is hypothesized that at least some nuclease activity depends in part on access of the binding site to target molecule in specific alignment [112]. Immobilization to electrode surface may restrict this access of the nucleic acid sequence to nuclease due to its proximity to a solid surface. This effect may be exacerbated by the shortness of the nucleic acid sequence, further reducing the length of nucleotide which can be affected by nuclease activity.

3.08b Kanamycin Aptasensor Titration against Target Molecule in Environmental Matrix, Chicken Faeces Matrix

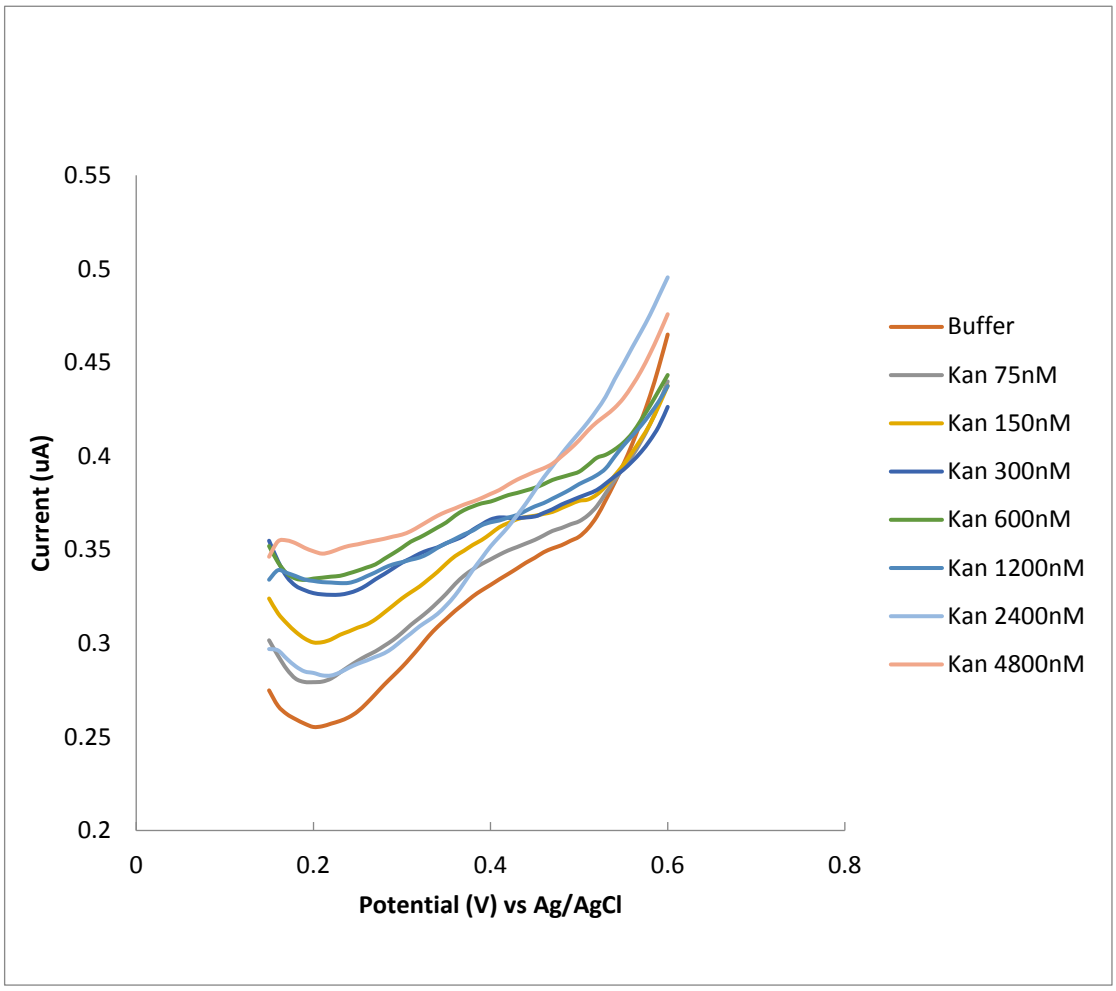

Fig 3.12 SWV of kanamycin fcn-aptamer biosensor's response to kanamycin titration vs Ag/AgCl, performedin faecal sample matrix

The titration curve is similar in overall shape to the titration curve obtained with clean buffer conditions titration and those of the soil sample assays. Investigation of the target titration under chicken faeces matrix enriched cell solution by SWV shows significant correlation between signal magnitude to target concentration. Similar to both previously assayed types, the titration plot profile is typically of a conventional binding curve (a signal drop followed by a plateauing at high concentration).

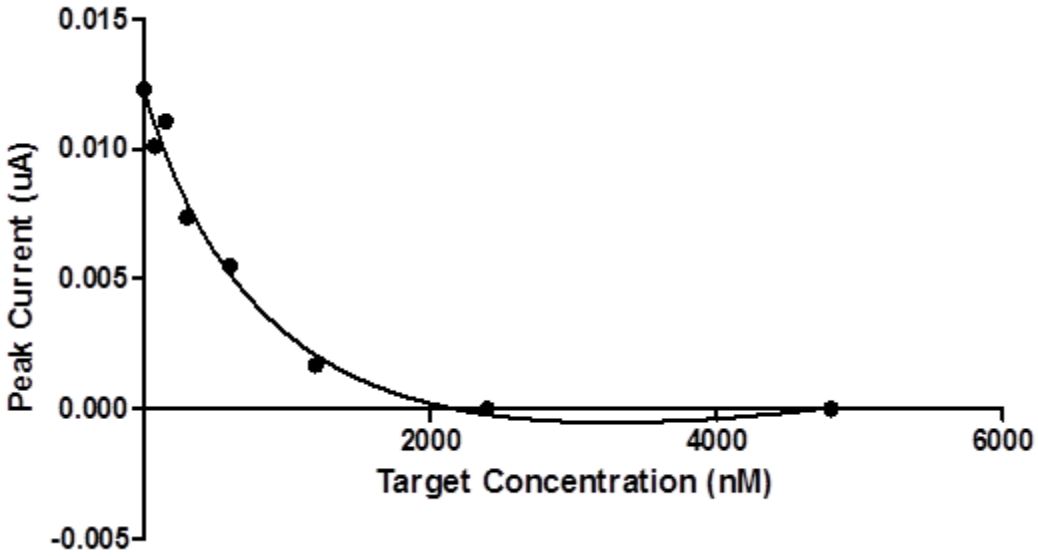

Fig 3.13 SWV derived peak current response of kanamycin Fcn-aptamer biosensor to kanamycin titration vs Ag/AgCl, performed in faecal sample matrix

According to the results of the target titrations, the detection limit of this sensor was at least 75 nM (this would support the previously proposed suggestion that the 75nM data point with reduced signal on a number of clean buffer condition experiments are outliers not representative of general signal trend). This is equivalent to a 150 nM, or 72.6 ng/ul, prior to the addition of 2x cell buffer solution. Since the total mass of chicken faeces mixed with liquid was 2g, this translates to a detection limit of at least 3.6 ug/gram of chicken faeces, assuming complete solubilisation. This is actually much more likely than in the case of soil, since the chicken faeces is dissolved much more easily than the soil sample, leaving much fewer residue visible to naked eye after significant agitation.

In total three independent titrations were performed in faecal environmental matrix buffer conditions with separate sensors in each case. The results of these replicate titrations can be found in Appendix B (page 276). In all cases the quantitative behavior followed the same pattern, with the current falling in correlation with an increase in kanamycin concentration.

Plotting the peak currents of target molecule response signals into the abovementioned mathematical models yields a Kd of 1238nM and 818 nM, with one titration indicating large standard error on the Kd value and poor r squared fit to the Langmuir binding model (the former being too wide to be calculated

by the Graphpad Prism software, and the latter being 0.89 respectively). All titration plot fits the Langmuir equation (fitted using model 2) to an r squared of at least 0.98 with the exception of the ambiguous curve mentioned above.

It was noticed that this Kd is significantly higher than those obtained for either the clean buffer or the Soil matrix conditions (which have an average Kd of 566nM and 356nM respectively). There are a number of potential causes for this:

1) The kannamycin target is being removed from the system by the chicken faeces matrix. One reason is that the kannamycin target is being destroyed by the chicken faeces matrix directly. It is reasonable to assume chicken faeces would contain a significant number of chicken gut flora bacteria and their products. Antibiotic resistance would be a significant advantage to a chicken gut bacteria, especially in the context of modern agriculture where use of antibiotics in feed as a means of improving feed to weight conversion ratio is widespread. At least three mechanisms of aminoglycoside resistance are dependent on enzymatic modification of aminoglycoside molecules [113], some of which are known to degrade Kanamycin [114][115].

2) An alternate cause of target molecule removal would be the loss of target molecule at the filtration stage of sample pre-treatment. Unlike the soil sample, the chicken faeces dissolves in water relatively readily, resulting in much fewer particles being removed at the centrifugation stage. However not all particles remaining suspended in solution after centrifugation is able to pass through the filter membrane pore (HAWP01300 filter has a membrane pore size of 0.45um). This results in a significant amount of blockage of the filter by suspended chicken faeces particles (indeed the filter has to be replaced many times in the filter process due to accumulation of blockage material on the membrane) which may result in the collateral entrapment of target molecule, resulting in decreased target concentration in the filtrate.

3) Another possible cause is the accumulation of non-target particles at the electrode interface, resulting in decreased access of the target molecules to the electrode surface, thus reducing effective target concentration at electrode interface.

It is unlikely that the increase in Kd value is the result of nuclease interference, since nuclease contamination would have resulted in loss of a proportion of signaling molecules, resulting in a general decrease of peak magnitude but no change in Kd, rather than a change in the signal trend seen here.

3.09 Electrode Reusability

One of the major potential advantages inherent to the structure of conformation change aptamers is the possibility of electrode reuse without the need for significant electrode surface restoration, due to the conformational change aptamer having a highly stable primary structure and being composed of a single covalently bonded unit. Since the primary structure will be significantly more stable than the target-aptamer interaction, removing target molecules is a simple matter of heating. After heating, the aptamer will simply return to its resting configuration.

This is not the case with configurational change systems, such as the Sandwich Aptamer Biosensor discussed in Chapter 5, where at the very least part of the structure (the component that is displaced into bulk solution, typically the redox label containing sequence) will need to be replaced in order for the electrode surface to be renewed. Antibody based sensing surface may not be renewable at all as the target-antibody separation temperature could also result in irreversible thermal degradation of the antibody coating.

In order to test whether the electrode would remain viable after harsh heat treatment and extended storage, the working electrode was stored after a target titration under lab conditions. This involved heat treatment at 90°C for 5 min in buffer, after which it was washed with MilliQ and stored in the fridge in autoclaved MilliQ water for approximately 1 week. The kanamycin titration was then repeated.

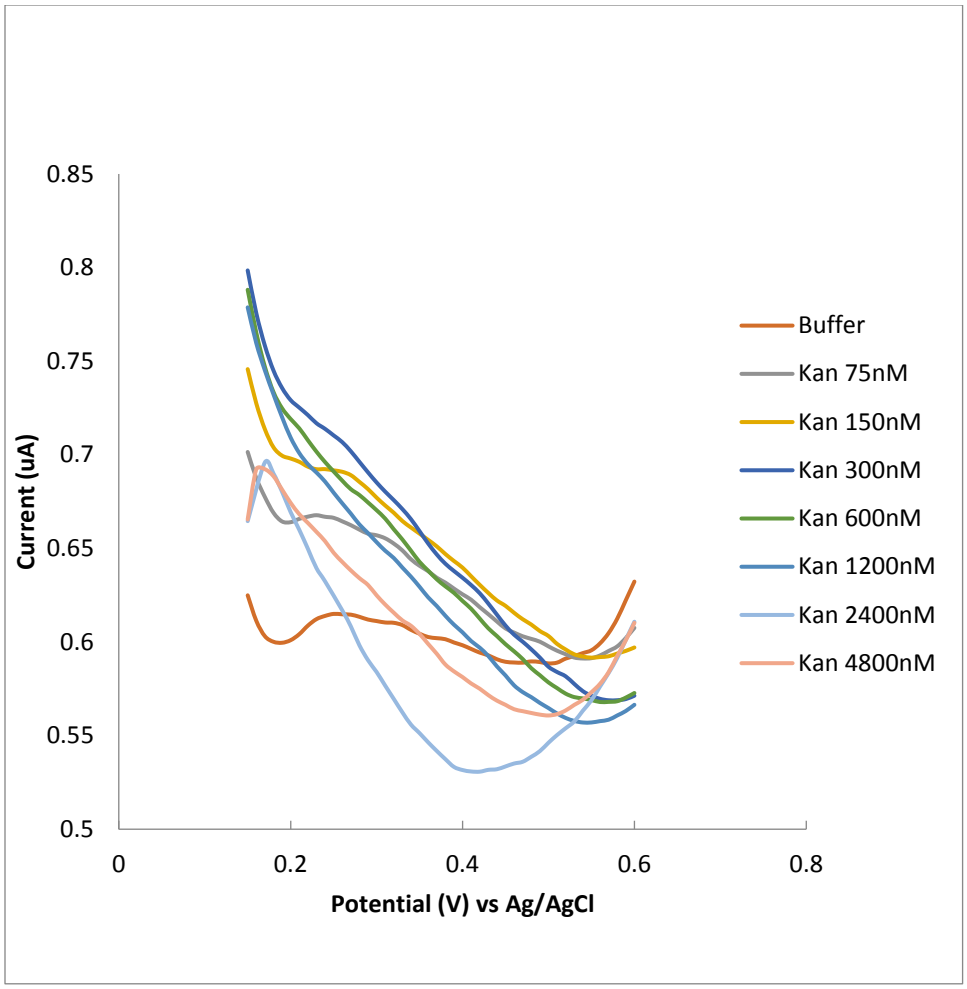

Fig 3.14 SWV derived peak current response of kanamycin Fcn-aptamer biosensor to kanamycin titration vs Ag/AgCl, performed using an pre-used electrode after heat based regeneration and one week of storage. SWV of this electrode during first use could be found in the Appendix A (Fig A.9, page 267)

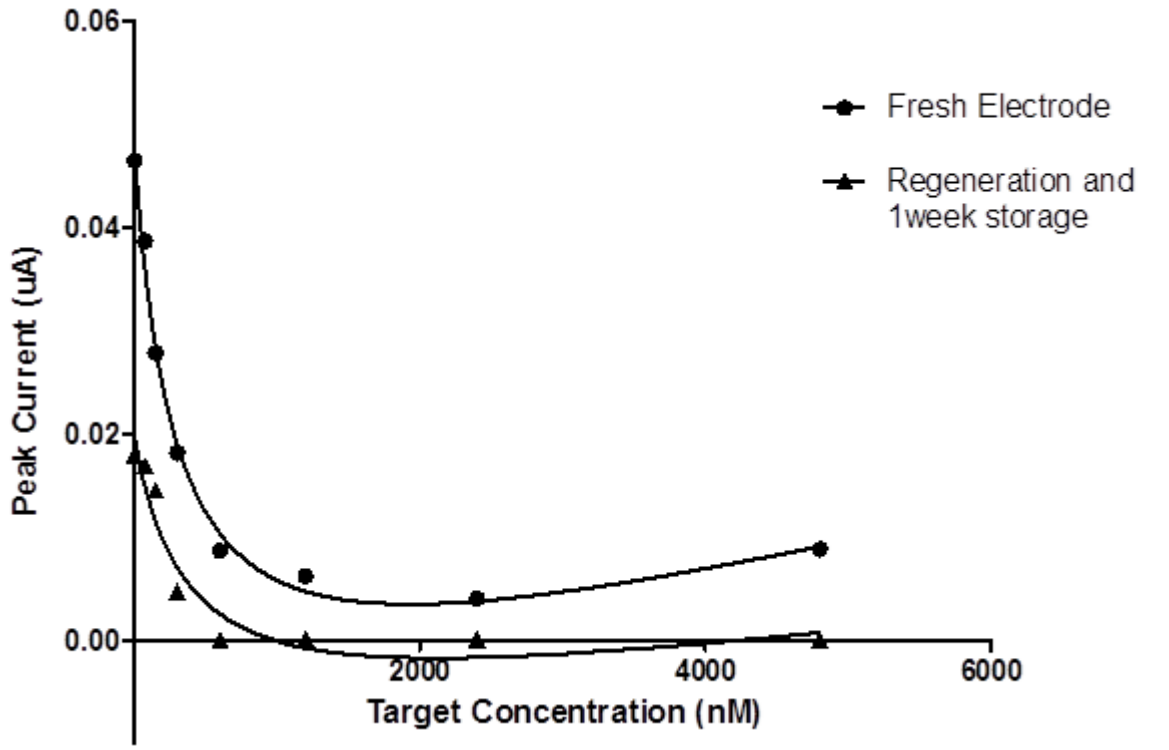

Fig 3.15 SWV derived peak current response of kanamycin Fcn-aptamer biosensor to kanamycin titration vs Ag/AgCl, performed in clean buffer. Blue) Profile using a fresh electrode after 12h DNA immobilisation and 24h storage, Red) Profile is the same electrode after heat based target dissociation and 1 week storage.

Comparing the two curves above, a significant signal amplitude decrease was noted between the first and second iterations. This is not surprising; it has always been observed that electrode stored for long periods of time suffer from signal loss (this is the reason why operational protocol demands that sensor electrodes be used within 7 days of sensor molecule immobilization). Given the 1 week wait time between the first and second iterations, the second experimental run was conducted close to the outer edges of what is considered the expiry date in a run operated using standard protocol.

Degradation over time can be linked to residual nucleases contamination during handling and storage process. In retrospect, storing the electrode in MilliQ may not have yielded optimal results. While MilliQ water can be assumed to be sterile, the electrode itself cannot. Any contamination introduced along with the electrode would retain activity due to the hydrated conditions of storage. In the future it may

be more beneficial to wash the electrode thoroughly with MilliQ and then covered up from air particles and stored after nitrogen blow drying.

The relatively harsh heating regimen the electrode has been subjected to would also have resulted in a net decrease in viable signaling molecule, primarily due to breakdown of thiol-gold interaction on the electrode surface.

However the trend of the data remains largely unchanged after heat treatment and 7 days of storage. Both show strong inverse correlation between target concentration and peak current signal strength at low target concentrations, followed by a target saturation induced plateau at very high concentrations. Sensor resolution remains unchanged at 75nM for both electrodes. Kd for the first week is 291 nM and the second is 374 nM. However this is likely to be a result of an abnormally low buffer signal in the second week, as well as non-detectible signals at high target concentration resulting in relatively skewed results.

3.10 Kanamycin Aptasensor electrode to electrode variations

Here the variation in signals trend and amplitude between the electrodes is reported. The nine electrodes used for standardised titration against target molecules under laboratory environment can be considered as baselines for study due to the well-controlled clean buffer condition used in all experiments. Also included are the soil sampled results, including those with the 120 min delay time, as the effect of processed soil sample on electrode signal appear to be minimal based on our results. Any negative effect to analysis of data as a result of soil sample matrix is compensated by the benefits of the increased sample size. For obvious reasons negative controls such as specificity control samples are not included as they are not expected to (and in the events did not) follow the signal trend of the target titration. Similarly variants to the soil matrix and clean buffer conditions titrations, such as electrode reusability tests, and poultry faeces matrix control were not included, since both tests showed changes in trends which could be explained by specific experimental variation factors.

Significant variation in voltammogram signal magnitude, but not in Kd values, was observed between the titrations sets investigated. In almost all cases, the peak current response to target concentration followed the same trend, showing a decrease in signal as a result of an increase in target concentration, followed by a plateau as the saturation point is reached. However, there was a significant variation in the signal magnitude between the result sets, with the lowest observable buffer peak (the strongest signal based on the signal trend of this sensor) of the clean buffer conditions tests being 21 nA in

magnitude and the highest being 83.7 nA, almost a 4 fold difference. Including the soil matrix sample increases this range to 16.1nA to 83.7 nA.

A total of 23 electrodes were used in assays against a titration of target molecule (12 under standard cell conditions, 8 against environmental sample). Fourteen electrodes in total displayed a signal trend typical of a Langmuir surface binding model (9 for the lab conditions target titration, 3 and 2 for the two types of soil matrix titrations). Two electrodes were lost as a result of accidents or human error. Of the remaining seven electrodes, four showed no signals at all, which can most likely be attributed to failed fabrication, either as a result of poor polishing or bad immobilization.

It is important to note that none of the profiles showed a generally positive trend. The single electrode showing a linearly negative response to titration could simply be the result of multiple outlier data points resulting in a skewed data trend. In the four cases where the sensor signal was not obtained, it is likely that the signal was insufficient to be noticeable over the background noise. This would suggest the electrode variation is the result of QC problems in sensor fabrication rather than a failure of the sensor design itself.

Attempts were made in order to determine the cause of signal amplitude variation between the data sets which have a signal consistent with the Langmuir binding model. Badly polished and prepared electrodes were noticed early to result in defective sensors with reduced or unreliable signals. Since badly fabricated and prepared electrodes have irregular sulphuric acid electrochemical cleaning profiles, they are discarded for reprocessing by default without undergoing the sensor molecule immobilization stage. Otherwise polishing should not have changed significantly between batches, and production methods were consistent.

3.11 Gel Encapsulated Electrodes

As discussed in the previous section, complex samples such as soil or faeces extract may contain nuclease enzyme. Nucleases are enzymes capable of hydrolyzing the phosphodiester bonds of nucleic acids. They are ubiquitous in nature, and they are therefore hypothesized to play a possible role in the degradation of surface bound nucleic acid molecules. In the environmental analysis section of this study, we have shown that the sensor retains most, if not all, of its signal amplitude even after extended incubation with environmental samples. This can be attributed to a number of reasons, such as low

nuclease concentration in the sample, obstruction of nuclease activity by the sensing surface or removal of nucleases by the pretreatment process. However these factors may not always apply, for example some samples may have greater nuclease concentrations than those of soil. The pre-treatment process in particular is not feasible or applicable for all sensing situations, for example in long term continuous sensing (no pre-treatment possible), such as in bioreactor monitoring, or extended environmental in situ monitoring for the presence (for example) of toxins.

It is therefore proposed that nuclease protection be implemented which does not require pre-treatment. Agarose gel is a commonly used tool, both in the SELEX affinity selection and many molecular biology processes. Agarose gels can entrap target molecules by forming three dimensional matrices of supercoiled masses of helical agarose molecules [116]. This results in a mesh like structure which inhibits the transport of materials larger than the average pore size. This nuclease exclusion strategy is analogous to the membrane filtration process used in environmental sample pretreatment, but with the barrier being at the electrode surface rather than as a separate pretreatment step.

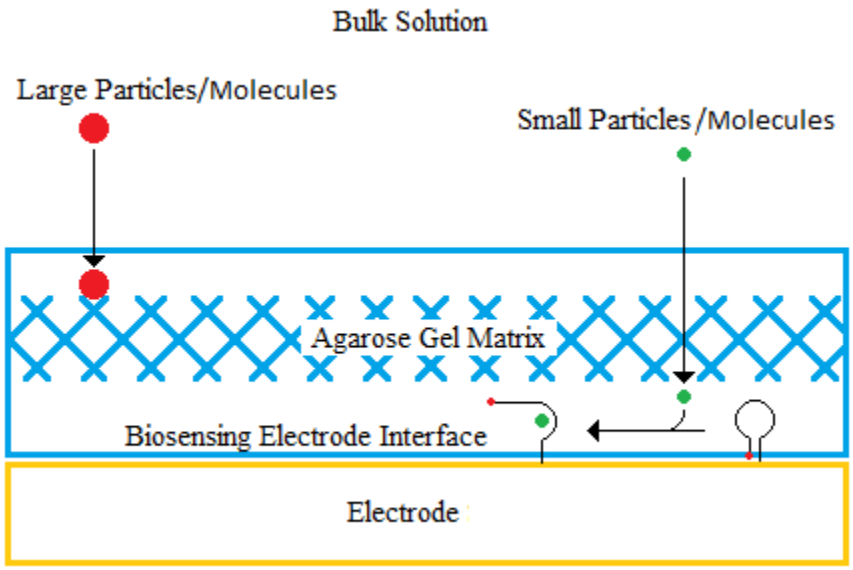

Fig 3.16 Hypothesized mechanism of biosensor surface protection as a result of gel encapsulation. Excluded particles include nucleases and redox active, noise generating large particles

The gel-coated electrode is fabricated first by preparing the kanamycin biosensor in a manner identical to that used for its preparation under regular laboratory and environmental conditions. Agarose is then

added to an electrolyte buffer pre-heated in a microwave oven for 5 min, to a final concentration of 3%. Then the aptamer-immobilised electrode is dipped to a length of approximately 30mm in the molten agarose solution for 5s, and the removed, inverted, and allowed to set. Dipping the gel up to at least 30mm in length is essential since it was noticed that a smaller cap will disaggregate from electrode tip when rehydrated in cell solution during use. The pore size of 3% agarose is 289nm [117]. While this is insufficiently dense to entrap large globular proteins, the density of the mesh should be sufficient to obstruct transport of large globular proteins to the electrode surface. However small molecules such as aminoglycoside secondary metabolites should be relatively unimpeded. The electrode is then stored in a cool, humid location to reduce dehydration of the gel tip.

The nuclease selected was S1 nuclease derived from *Aspergillus oryzae*. This nuclease was selected as it a non-specific nuclease that primarily targets single stranded DNA substrates [118]. The pre-prepared electrode is incubated in 1U/10ul solution of nuclease in nuclease buffer (20mM Tris-HCl pH 7.5, 50mM NaCl and 0.1 mM $ZnCl_2$) containing Zinc cofactor of S1 nuclease, at 37°C for 2 hours. The electrode is then used in a cell setup identical to the laboratory condition assay.

A series of negative control assays were also carried out to determine the degree of activity of S1 nuclease on an unprotected electrode. These assays were conducted in a manner similar to the gel coated assays, including nuclease incubation time, but without the presence of the gel coat.

Two key objectives must be fulfilled for the gel encapsulation of electrode to be considered a viable process from a practical standpoint:

1) The gel encapsulation process must not decrease the signal amplitude and sensitivity of the electrode to the point where the electrode is no longer feasible as a kanamycin sensor.
2) The gel encapsulation process must be useful, in that the absence of gel encapsulation leads to a significant loss in sensor signal.

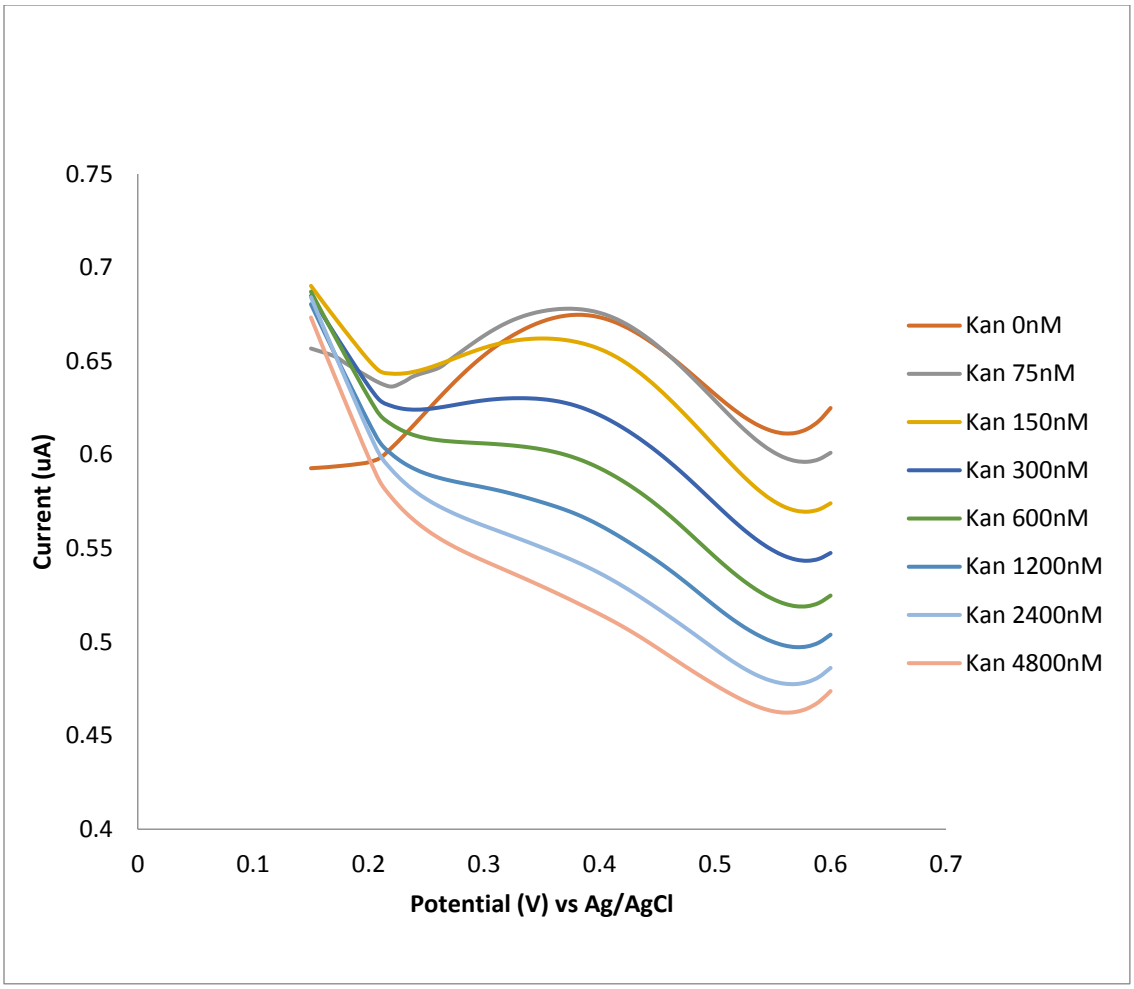

Fig 3.17 SWV of gel encoated kanamycin fcn-aptamer biosensor's response to kanamycin titration vs Ag/AgCl, performed in clean buffer following 2h incubation in nuclease solution

The results of the gel encapsulated electrode show an average signal amplitude comparable to that obtained in laboratory condition assays, which would indicate that the encapsulation process does not significantly interfere with the signaling process. Signal amplitude of gel coated biosensors range between 51nA to 84nA, with an average of 70nA. This is slightly higher than the average amplitude of electrodes performed under laboratory conditions (54nA), although the difference is not statistically significant. The range of amplitude was much narrower than those obtained in the clean buffer experiments (max 84nA, min 23nA), although this can be attributed to the much larger dataset of the clean buffer experiment compared to the gel encapsulated experiment (9 to 4).

In total four independent titrations were performed under gel encapsulated clean buffer conditions with nuclease pre-incubation. The results of these replicate titrations can be found in Appendix C (page 282). The results of the gel encapsulated electrode also show similar quantitative behavior to the clean buffer condition, with the current falling in correlation with an increase in kanamycin concentration. Fitting the peak currents as a function of target molecule concentration using a Langmuir Isotherm yields an average Kd of 385.6 nM which compares closely to the to the results of the clean buffer samples described previously (average Kd of 565.8 nM). R squared was calculated to be greater than 0.9 in all cases, and in all but one of the titration the r squared was calculated to be greater than 0.98.

Based on these observations it is possible to conclude that the gel encapsulation process did not significantly interfere with the sensing process, and that gel encapsulated electrode therefore remains a feasible kanamycin biosensor.

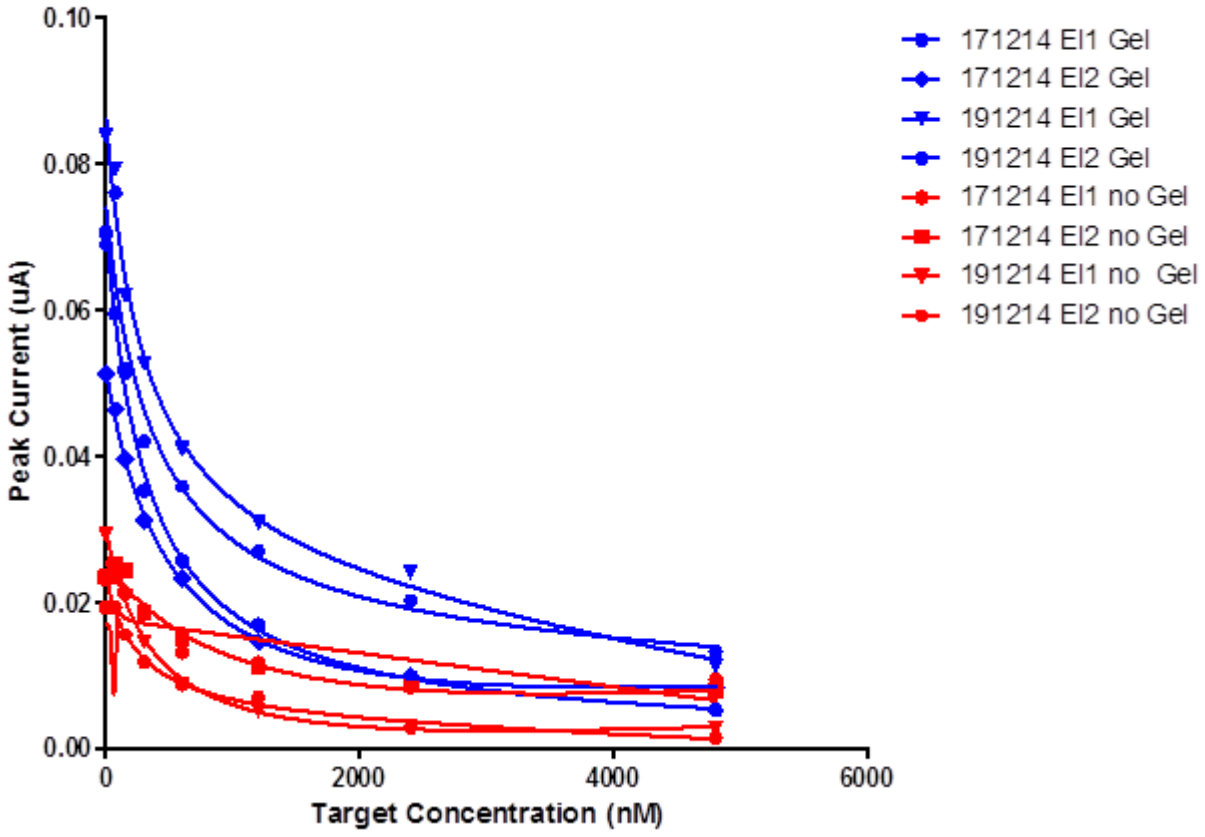

Fig 3.18 SWV derived peak current response of kanamycin Fcn-aptamer biosensor to kanamycin titration vs Ag/AgCl, gel encoated electrode in blue and unprotected electrodes in red. All electrodes are limited

to two consecutive production batches, and performed using ALS electrode only, to further decrease intrabatch variation.

The negative control continue to show a significant signal amplitude after 2 h of incubation in 1U/10ul nuclease without gel protection. This is in contrast with gel electrophoresis of the sensing molecules in solution, incubated for the same duration, which no discernable bands at all (which would indicate significant hydrolysis). This would support the conclusion raised in the environmental matrix assay section of this chapter, that the immobilisation process provides some inherent protection to the immobilized biosensor molecule even in the absence of gel encapsulation (additional details can be found in section 3.08 of this chapter).

However it should be noted that while negative control signal remained clearly discernable, the signal amplitude of the negative control is consistently lower than that of the gel encapsulation protected electrode. Eight electrodes, including four electrodes of each type, were assayed in this test in total. Of these eight the four electrodes displaying the highest maximum signal (for this molecular beacon type biosensor this is in the absence of kanamycin) are all gel protected, while the four lowest are all unprotected electrodes. Out of all data points obtained (64 total) only two data points of the gel encapsulated sets were not within the 50^{th} percentile in terms of signal amplitude at any given concentration, and these are found at the highest concentration (lowest signal amplitude) where the effect of noise would be greatest.

Signal trends for the negative control is comparable to those of the gel encapsulated sample and the laboratory condition assay, with an average Kd of 452nM. This is not surprising as nuclease digestion would result in a decrease in density of biosensing molecules on electrode surface (and therefore signal amplitude), but otherwise should not interfere with the signaling process, resulting in no change in the signal trend.

As a whole, these results would indicate that while gel encapsulation clearly does not inhibit sensor activity, and may reduce loss of signal amplitude as a result of nuclease hydrolysis, it is not strictly essential for the preservation of the sensing surface even with extended exposure to high nuclease concentration. Therefore the lack of nuclease activity is not exclusively the result of exclusion by molecular weight partition, but is also the result of other factors discussed in the environmental sample section of this chapter.

3.12 Sensor Specificity

Control experiments were conducted in order to determine whether the sensing molecule would bind to non-target molecules structurally similar to the kanamycin target. Controls selected for these purpose were other antibiotics of the aminoglycoside class, all of which have the same basic amino groups attached to glycosides rings structure. Although chemically distinct, all aminoglycoside have the same mechanism of action, binding to the aminoacyl-tRNA ribosomal site (commonly referred to as the A site) of the 30S subunits, a highly conserved feature of many gram negative bacteria. This gives aminoglycosides a very broad spectrum of activity.

Typically high specificity can be considered a positive characteristic in a biosensor. It should be noted however that specificity to kanamycin could be a double edged sword. Aminoglycosides in general is already a fairly restrictive category. Whether high specificity is a positive or negative characteristic depends significantly on what the sensor's particular function will be. In the case of microbial product discovery it is a positive trait if the aim of the assay is to find a new producer organism of kanamycin, but it can also be a negative trait if the aim of the assay is to find a novel aminoglycoside antibiotic with relatively subtle differences to kanamycin. Even relatively small structural differences could result in a significant difference in practical value of an antibiotic (beta lactams ampicillin and methicillin for example have very similar structures but methicillin is beta lactamase resistant). Similarly for an environmental pollutant sensor specificity is a positive trait if the aim of the assay is to identify a specific antibiotic residue, but a negative one if the sensors purpose is to discover aminoglycoside residues in general. In the case of sensors for industrial bioproduct synthesis quality control (such as a QC sensor in a bioreactor for example), specificity is a highly positive characteristic, since a specific product is the operational aim.

For obvious reasons response to non-aminoglycosides could be considered a universally negative characteristic. However 'non-aminoglycoside' is too broad a category to be practically tested. Should the sensor not respond to other aminoglycosides there is no reason to assume that it will respond to a random non-aminoglycoside either.

3.12a Specificity Control

Control experiments were conducted in order to determine the specificity of the biosensor to kanamycin target. Aminoglycosides streptomycin and gentamycin were selected, largely due to ease of access. All three molecules are of comparable sizes (MW of 581.6 for streptomycin, 477.6 for gentamycin and 484.5 for kanamycin, and similar solubility (references generally state 50mg/ml for all three). All three are built around of amine-rich triplet sugar ring. Streptomycin is slightly larger, with a pentose without amine groups on the second ring, the third ring contains two guanidine groups, resulting in a molecule with more proton acceptors than donors (19/16). Kanamycin and gentamycin are structurally quite similar, although gentamicin's active groups and rings has significantly greater degree of methylation, proton acceptor/donor ratio for both are quite balanced at 15/15 and 12/11 respectively.

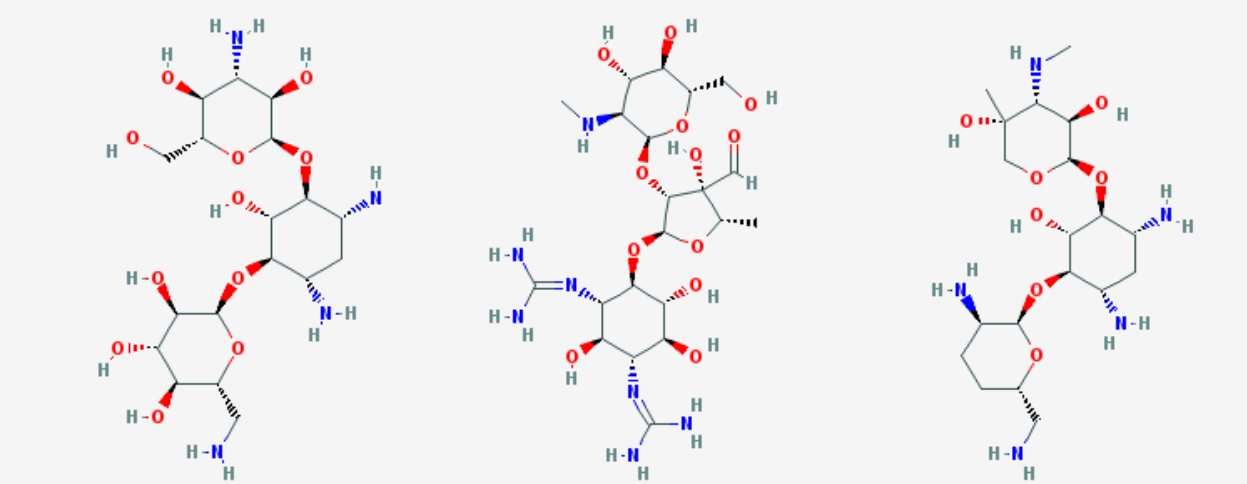

Fig 3.19 From left to right, the chemical structures of Kanamycin, Streptomycin and Gentamycin, quoted without modification from [119]

3.12b Kanamycin Aptasensor Titration against Streptomycin

The concentration range was selected to be similar to that of the target titration, with the highest concentration doubling the highest target concentration investigated.

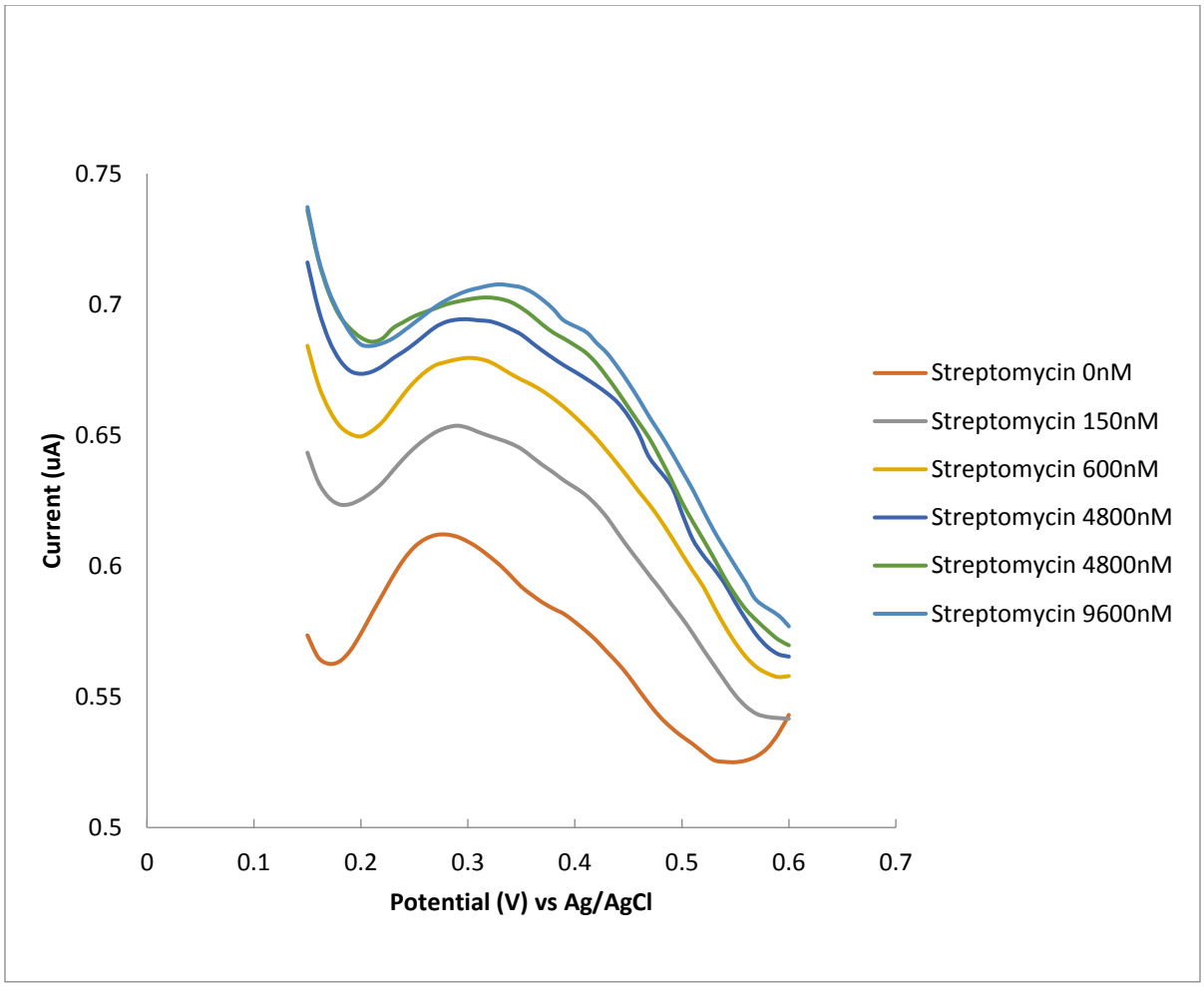

Fig 3.20 SWV of kanamycin fcn-aptamer biosensor's response to Streptomycin titration vs Ag/AgCl

In total three independent titrations were performed against Streptomycin negative control with separate sensors in each case. The results of these replicate titrations can be found in Appendix D (page 291).

Analysis of the data shows no clear correlation between peak current and concentration of streptomycin control. Change in signals as a result of streptomycin titration is relatively low in amplitude compared to the target titration. Comparison of the peak response of the voltammogram of the Streptomycin titration shows no reproduced trend in signal. This would support the conclusion that there is no comparable affinity between the sensing molecule and streptomycin under these conditions.

Highest to lowest signal ratio was respectively 1.09, 1.56 and 1.13, again significantly lower than the high/low signal difference of the kanamycin titration. Standard deviation within data set is 1.9, 1.1 and 3nA, a comparatively very small deviation within data set which indicates low signal difference between

data points (by comparison the standard deviation of the same nine working electrodes show a standard deviation average of 18.7nA). This indicates that titration of non-target molecule does not result in significant signal change relative to target titration. Concentration with highest signal was respectively 0nM (1st), 75nM (2nd) and 300 nM (3rd), lowest signal was respectively 4800nM (5th), 0nM (1st) and 9600nM (6th), indicating a more or less random data trend. This would indicate there is no significant correlation between streptomycin concentration and peak current.

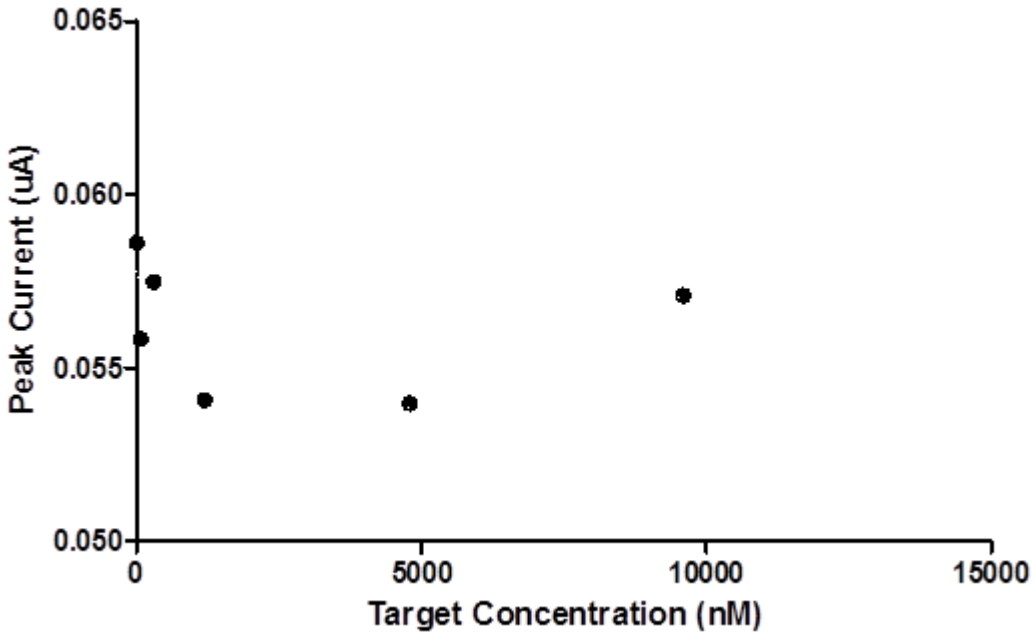

Fig 3.21 SWV derived peak current response of kanamycin Fcn-aptamer biosensor to Streptomycin titration vs Ag/AgCl.

3.12c Kanamycin Aptasensor Titration against Gentamicin

The concentration profile of the gentamicin control is limited by the highest concentration which could be obtained, which was 47.8 mg/ml (100 uM). This meant the highest concentration realistically achievable was 1000 nM. The concentration range was selected to be similar to that of target titration, with the highest concentration being 1000nM.

Unlike most tests, which were repeated in triplicate, only two assays were performed due to limitations in stock availability of gentamicin.

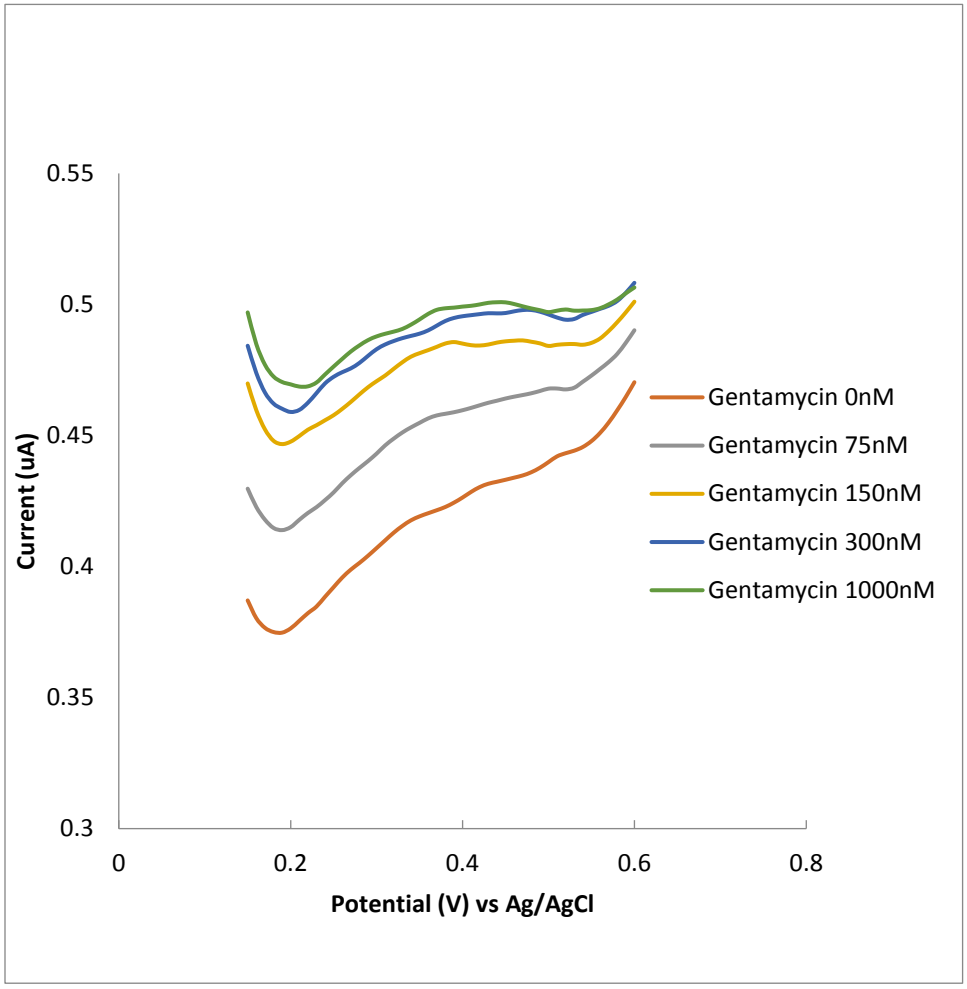

Fig 3.22 SWV of kanamycin fcn-aptamer biosensor's response to Gentamicin titration vs Ag/AgCl

In total two independent titrations were performed against Gentamicin negative control with separate sensors in each case. The results of the replicate titration can be found in Appendix D (page 291).

Analysis of the data shows no clear correlation between peak current and concentration of gentamicin n control. Like in streptomycin titration change in signal as a result of gentamicin titration is relatively low in amplitude compared to the target titration. Comparison of the peak response of the gentamicin titration shows no reproduced trend in signal. This would support the conclusion that there is no comparable affinity between the sensing molecule and gentamicin under these conditions.

Highest to lowest signal ratio was respectively 1.47 and 1.12, which is a significantly lower signal difference than that observed in the target titration, where the lowest signal was generally below detection limit. Standard deviation within the data set is respectively 1.9 and 1.6 nA respectively, a comparatively small deviation within the data set, indicating low signal difference between data points. Highest signal was respectively 150nM (3rd)and 0 nM (1st), lowest signal was respectively 0nM (1st) and 75nM (2nd), indicating a more or less random data trend. This would indicate there is no significant correlation between gentamicin concentration and peak current.

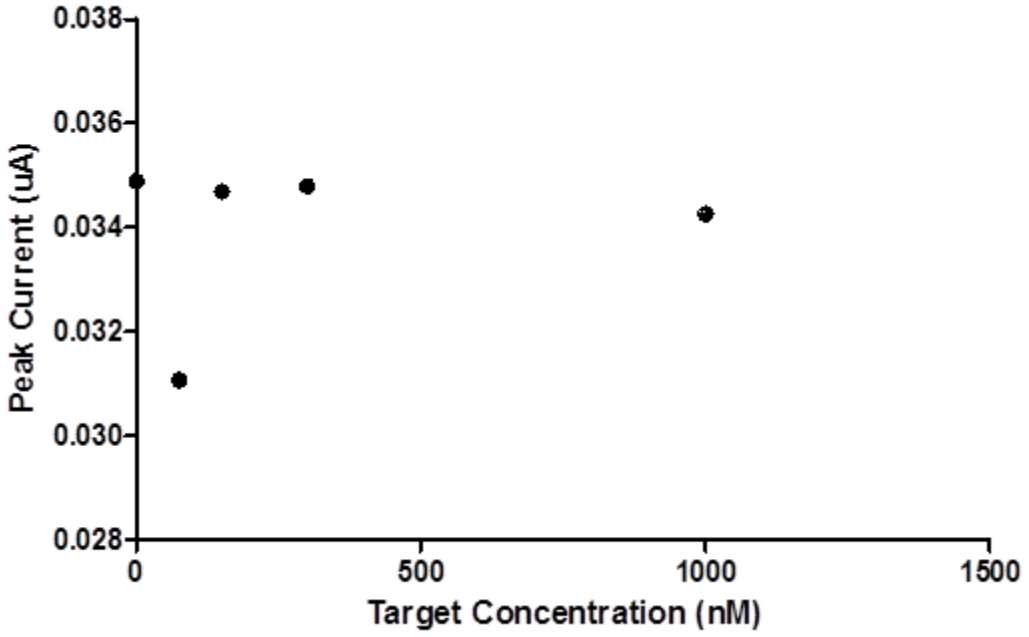

Fig 3.23 SWV derived peak current response of kanamycin Fcn-aptamer biosensor to Gentamicin titration vs Ag/AgCl.

3.13 Tetracycline Sensing with a Ferrocene Modified Aptamer

Unlike the aptamer sequence for kanamycin described by Song et al [102], where the priming sequence had been removed, that of tetracycline (Niazi et al [120] still contains the priming sequences. The Kd of the aptamer as published was determined to be 64 nM by equilibrium membrane filtration, which separates aptamer bound from unbound tetracycline. The SELEX protocol of the original paper specifically includes counter-selection against the similar molecule, oxytetracycline, with the aim of increasing specificity of the aptamer for its target.

The combinatorial library from the original publication was 75 bases in length, which is considered too long for an ideal molecular beacon, since binding a small target to such a long sequence may not result in the dissociation of the molecular beacon. Sequence in a SELEX library is composed of randomized region flanked by primer binding region. The target binding affinity of a sequence isolated by the SELEX process is driven by the randomized region of the sequence, with the flanking region being present primarily for the amplification process. While it is possible that the flanking region may play a role in target binding (and in some cases the flanking region is indeed essential for successful target binding [121]), truncating the flanking region is less likely to damage the ability of the aptamer to bind target molecule than truncating the random region. There are a number of previous studies where the truncation of a SELEX selected sequence at the primer binding region results in significant increase in target affinity [122][123]. Analogous studies to silence the fixed sequence of selected nucleotide libraries have also been undertaken, resulting in increased affinity to target [121]. A recently published SELEX protocol attempts to minimise the effect of fixed regions on the sequence by performing affinity selection with such regions silenced by complimentary binding [124].

Thus in order to reduce the length of the sequence, the sequence was truncated by removing primer binding sites flanking the random region.

Published Sequence:

5'-
CGTACGGAATTCGCTAGCGGGCGGGGGTGCTGGGGGAATGGAGTGCTGCGTGCTGCGGGATCCGAGCTCCACGT
G-3'

Original aptamer was selected to bind tetracycline taken from original paper published by Niazi et al [120], and contains flanking primer binding sequence needed in the process of SELEX for amplification via PCR. The sequence utilized for this study is shown in green.

Complementary sequences were then added in order to produce a hairpin loop secondary structure.

Molecular Beacon Design:

5’-GGGCGGGGGTGCTGGGGGAATGGAGTGCTGCGTGCTGCGGCCGCCC-3’

The beacon-forming added sequence is displayed in red, and was designed to be complementary to the 5’ sequence present in the aptamer and shown in blue. In the original paper of Niazi et al, the target binding sequence is predicted to be at the 5’ end of the truncated sequence, based on its presence in sequences isolated from the final SELEX library with high affinity to the target molecule. This makes it an attractive region for design of a hairpin loop, since involvement in target binding would result in a dissociation of the redox label bearing complementary strand.

Like the kanamycin biosensing molecule, the sequence selected was adapted for electrochemical conformational sensing by the addition of a C6 mixed disulphide group at the 5’ end of the sequence and a ferrocenyl modified base at the 3’ end.

Finalised Biosensor Sequence:

5’-C_6H_{13}-S-S-GGGCGGGGGTGCTGGGGGAATGGAGTGCTGCGTGCTGCGGCCGCCC-Fcn-3’

3.14 Tetracycline Aptasensor Titration against Target Molecule

The results of the tetracycline aptamer titration show a significant signal increase in response to an increase in target concentration.

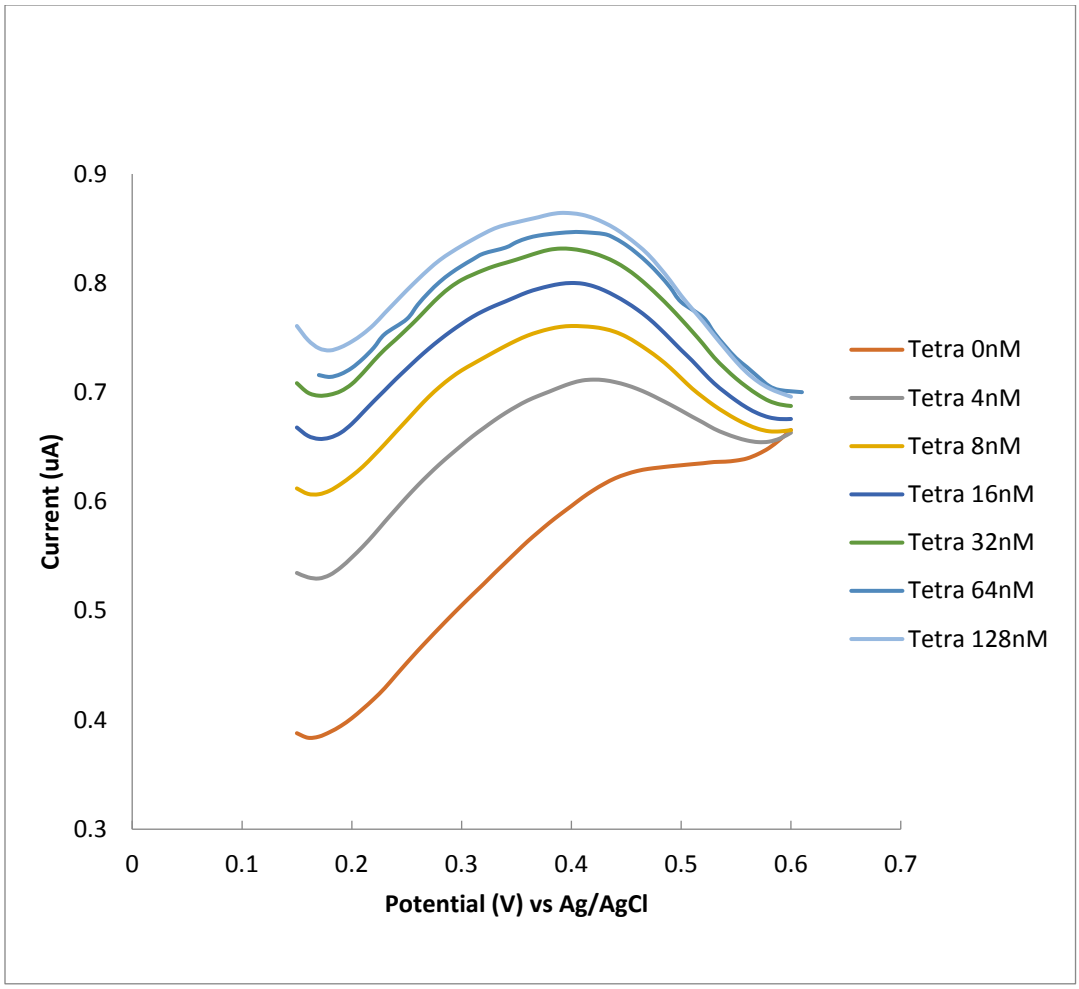

Fig 3.24 SWV of tetracycline fcn-aptamer biosensor's response to tetracycline titration vs Ag/AgCl, performed in clean buffer

While at present there are no available nucleic acid structure model which predicts G-quadruplex secondary structures thermodynamically, computational tool are available which compare DNA sequences to a database of sequence motifs that are believed to be associated with G-quadruplexes. One such resources is the G-Quadruplex Resource Site's QGRS Mapper [125] [126].

The results of a search of the database yielded 1 exact match, and 227 similar sequences including overlap, which would indicate a strong likelihood of the sequence forming a G-quadruplex structure. The sequence can be found below in fig. 3.24.

5'-GGGCGGGGGTGCTGGGGGAATGG-3'

5’-GGGCGGGGGTGCTGGGGGAATGGAGTGCTGCGTGCTGCGGCCGCCC-3’

Fig 3.25 The exactly matching G-quadruplex forming sequence discovered by a search of the QGRS mapper database, its location on the truncated tetracycline aptamer biosensor is in red.

Like the kanamycin aptamer the titration plot profile is typical of a Langmuir type binding curve, with the signal drop correlating to target concentration at lower concentrations before plateauing at high concentration as the sensing surface is saturated with target molecules.

Peak current was acquired using the same method as that used in the kannamycin aptamer biosensor study. Fitting the peak currents as a function of target molecule concentration using a Langmuir type fitting yields an average Kd of 6.8 nM, which is significantly lower than the literature value for the Kd of 64 nM. This is not unexpected since the sequence has undergone significant change by the truncation of primer binding region and addition of a stem forming sequence. It is also possible that, like the kanamycin aptamer, variation between experimental condition such as the addition of 5’ and 3’ end modification and change in environment (buffer conditions and immobilisation to electrode surface) may also play a role in influencing Kd.

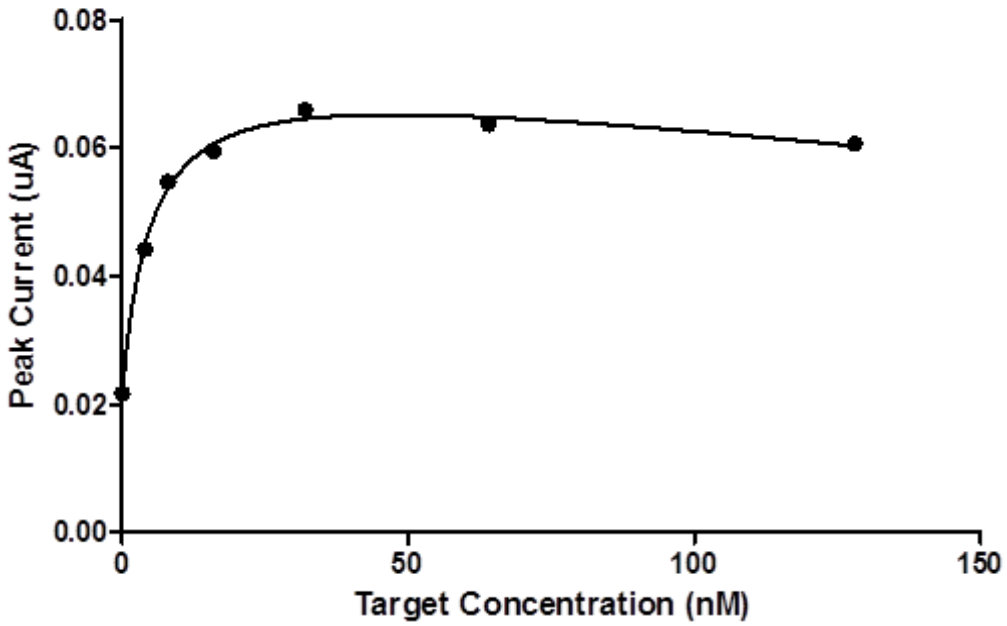

Fig 3.26 SWV derived peak current response of tetracycline Fcn-aptamer biosensor to tetracycline titration vs Ag/AgCl, performed in clean buffer

In total five independent titrations were performed under simple matrix clean buffer conditions with separate sensors in each case. The results of these replicate titrations can be found in Appendix E (page 295). In all the cases the dose response behavior followed the same pattern, with the current rising in correlation with an increase in tetracycline concentration. However sensor to sensor variation meant that the Kd values varied from a K_{max} of 17nM to K_{min} of 2.6 nM. The K_{max} is a probably an outlier as the average Kd (including the K_{max}) is 6.8 nM (second highest Kd is 5.7nM) and also has a relatively poor fit to the Langmuir binding model (r squared of 0.96). R squared was calculated to be greater than 0.95 in all cases, and in all but the outlier the r squared was calculated to be greater than 0.98.

Based on the results of the target titrations, the detection limit of this sensor is at least as low as 4 nM. This level of sensitivity is considerably superior to even the most optimistic detection limit of conventional antibiotic productivity selection based on observation of zones of growth inhibition (toxic dose of Tetracycline to target organism is equal to or greater than 203 nM [127]).

3.15 Tetracycline Aptasensor Titration against Target Molecule in Environmental Matrix

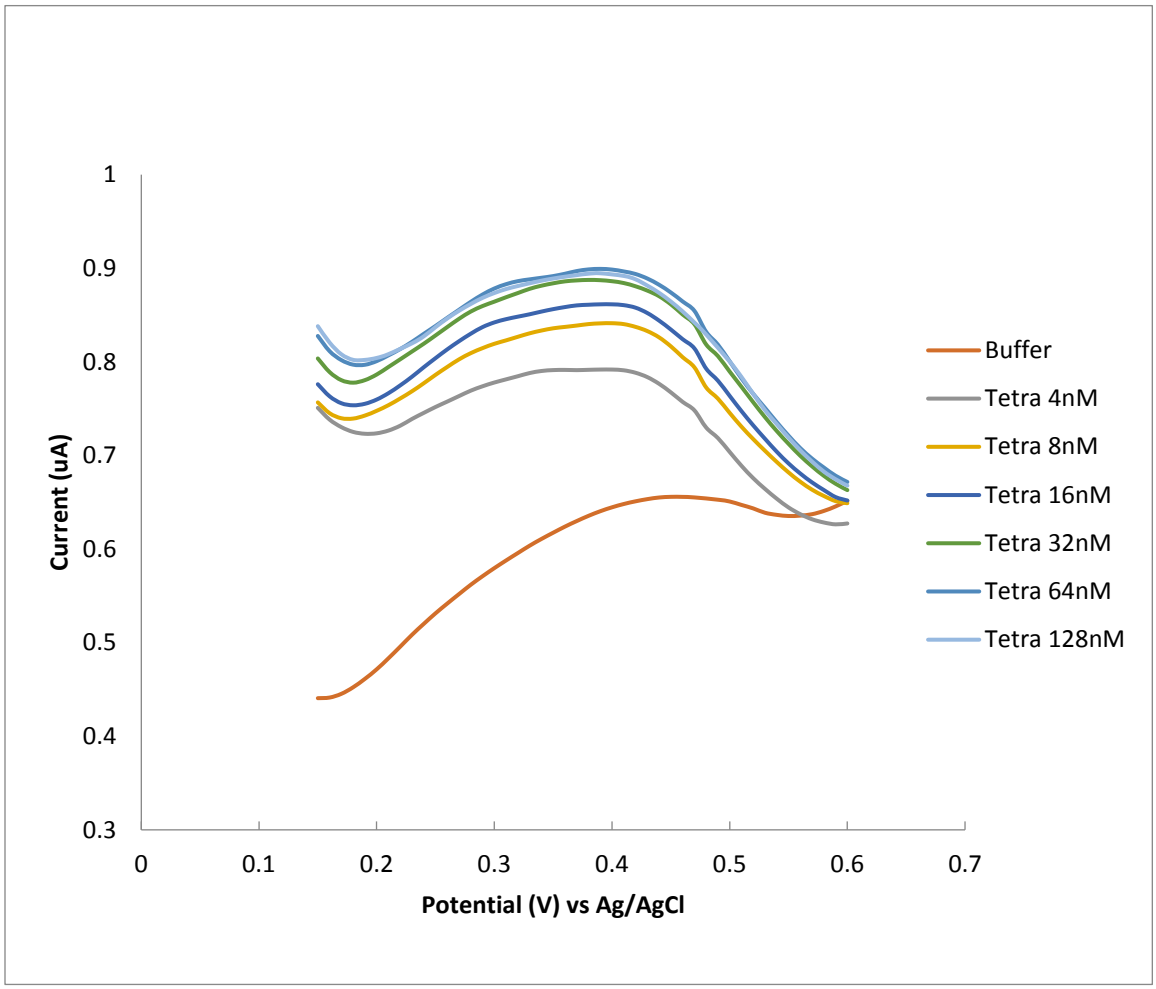

Fig 3.27 SWV of tetracycline fcn-aptamer biosensor's response to tetracycline titration vs Ag/AgCl, performed in soil sample matrix

Like the environmental matrix enriched target titration of the kanamycin aptamer, the titration curve under these conditions show minimal difference in trend to the titration curve of the assay performed using clean buffer. Investigation of target titration in an environmental matrix enriched cell solution by SWV shows significant positive correlation between signal amplitude to target concentration. Similar to an assay under clean buffer conditions, the titration plot profile is typical of a conventional Langmuir type fitting (a signal increase followed by a plateauing at high concentration).

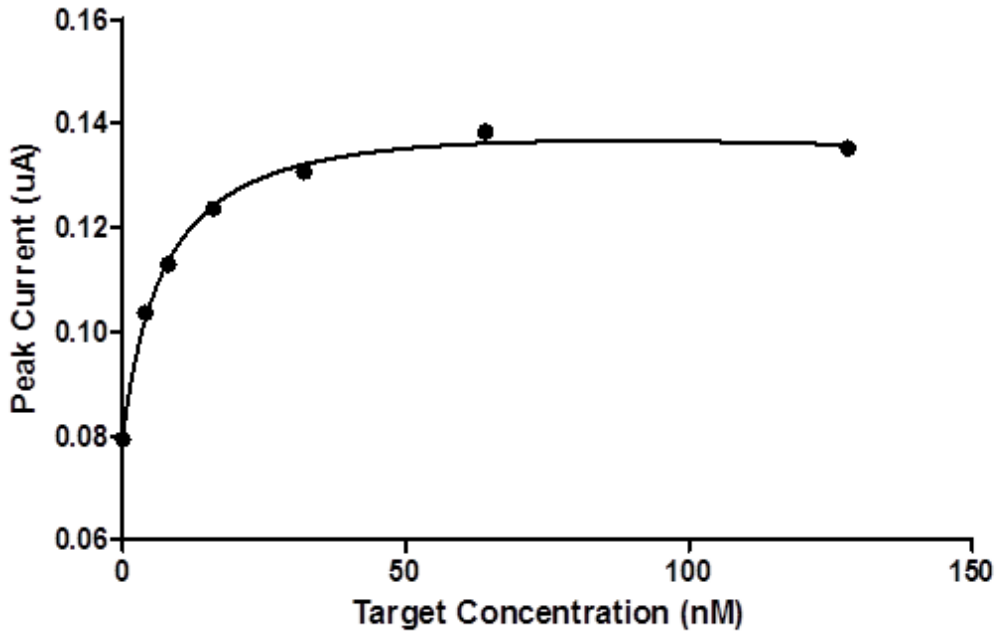

Fig 3.28 SWV derived peak current response of tetracycline Fcn-aptamer biosensor to tetracycline titration vs Ag/AgCl, performed in soil sample matrix

From the results of the target titrations, the detection limit of this sensor was determined to be at least 4 nM. This is equivalent to 8 nM, or 3.6 ng/ul, prior to the addition of 2x cell buffer solution, or 72 ng/gram of soil. The same assumptions regarding solubilisation and water accessibility discussed in the kanamycin biosensor section also applies here.

In total four independent titrations were performed in soil environmental matrix buffer conditions with separate sensors in each case. The results of these replicate titrations can be found in Appendix F (page 301). In all cases the quantitative behavior followed the same pattern, with the current rising in correlation with an increase in tetracycline concentration.

Fitting the peak currents as a function of target molecule concentration using a Langmuir type fitting yields an average Kd of 5.9 nM, which compares closely to the to the results of the clean buffer samples described previously (Kd average of 4.8 nM). Like the clean buffer sample, this Kd is significantly lower than that reported in the literature of 64 nM.

Signal amplitude at the highest target concentration (typically the maximum signal amplitude within the titration set) of the environmental condition titration (average 130nA) is slightly higher than, but still comparable to, those performed under clean buffer conditions (average 88nA). This would support the conclusion noted in the kanamycin biosensor section that the presence of the soil environment matrix does not significantly affect the performance of the sensor.

Since the protocol used here are similar to those used in the analogous Kanamycin environmental condition titration, and both sensors display (with reverse signal direction) the same signal trends, it can be reasonably assumed that the analysis discussed in the Kanamycin section concerning the effect of the environmental matrix on the biosensor also applies here.

3.16 Tetracycline Aptasensor Electrode to Electrode Variations

Variation in the signal magnitude between titration sets is significantly smaller between tetracycline sensors than between kanamycin sensors. Resting signal averages at 62.3 nA, with an upper and lower quartile of 81.8 nA and 50.4 nA, and a standard deviation of 28.2. Saturation signal (7^{th} concentration, 128nM) averages at 112nA, with upper and lower quartiles of 138 nA and 95 nA respectively, and a standard deviation of 41 nA. This represents a relatively greater consistency in signal magnitude compared to most other sensors investigated in this study. As in the case of kanamycin sensors, all cases where peak could be observed show the same trend of peak response to target concentration, though in this case showing an increase as opposed to a decrease in signal as a response to target concentration increases.

A total of thirteen sensors were created, of which three yielded no detectable signal. In this case 75% of the failed electrode came from the same production batch, which makes it highly likely this is a batch based phenomenon. The remaining electrodes displayed a signal trend typical of a Langmuir surface binding model. In total four out of thirteen electrodes displayed irregular signals, giving a failure rate of 31%

3.17 Tetracycline Aptasensor Specificity

Control experiments were conducted in order to determine whether the sensing molecule would bind to non-target molecules structurally similar to the tetracycline target. Controls selected for this purpose is Erythromycin, another antibiotics of the polyketide class. Unlike the aminoglycosides which all have the same basic structure, polyketides is a highly diverse family structurally, therefore care was taken to ensure the control is structurally similar to Tetracycline.

3.18 Tetracycline Aptasensor Titration against Erythromycin

Control experiments were conducted in order to determine the specificity of the biosensor to tetracycline target. Erythromycin were selected, largely due to ease of access and low price. erythromycin and tetracycline have similar solubility (references generally state 2 mg/mg for erythromycin vs 10mg/ml for Tetracycline).

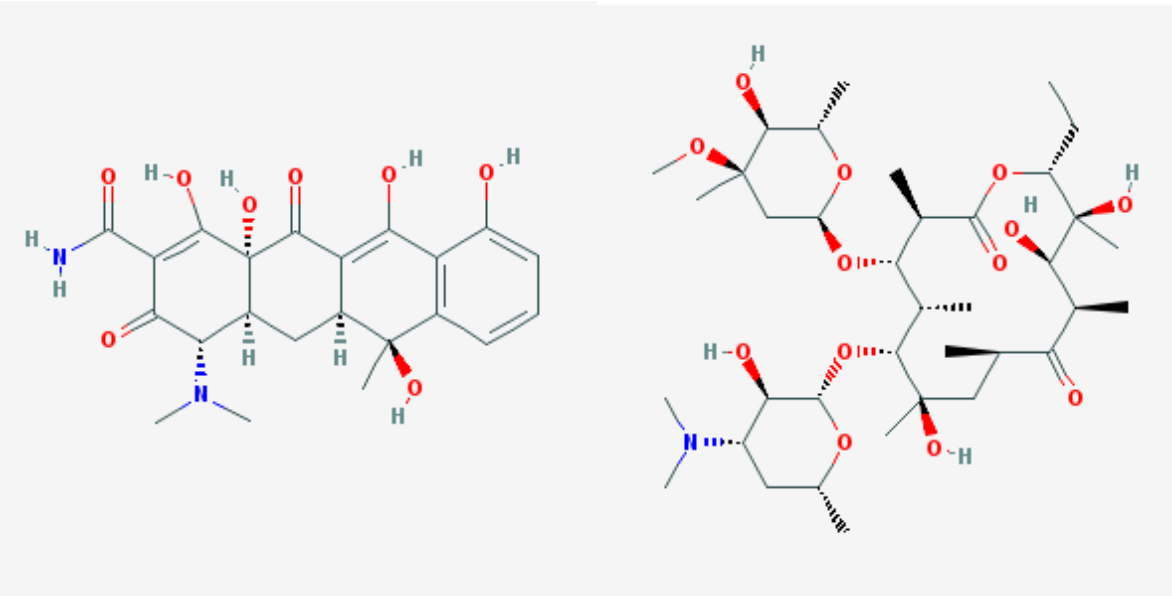

Fig 3.29 From left to right, the chemical structures of Tetracycline and Erythromycin, referenced without modification from [119]

Concentration range was selected to be similar to those of target titration, with the highest concentration doubling the highest target concentration investigated.

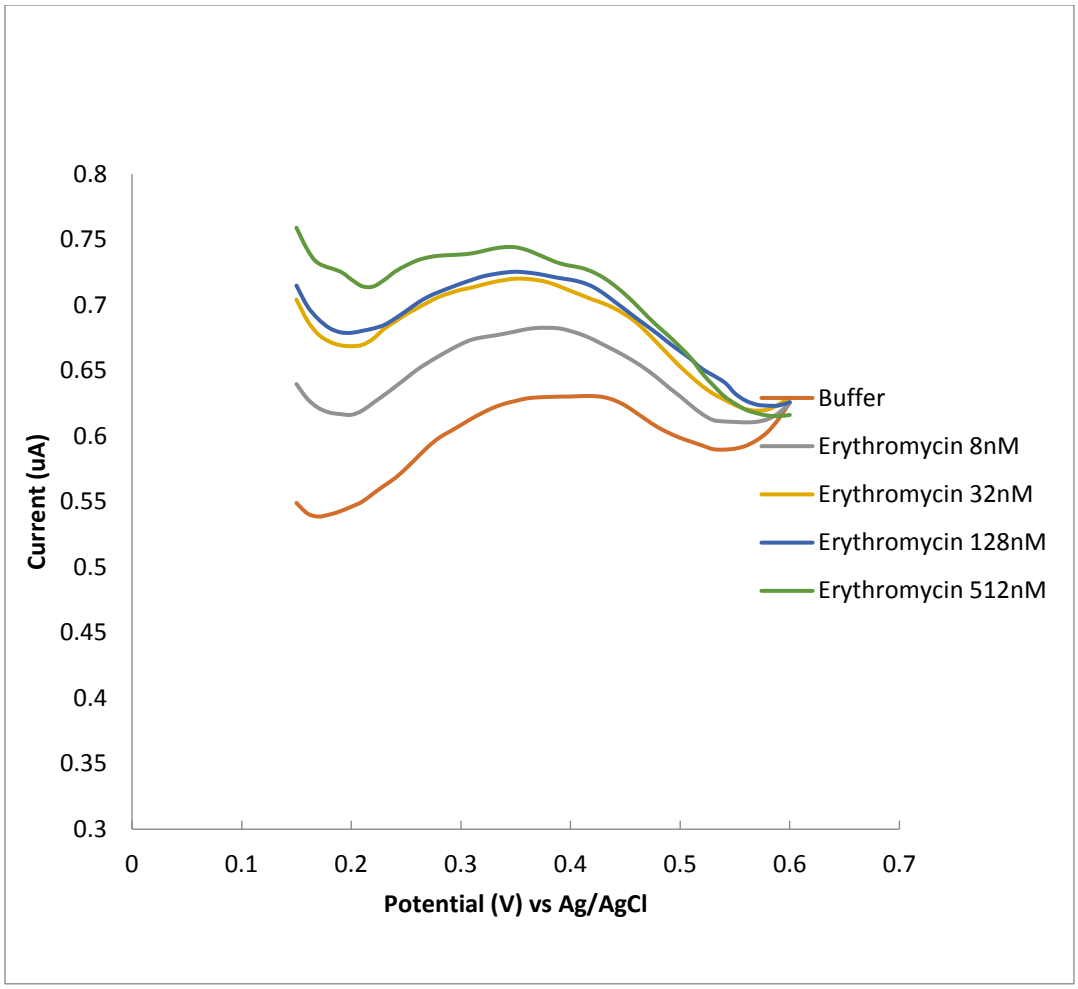

Fig 3.30 SWV of tetracycline fcn-aptamer biosensor's response to erythromycin titration vs Ag/AgCl, performed in clean buffer

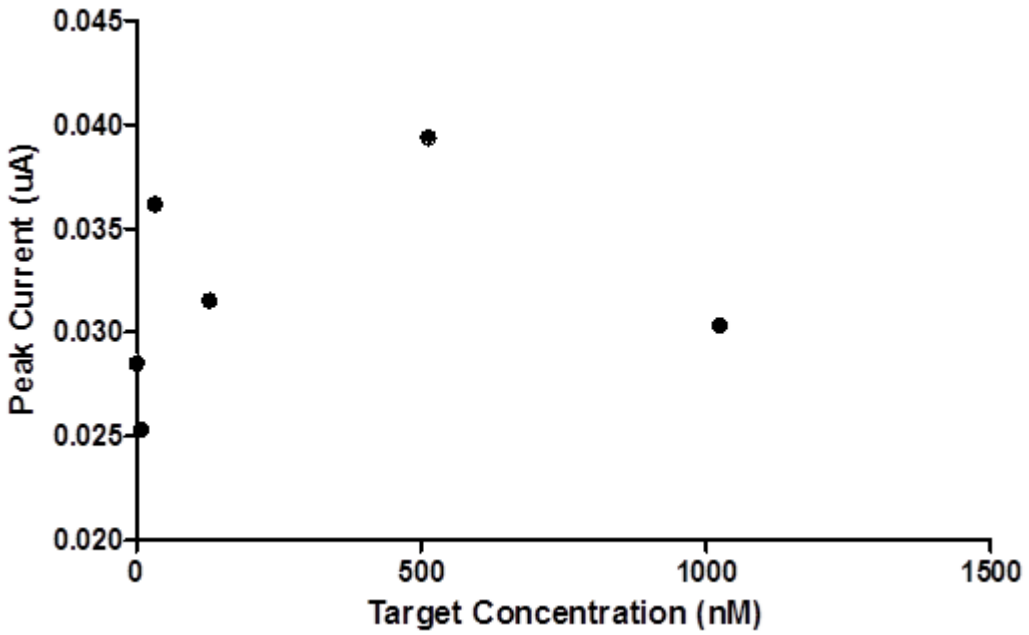

Fig 3.31 SWV derived peak current response of tetracycline Fcn-aptamer biosensor to erythromycin titration vs Ag/AgCl, performed in clean buffer

In total three independent titrations were performed against Erythromycin negative control with separate sensors in each case. The results of these replicate titrations can be found in Appendix G (page 306).

Analysis of the data shows no clear correlation between peak current and concentration of Erythromycin control. This would support the conclusion that there is no comparable affinity between the sensing molecule and erythromycin under these conditions.

Highest to lowest signal ratio was respectively 1.26, 1.56 and 1.88, again significantly lower than the high/low signal difference of the Tetracycline titration (2.63 average between 5 results). Standard deviation within data set is 4.6 nA, 5.1 nA and 3nA, a comparatively small deviation within data set, indicating low signal difference between data points (by comparison standard deviation for target titration is 20.3nA). Concentration with highest signal was respectively 128nM (4^{th}), 512nM (5^{th}) and 512 nM (5^{th}), lowest signal was respectively 0mM (1^{st}), 8nM (2^{nd}) and 1025nM (6^{th}), indicating a more or less random data trend. This would indicate there is no significant correlation between erythromycin concentration and peak current.

3.19 Concluding Remarks:

This study has shown the potential of using conformation change aptamer to sense antibiotic targets not only in the controlled laboratory environment in simple solutions, but also in relatively complex environmental matrix.

Author	Bioreceptor molecule	Sensor Format	Sensing Mode	Detection Limit	Target	Nucleotide	Ref
Kannamycin CCA	Aptamer	Conformation Change Aptasensor	Electrochemical	75 nM	Kanamycin A	DNA	NA
Tetracycline CCA	Aptamer	Conformation Change Aptasensor	Electrochemical	4 nM	Tetracycline	DNA	NA
Zhang et al	Aptamer	Target-Aptamer complex mediated impedence of electrode surface access to redox label	Electrochemical	1 nM	Tetracycline	DNA	[128]
Dong et al	Aptamer	Competition Assay	SPR	1.55 nM	Chloramphenicol	NA	[129]
Zhang et al	Aptamer	Target-Aptamer complex mediated impedence of electrode surface access to redox label	Electrochemical	2.17 nM	Tetracycline	DNA	[130]
Zhou et al	Aptamer	Target-Aptamer complex mediated impedence of electrode surface access to redox label	Electrochemical	5nM	Tetracycline	RNA	[131]
González-Fernández et al	Aptamer	Target-Aptamer complex induced assembly of transducer enzyme	Electrochemical	100 nM	tobramycin	RNA	[132]
Wochner et al	Aptamer	Competition Assay	Optical	159 nM	Duanomycin	DNA	[133]
Nikolaus et al	Aptamer	Induced assembly configurational aptamer biosensor	Optical	5 uM	Kanamycin A	DNA	[134]

Table 3.01 A comparison of the Conformation Change Aptasensors and a selection of recent antibiotic aptamer biosensors.

Based on the results of the target titrations, the detection limit of this sensor was determined to be at least as low as 75 nM and 4nM for the Kanamycin and Tetracycline CCA biosensors respectively. This is comparable to published literature of antibiotic aptamer biosensors, which typically describes aptamer

biosensors with nanomolar detection limits. Sensors with limits of detection within the micro and picomolar range exist, but these tend to be the exception rather than the norm.

Both kanamycin and tetracycline sensors showed high specificity to their targets, showing no significant response to structurally similar molecules.

Further enhancement of the sensor by gel encapsulation has shown that it is possible to prevent signal loss from extended exposure to high nuclease concentrations. However tests of electrodes exposed to high concentrations of nucleases in the absence of protection by gel encapsulation also shows significant resistance against signal loss.

Some of the well-known factors which adversely affect biosensor performance in practical applications have been listed in the Field Biosensor Section of the First Chapter (see page 66). The results would indicate that these issues have been successfully addressed with the aptasensor designs presented here, either by sample pre-treatment and/or electrode design. All these countermeasures could be easily implemented in the field, even with limited availability of resources.

Potential interfering factors	**Mitigation**
Competition by target-similar molecules	Negative control against target-similar molecules
Background Noise	Noticeable difference between background and target-bound signals
Degradation of Target	Pre-treatment (cool storage of solution sample)
Degradation of Sensor	Gel encapsulation, suitable sensor storage practices
Fouling of Electrode Surface	Sample pre-treatment (centrifugation and filtration)

Table 3.01 Potential factors affecting biosensor performance and countermeasures undertaken to reduce their effect.

Future work conducted following this line of investigation is described in the fourth chapter of this thesis, where the kanamycin and tetracycline aptamer biosensor has been merged into an automated multichannel sensing system.

Chapter 4: Automated Multichannel Aptamer Biosensor

4.01 Introduction

The previous sections of this study has established the basic functionality of the kanamycin and tetracycline aptamer biosensors, both in simple clean buffer solution and in the relatively more complex matrix of likely investigated environments. Here an attempt was made to increase applicability of the aptamer biosensor system by increasing the sampling range of the sensor and decreasing the operational steps of the sensing requiring human intervention. The ultimate aim of which should be a more versatile sensor setup with decreased operational human-hour requirement.

4.02 Type 2 Automated Sampling Platform

Decreasing the steps requiring human intervention was achieved largely through the fabrication and integration of an automated sampling platform into the sensing device.

The Type 2 Automated Sampling Platform (T2ASP) was developed directly from a RepRap type 3D printer. The electronics and hardware components of the 3 axis robot was largely retained, since the mechanical functions of a 3D printer and a mechanical automatic sampler share similar purposes, namely the movement of an effector head (an extruder nozzle in the 3D printer, a sampling tip in the case of the autosampler) to a desired location over an area of activity (a printing plate for a 3D printer, a sampling surface for an automatic sampler). Details regarding the design and fabrication of the automatic sampler can be found in the methodology section.

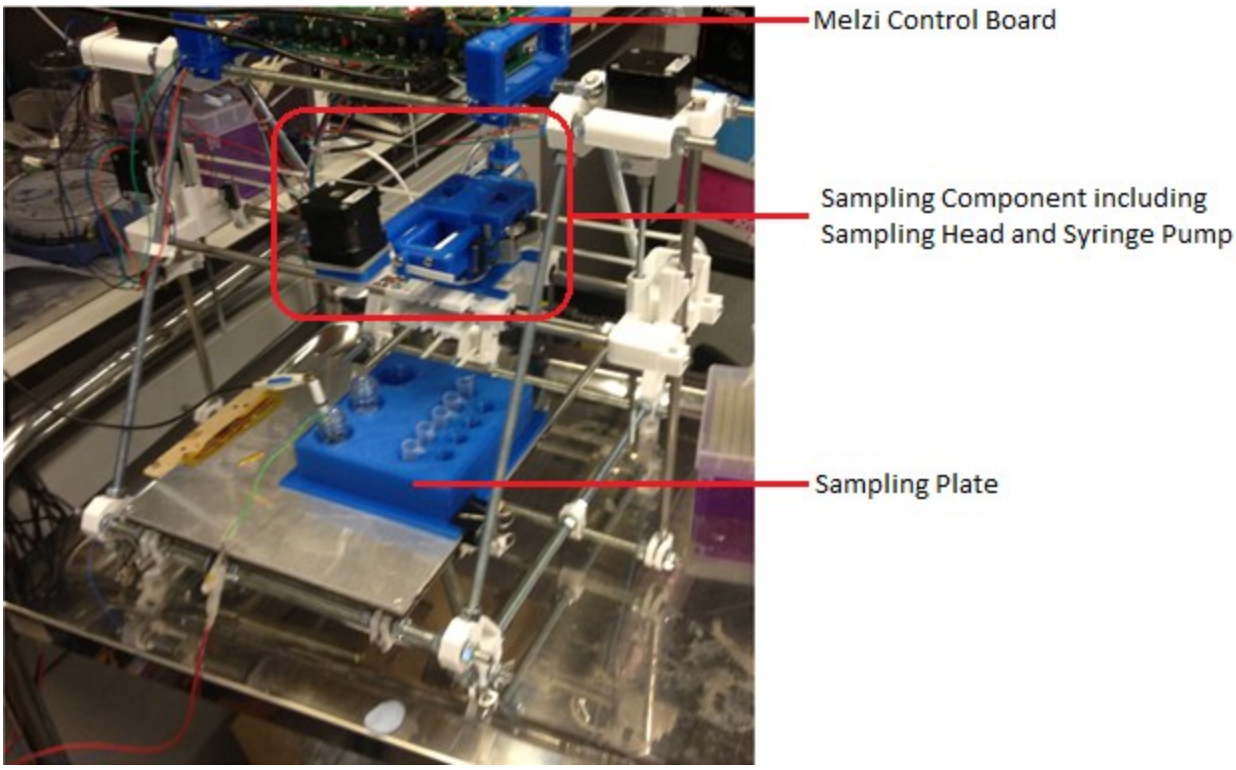

Fig 4.01 Early T2ASP being used to conduct electrochemical assay of ferrocene control.

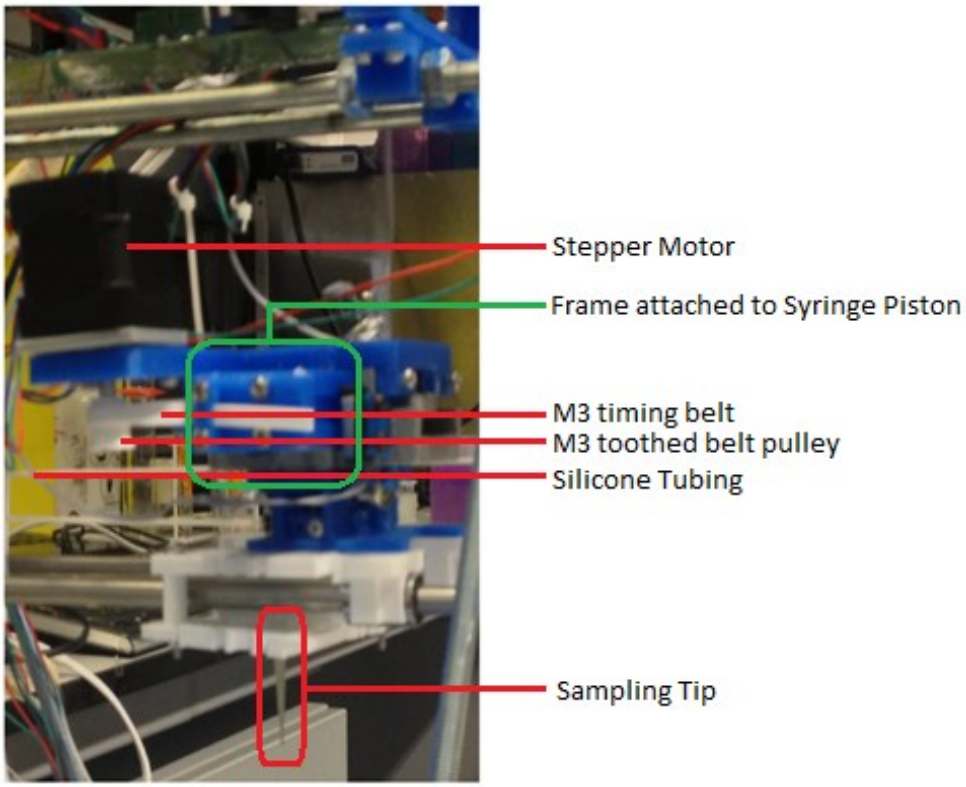

(left) Fig 4.02 The sampling component, composed of a syringe pump and sampling head.

The above displayed model uses the same sampling head as the autosampler used for the multichannel aptamer biosensor, and largely similar operational layout. This device could be considered more complex than those used in the final multichannel aptamer biosensor experiment, with a 3 axis movement capability (it utilizes both the X and Y axis of the 3D printer). Control scheme is much more complex (perhaps unpractically so) utilizing two Melzi control boards, one controlling the 3 axis scaffold and one controlling the sampling pump, and controlled by two time synchronized software interfaces. In the final multichannel sampler, only one Melzi control board is used, controlled with one interface.

4.03 T2ASP Performance

In order for the T2ASP to be a successful liquid handling robot the sampler must be able to achieve its main objective, which is firstly to reliably uptake a set volume of liquid from a starting point, secondly to transport that liquid to an end point, then to eject the volume of liquid at that point.

Thus a Gcode script is written with the following feature:

1) To move from start (X0) to sampling point (X20)
2) To lower sampling tip into the well and uptake sample (Z40 to Z10)
3) Raise sample head height to clear the sample well (Z10 to Z40), move to sample release point (X 70).
4) Sample head is lowered (Z 40 to Z 10) and liquid is released to a pre-weighted measuring boat.

The measuring boat is then weighted on a Sartorius balance, weight difference indicating the volume of pumped liquid. Liquid used in entire process was MilliQ water.

A trial run was conducted prior to mass testing (results not included). Two key errors were noticed on these runs. Firstly small amounts of liquid may be lost during transportation (step 3) by dripping from sampling tip during movement. This was resolved by adding a 1mm syringe movement step after tip is raised from sampling point, creating an air bubble between the liquid and the sampling tip during movement. The second is that the liquid ejection at release point was occasionally incomplete, leaving a small droplet of unreleased liquid at pipette tip. This was resolved by adding a 4mm air uptake stage prior to the liquid uptake stage. At the release stage the liquid is ejected followed by the air in the

cylinder resulting in the expulsion of any remaining liquid droplets via air pressure. This should minimize the volume of residual liquid within the sampling tip, thereby reducing chance of cross-contamination.

Contamination could potentially be minimized by mechanical pumping with the sampling tip in a reservoir containing buffer solution, a practice commonly used in commercial liquid handling robots. This was not implemented in the protocol described, however, as the number of sampling points is relatively small and generally results in the saturation of the first sampled biosensor (details can be found in section 4.06 and 4.07 of this chapter).

Results:

Three syringe movements were tested, 2.7mm, 5.4mm and 8.1mm, equivalent to 50ul, 100ul and 150ul. Improved Gcode were used for all runs.

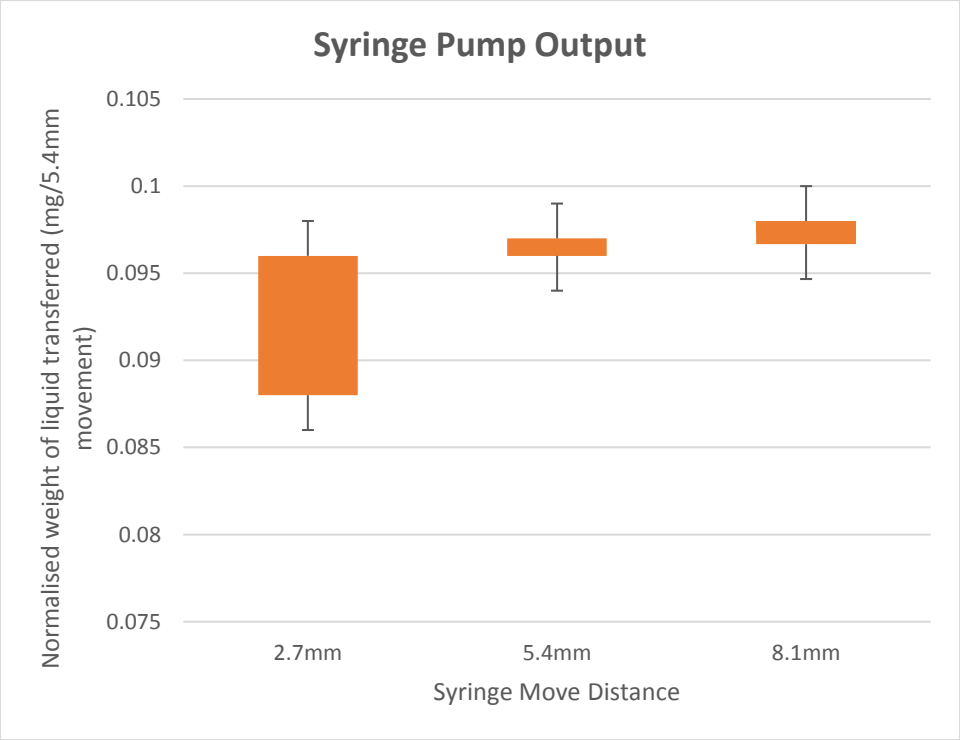

Fig 4.03 Syringe output in weight of liquid transferred per 5.4mm effective movement. This translates Gcode based movement commands into syringe movement, which should in turn determine volume pumped. Volume is measured in weight due to mode of measurement (a Sartorius scale)

In general the pump would appear to be suitable and to meet its requirements. The results would indicate that there is a loss of a relatively fixed amount of volume during each transfer. This is most

likely as a result of the stepper motor missing some steps as a result of overcoming friction on the syringe piston. Alternately this could be as a result of loss of volume during transport, either in raising or lowering sampling head or one of the lateral movement steps. No obvious liquid loss was observed in transit however.

In any case loss of volume is relatively small. Even the highest error in smallest sampling volume, total volume lost was 14ul per 100ul draw, with the average volume error for 2.7mm movement being 7.2 ul. Average volume errors for 5.4mm and 8.1mm movement are respectively 96.8 ul and 97.2 ul per 5.4mm movement, a 3.2% and 2.8% decrease from calculated volume, with the biggest deviation being 96ul per 5.4mm movement for both 5.4mm and 8.1mm results. This means a maximum difference from estimate of 4%. This compares favorably to ISO-8655 standards for a 1000ul Gilson's pipette which allow for an error of 8% at 100ul, though by the same standards a 200ul Gilson's pipette should have an error of no more than 1.6% at 100ul.

4.04 Test of T2ASP for single electrode on/off assay.

The T2ASP was tested in a single electrode assay. This test was conceived partially as a more real-operation condition test of T2ASP, and also as a pilot run for automated cell to be used in the multichannel assay.

In order to streamline the number of steps in the multichannel sensor, it was decided that a full range titration should be replaced by a single concentration on/off type titration. Sampling occurs purely by automation. Stock solution is composed of a 250uM Kannamycin solution. Pipetted volume is 100ul, creating a 5uM solution in a 5ml cell. Electrode conditions are otherwise identical to those of the laboratory condition experiments as described in the CCA section of the Third Chapter.

Kanamycin aptamer was selected as it was the most well studied conformation change aptamer available at the time. As a stirrer could not be directly incorporated into the current automatic sampler design, a 5 min wait time was provided for the solution to mix by diffusion and convection.

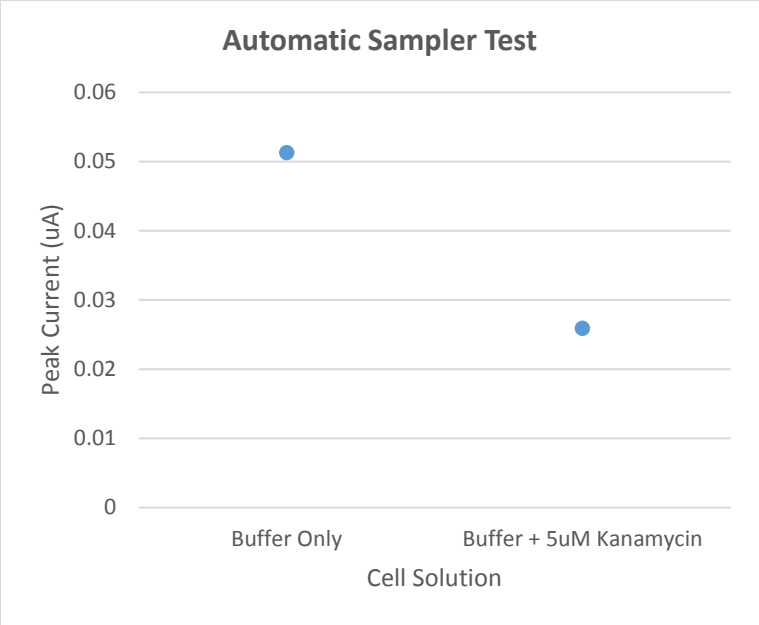

Fig 4.04 Comparison of SWV derived peak current response of Kanamycin Fcn-aptamer biosensor vs Ag/AgCl to buffer and a 5uM Kanamycin solution, used to display feasibility of automatic sampling system.

The result indicates a significant signal decrease as a result of target addition. The amplitude of the signal change between buffer and target solution is 25nA, which is somewhat smaller than the average signal change seen previously. The average amplitude change between Buffer and 5uM Kanamycinin the comparable sensor format was 47nA on average, with a range of 22nA to 72nA. The signal amplitude in the absence of Kanamycin target was which is not considered statistically significantly different from that observed previously (54nA).

Based on these results it can be concluded that migration of the Kanamycin biosensor to the T2ASP automatic sampling platform does not significantly affect the performance, and that this process could be evolved further for multi-channel testing.

4.05 Test of T2ASP for Multichannel assay against multiple test samples

Having established the functionality and reliability of the T2ASP, the sampling platform was the used in a multi-electrode assay with multiple samples. Kanamycin and Tetracycline aptamer biosensors were selected since they have been used in previous studies conducted by this project using the same electrochemical cell conditions, particularly regarding cell buffer. Thus it is known that these two

electrodes will be able to operate under common conditions. Electrode assay protocol used was the same as the T2ASP single electrode test (see above), with the exception of an additional reservoir added for a 2nd sample solution and additional cycle of SWV for added test samples.

Like the single electrode automated assay, sampling occurs purely by automation. Stock solution is composed of a 250uM Kannamycin and 6.4uM Tetracycline solution, thus 100ul of pipetted stock creates a 5uM and 128nM solution in a 5ml cell respectively.

4.06 T2ASP Multichannel Test 1

Test 1 of the multichannel assay automatically adds 100ul stock Tetracycline to buffer to produce the first and 100ul stock Kanamycin to produce the second solution.

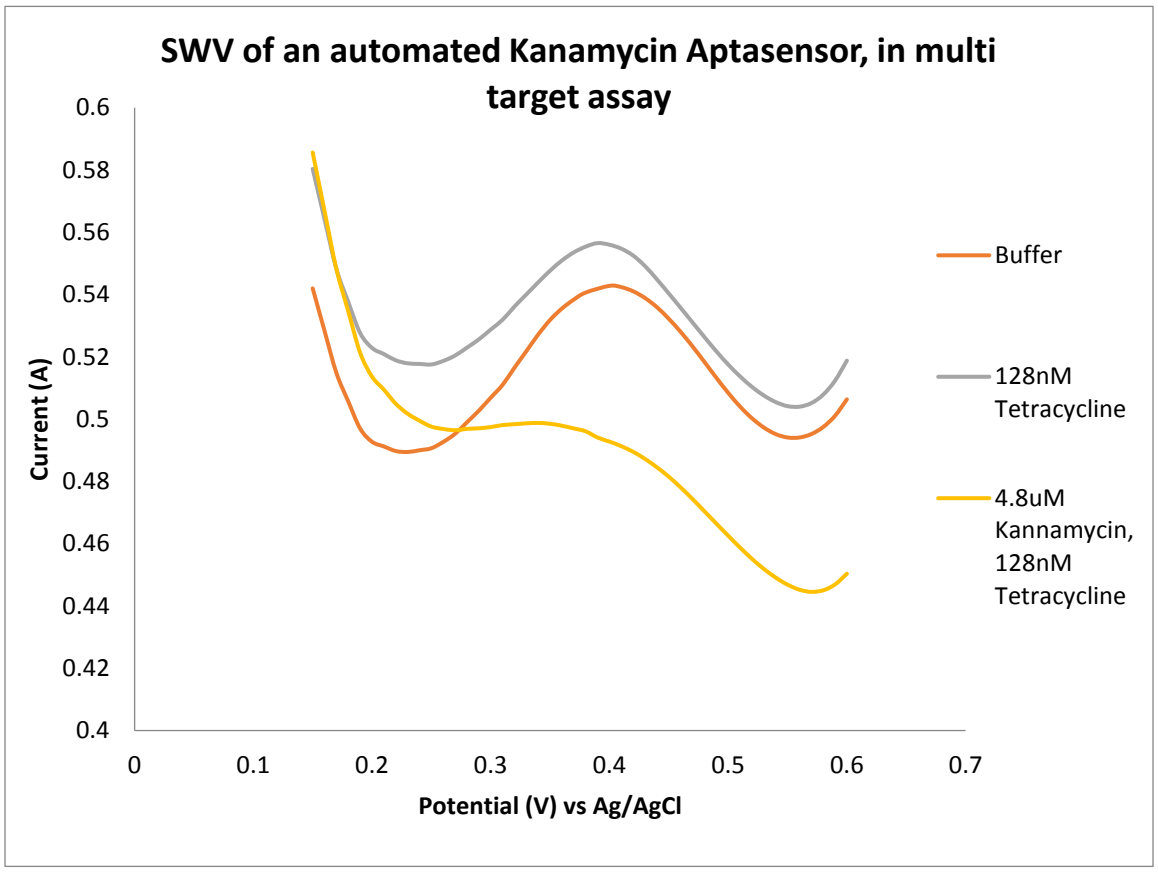

Fig 4.05 SWV of ferrocene labeled Kanamycin biosensor vs Ag/AgCl, performed in clean buffer in a multi electrode cell. First solution added results in a 128nM Tetracycline solution, Second solution added results in a 5uM Kanamycin and 128nM Tetracycline solution

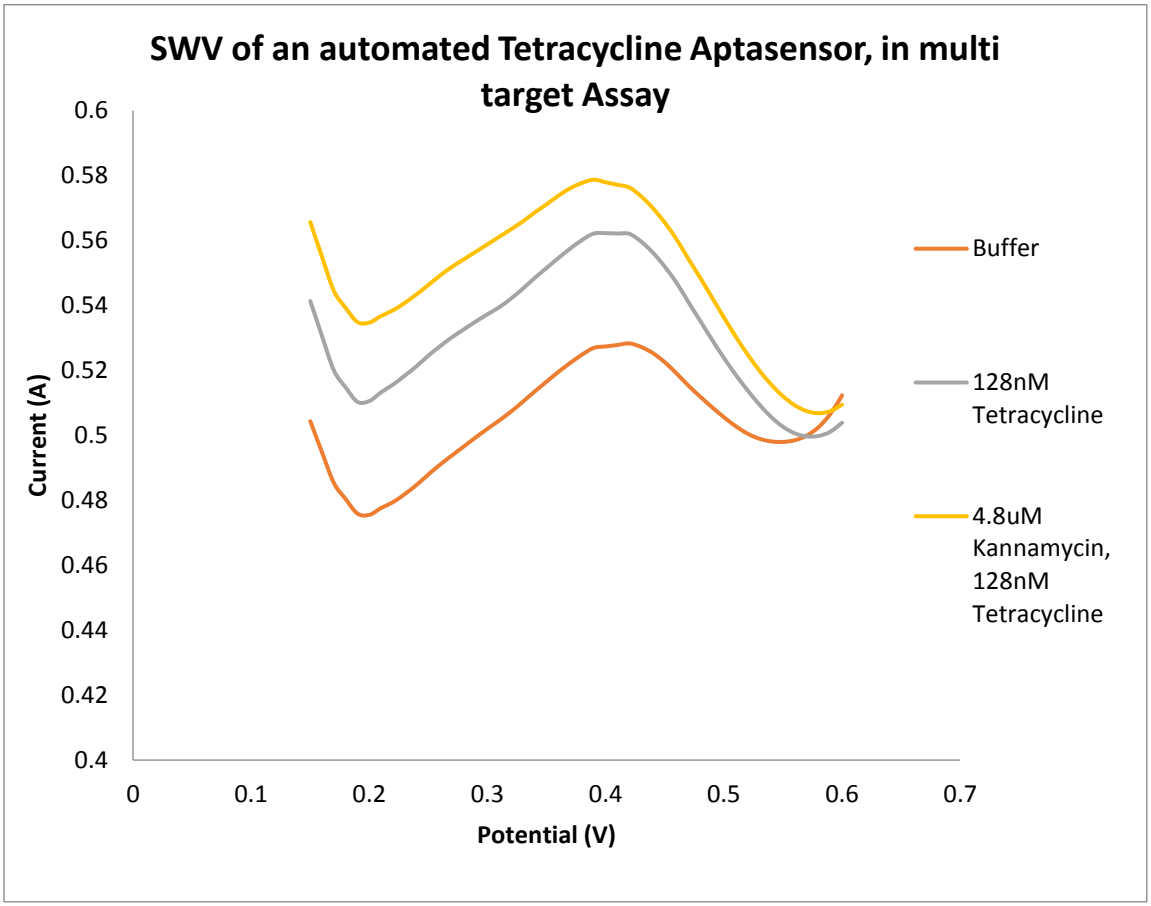

Fig 4.06 SWV of ferrocene labeled Tetracycline biosensor vs Ag/AgCl, performed in clean buffer in a multi electrode cell. First solution added results in a 128nM Tetracycline solution, Second solution added results in a 5uM Kanamycin and 128nM Tetracycline solution

The result shows a significant increase in current by the tetracycline biosensor, and an insignificant signal change by the kanamycin aptamer, as a response to addition of tetracycline solution. Conversely the result shows an insignificant response by the tetracycline biosensor, and a significant decrease in current by the kanamycin aptamer, as a response to addition of kanamycin solution. These result would indicate that the multichannel arrangement does not result in cross reaction between the sensors and that the respective sensors are still able to selectively detect their target molecule.

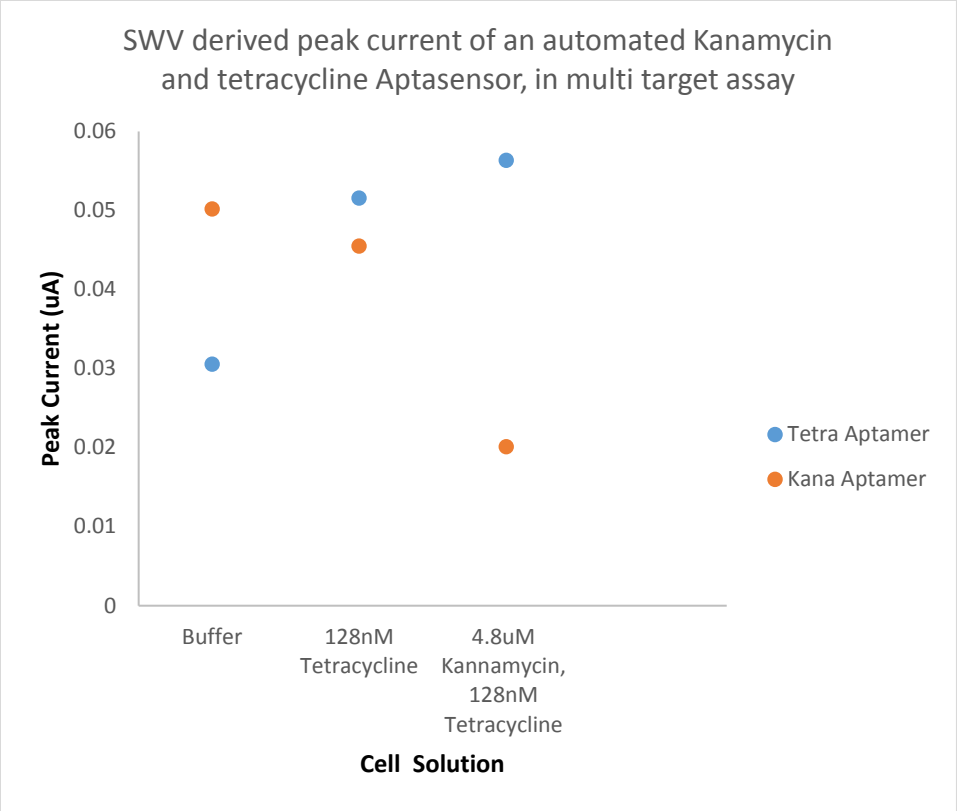

Fig 4.07 SWV derived peak current response of Kanamycin and Tetracycline Fcn-aptamer biosensor vs Ag/AgCl to a 128nM Tetracycline cell solution, and a cell solution containing both 5uM Kanamycin and 128nM Tetracycline.

A single replicate of this experimental setup was conducted, with similar results. This result can be found in Appendix H (page 309).

4.07 T2ASP Multichannel Test 2

To test whether the order of the sample addition has an effect, a second series of measurement were made in which the order of addition of samples was reversed. The results are shown below.

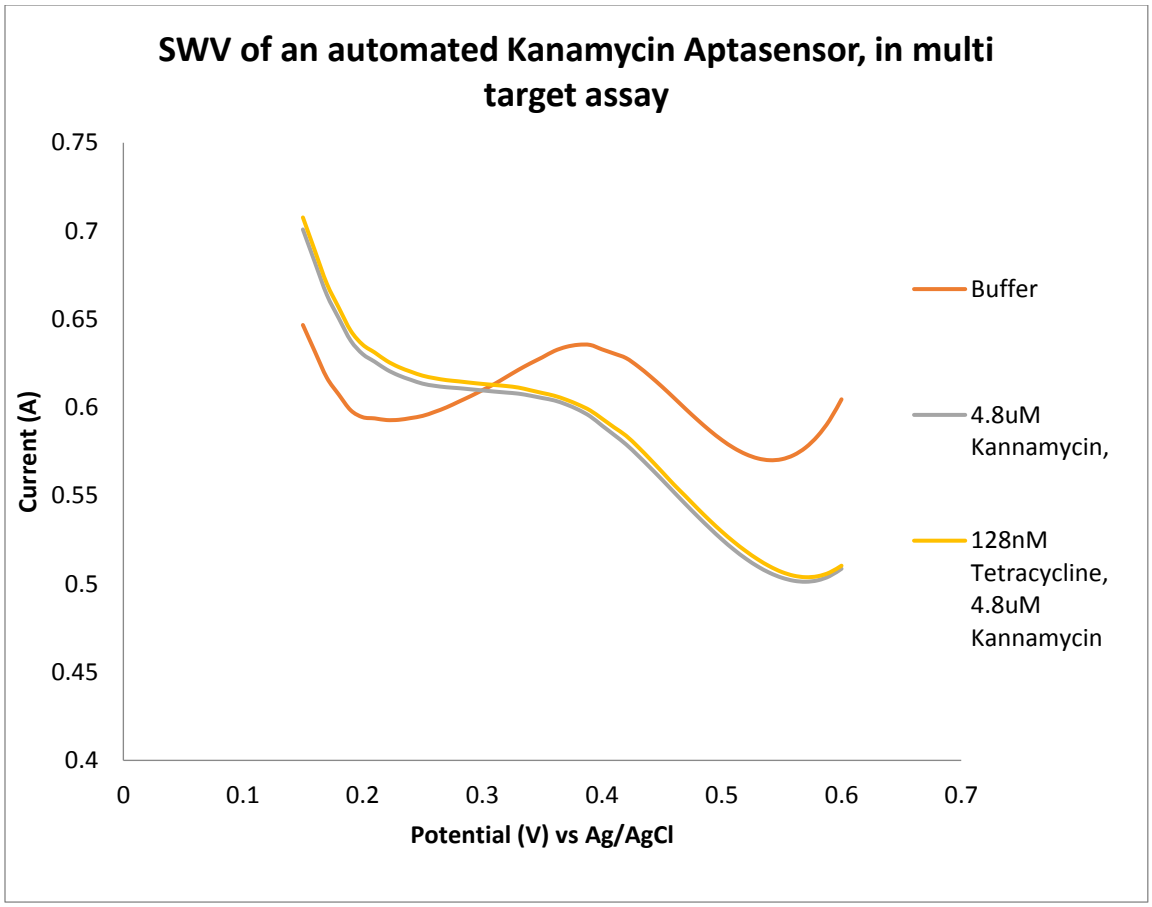

Fig 4.08 SWV of ferrocene labeled Kanamycin biosensor vs Ag/AgCl, performed in clean buffer in a multi electrode cell. First solution added results in a 5uM Kanamycin solution, Second solution added results in a 5uM Kanamycin and 128nM Tetracycline solution

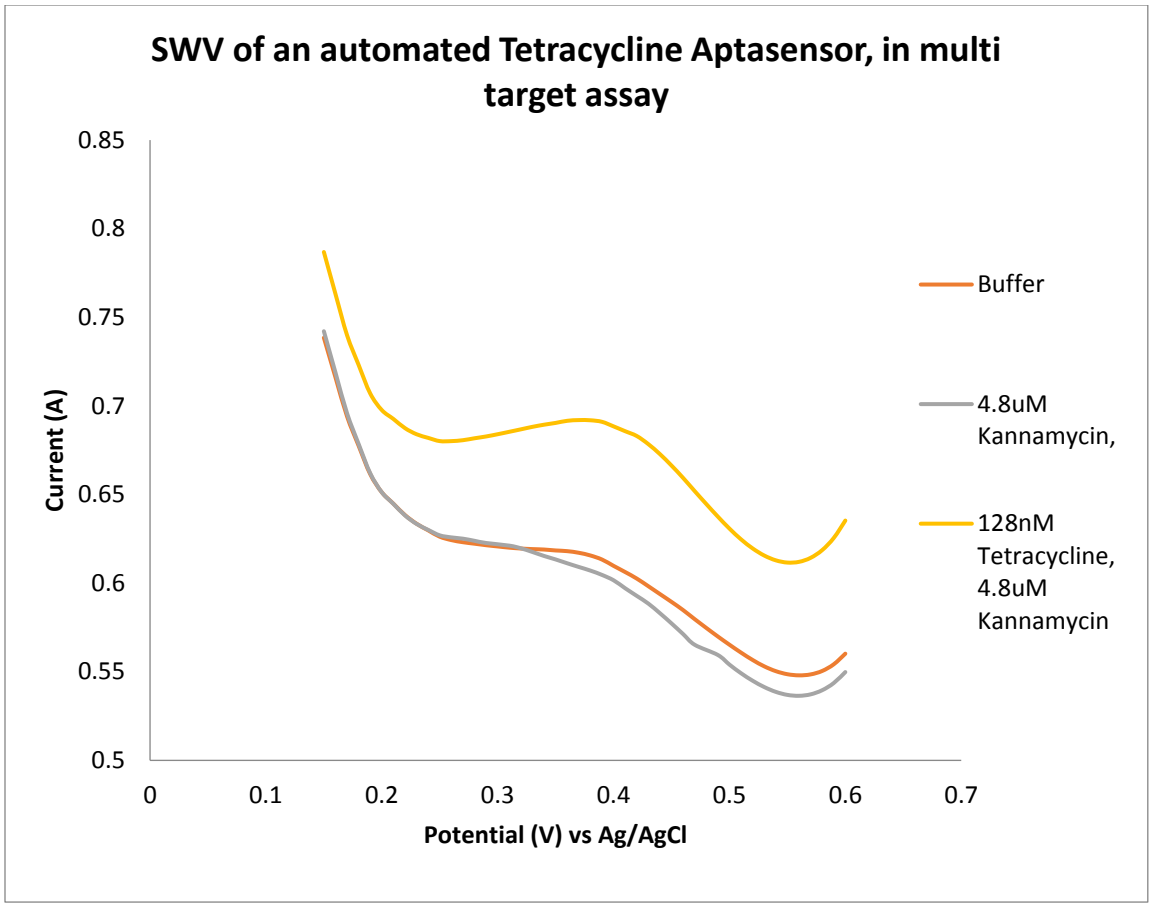

Fig 4.09 SWV of ferrocene labeled Tetracycline biosensor vs Ag/AgCl, performed in clean buffer in a multi electrode cell. First solution added results in a 5uM Kanamycin solution, second solution added results in a 5uM Kanamycin and 128nM Tetracycline solution

The result shows a significant decrease in current by the kanamycin biosensor, and an insignificant signal change by the tetracycline biosensor, as a response to addition of kanamycin solution. Conversely the result shows an insignificant response by the kanamycin biosensor, and a significant increase in current by the tetracycline aptamer, as a response to addition of tetracycline solution. These result would confirm test 1's observations, which indicate that the multichannel arrangement does not result in cross reaction between the sensors and that the respective sensors are still able to selectively detect their target molecule, irrespective of the order of addition.

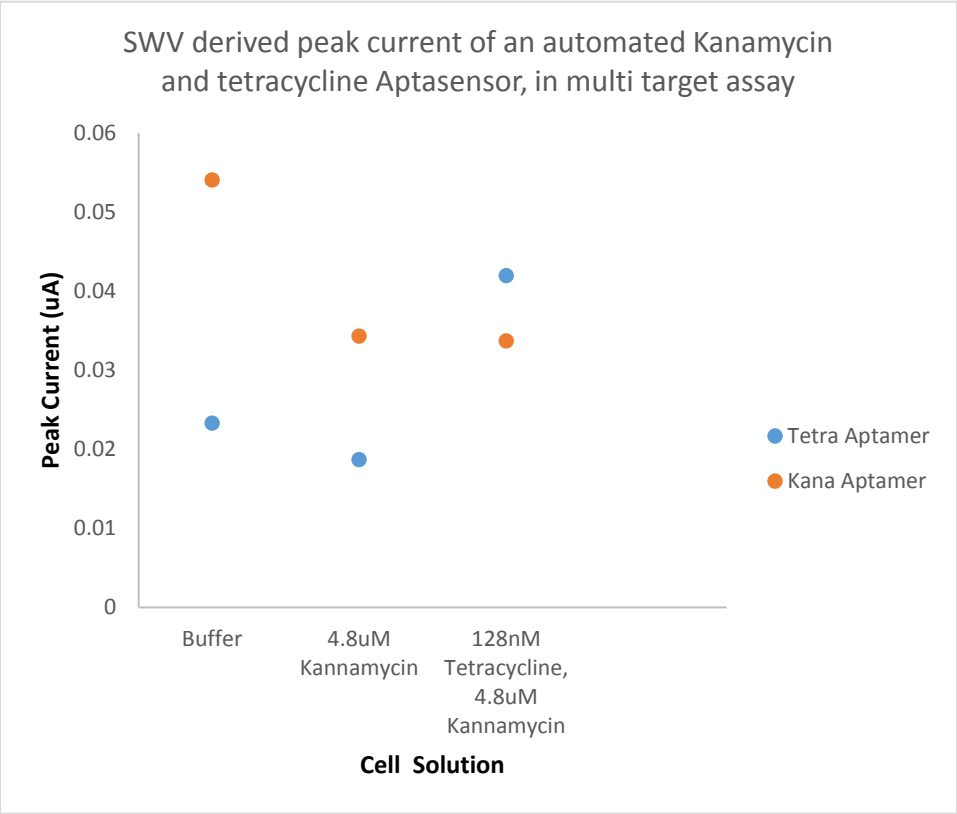

Fig 4.10 SWV derived peak current response of Kanamycin and Tetracycline Fcn-aptamer biosensor vs Ag/AgCl to a 5uM Kanamycin cell solution, and a cell solution containing both 5uM Kanamycin and 128nM Tetracycline.

A single replicate of this experimental setup was conducted, with similar results. This result could be found in Appendix H (page 309).

4.08 Additional Analysis

The results of test 2 confirm that the change in signal is not a time or non-target condition induced phenomena. The addition of target results in a significant response exclusively in the biosensor specific to that target, with much less significant response in the other electrode. Due to the specific binding properties of the aptamers discussed in their respective sections the Kanamycin aptamer could be considered Off in High, and On in Low, and vice versa in the case of Tetracycline aptamer, with the signal

being On in High and Off in low. The results of the multichannel tests can be summarized in the table below.

Electrode	Solution Compostion	Peak Current Amplitude (nA)	Signal State	Sensor State	Solution Compostion	Peak Current Amplitude (nA)	Signal Change Amplitude (nA)	Change Significant?	Signal State	Sensor State	Solution Compostion	Peak Current Amplitude (nA)	Signal Change Amplitude (nA)	Change Significant?	Signal State	Sensor State
Test 3 Tetra	Buffer	36.8	LOW	OFF	Tetra	52.6	15.8	Yes	HIGH	ON	T/K	52.3	-0.3	No	HIGH	ON
Test 3 Kana	Buffer	52.9	HIGH	OFF	Tetra	45.5	-7.4	No	HIGH	OFF	T/K	20.7	-24.7	Yes	LOW	ON
Test 5 Tetra	Buffer	30.6	LOW	OFF	Tetra	51.6	21	Yes	HIGH	ON	T/K	56.3	4.8	No	HIGH	ON
Test 5 Kana	Buffer	50.2	HIGH	OFF	Tetra	45.5	-4.7	No	HIGH	OFF	T/K	20.1	-25.4	Yes	LOW	ON
Test 6 Tetra	Buffer	15.6	LOW	OFF	Kana	16.5	0.9	No	LOW	OFF	T/K	33.9	17.4	Yes	HIGH	ON
Test 6 Kana	Buffer	58.4	HIGH	OFF	Kana	28.3	-30.1	Yes	LOW	ON	T/K	26	-2.2	No	LOW	ON
Test 8 Tetra	Buffer	23.3	LOW	OFF	Kana	18.7	-4.6	No	LOW	OFF	T/K	42	23.3	Yes	HIGH	ON
Test 8 Kana	Buffer	54.1	HIGH	OFF	Kana	34.3	-19.7	Yes	LOW	ON	T/K	33.7	-0.6	No	LOW	ON

Table 4.02 Summary of Results for Multichannel Aptamer Bosensor

The results show an off signal for both biosensors in target absent buffer. Addition of the first solution (Tetracycline solution in Test 1, Kanamycin solution in Test 2) result in On signal for Tetracycline biosensor in Test 1 and Kanamycin biosensor in Test 2 respectively and no signal change in the other electrode. Addition of second solution result in the switching on of the second electrode, Kanamycin biosensor in Test 1 and Tetracycline biosensor in Test 2.

4.09 Concluding Remarks

This study has shown that the aptamer biosensors discussed in the Conformation Change Aptamer Biosensors chapter of this thesis could be integrated into an automated multichannel system, thereby increasing the applicability of the sensors in a real world setting.

Future work conducted following this line of investigation should concentrate on diversifying the multichannel aptasensor onto other potential targets of interest. These sensor should target analytes whose detection would be beneficial in the environment investigated, such as valuable secondary metabolites for microbial product discovery, or toxic contaminants for agricultural regulation.

Another potential area for future works for CCA based systems is to test this sensor format in other environments where antibiotic detection could be useful, such as bioreactor monitoring for example. Alternatively the sensor could be tested against a more diverse range of soil and agricultural effluence samples.

While the gold disc electrode is useful for prototype sensor testing due to its simplicity, it is not amenable to scaling up for commercial scale production. Using multiple large GDEs in a multichannel array also necessitates a large electrochemical cell, which results in wastage of reagents. It may be beneficial in future works to integrate multiple biosensors into microelectrode arrays.

Chapter 5: Aptamer Biosensors based on Gold Nanoparticles

5.01 Introduction

This part of the thesis describes the development of a biosensor based on Enzyme-Linked Oligonucleotide Assay (ELONA) technology utilized as part of the affinity selection component of the SELEX process (see page 243). Two sub-types of ELONA-like biosensors were originally envisioned, based respectively on direct and indirect ELONA. Both sub-types depend on the aggregation of redox label rich Gold Nanoparticles (GNPs) at the electrode as a means of signal generation.

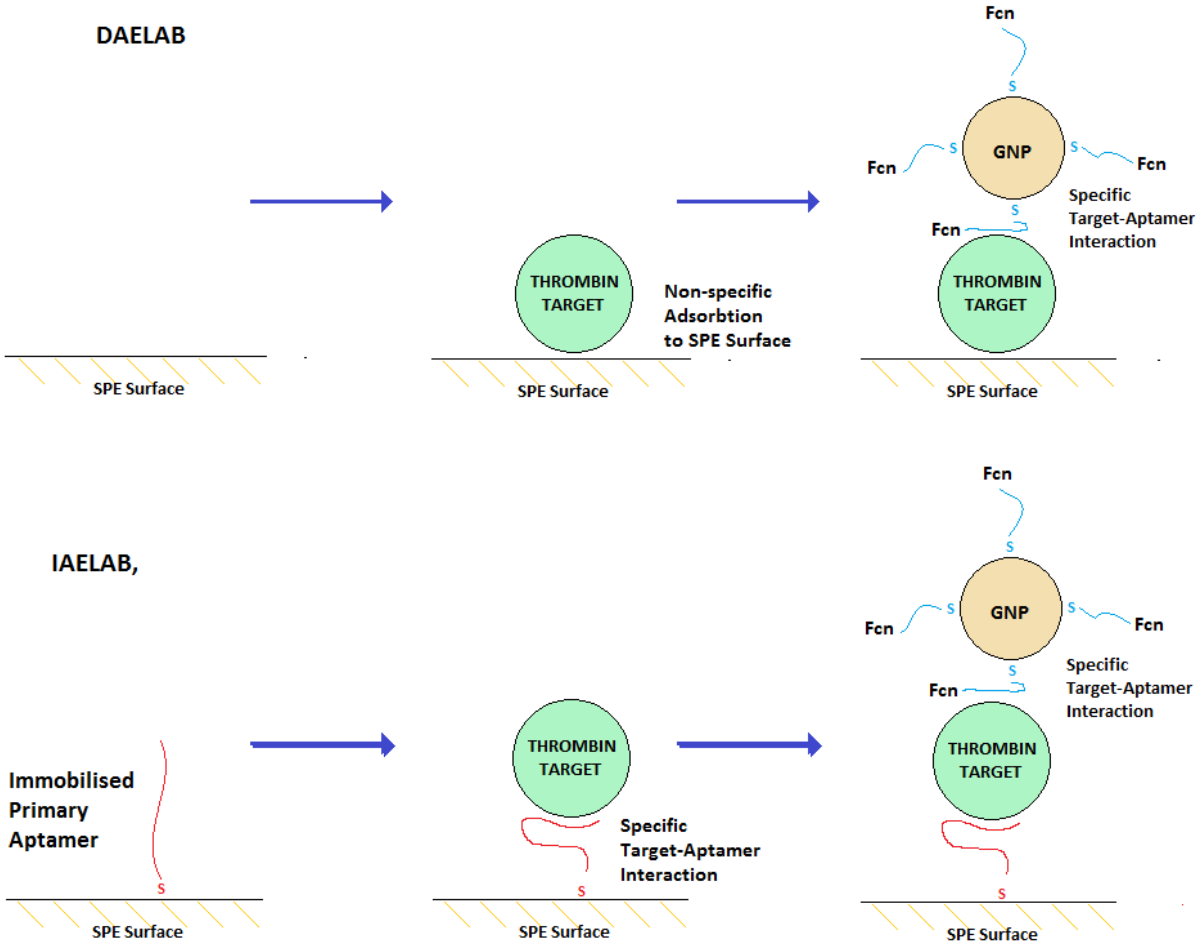

Fig 5.01 Hypothesized sensing mechanism of DAELAB and IAELAB, the sensing mechanism is described in section 5.09 and 5.10 of this chapter.

5.02 Gold Nanoparticles (GNP)

Metal nanoparticles have generated considerable interest in recent times [135] [136][137] particularly regarding their use as components of biosensors. A number of different metal nanoparticles have been integrated into biosensor systems. Nanoparticles based on metal oxides [138] and semiconductor [139] have also been investigated.

Metal nanoparticles, due to their small size, can exhibit unique properties not present in bulk material made from the same metal [140][141]. The final properties of these nanoparticles are influenced by the particle size, concentration and material of the composite nanoparticles, as well as the modifications present on the nanoparticle surface.

Perhaps the most common metal nanoparticles to be used in the field of biosensing are Gold Nanoparticles (GNPs). GNPs are most commonly used with a size range of 1nm-100nm [142], and have high surface to volume ratio compared to the bulk structures (such as a conventional gold electrode). Methods of GNPs synthesis are well researched and reproducible [90] [143], with proven consistency in inter and intra-batch nanoparticle size.

GNPs are frequently used in electrochemical sensing applications, because of their high conductivity [144], which allows relatively uninterrupted electron transfer between redox species and the electrode surface. The biosensor design explored in this part of the study seeks to exploit this property and the high surface area of GNPs in order to increase the loading of redox label at the electrode surface. By immobilizing multiple redox labeled aptamer biosensor molecules on the GNPs, it is hoped that the signal of a single target molecule-aptamer interaction would be amplified due to the enhanced mass of redox labels present. GNPs has been used successfully to increase the quality and surface area of electrode biosensors including, for example, thrombin sensing [145].

GNPs have been used in the past to provide a conductive core through which charge could tunnel to the electrode surface [142]. This is in contrast to non-conductive nanoparticles (for example latex) where electron transfer can only take place with redox label spatially located close to the electrode surface.

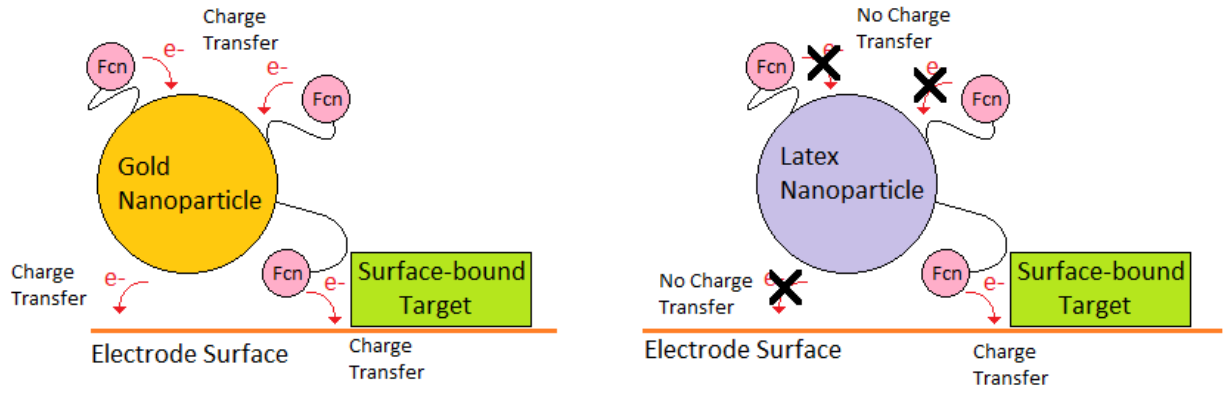

Fig 5.02 Schematic comparison of conductive and non-conductive nanoparticle sensors.

GNPs are also compatible with immobilisation of thiol modified aptamers [146], providing a short path between the redox label and the conductive GNP core.

5.03 Sensing Mechanism

Signal change is the result of change in the density of redox label at the electrode interface as a result of target-aptamer complex induced aggregation. Based on the known mechanisms of ELISA and ELONA on which this design is based [147][148], sensing mechanism occurs in two phases. For the Indirect Adsorption ELONA-Like Aptamer Biosensor (IAELAB) the first step involves the specific binding of target molecule to the electrode surface by surface bound target specific aptamer (analoguous to the primary antibody on a sandwich assay). The second step involves the specific binding of a different, GNPs bound, aptamer (analogous to the detection antibody on a sandwich assay) to the target molecules immobilized at the electrode interface (see fig 5.01 above). This aptamer contains bioconjugated redox label, allowing it to generate electrochemical signal at electrode interface. This is in contrast to ELISA and ELONA, which typically uses HRP or similar enzymes as signal amplifier.

Therefore in IAELAB the function of the primary aptamer is to enhance the target affinity and specificity of the electrode surface, thereby effectively increasing the concentration of target molecules at the electrode interface. The concentration of ferrocenated, GNPs bound, detection aptamer which binds to the immobilized target should determine the signal amplitude. The amount of immobilized target is in turn dependent on the target concentration, as well as its binding affinity to and the number of primary aptamer molecules at electrode surface (see Section 3.03 of the 3rd Chapter, page 93). Thus both sensor

molecules affinity for the target molecule play a role in signaling. Without the immobilized aptamer the target may not be bound sufficiently tightly to electrode surface, to be retained during the wash, resulting in a low surface concentration.

The Direct Adsorption ELONA-Like Aptamer Biosensor (DAELAB) is similar, but the first step involves the direct adsorption of target molecule to electrode surface.

5.04 Thrombin Aptamers TBA and HD22

The IAELAB format requires a pair of aptamers that bind the target at different sites on the molecule. The best established example of this are thrombin binding aptamers. The aptamer sequence selected for immobilisation on GNPs is the 15 bp long TBA aptamer sequence originally published by Bock et al [149]. The SPE side aptamer is the 29 bp long HD22 aptamer sequence originally published by Tasset et al [150].

TBA

5'-GGTTGGTGTGGTTGG-3'

HD22

5'-AGTCCGTGGTAGGGCAGGTTGGGGTGACT-3'

Fig 5.03 Published sequence for selected thrombin binding aptamers.

The TBA sequence selected was adapted for binding to gold by the addition of a C6 mixed disulphide group at the 5’ end of the sequence and for bioconjugation with ferrocene carboxylic acid through an amine group at the 3’ end as shown in fig 5.04.

Since the HD22 is also immobilized onto gold it too needs to be modified with the mixed disulphide group at the 5’ end. An amine group was added to the 3’ to increase the versatility of this aptamer should additional functionalization be required (e.g. by the addition of a fluorophore).

TBA, disulfide and NH_2 modified (pre-bioconjugation with ferrocene carboxylic acid)

5'-C_6H_{13}-S-S- GGTTGGTGTGGTTGG -*NH_2*-3'

TBA, disulfide and ferrocenyl modified (post-bioconjugation)

5'-C_6H_{13}-S-S- GGTTGGTGTGGTTGG -Fcn-3'

HD22, disulfide and NH2 modified

5'-C_6H_{13}-S-S- AGTCCGTGGTAGGGCAGGTTGGGGTGACT -*NH_2*-3'

Fig 5.04 Finalised Thrombin Biosensor Sequences.

These two sequences have been extensively studied [151][152][153], including the 3D structure of the aptamer-target interaction [154][150]. HD22 and TBA do not share a common target binding site, so it is unlikely that competition for binding site will take place, which is important for IAELAB. Further evidence of this is that HD22 and TBA when dimerised, through a linker, display an avidity effect resulting in significant increase in binding [155] to Thrombin. Due to the extensive literature already available on these two aptamers as well as the fact that, unlike the conformation change aptamer, this mode of sensing does not rely on detailed knowledge of aptamer structure, no further study by modeling was deemed necessary.

5.05 Negative Control Selection

Two negative controls were selected for the assays, these being bovine serum albumin (BSA) and lysozyme. BSA was selected due to its high concentration in most the likely sample of a practical human thrombin biosensor, which is blood plasma in a biomedical sensor setting. Lysozyme was selected due to its highly positive charge, which should result in significant non-specific affinity to negatively charged DNA bioreceptor molecule. Thus the lysozyme titration would represent a good worst case scenario for non-specific false positive results [156].

5.06 Determination of success of Bioconjugation Process and Confirming the Electrochemical Characteristics of Ferrocene

Unlike conformational change aptamer biosensor, thrombin aptamer was purchased without pre-attached ferrocenyl group. These control experiments were conducted in order to determine the success of the process of bioconjugation, as well as to confirm the utility of ferrocene as a redox label. A complete sensor tip containing sensing surface immobilized on a gold disc electrode was set up in an electrochemical cell, and SWV was conducted in a manner similar to that used for conformational change biosensor process.

Five electrodes, each containing different oligonucleotides immobilized on the surface, were tested. First an electrode with immobilized NH_2 capped thrombin aptamer was tested to provide a baseline for an electrode with a self-assembling monolayer of DNA but in the absence of a redox label; this acts as label-free negative control. The second electrode had thrombin aptamer bioconjugated with Ferrocene carboxylic acid using the method provided in the methodology section. For comparison electrodes with commercially supplied ferrocene conjugate kanamycin and tetracycline aptamer were used. The fifth electrode is blank electrode.

Special care was taken to ensure all electrodes used in this test had been extensively rinsed in order to remove any oligonucleotide sequences not covalently bonded to the electrode surface.

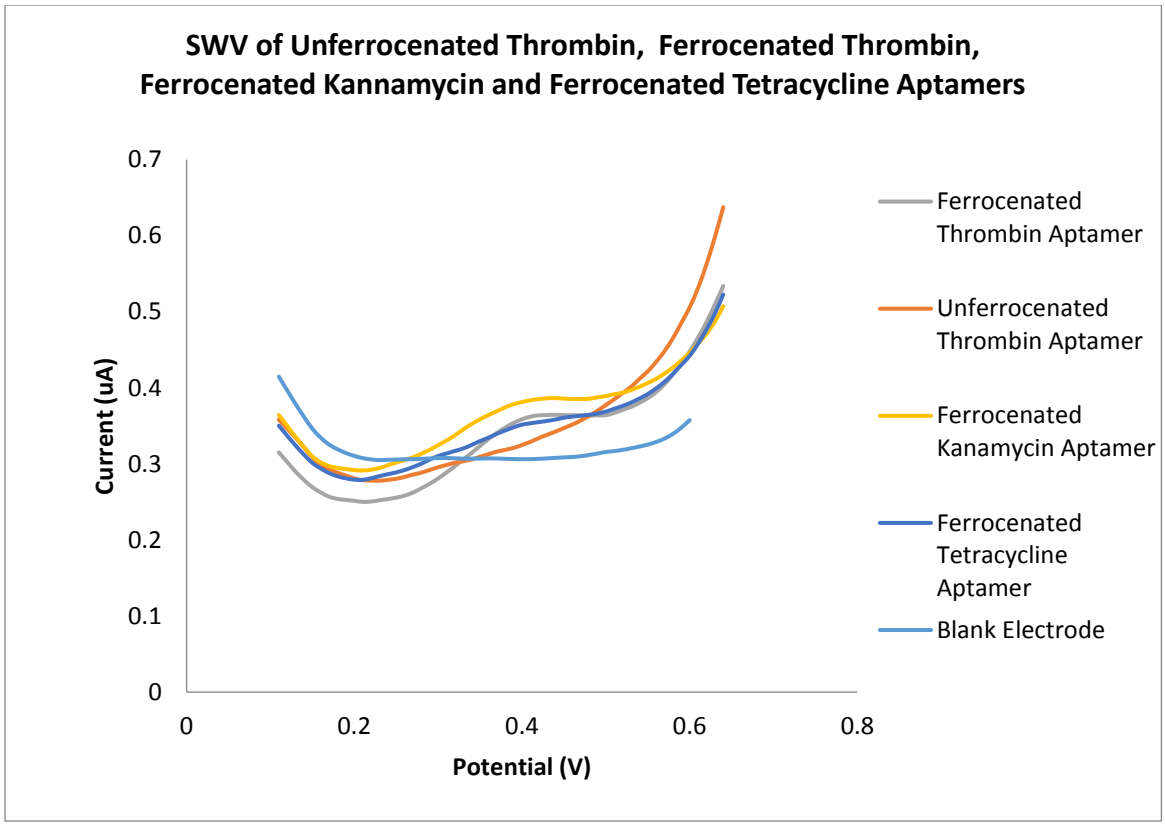

Fig 5.05 SWV of ferrocene labeled biosensor and control electrodes vs Ag/AgCl, in under target-free (buffer only) conditions.

A voltammetric peak was clearly observed at in all the ferrocenated aptamer electrodes. Since no other peaks of similar magnitude were noted within this potential scan range, and the peak being sufficiently close the literature value, it is concluded to be the ferrocene peak.

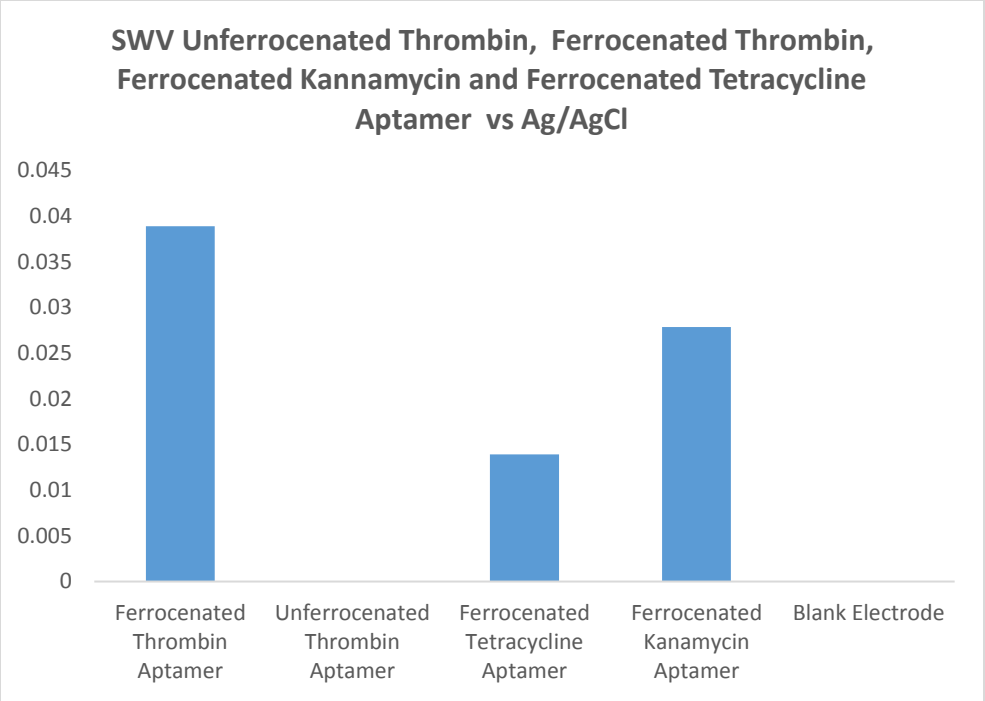

Fig 5.06 Peak current amplitude of the biosensor and control electrodes in buffer vs Ag/AgCl

Peak magnitude is within the same order of magnitude as those of Ferrocenated Kanamycin aptamer in resting (unbound) state. Our study of conformation change aptamer show that electrodes could display considerable variation in maximum signal amplitude, most likely as a result of quality of electrode polishing. Comparison of thrombin electrode signal to tetracycline aptamer in its resting state shows significant difference in signal magnitude, though this comparison would perhaps be less useful than a comparison of the signal of thrombin aptamer to a target saturated tetracycline biosensor electrode (which is in its maximum signaling state).

5.07 Characterizing Synthetic GNPs

In order to determine the uniformity in shape and size of gold nanoparticles, samples were observed in a transmission electron microscope (TEM).

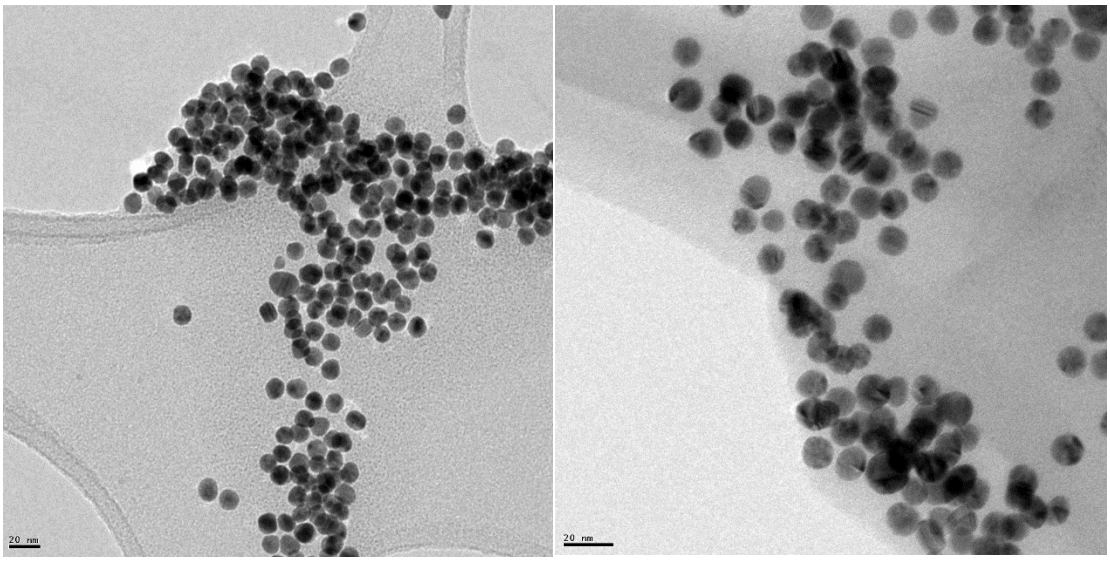

Fig 5.07 Transmission Electron Micrograph of GNPs particles fabricated using the Frens Method

By measuring several samples of GNP using TEM, the average size of GNP was determined to be 10.2 nm, with fewer than 1% of the particles being outside the 9-11 nm range. The shape of the nanoparticles appear to be uniform enough to be utilized in aptamer coated GNPs production.

The GNPs were also observed by UV/Vis spectrophotometry as the wavelength of the absorbance maximum depends on the particle diameter and the absorbance peak magnitude on the concentration. Spherical GNP with particle size of <40 nm is well studied to have absorbance peak at close to 520nm [157].

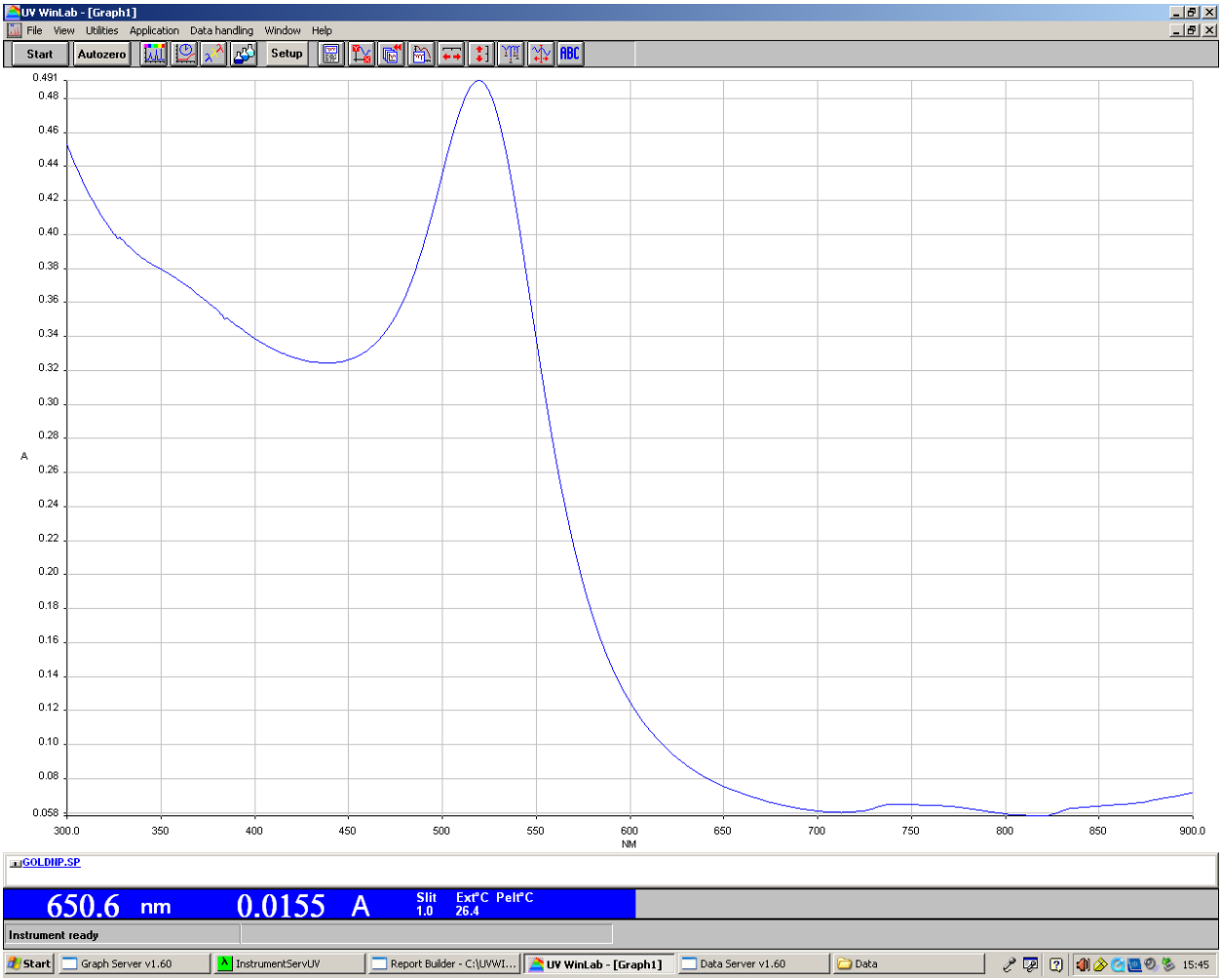

Fig 5.08 UV/Vis spectrograph of bare GNPs particles fabricated using the Frens method [90].

The result of the UV/Vis spectrograph would indicate that GNP within the correct size range has been successfully synthesised.

5.08 Determining the Presence of Aptamer on GNPs

Dynamic Light Scattering (DLS) is a technique for measuring the hydrodynamic radii of particles in the submicron region by measuring the change in the intensity of scattered light as a result of the influence of Brownian movement on the drift of particles. The larger the particle, the slower the Brownian motion. The diffusion coefficient measured by DLS does not depend solely on the size of the particle core, but also on the co-transported mass (such as for example the double layer which forms on any charged surface in liquid) on the surface of the investigated structure, as well as the concentration and type of ions in the medium. This combined size is known as the hydrodynamic diameter. This results in a measured hydrodynamic size larger than the actual GNPs core.

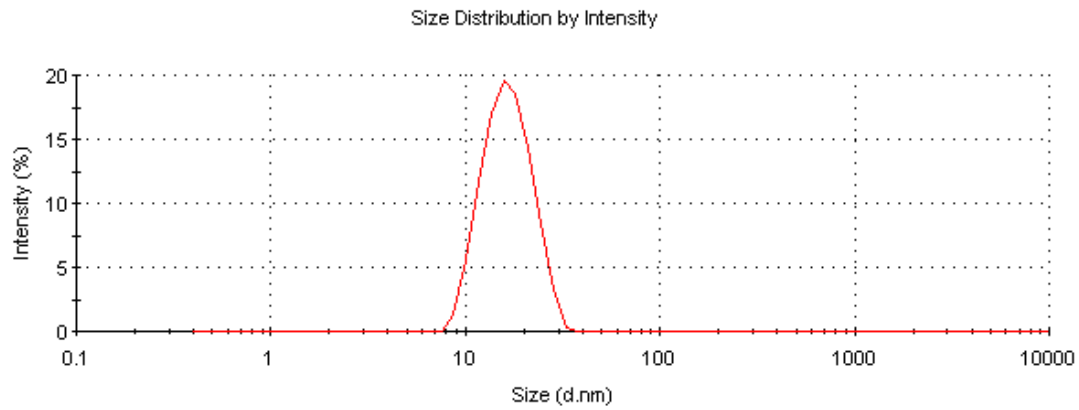

Fig 5.09 DLS results for bare gold nanoparticles

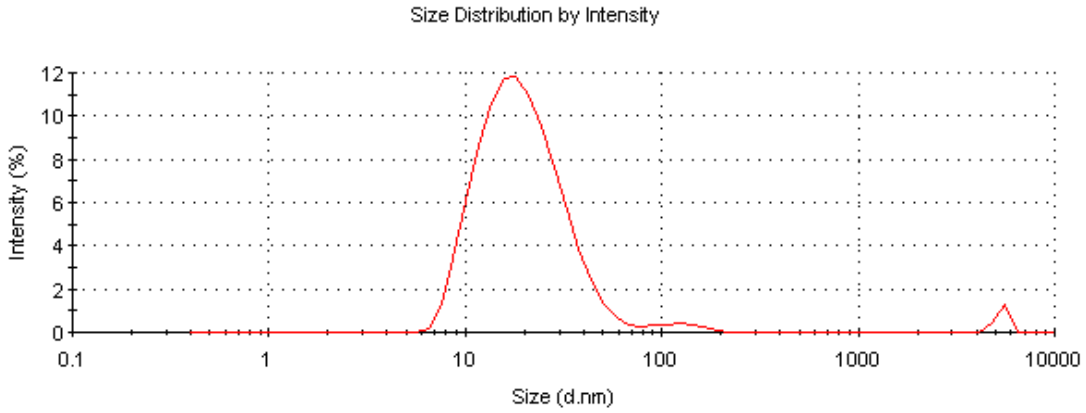

Fig 5.10 DLS results for aptamer coated GNP

The results show a noticeable increase in the size of the hydrodynamic radii from 15.6 to 19 nm, which supports the assessment that the gold nanoparticles have been successfully loaded with aptamer. An increase in the size distribution suggests greater variation of particle sizes.

There is a considerable difference between the radii of the unmodified GNPs determined by TEM and DLS. This could be explained by the presence of the hydrodynamic layer, which would be detected by the DLS but not the TEM. The significant change in DLS measured diameter could also be the result of an organic layer formed during citrate dependent GNPs synthesis such as the Frens method. Further, the

DLS method of data analysis is dependent on the particle model, and may therefore generate anomalous results if the model is not a good representation of the actual particles being measured.

Another method for determining successful DNA immobilization on GNPs is through UV/Vis spectrophotometry.

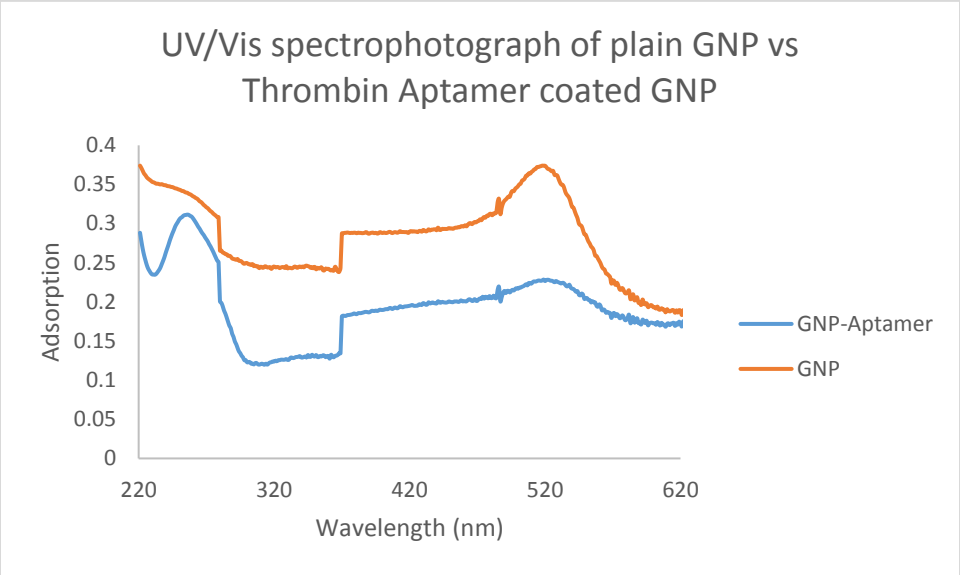

Fig 5.11 UV/Vis spectrograph comparing DNA enriched and bare GNPs particles. The "drop" located between 340 to 380 nm is due to a filter change in the spectrometer.

Both GNPs and DNA-GNPs displays a clear peak at 550nm as a result of GNPs's contribution to solution adsorption. This peak is more pronounced in the original sample than in the DNA-GNP sample. This was expected since the dilution factor of the DNA-GNPs is at least 250% greater than of the original GNPs sample (the resuspension ratio is typically 250ul for every 100ul original GNPs solution), and it is almost certain that some loss of GNPs would have occurred as part of the immobilization process (either due to adhesion to surfaces or loss with supernatant).

However the DNA-GNPs shows a significantly more pronounced peak at 260 nm as a result of DNA's contribution to adsorption, which would support the conclusion that significant DNA is present in the DNA-GNP sample. Peak at 260 nm for the original GNPs sample is very small compared to the height of the 260 nm peak of the DNA-GNP sample.

In order to prove that the DNA mass in the DNA-GNP sample has been successfully immobilized onto the GNPs and not simply present in the solution, the DNA-GNP is spun down using a centrifuge. This is

should not result in the precipitation of unbound DNA along with GNPs sample, since the very short 17bp aptamer precipitation protocol requires 10000g centrifugation for at least 10 min, preceded by at least 2h (preferably 12h) incubation in 100% ethanol at -20°C. The supernatant is then extracted and sampled in a nanodrop device. The results show no noticeable concentration of DNA, which would support the conclusion that the concentration/resuspension cycles have been successful in removing unbound DNA, and that the only remaining mass of DNA in the DNA-GNP sample is bound to the GNPs surface.

5.09 Direct Adsorption ELONA-Like Aptamer Biosensor (DAELAB) results

Investigation of a target titration by SWV shows no clear correlation between observed current to target concentration. Indeed 3 out of the 4 full target titration DAELAB runs investigated yielded no quantifiable signals at all. In one instance of DAELAB, a peak was observed, but only at the highest target concentrations. A further 7 test runs were conducted at the highest thrombin concentration only (no titration below a concentration of 1000nM), two of these runs yielded quantifiable signals (peak magnitude of the three peaks were 115.5 nA, 8.7 nA and 76.5 nA. This would indicate that the DAELAB sensor is capable of detecting Thrombin at the highest concentration with a 30% reliability. Voltammograms derived from both electrode variation, one showing no signal response to concentration and one where signal is only observed at the highest concentration, is displayed in the figure below.

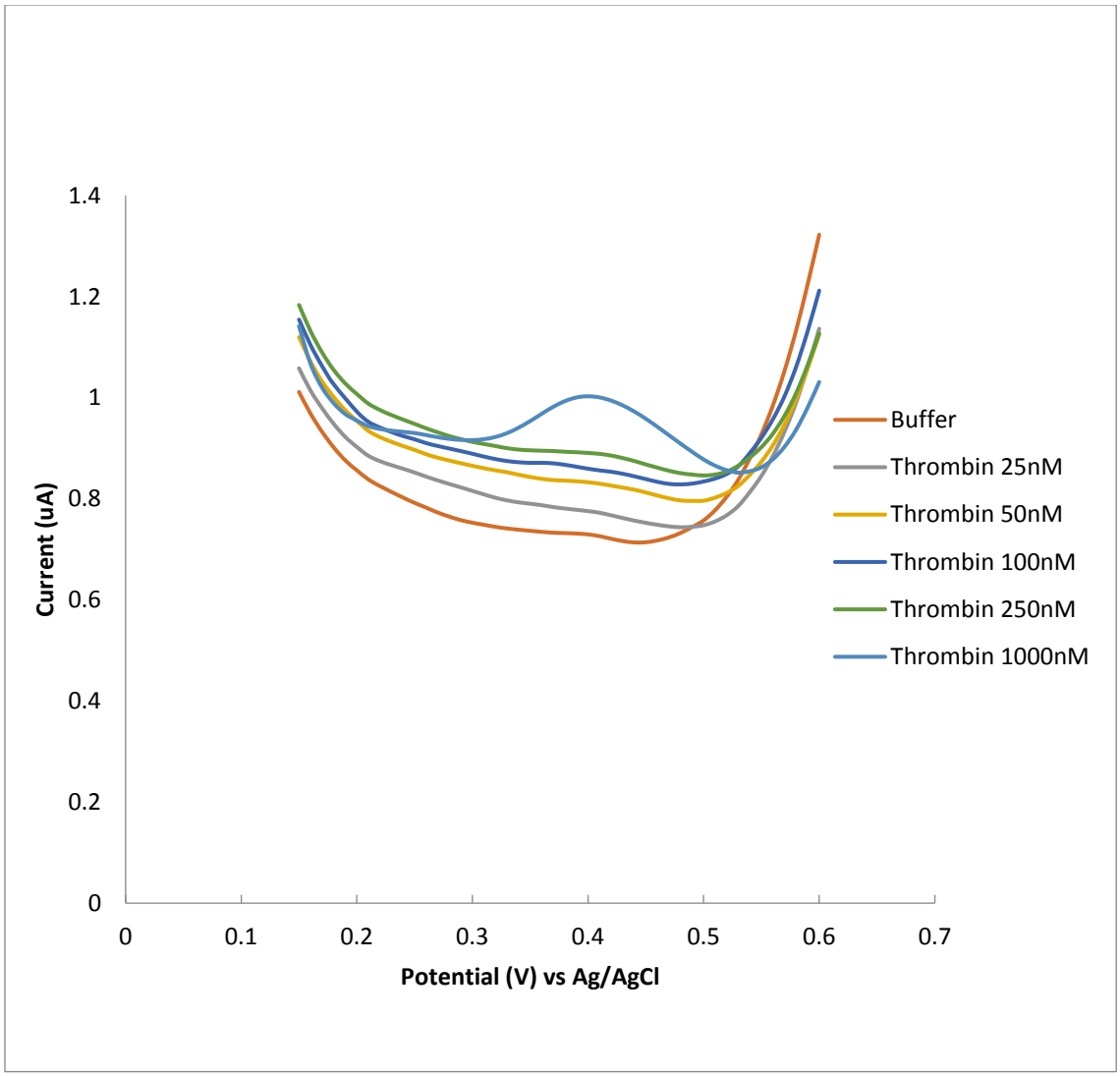
1.4
1.2
1
0.8
0.6
0.4
0.2
0
Current (uA)
0
0.1
0.2
0.3
0.4
0.5
0.6
0.7
Potential (V) vs Ag/AgCl
Buffer
Thrombin 25nM
Thrombin 50nM
Thrombin 100nM
Thrombin 250nM
Thrombin 1000nM

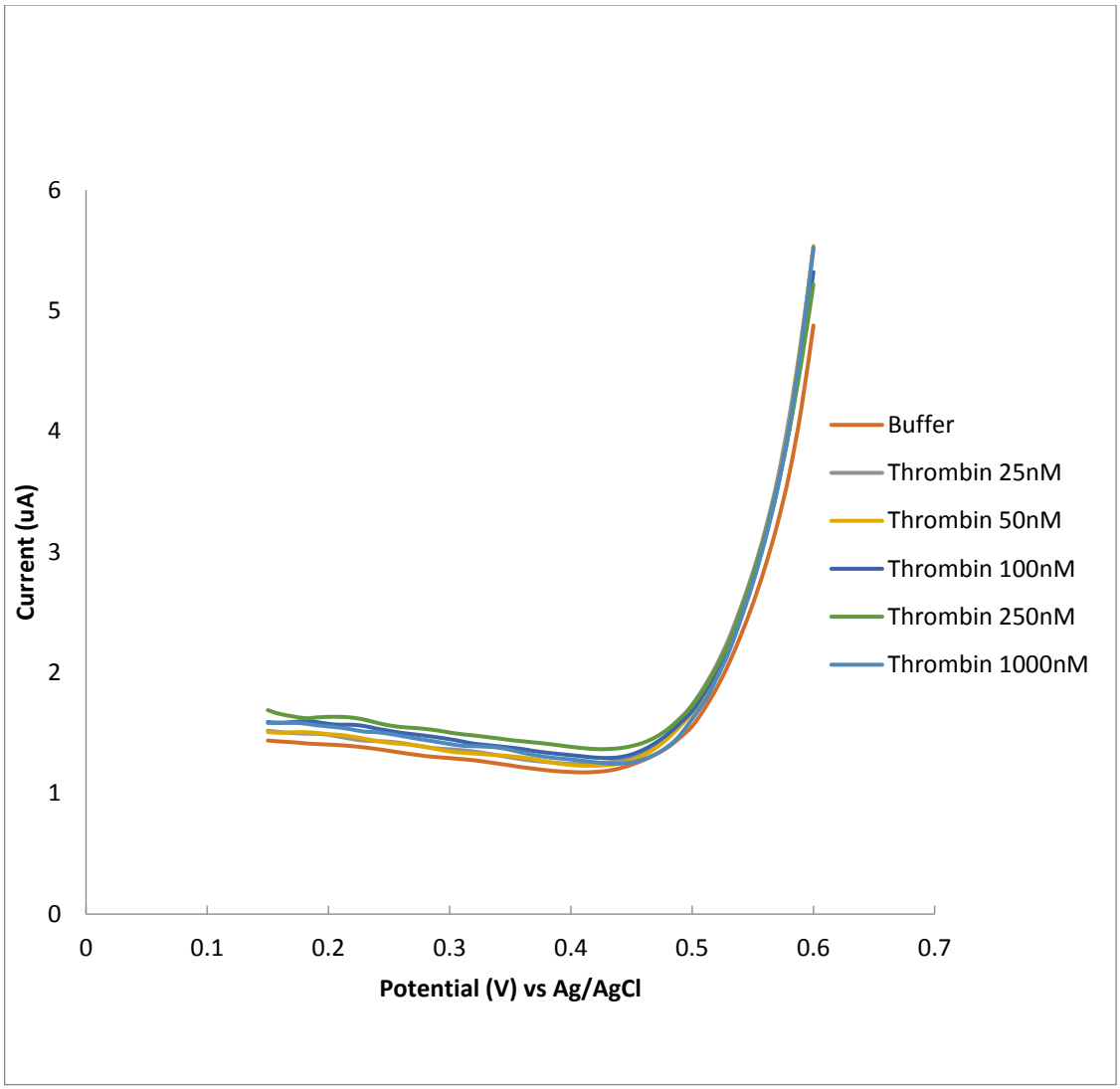

Fig 5.12 SWV of Thrombin fcn-aptamer biosensor with direct adsorption configuration (DAELAB)'s response to Thrombin titration vs Ag/AgCl, showing both observed electrode variations.

Direct ELONA (and the much more ubiquitous direct ELISA from which ELONA is developed) is considered a robust technology, and is frequently used in the determination of Kd for SELEX process. This technique has been used by this study itself to determine increase in target affinity of DNA library in the automated devices section. The success of direct ELONA proves that it is possible to bind large globular protein targets to non-specific surfaces. However in the case of using a redox label rather than an enzyme the additional constraint of the former is that it requires the label to be close to the surface. Additional factors that could result in no detectable signal include the following:

1) Differences in binding surface unrelated to the binding protocol could also have played a role in decreased adsorption. SPE surface is a gold film, microplate reader plates are usually fabricated out of polypropylene or polystyrene. This could result in a number of reasons for loss of signal. It is possible that the gold surface simply has a lower affinity for the thrombin target than the polymer surfaces. It is also quite possible that thrombin-gold interaction does not result in adsorbed molecules that can interact with the GNPs-bound aptamer. One of the benefits of IAELAB's specific adsorption of target molecule onto the electrode surface is that any target retained by this method is likely to have a relatively uniform deposition on the electrode surface, as a result of orientation of the 29 aptamer binding site towards the 29 bp aptamer immobilized at the electrode surface. Deposition of target onto the SPR surface would be harder to predict, and also potentially more random. This could result in the adsorbed molecules losing their binding sites to the 15 aptamer as a result of denaturation in the process of adsorption. Alternately gold-Thrombin direct interaction could favour an interaction which hides the 15 aptamer binding site, effectively burying it in the process of adsorption.

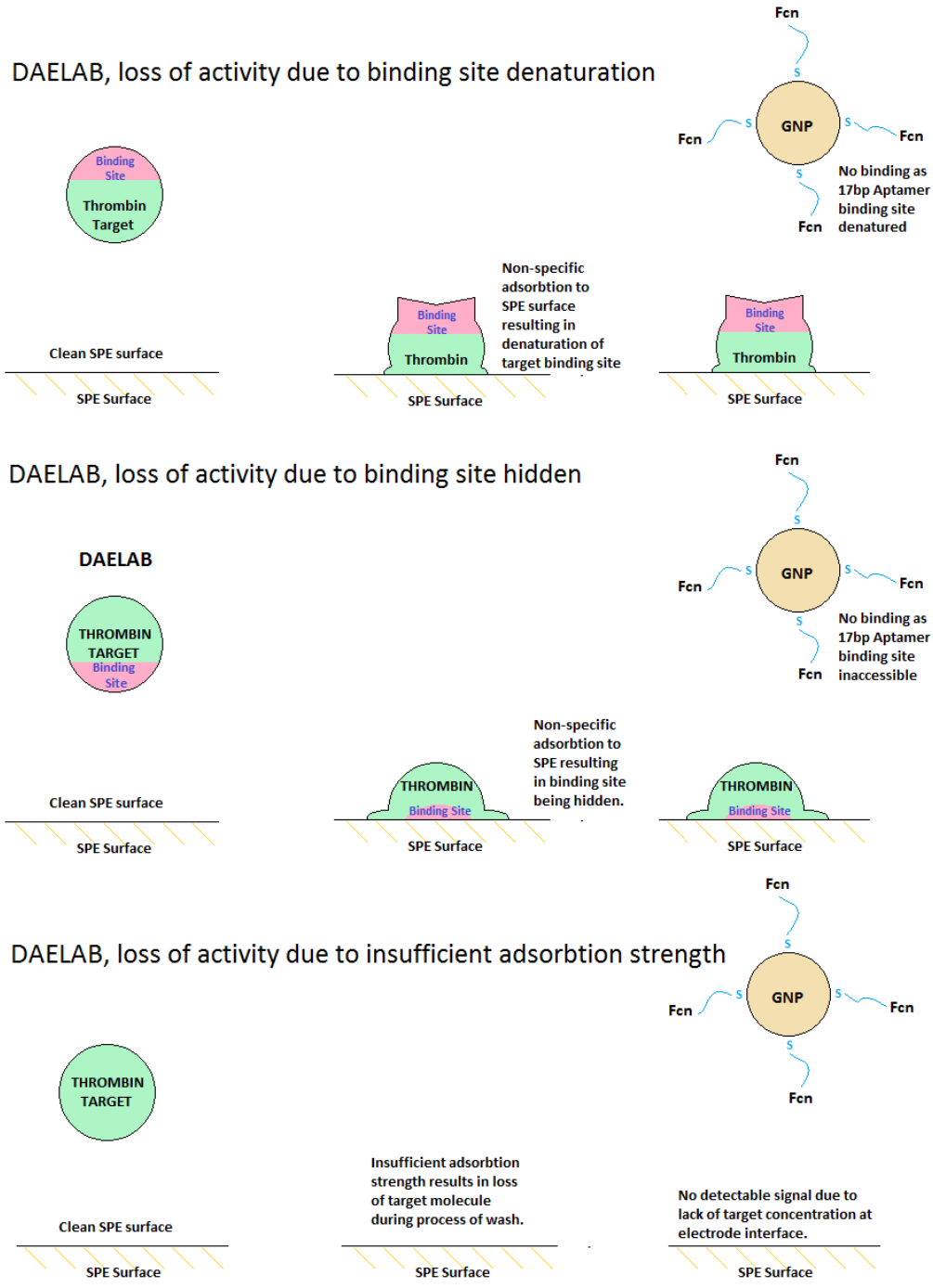

Fig 5.13 Potential causes for the failure of DAELAB sensing method.

2) Immobilisation conditions. Indirect ELONA of the protocol used in the SELEX device part of this study was optimized to facilitate adsorption. This includes immobilization temperature (4°C in ELONA vs 25°C in DAELAB), Immobilization buffer (ELONA adsorption buffer for lysozyme had same charge as target, increasing precipitation, Thrombin has a relatively net neutral charge at pH7 (compared to lysozyme, for example)) and immobilization time (12h for ELONA vs 60 sec for DAELAB).

3) In the ELONA assays a much less stringent washing procedure was used as compared to that used with the sensors.

Thus it could be concluded that the conditions of direct ELONA are not comparable to those of DAELAB. Any of the factors above could result in the loss of effective target concentration at the electrode interface. In the absence of target molecules at electrode surface after the first wash, there is a decreased affinity to the Fcn labelled GNPs, leading to the loss of redox label during the 2nd wash, resulting in decreased signal.

5.10 Indirect Adsorption ELONA-Like Aptamer Biosensor (IAELAB) results

Investigation of a target titration by SWV shows significant correlation between signal magnitudes to target concentration. The titration plot profile is typical of a conventional binding curve, with the signal drop correlating to target concentration at lower concentrations before plateauing at high concentration as the sensing surface is saturated with target molecules at high concentrations.

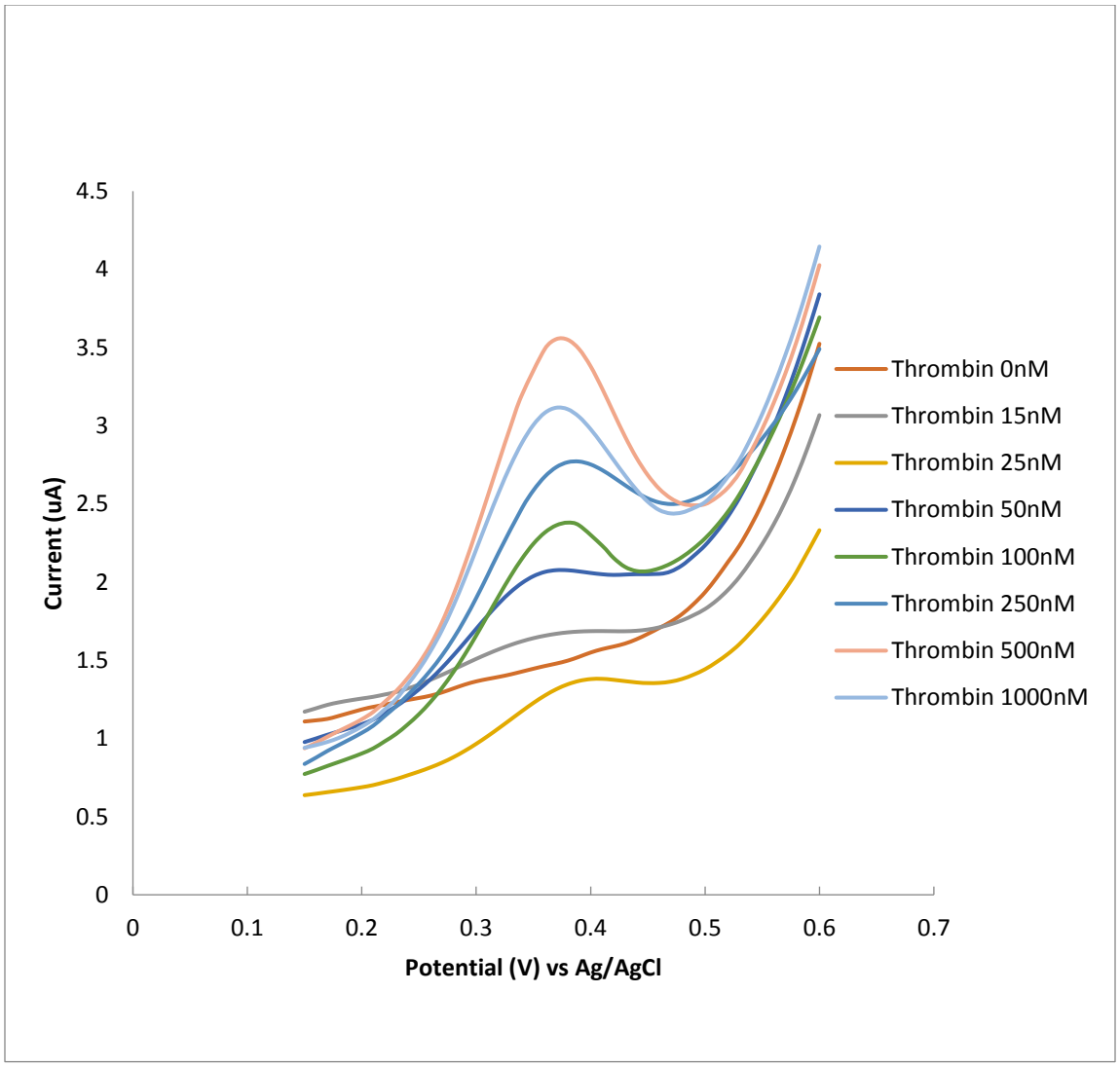

Fig 5.14 SWV of thrombin fcn-aptamer biosensor with sandwich configuration (IAELAB)'s response to thrombin titration vs Ag/AgCl

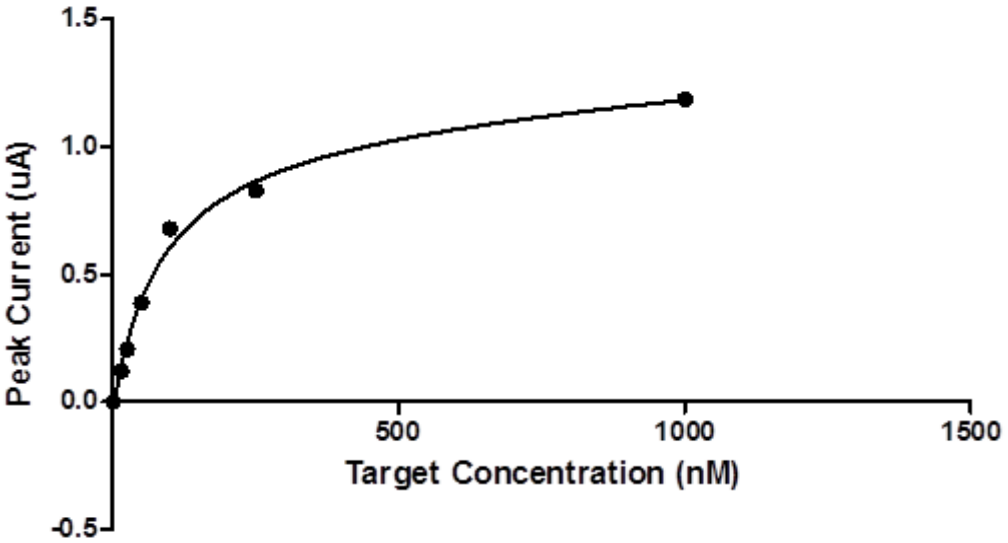

Fig 5.15 SWV derived peak current response of thrombin Fcn-aptamer biosensor with sandwich configuration (IAELAB) to thrombin titration vs Ag/AgCl. The data point at 500 nM has been eliminated as an anomalous data.

Mathematical processing using Graphpad Prism 5 Software yields an average Kd of 46.2 nM, with an upper and lower quartile values of 50.7nM and 32.2nM respectively, and a Kd standard deviation of 22.7. The reference Kd for the GNPs bound aptamers used in this assay is complicated by the popularity of this aptamer, and therefore the range of techniques used to estimate its Kd, which ranges from 2.68 to 450 nM [158].

Estimates of the Kd based on the results of this study would be within the typical range shown in previous publication for the GNPs based aptamer, but much higher than the Kd of the SPE based aptamer. It is unclear how relevant literature Kd is relative to the Kd of this experiment however, as conditions of this assay is significantly different from most Kd determination protocols. The wash step for example will almost certainly result in a decrease in signal as a result of removal of surface adsorbed particles by hydrodynamic shear.

R squared value of the data sets fit the linear regression of the one site binding – saturation, one site – total model of the prism software by >0.98 for 4 result, >0.95 for 1 result and >0.90 for 1 result.

All data sets show consistent signal increase between 0 to 100 nM. There is much less agreement in the magnitude of signals and signal trend between 250 nM to 1000 nM. Three results show a clear non-linear trend of increase between 0-150nM, followed by a linear increase between 250 to 1000 nM, five

results show an increase between 0-150nM, followed by a signal plateau between 250 to 1000 nM. These results can be found in Appendix I.

Author	Bioreceptor molecule	Sensor Format	Sensing Mode	Detection Limit	Reference
IAELAB	Aptamer	Induced assembly configurational aptamer biosensor	Electrochemical	15 nM	
Liu et al	Aptamer	Induced assembly configurational aptamer biosensor	Optical	89 pM	[159]
Xiao et al	Aptamer	Conformation change aptamer biosensor	Electrochemical	6.4 nM	[160]
Li et al	Aptamer	Induced assembly mediated retainment of transducer enzyme	Optical	20 nM	[161]
Zhang et al	Aptamer	Induced disassembly configurational aptamer biosensor	Optical	20.5 nM	[162]
Mir et al	Aptamer	Induced assembly configurational aptamer biosensor	Electrochemical	80 nM	[163]
Zheng et al	Aptamer	Target-Aptamer complex imhibition of enzyme digestion	Optical	680 nM	[164]

Table 5.01 A comparison of the IAELAB sensor relative to a selection of recent thrombin aptamer biosensors.

Based on the results of the target titrations, the detection limit of this sensor was determined to be at least as low as 15 nM. This is comparable to published literature of Thrombin aptamer biosensors, which typically describes aptamer biosensors with low nanomolar detection limits. Sensors with limits of detection within the picomolar range exist, but these tend to be the exception rather than the norm.

5.11 Thrombin Titration with full IAELAB setup in the absence of redox label

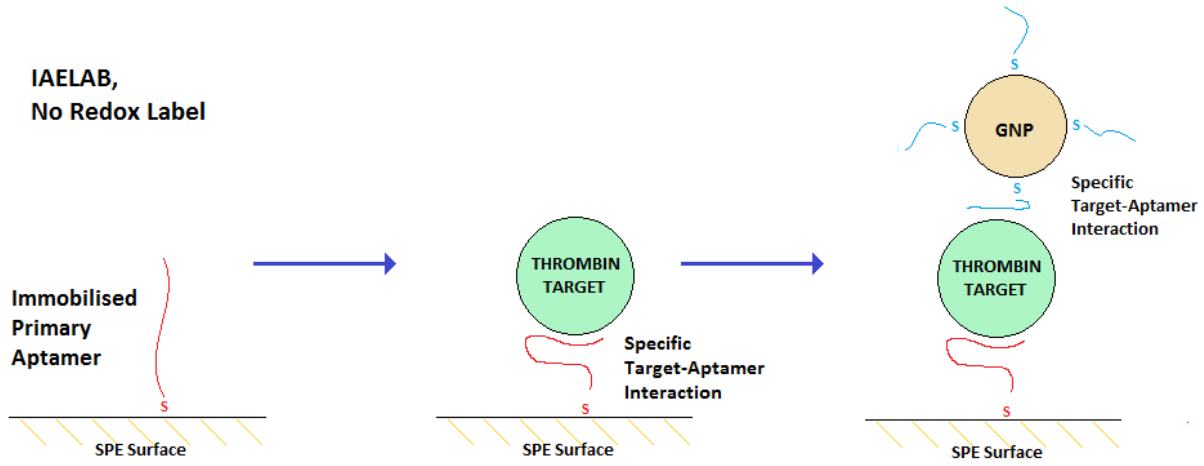

Fig 5.16 Binding mechanism of redox-label free negative control

These control experiments were conducted in order to determine whether the voltammetric responses observed in the IAELAB results were due to the presence of the ferrocene label at the electrode surface. Controls were set up using the same protocols as that listed in the methodology section for IAELAB, with the only exception being that the aptamer immobilized onto the GNPs was not conjugated with ferrocene label prior to the assay.

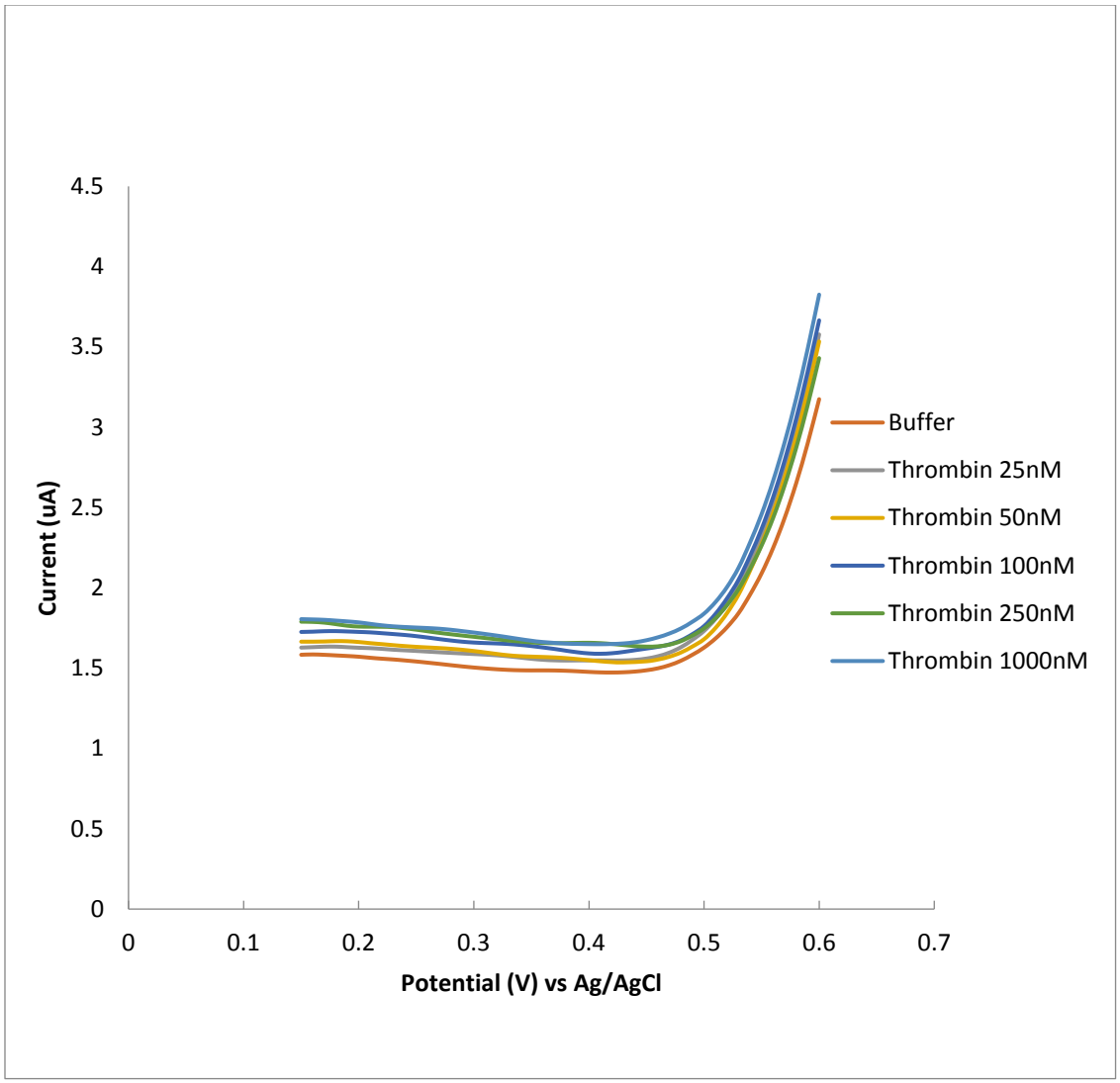

Fig 5.17 SWV of unferrocenated Thrombin aptamer with sandwich configuration (IAELAB)'s response to Thrombin titration vs Ag/AgCl

The result showed no noticeable peak in the absence of redox label. The lack of any distinct peak indicates that the target is not oxidised in the range and conditions of the experiment, and that the distinct peak detected at approximately 0.45 V in titrations are the result of charge transfer to the redox label. While the effect of the charging current could be observed, the magnitude relative to a typical ferrocene signal is minimal within the investigated range, and could therefore be considered negligible for the purposes of data analysis.

5.12 Sensor Specificity

Control experiments were conducted in order to determine whether the sensing molecule would bind to non-target molecules similar to the Thrombin target. Lysozyme and Bovine Serum Albumin (BSA) were eventually selected, for reason of low cost and availability. Lysozyme was selected due to its strong overall positive charge, which was expected to give it at least some degree of non-specific affinity to negatively charged oligonucleotides. This should provide a near maximum baseline non-specific signal for non-target globular proteins. BSA was selected due to its prevalence in the serum, which is the natural working environment of a practical real-life thrombin biosensor. Both specificity controls were also chosen due to their relatively similar size to target molecule (14.3kDa for lysozyme and 66kDa for BSA, compared to 37.4 kDa for thrombin), allowing them to represent globular proteins in general.

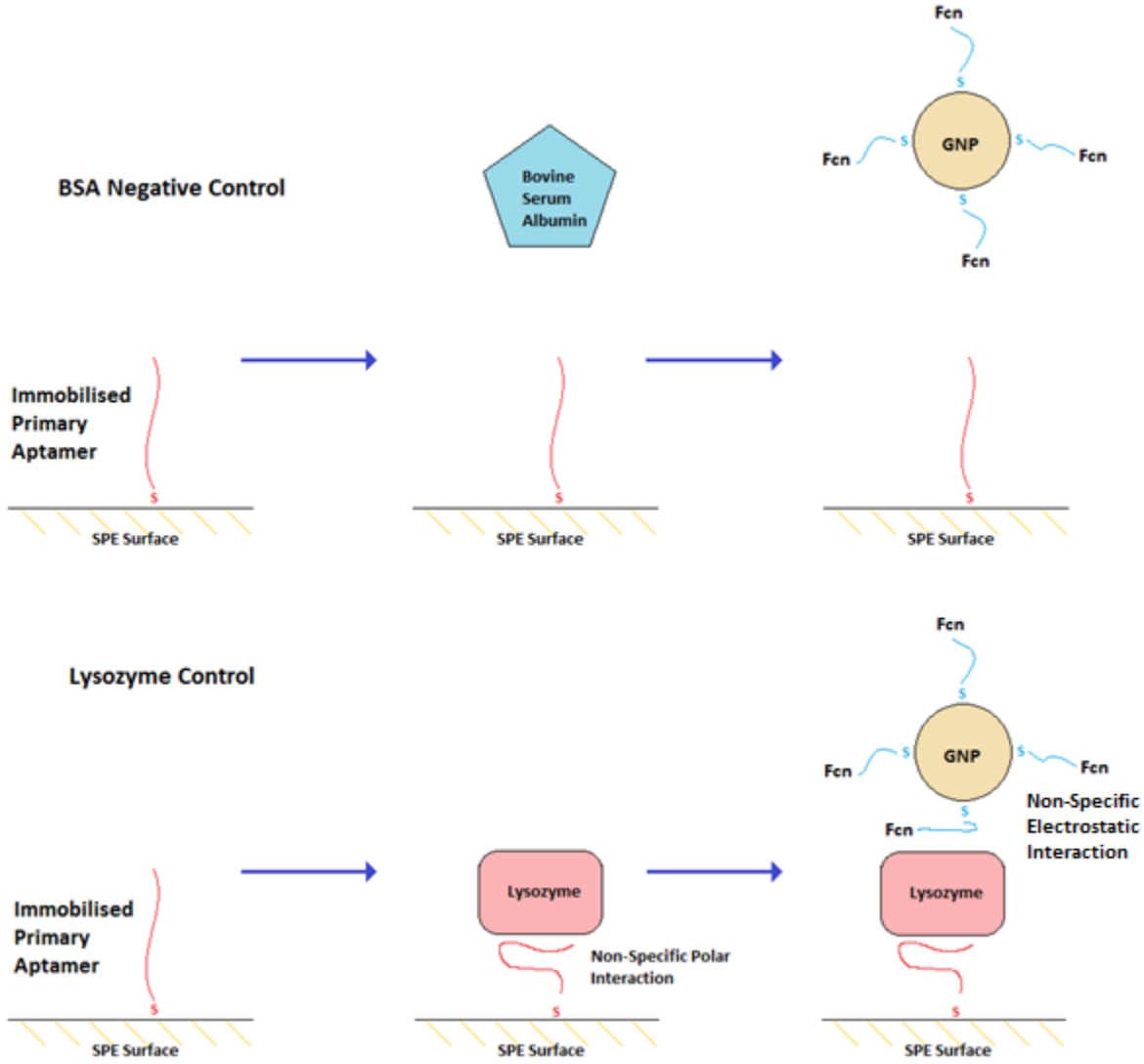

Fig 5.18 Hypothesised mechanism of BSA and Lysozyme negative control

5.12a Titration against Bovine Serum Albumin Negative Control

Concentration range was selected to be similar to those of target titration, with the highest concentration being double the highest target concentration investigated.

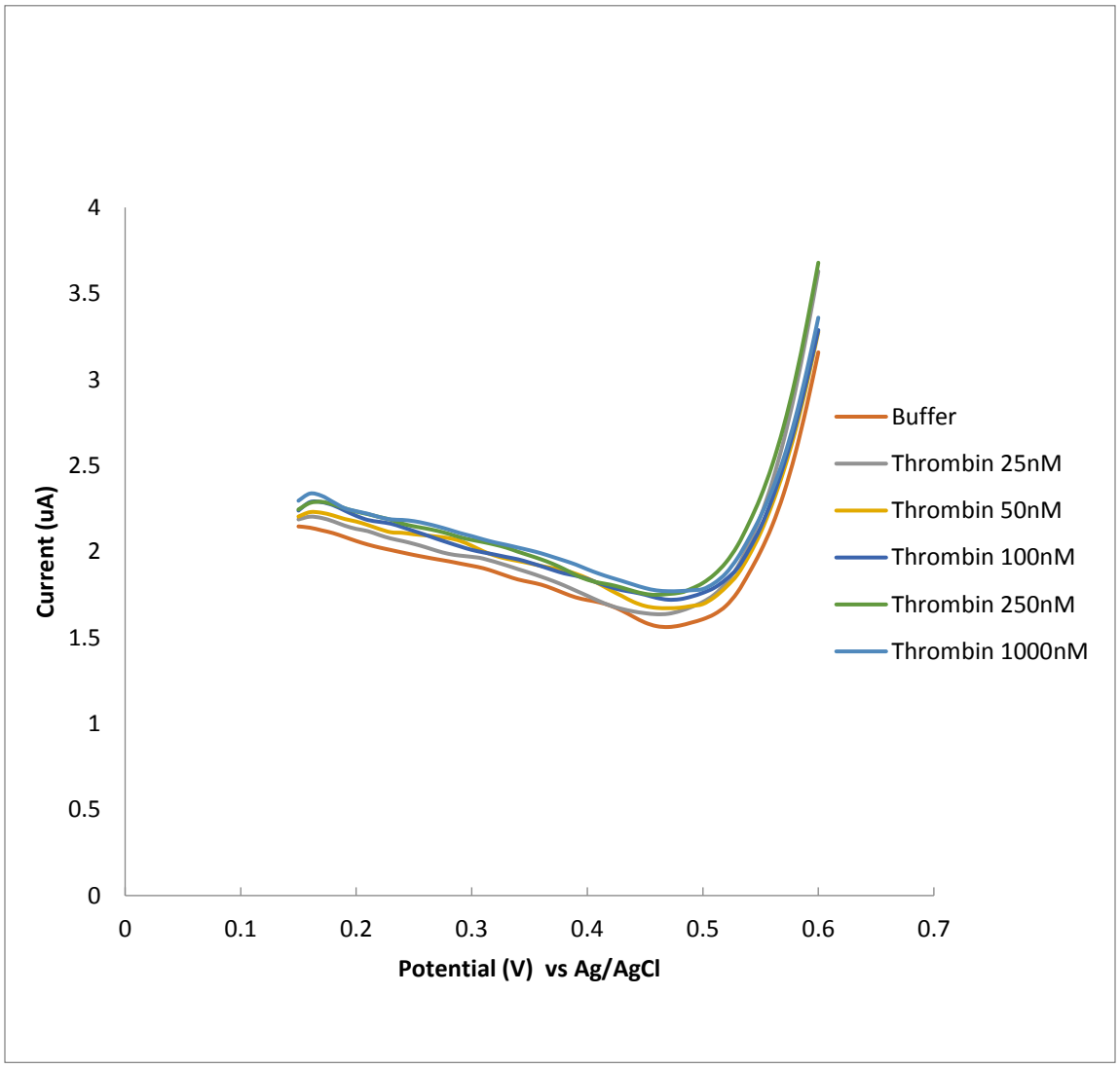

Fig 5.19 SWV of Thrombin fcn-aptamer biosensor with sandwich configuration (IAELAB)'s response to BSA negative control titration vs Ag/AgCl

Analysis of the data shows no clear correlation between peak current and concentration of BSA control. This would support the conclusion that there is no comparable affinity between the sensing molecule and BSA under these conditions.

No discernible signal was detected on this control at all, which would indicate that there is very little (if any) non-specific binding of at least the GNPs end of the aptamers to BSA. This is very desirable as albumin is the primary protein component of serum [165] (typically forming half of blood protein mass in a healthy human, the vast majority of the remaining being globulins). From a real world perspective, any practical application of a thrombin sensor will almost certainly be in a biomedical context, with the environmental matrix being composed of blood plasma, which is the medium of activity for the coagulation cascade.

Serum albumin concentration in blood varies from person to person, potentially with very significant outliers as a result of illness, but 34 to 54 mg/ml is considered typical. 54 mg translate to 818 uM, which makes the 1uM result particularly significant.

5.12b Titration against Lysozyme Negative Control

Concentration range was selected to be similar to those of target titration, with the highest concentration be double the highest target concentration investigated.

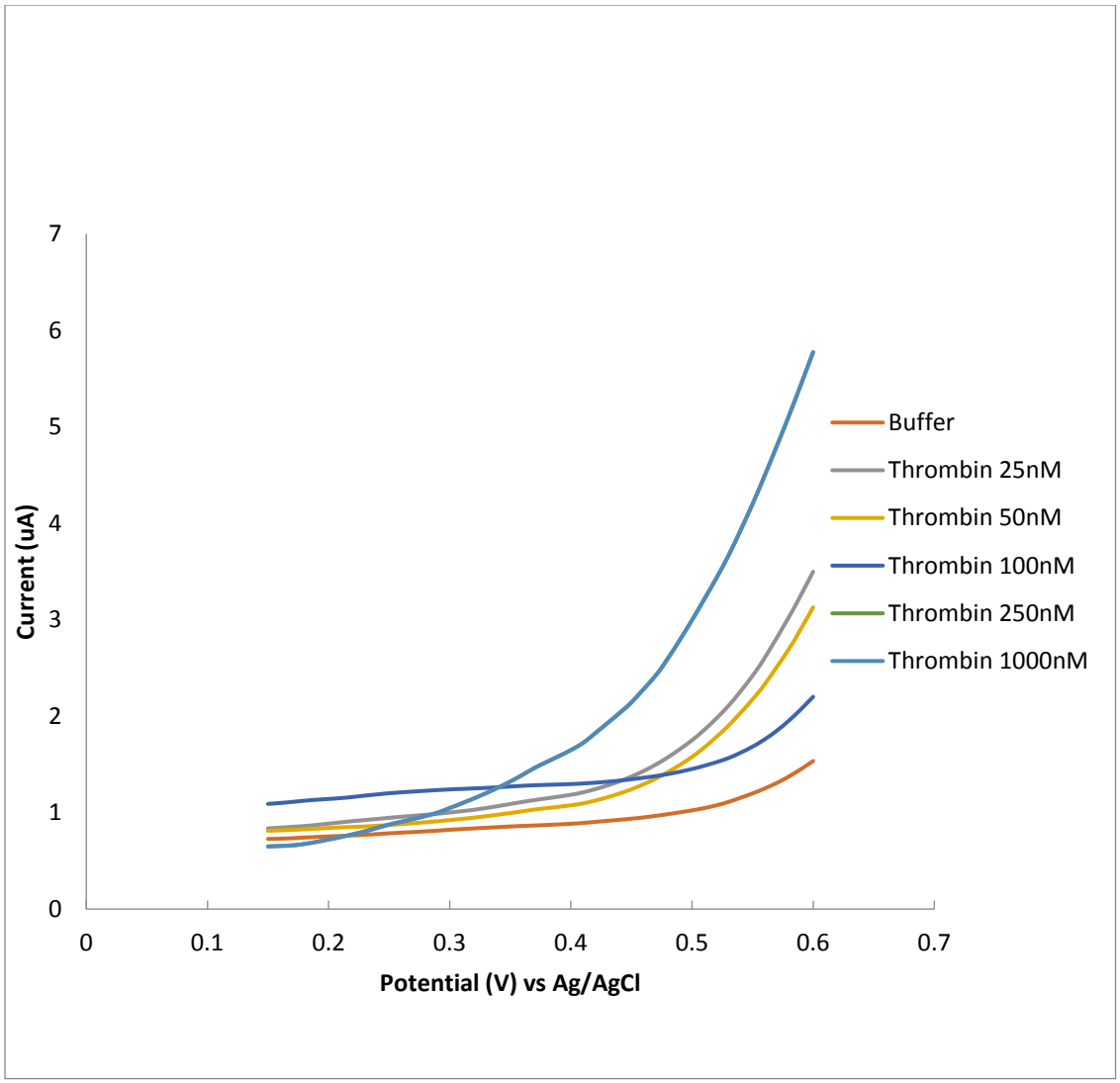

Fig 5.20 SWV of Thrombin fcn-aptamer biosensor with sandwich configuration (IAELAB)'s response to lysozyme negative control titration vs Ag/AgCl

Analysis of the data shows no clear peak in the current response as a result of a titration of lysozyme control. This would support the conclusion that there is no comparable affinity between the sensing molecule and lysozyme under these conditions.

The contrast between the voltammetric responses in the presence of thrombin and those in the presence of albumin and lysozyme supports the lack of non-specific binding.

This result is supported by the results of the DAELAB assay, which display a very low signal response as a result of target concentration, indicating that adsorption is insufficiently strong for the thrombin to adhere to the electrode through the wash process. In the case of DAELAB it is almost certain that it is the electrode-target interaction has failed (rather than the target-GNPs component, which would be identical to those used in the IAELAB, which displays clearly defined signals). Here the failure could have occurred at either of these points, with the same empirical result of reduced signal response.

5.13 A Comparison of Sandwich Aptamer Biosensor and Conformation Change Aptamer (CCA)

The two sensing modes described in this thesis are quite different. And table 5.01 summarizes these differences.

Factors affecting sensor performance	**Conformation Change Aptamer (CCA)**	**IAELAB**
Signal to baseline ratio	Low	High
Effect of electrode quality	Highly dependent on smoothness and cleanness of electrode surface	Can work with lower quality/less smooth electrodes such as SPE
Assay complexity	Low after initial sensor electrode preparation	Complex, multi-step assay.
Ease of automation	Easy	Relatively more difficult
Potential for miniaturization	Simple	More difficult
Potential for expansion to other targets	Simple, wide range of potential targets	Potentially limited to large targets with multiple binding sites.

Table 5.02 A comparison of DAELAB sandwich aptamer biosensor to Conformation Change Aptamer biosensor discussed in chapter 3

Perhaps the greatest weakness of the sensor discussed in this chapter is its lack of potential for future development. The IAELAB design takes advantage of the extensive knowledge available regarding target-aptamers both the 15 bp long Bock et al TBA aptamer [149] and the 29 bp long HD22 Tasset et al [150] aptamer, as well as the fact that both aptamer do not compete for the same binding site or otherwise obstruct the binding of the other aptamer. This degree of knowledge is uncommon for most aptamers, making it hard to extend this design philosophy to other targets, where two aptamers capable of binding to the potential target may not exist at all, let alone possess already studied target bound structures.

The need for two aptamer binding sites on the target also makes it unlikely this design philosophy could be used for the sensing of small molecular targets, which would limit the realistic potential targets for this sensing philosophy to relatively large molecules such as globular proteins.

These factors are in contrast to the CCA which could be expanded onto other potential targets, including low MW targets or targets with highly repetitive subunits, with relative ease. Indeed the third chapter chapter of this study has already shown that this mode of sensing could be expanded onto two different targets.

The IAELAB system is also more complex compared to CCA, requiring both more reagents and more human hours per operation, and therefore increased cost of assay. In particular CCA requires minimal skill to operate after successful fabrication of the sensor device (so simple in fact that the previous chapter has shown that target sensing operation could be performed using a minimally modified 3 axis robot). IAELAB on the other hand require extensive human interaction even after sensor assembly. This can prove to be significant problem should the device be expanded to a commercial production, since operating the sensor will require technical skill on the user end. This could make the device less applicable in LEDCs due to shortage of human resources, and increases the cost of operation to some extent in both LEDCs and MEDCs.

On the other hand the IAELAB has a number of significant advantages of over the CCA mode of sensing. Compared to CCA, IAELAB's signal to noise ratio is relatively high, with the buffer signals being uniformly low or undetectable compared to its target bound states. This is most likely because the CCA's redox label is tethered to the electrode surface, and thus spatial relocation of the redox label is at most equal to the length of the aptamer molecule. In IAELAB, unbound biosensor molecule is completely removed from the system by the wash, resulting in decreased noise.

This also makes the IAELAB sensor less sensitive to badly polished or less smooth electrode surfaces. Smooth and chemically cleaned electrode surfaces on the other hand are essential for the successful application of CCA. Reduced sensitivity to electrode surface quality could facilitate the scaling up of IAELAB based sensing method, since methods of mass producing electrodes (such as screen printing) could be used.

Signal amplitude in general for IAELAB is also significantly higher than those of CCA, which would indicate a greater redox label load than those of CCA. Maximum peak amplitudes for IAELAB (average 1uA, max of 1.18, min of 0.9) is typically over an order of magnitude higher than those of CCA (average of 54 nA, max of 84nA, min of 23nA). This could be a significant advantage in environments where there is a significant amount of redox noise.

5.14 Concluding Remarks

In this section of the study, it is shown that the sandwich aptamer biosensor (IAELAB) format can be used to detect thrombin target at a concentration within the nanomolar range. It is also possible that the direct adsorption (DAELAB) mode of sensing could detect thrombin target at a higher (at least micromolar) range, though this could not be determined with the resources available to this study.

The sensor showed high specificity to its target, showing no significant response to other globular proteins, including both BSA (highly ubiquitous in target environment) and lysozyme (positively charged and therefore a good representative of a worst case scenario for non-specific false positive results).

Sensor Setup	**Format**	**Ligand Molecule**	**Detection Limit**
DAELAB	DAELAB	Thrombin	(1uM)*
IAELAB	IAELAB	Thrombin	15nM
Label-Free Control	IAELAB	Thrombin	No Signal

Albumin Negative Control	IAELAB	Albumin	No Signal
Lysozyme Negative Control	IAELAB	Lysozyme	No Signal

*Signal present in 30% of electrode variations only

Table 5.03 Summary of Results for Aptamer Biosensor based on GNP

Future works could take one of two directions. The first would be to test the sensor in its most likely target environment (simulated by animal serum perhaps). The second would be to automate the IAELAB, which should reduce the effect of one of its greatest weaknesses (human hour needed for operation).

Automation of IAELAB would without doubt be more difficult than those of CCA, but should still be relatively easy. The wash steps could be implemented using a peristaltic pump similar to those discussed in the LHS section of Chapter 6 (see 212), and the drying could be performed through the implementation of a valve actuator controlled nitrogen source.

However the ability to generate aptamer pairs is still the major limitation in the more general use of IAELAB. Until a method becomes available that can reliably produce such aptamer pairs it is likely to remain a niche format.

Chapter 6: Automated SELEX Device (ASD)

6.01 Introduction

This part of the thesis describes an attempt to design and fabricate an automated mesofluidic flow device to perform Systematic Evolution of Ligands by Exponential Enrichment (SELEX), the process commonly used for the isolation of aptamers sequences [21][22].

In Chapter 1 it was discussed that automation could be of great benefit in increasing throughput, decreasing cycle time and reducing human time and financial expense of the SELEX process. Based on a literature review of automated SELEX devices it is also possible to conclude that at present automation of the SELEX process generally takes one of two design directions, one of which is mimicking human action with an automatic sampler [70], the other uses microfluidic based systems [72]. The inherent advantages and disadvantages of both systems were discussed and evaluated in the introduction and it was concluded that there may be some potential benefit in attempting to create an automated SELEX device based on mesofluidic channels. It is hoped that by increasing the scale of microfluidic channels from a micrometer to millimeter scale, it would be possible to gain the primary advantages of the large volume SELEX (large library and sequence variation), while also retaining the primary advantages of microfluidic SELEX (reduced contamination risk, low initial cost and maintenance).

Numerous configurations of SELEX devices have been studied, however all Automated SELEX Devices (ASD) share a number of common components that perform the following operations:

1) Liquid handling
2) Flow Rate Control
3) Temperature Control
4) Partition and Separation

Under suitable software control.

Liquid handling and flow rate control determine the movement of liquid to the correct reaction chambers. This is typically either a pipette actuator and 3 axis robot in a conventional (auto-sampler based) SELEX device or a pump and solenoid valve manifold in a fluidic SELEX device.

Temperature control is primarily required for thermal cycling for the PCR amplification, and is typically implemented using a simple thermostat. Temperature is also frequently used for the dissociation of bound DNA from target.

Partition and separation system is involved in the removal of low affinity sequences from the target bound library, and subsequent separation of target bound from unbound sequences. The design of these system is by far the most diverse, since target properties play a significant role in determining partition and separation protocols.

In addition to these components, an important aspect in the design of any ASD is the electronics hardware and software which power and control the ASD.

Contamination and the control thereof is one of the central aspects of automated molecular biology process system design. As such contamination control is considered one of the key considerations in device design, despite not being a direct part of the SELEX process.

These components could be implemented in a diverse variety of ways. How they are implemented would necessarily depend on the overall format of the automated SELEX device which will be discussed in the following section.

6.02 Operational Protocol

The essential design of the Automated SELEX Device (ASD) is based on a manual SELEX protocol which has been successfully and widely employed in the past by many research groups to isolate aptamers [64][71]. The automated protocol is analogous to the manual one, with the central difference being that a flow type liquid handling robot is used to perform the tasks typically carried out using a manual pipette.

Initially most cases of SELEX were performed using the original protocol of [21][22], where the retention of the target-nucleic acid complex is by filter binding or affinity chromatography. In the work described here a protocol using target molecule covalently bonded to magnetic nanoparticles (MNP) is used instead, since it is much easier to implement MNP based separations by automation. Several groups have successfully used SELEX protocols with an MNP based partitioning step [55][56][57].

A comparison between a typical Manual SELEX protocol and the automated SELEX protocol used in this thesis are as follows:

	Manual SELEX Protocol	**Automated SELEX Protocol**
Denaturation	Library is heated at 90°C for 2 minutes within a thin wall eppendorf tube on a heating block, then allowed to cool for 10 min.	DNA is fed into the PCR chamber and heated to 90°C for 2 min, and then allowed to cool for 10 min.
Affinity Selection	Target bound MNP suspension in buffer is placed in a reaction vessel. Denatured DNA solution is then added to the target-MNP solution and incubated for 2 hours. Solution may be agitated manually by Gilson's pipette.	Target bound MNP suspension is pumped gently into the Affinity Selection chamber (AS chamber), and MNP deposition is achieved by turning the electromagnet on, after which liquid is pumped forwards and backwards over a short distance (this will be referred to as "shaking") several times to ensure as much MNP is retained as possible. Denatured DNA in the PCR chamber is pumped into the affinity selection chamber, after which the MNP is released by turning the electromagnet off, followed by "shaking". Solution is left to incubate with the DNA library for 2 hours.
Post Selection Extraction	After incubation a magnet is placed at the bottom of eppendorf, resulting in deposition of DNA-Target-MNP at the bottom of the eppendorf. Supernatant is pipetted out, and a fresh buffer is added, MNP is resuspended and the solution is heated at 90°C for 2 min. MNP is deposited using magnet. Solution containing DNA is pipetted out and retained.	Magnet is switched on, and the MNP deposited out of solution. AS chamber is then washed with buffer, after which the AS chamber is filled with PCR mastermix. MNP is resuspended, after which the solution is heated at 90°C for 2 min to release target bound DNA. MNP is then redeposited, and the Selected-DNA/Mastermix Solution is pumped into the PCR chamber.

PCR	The enriched library is added to PCR mastermix. Solution is divided into thin walled PCR tubes and placed into a thermocycler.	PCR is carried out in PCR chamber containing selected DNA template and mastermix.
ssDNA separation	After PCR is completed, PCR product is pooled and streptavidin coated MNP is added. Solution is left to incubate for 1 hour. Solution is then heated at 90°C for 2 min. A magnet is then used to deposit MNP, and the solution is extracted for post processing.	After PCR is completed, the reaction mixture is pumped to the affinity selection chamber containing streptavidin coated MNP, and left to incubate for 1 hour. Solution is then heated at 90°C for 2 min. MNP is then deposited, and the solution could be either pumped forward for post processing or alternately backwards to the PCR chamber so that affinity selection chamber could be refreshed with new Target-MNP, and allow another round of SELEX to take place.

Table 6.01 Comparison between Manual SELEX protocol and Automated SELEX protocol

The sequences resulting from the SELEX process should be a pool of relatively more homogenous than the initial selection library, and with greater affinity to target molecule.

The post processing protocol is shared by both the automated and manual PCR procedures. The amplified sequences undergo phenol chloroform extraction followed by ethanol precipitation. This yields purified DNA. Some of this is either used in the following round of SELEX or retained as a stock sample, either for reference purposes in case of further analysis (such as by ELONA, Gel electrophoresis or UV/Vis spectrophotometry) or as fallback stock in case of contamination or general decrease in affinity in subsequent rounds.

In order achieve the above automated protocol, the actions steps needed are as follows (absolute essential steps are shown only, optimization is excluded):

Diagram labels

Red represents active solenoid valves or heating elements

Pink represents position of Target-MNP

Orange represents position of unenriched streptavidin-MNP

Dark Blue represents location of original DNA library

Yellow reperesents Selected DNA sequence without master mix

Green represents Mastermix containing Selected DNA template

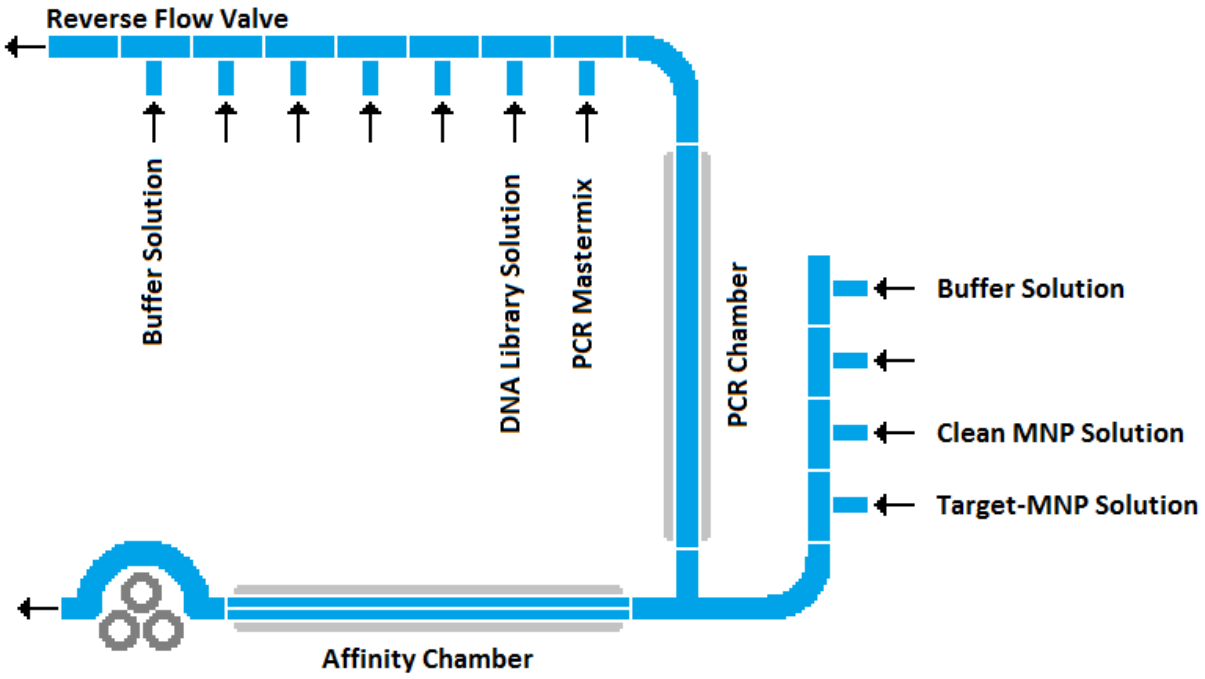

Starting State: For the starting state, the device is purged with one or more solutions as a means of cleaning the flow tubes and reaction vessels of potential contaminants, followed by thorough wash with sterile buffer.

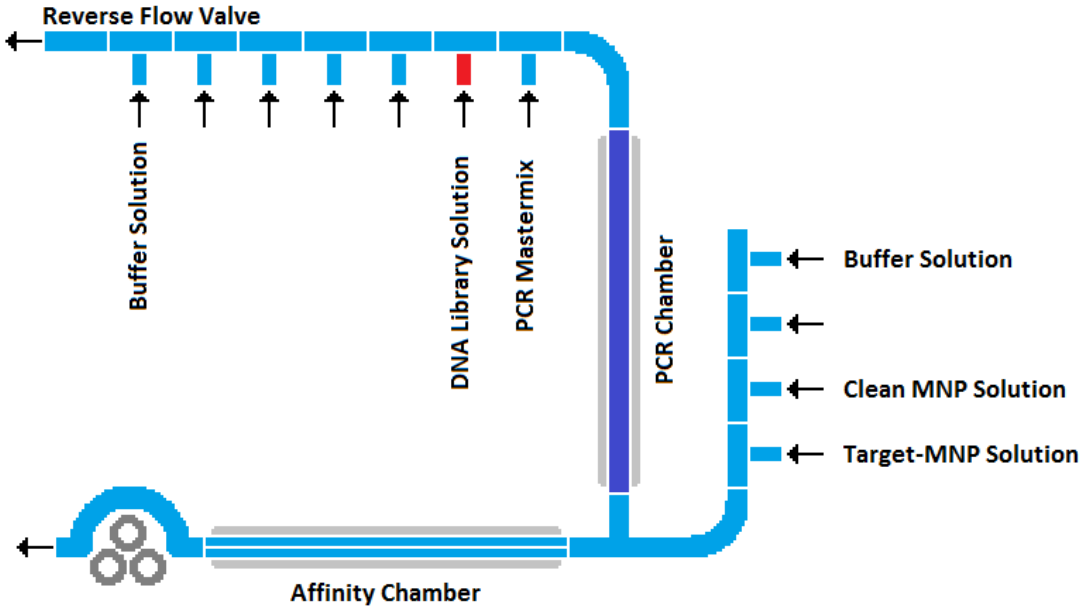

Denaturation: DNA library valve open, pump forward, DNA library valve close, Buffer valve open, pump forward, Buffer valve close, heat to 90℃ 2 min, wait 10min

A comparatively small quantity of DNA library is pumped into the system. This creates a segment of tube containing DNA library flanked with buffer solution called a "plug". A volume of buffer is pumped, pushing the plug of DNA library into the PCR chamber.

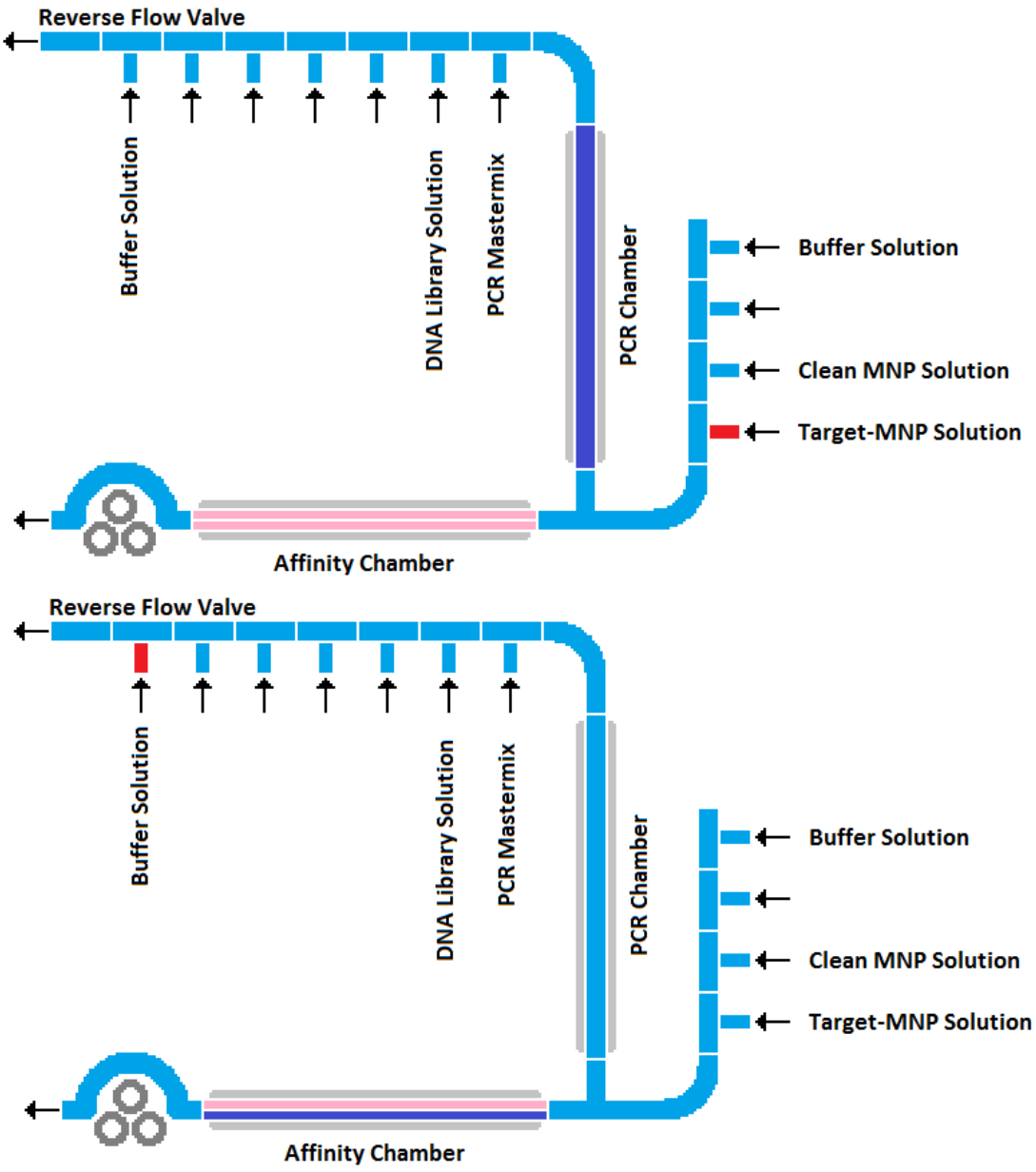

Affinity Selection: Target Enriched MNP valve open, magnet on, pump forward, Target Enriched MNP valve close, Buffer (2nd Manifold) valve open, pump forward, Buffer (2nd Manifold) valve close, Magnet on, "shaking",

A plug of Target-MNP is pumped into the system. A volume of buffer is pumped, pushing the plug of DNA library into the PCR chamber. Magnet is then turned on and the MNP solution deposited to affinity chamber wall.

Buffer valve open, pump forward, Buffer valve close, magnet off, "shaking", wait 120 min

DNA library plug is driven into the affinity selection chamber. MNP is then resuspended in the DNA library solution. Solution is incubated for 120 min.

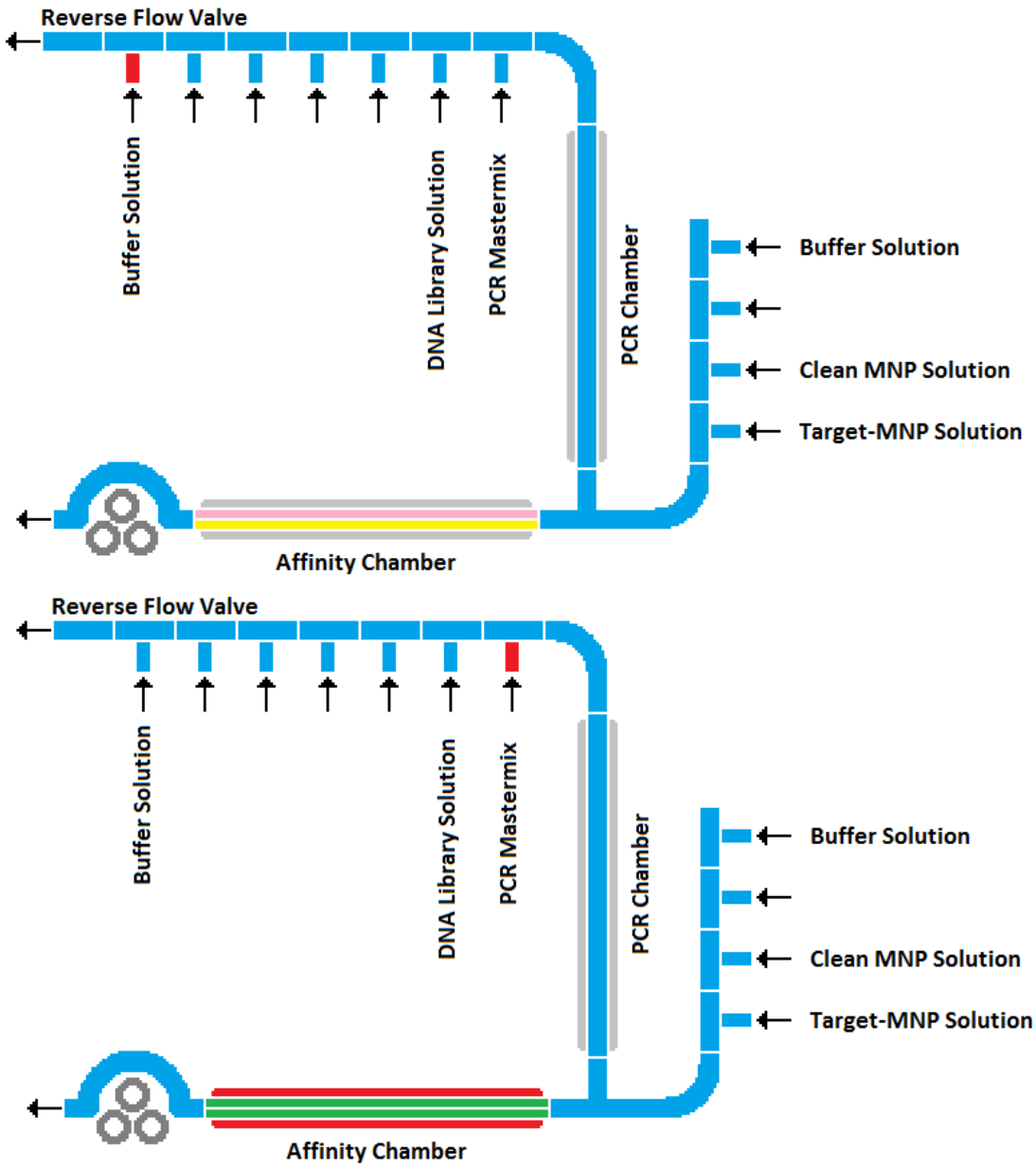

Post Selection Extraction: Magnet on, "shaking", Buffer valve open, pump forward, Buffer valve close,

Aptamer-Target-MNP particles deposited onto affinity selection chamber wall, wash removes any unadsorbed DNA library.

Mastermix valve open, pump forward, Mastermix valve close, Buffer valve open, pump forward, Buffer valve close, "shaking" , magnet off, Heat on 90℃ 2 min, magnet on, "shaking", reverse flow valve open, pump reverse, reverse flow valve close,

PCR mastermix minus template is driven affinity selection chamber as a plug. Aptamer-Target-MNP is resuspended in mastermix solution. High affinity sequence is driven into mastermix by heat, MNP is redeposited, master mix containing selected template is driven into PCR chamber by reverse flow.

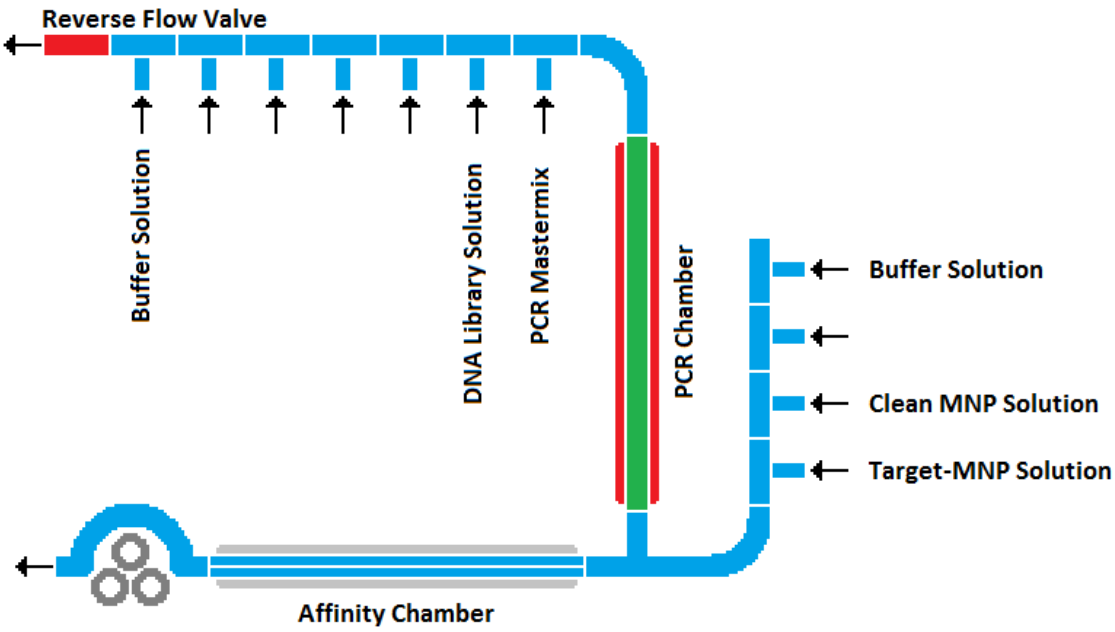

PCR: Heat on 90°C 2 min, Repeat X cycles [Heat on 90°C 30s, heat on 57°C 30s, heat on 72°C 30s]

PCR thermal cycle operation, no final extension as sequence fairly short/avoid non-specific long sequence

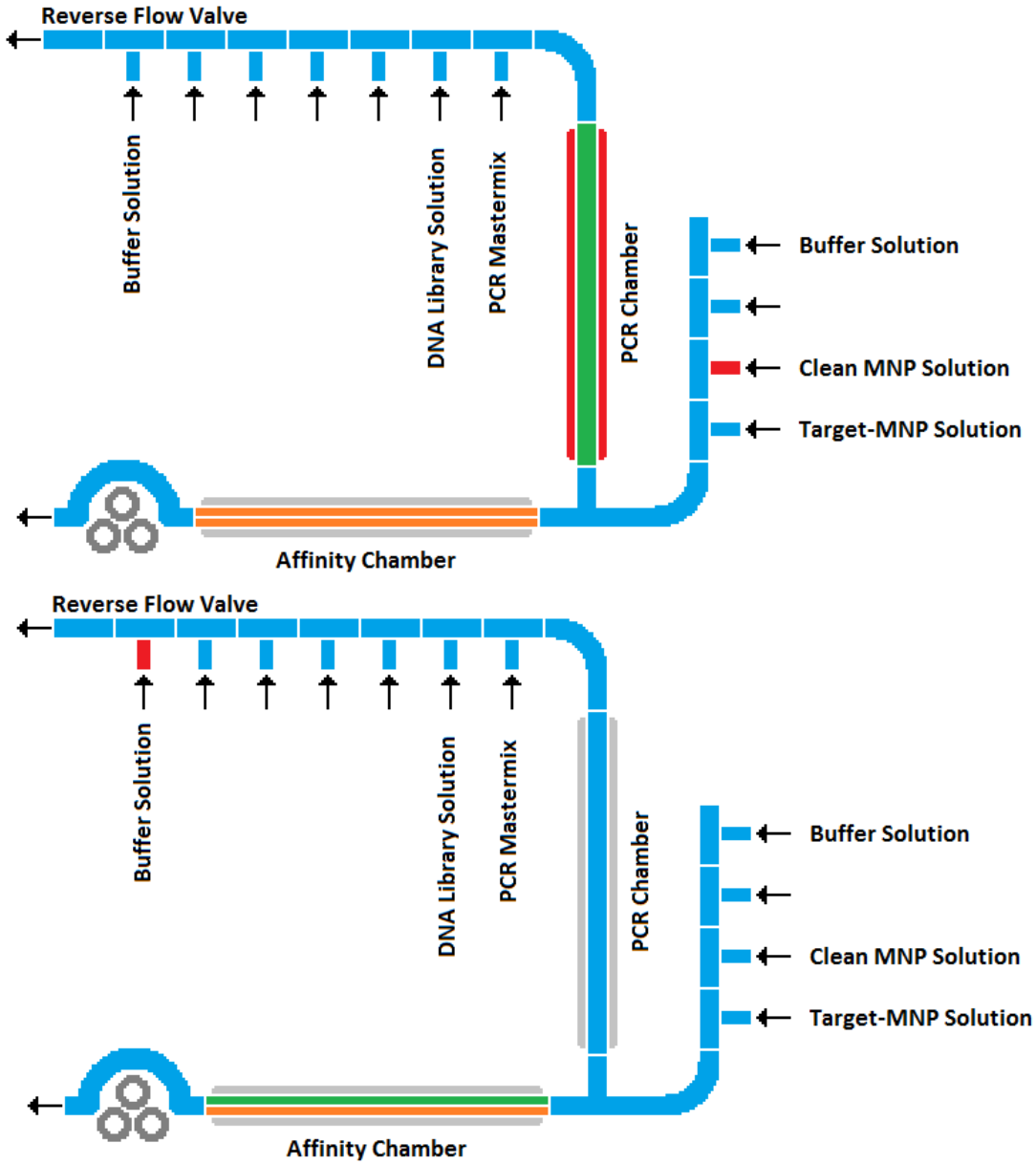

ssDNA separation: Fresh MNP valve open, pump forward, fresh MNP valve close, Magnet on, Buffer (2nd Manifold) valve open, pump forward, Buffer (2nd Manifold) *valve close*

Fresh MNP plug is driven into affinity selection chamber (buffer for this operation comes from 2nd manifold buffer feed).

Buffer valve open, forward pump, buffer valve close, magnet off, “shaking”, wait 60 min, heat on (affinity chamber) 90°C 2 min, magnet on, “shaking"

Amplified solution driven to affinity selection chamber. Fresh MNP resuspended and incubated for 60 min. DNA sequences not covalently bonded to MNP resuspended by heat, MNP redeposited.

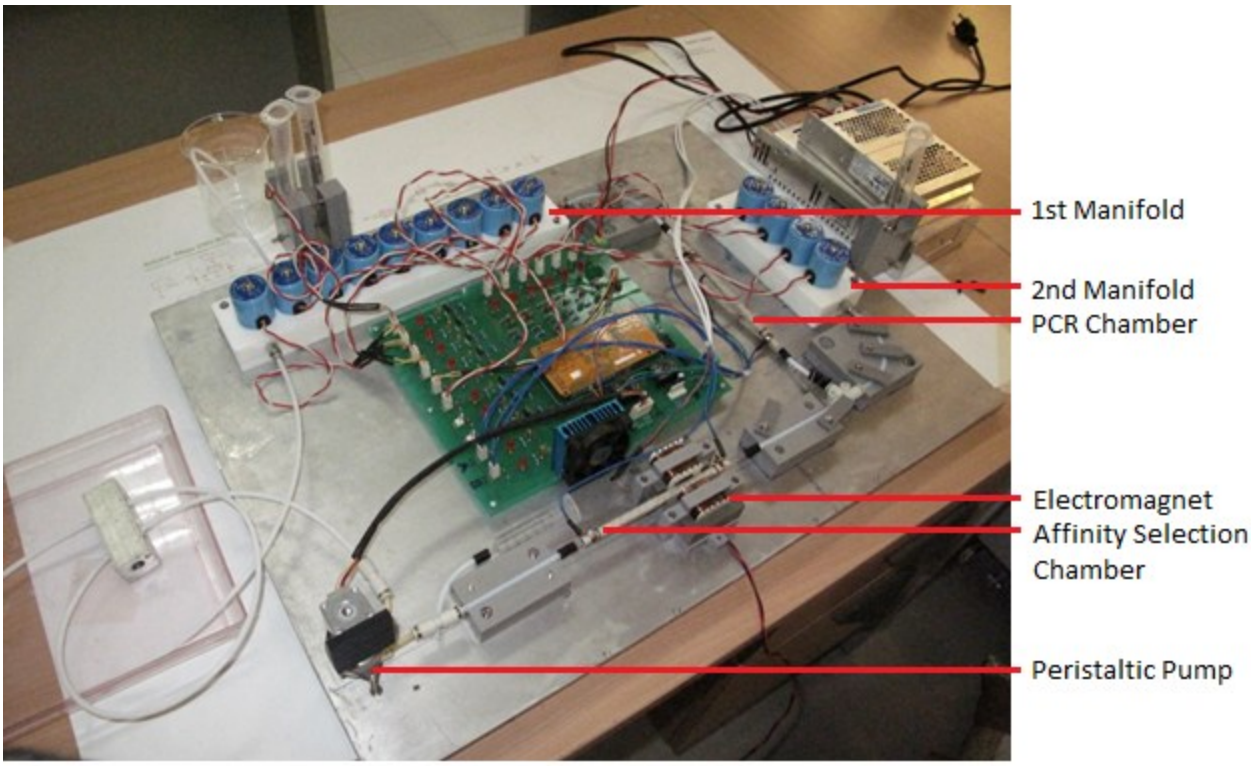

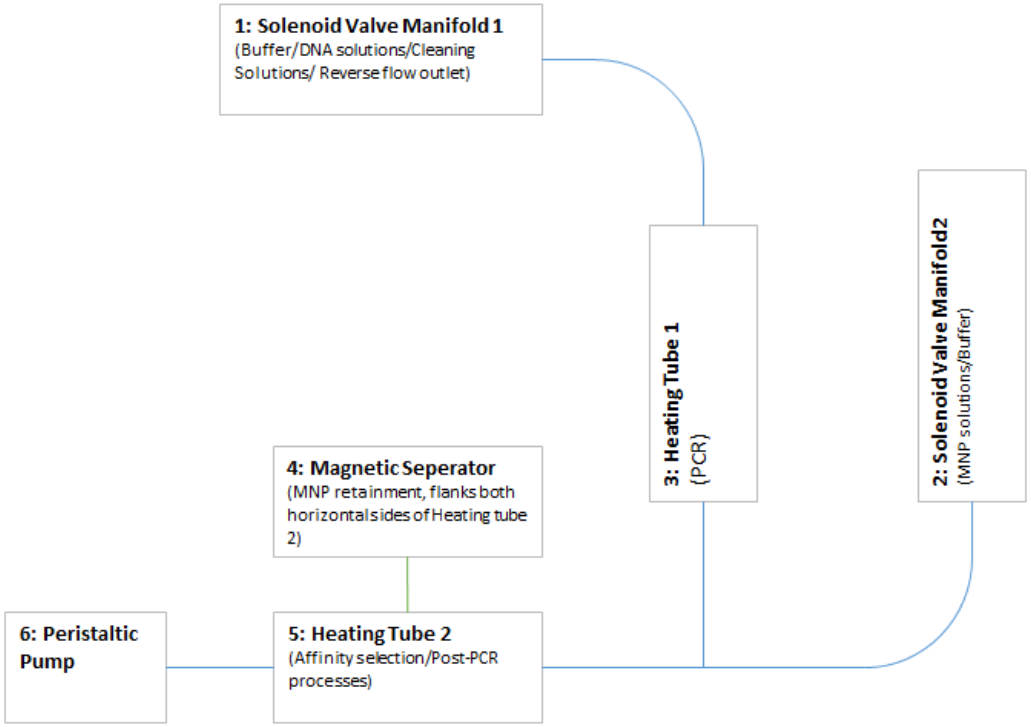

Fig 6.01 Photograph shows arrangement of the components of this protocol on a late model ASD, below is a simplified diagrammatic representation of the device photographed.

If process is immediately followed by another round of selection:

Reverse flow valve open, pump reverse, reverse flow valve close, target-MNP valve open, pump forward, target-MNP valve close.

If process is followed by post processing, solution is collected from drain:

Buffer valve open, pump forward, buffer valve close.

"Shaking" is a multiple step process involving a short forward pulse followed by a short reverse pulse:

Repeat X times [Buffer valve open, pump forward (short), buffer valve close, reverse flow valve open, pump reverse (short), reverse flow valve close]

The automated protocol described above is a very broad overview of the process. Optimization and other essential tweaking during development has resulted in a relatively complex final Gcode protocol with several hundred actions steps (the majority of it essential optimization steps such as "shaking"), the full version of which would be impractical to describe here. Examples and description of the action steps which form the building block of the final Gcode script can be found in the software section of this chapter (see page 235).

Having proposed a basic operational outline for the SELEX device, it is now possible to determine the optimal configuration in which the SELEX automation components discussed in the previous section could be implemented. Since these systems (other than the software and electronics control components) operate in a largely modular nature, the design and development of these components would be discussed below separately.

6.03 Temperature Control and the design of PCR protocol

SELEX is comprised of repeated cycles of selection and amplification. Since in conventional SELEX amplification is achieved by PCR (a thermal cycling process), it follows that any SELEX device must have accurate temperature control.

Temperature was also used in the final model of the ASD as a means of separating affinity selected aptamers from Target-MNP, and also (after second strand synthesis and PCR with a biotinylated reverse primer) in removing the biotinylated ssDNA strand prior to another round of selection.

6.03a Model 2 Temperature Control System (TCS)

While some success was achieved using heating block based Temperature Control System (TCS) (based on the extruders of 3D printers), practical test showed that these earlier models were incapable of sufficiently rapid heating.

In the final design of the TCS, a concentric thin walled aluminium pipe (4.2 mm ID, 5.8 mm OD, 140mm long) was used as the heating element around the glass tube of the PCR and AS chamber. This minimizes the mass that needs to be cooled and heated while maximising surface of area of contact with the flow tube, thus optimizing both heating and cooling times.

A feedback thermistor is placed into a 1mm x 2mm, 0.6mm deep trench cut into the pipe surface made using a CNC milling machine. Thermal paste was applied to fill this trench, in which a Murata Electronics NXFT15XH103FA2B100 [166] thermistor was embedded. The entire aluminum pipe was covered with adhesive PTFE tape to provide electrical insulation from the nichrome heating tape. This reduces the rate of heat transfer, but is essential in order to prevent short circuit.

The heating element is a nichrome tape, 5mm wide which is twisted around the PTFE coated aluminum pipe, with an even gap of approximately 8mm between turns. A tag was left at each end of the nicrome wire where contact with the circuit wire could be made. The heating tube is then wrapped in another layer of PTFE tape to provide thermal insulation, as well as to reduce the danger of contact. Special care is taken to prevent nichrome wire coming into contact with any element of the thermistor's leads, and that a gap is made in the outer PTFE sheath to enable access to the thermistor leads.

In later production runs, rigid metal wire was tightly wound around intervals of the heating element to prevent PTFE tape splitting as a result of heat expansion.

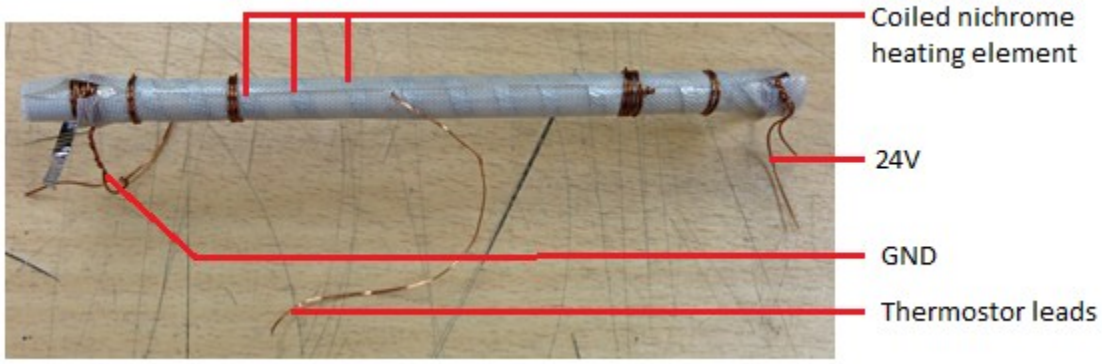

Fig 6.02 A Model 2 TCS

6.03b PID Controller

Although the 3D printer thermal head was not suitable as a heat source, as described at the start of this section, its control firmware, Sprinter, was integrated with a third party open source PID software which had been developed by B Beauregard [167] in an unmodified state as a custom library. This PID software was selected due to its stability, good temperature response and ease of integration into a preexisting Arduino firmware. It is also one of the most commonly used PID libraries developed for the Arduino system, and is thus well known among the 3rd party community, making the system both well tested and documented.

Another essential improvement imported from previous models was the addition of a fan in order to reduce the cooling time. This fan is powered directly from the main power supply, and left in an always on state.

6.03c Feedback Control Mechanism

Heat sensing for signal feedback is similar to that used in 3D printers, and utilizes a pull-up/pull-down resistor couple, with the pull down resistor being a thermistor. Temperature is calculated by the voltage at an analogue pin (Vout) compared to reference data. For this system, Vout can be represented with this equation:

$$Vout = Vcc\left(\frac{RThermistor}{RThermistor + R2}\right)$$

R2 being the resistance of the fixed value resistor coupled with the thermistor.

Eq 6.01 Determining the value of voltage at analogue pin

Since R1 is kept at a constant (10kOhm), the only variable governing Vout is the resistance of the thermistor, which in turn is governed by the environment temperature.

Temperature is determined by the PID program by comparing of the feedback signal at the analogue pin to a database of known signal response to temperature, and using it to extrapolating an estimate of the temperature of the heating tube. Since the data points of the database is 1 degrees wide, the resolution of the temperature sensor can be assumed to be 1 degree wide at most.

The feedback signal at the analogue pin is used by the PID controller to determine the difference between the set temperature and the actual temperature, which in turn allows it to generate a response in order to bring the temperature back to target. The overall schematic of feedback regulation could be found in fig 6.03 below.

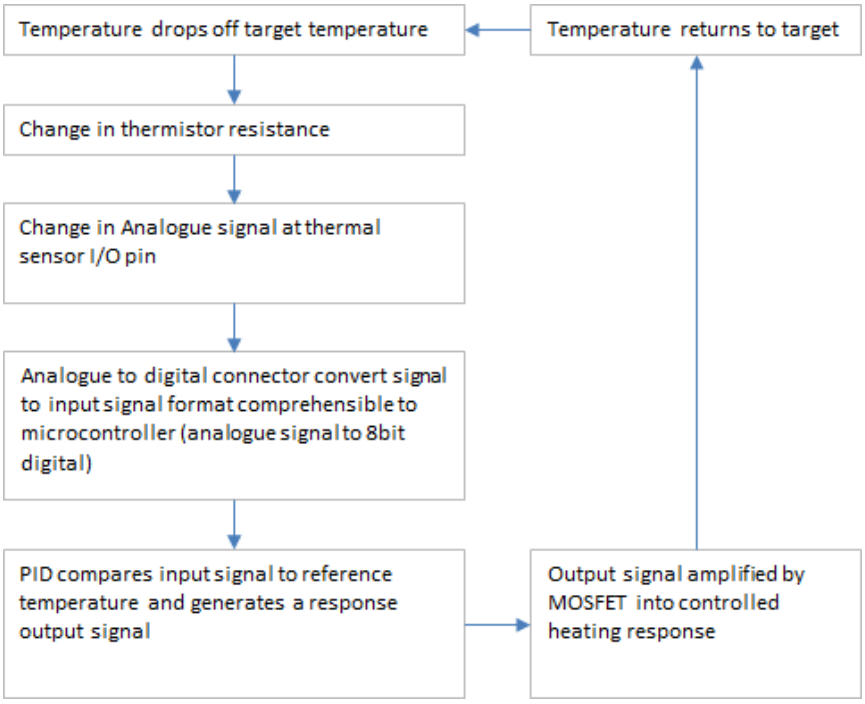

Fig 6.03 Summarised scheme of feedback temperature regulation.

6.03d Results of Model 2 TCS

Heating unit was able to achieve all 3 key PCR temperatures, and could maintain the temperatures once target is reached with reasonable stability.

The heating unit was able to perform the correct thermal cycling profile required by the PCR conditions, in terms both of the speed of temperature change and the stability of the temperature once attained. This is illustrated in fig 6.04 below.

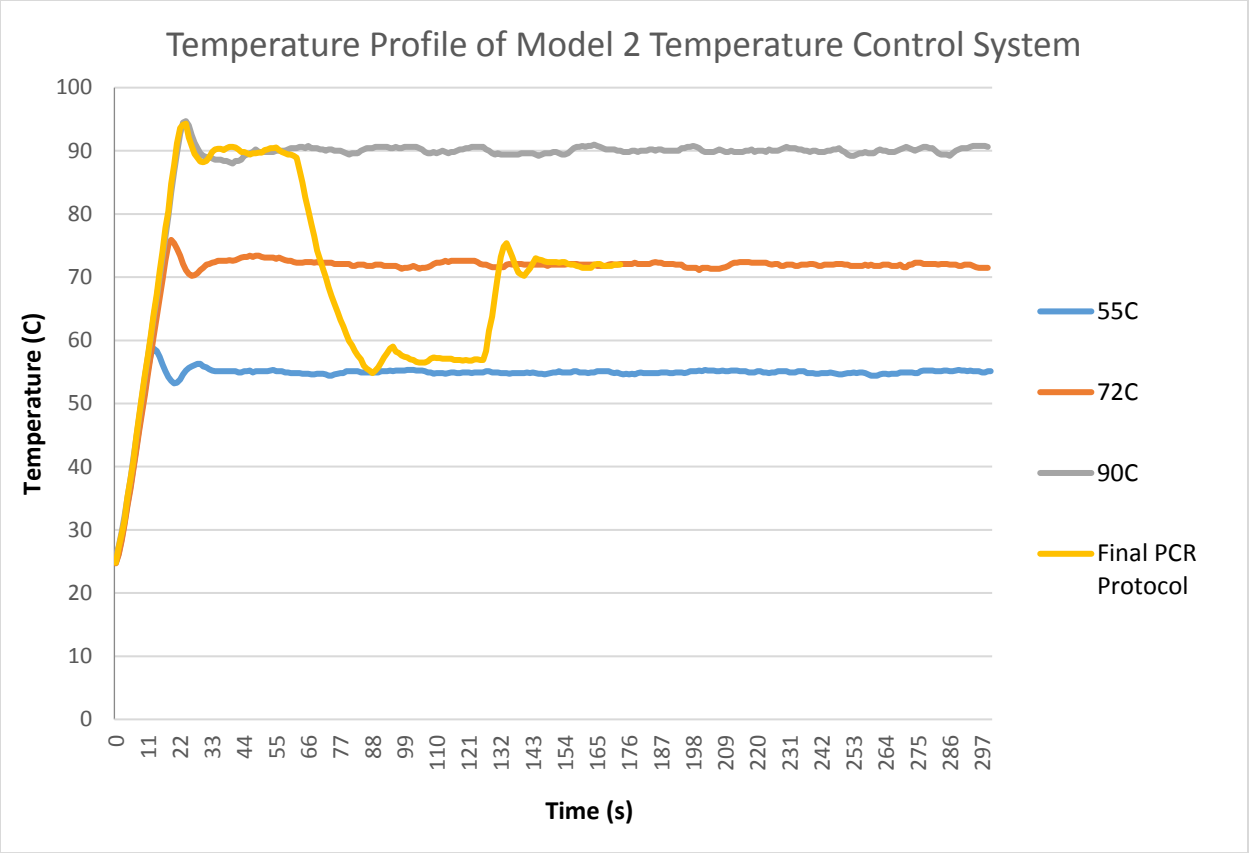

Fig 6.04 Heating profile of the final model TCS (18 coils).

All temperatures could be definitively reached within 25s of initial heating, faster than original target design specification of 45s. This is considered acceptable, and is comparable to the specifications of commercial PCR machines [168].

The temperature control was resistant to changes in ambient thermal fluctuations.

6.03e Aspects of PCR

Originally the PCR temperature targe was 60s at 90°C, 60s at 54°C and 60s at 72°C, for 40 cycles. During initial testing it was determined that the results of this protocol yielded a significant number of non-specific bands larger than the template.

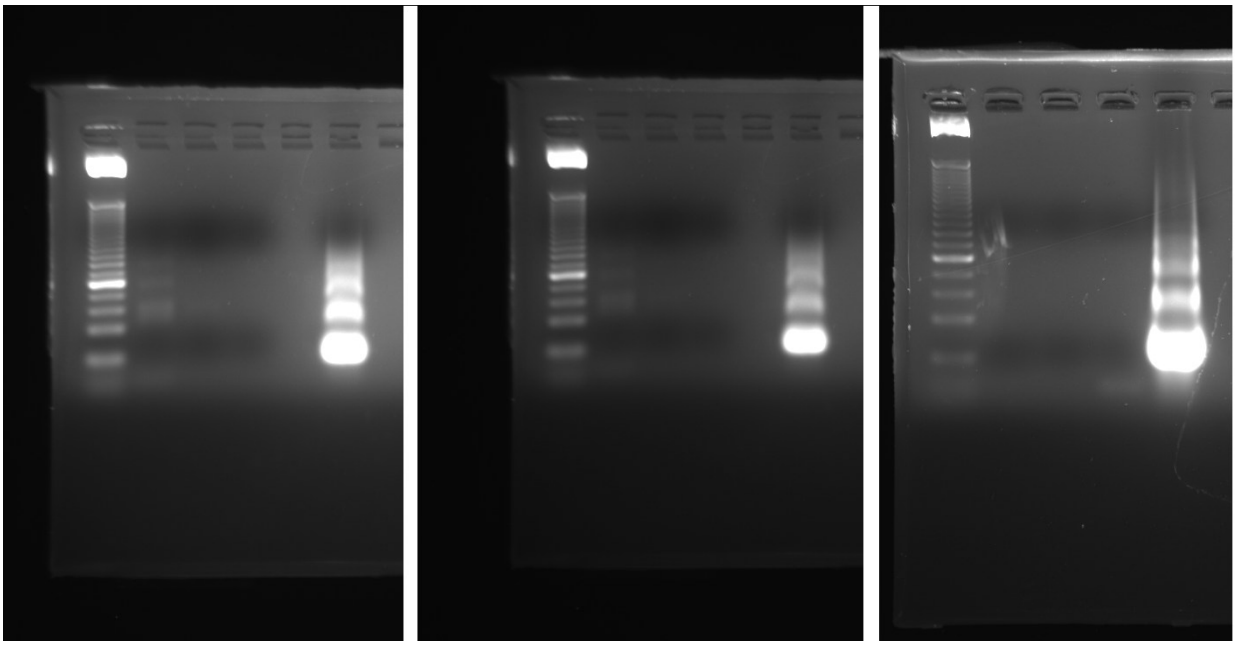

Fig 6.05 Gel Electrophoresis of products of original PCR protocol

These sequences are generally caused by non-specific binding of primer regions to the N30 sequences. TaqPol is not sequence specific, thus hybrid formed of two non-specific binders sharing complementary sequence will result in the extension and eventual conjugation of the couple into a single long sequence. This sequence will contain primer binding sites, and thus is capable of reproduction in the process of PCR. Since non-specific binders generally has less affinity than primer to its complementary sequence, increasing stringency could be said to be a good method of decreasing non-specific amplicons. Potential areas of improvement, both avoidable and unavoidable, as well as action taken are listed below:

Causes	Reason	Countermeasure
Too much template	High concentration of initial template results in higher chance of template hybridisation.	This cannot be avoided in sequential SELEX, as there would be no way to investigate template concentration and remove template concentration between rounds of automated SELEX.
Too many PCR Cycles	Excess PCR cycles provide opportunity for non-specific amplification. Primers generally used up in earlier cycles.	Reduced initially planned 40 cycles down to 22 (number reached by trial and error)
Extension time too long	Enables non-specific amplification. Less an issue in this case due to shortness of sequence.	Extension time reduced from 60s to 30s. May not be applicable here due to shortness of aptamer sequence.
Annealing time too long	Increase chance of non-specific annealing.	Annealing time reduced from 60s to 30s.
Annealing temperature too low	Increase chance of low affinity non-specific binders.	Primer have theoretical Tm of 59°C. Thus temperature was raised to 57°C during annealing phase of PCR.
Thermal cycler heat increase too slow	Same as above. Creates period of low temperature during ramping.	Optimization of temperature control system from a previous block format into tube format described in this chapter.

Table 6.02 Causes of large non-specific amplicons, and measures taken to prevent their formation

Implemented PCR improvement countermeasures resulted in a significant decrease in non-specific bands (results can be seen below). Reduction in template extension time may have resulted in a small amount of noticeable short sequence smear located below the desired sequence band. This is not considered a major problem, since lacking a primer binding site complement the sequence would simply not be amplified in the next SELEX run and is therefore not a long term problem. The single distinct thin band represents the exponentially amplified target sequence and is the typical products of successful PCR.

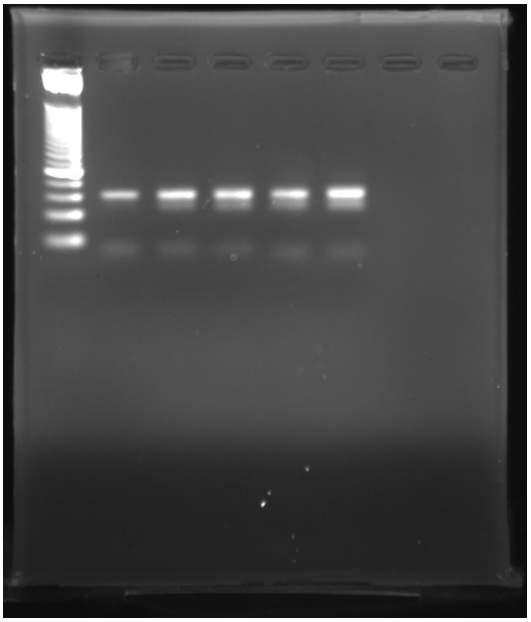

Fig 6.06 Gel Electrophoresis of products of new PCR protocol Left to Right Well 1) DNA Ladder Well 2) PCR products from pilot PCR runs using new protocol

6.04 Liquid Handling System (LHS)

The liquid handling system, together with the flow rate control system, ensure the correct reagent is transported to the correct location at the correct time. The liquid handling system also covers the flow channel design aspect of this study.

6.04a Solenoid Valves

Solenoid valves are ubiquitous electromechanical devices commonly used as control components in many fluidic applications. Multiple solenoid valves are frequently arrayed in a manifold in order to regulate flow between pumps and actuators. Different combinations of open/closed states of these

valves allow for complex fluid regulation behavior to be controlled electronically. Solenoid valves are generally considered to have fast response, long operational lifespan, and high reliability. Flow direction and rate is controlled by the motor pump, which will be described in the next section of this chapter.

The most common type of hydraulic solenoid valves are composed of a solenoid coil, a plunger and a counter spring. The plunger is very commonly encased in a plunger tube, and closed on the liquid end with a heat and chemically resistant rubber seal. This assembly sits on top of a chamber, directly atop of the source and drain port. In an NC resting state solenoid valve, the compression spring pushes down the plunger into a (closed) position in the absence of power to the electromagnetic coil. This results in the source and drain ports being disconnected. Application of power to the electromagnetic coil results in the magnetic force overcoming the compression spring, resulting in the plunger being pulled up. This creates a flow chamber which connects the source and drain port, enabling flow. Solenoid valve selected was a Roundstar RSC-2 RO, specifications for which can be found here [169].

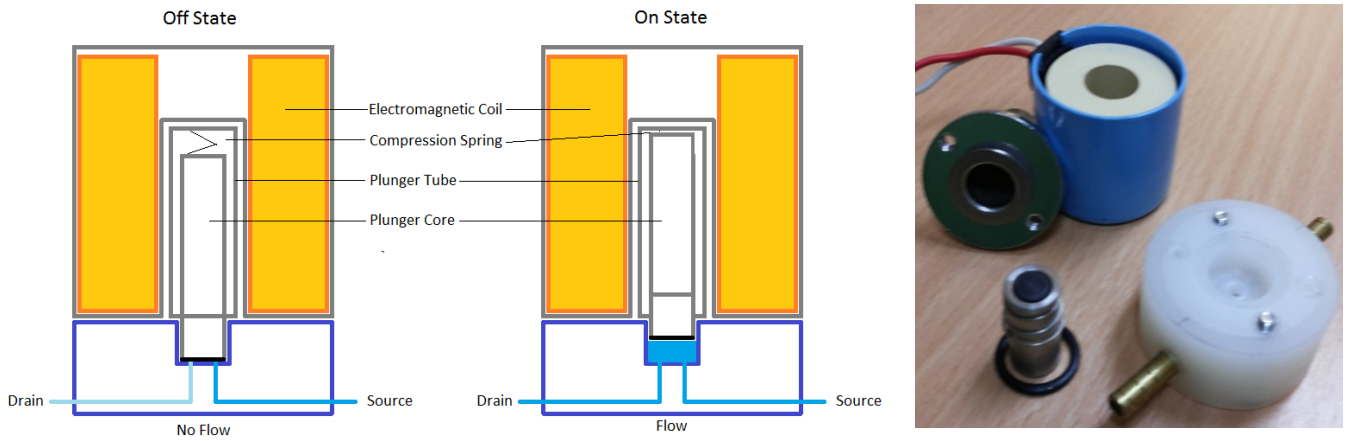

Fig 6.07 This diagram shows the operation mechanism of a typical NC Solenoid Valve. Left) a solenoid valve in the closed “off” state, Center) a solenoid valve in the open “on” state, Right) a photograph of a disassembled solenoid valve.

6.04b Design of Solenoid Valve Manifold

It was decided that the primary material for manifold (including all parts in contact with liquid flow) should be made out of PTFE. PTFE is known to have excellent resistance to both thermal and chemical

stress, as well as being a relatively non-adsorptive material. PEEK was also considered as a manifold material [170].

Ideally the manifold would be composed of solenoid valve flow chambers placed above a single long flow tube drilled through the manifold. However this proved impossible to implement, since it was impossible with the resources available to drill a straight 300mm long channel though a block of PTFE, with a uniform diameter of 2mm. The friction on drill bit overcomes the grip of the chuck on the bit typically within 10cm of drilling, preventing further drilling. It was also noticed that, due to elasticity of PTFE, there is significant twisting of the drill bit which results in noticeable increase in drilled chamber diameter after 5cm.

In practice the manifold was composed of two PTFE blocks, the top blocking containing the solenoid valve chambers and a drain connected to vents leading down to the second block. The second block contains only the single long channel, surrounded by a 1 mm wall surrounded in turn by a 2mm groove. An EPDM Rubber O ring is pressured into this groove, and acts as sealant when the two parts are compressed when the manifold is assembled, producing an object analogous to a single block containing a single straight 2mm channel. On the primary manifold, the solenoid valve chamber located at the opposite end to the drain is aligned in a reverse direction (with the chamber's source connected to the long flow channel and the drain leading away from the manifold) and acts as a reverse drain.

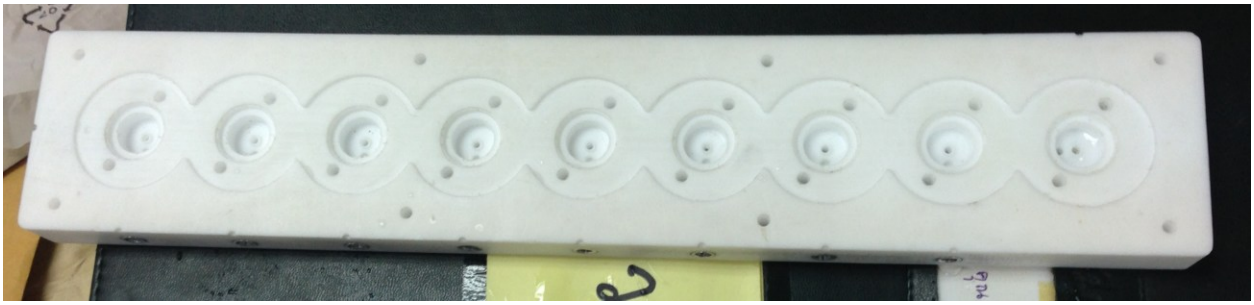

Fig 6.08 Part 1 (top) of solenoid valve manifold, containing vents and solenoid valve chambers.

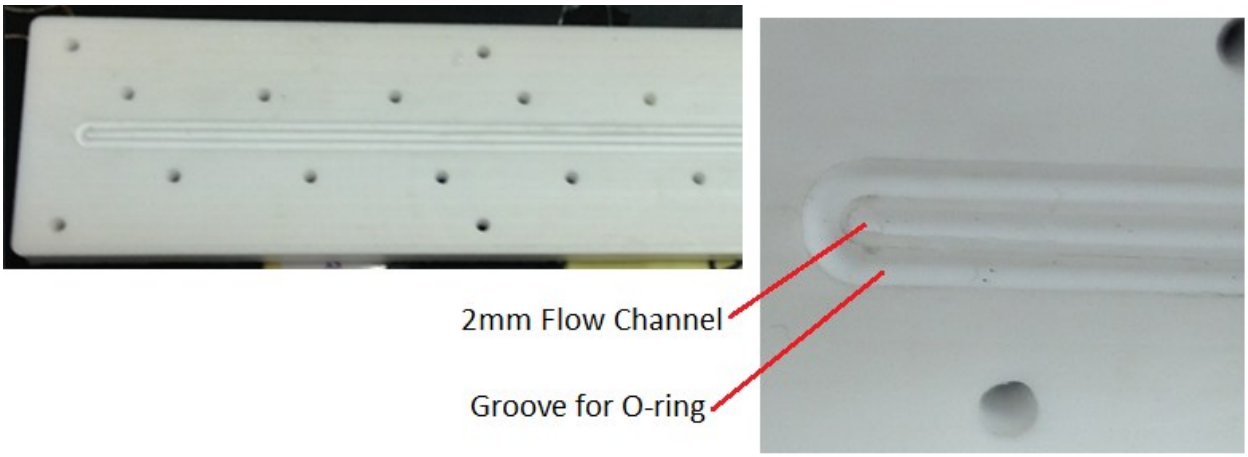

Fig 6.09 Part 2 (bottom) of solenoid valve manifold, 2mm flow channel and O-ring groove.

It should be noted that PTFE proved to be an exceptionally difficult material to machine, since it is soft and elastic enough to not be abraded easily by a tool bit. This makes the creation of precise machine parts out of PTFE difficult, since the plastic deforms and flakes on contact with tool bit, rather than being abraded. Nevertheless all requisite PTFE parts were successfully fabricated after extensive optimization, primarily by CNC milling. Some design compromises which should minimally affect performance was also undertaken to allow replicate parts to be fabricated reproducibly within realistic time frames (for example the wall separating the 2mm flow channel from the groove, a particularly difficult part to machine, was expanded from 0.5mm in the original design to 1mm in width).

Fig 6.10 The primary solenoid valve manifold in fully assembled state.

6.04c Overview of important considerations in the design of solenoid valves and flow tubes

It should always be remembered that the flow system is a means of transportation, either of reactants into reaction vessels or of waste materials to drain. While an enclosed flow system is isolated from outside contamination, some mixing can occur as a result of simple diffusion at the boundaries between two solutions at the flow tubes. This is not a major concern for wash solutions and buffers, which are cheap and employed in large volumes. However, DNA solutions and PCR mixes must be fed as solution segments pushed by buffer or other solutions (plugs) for reasons of economy. In operational terms this generally means a relatively short segment of fluid flanked on either end by a buffer solution. The plugs envisioned for this SELEX device will be approximately 500 ul in volume, which equates to 79.58 mm^3 of volume per mm^2 of diffusional interface with a 2mm inner diameter tube. Thus the degree of diffusional mixing of the system at a static state, or even during movement along a smooth tube, should be relatively insignificant. The absence of significant (>2mm) expansion of the solution boundaries observed during long static phases of device operation (the 2 hour long affinity selection for example) would support this conclusion.

In theory the degree of mixing taking place in the flow system could be predicted using the Reynold's number [171]. The Reynolds number is a dimensionless quantity used to categorize of whether a fluid flow will in a laminar or turbulent. A Reynold's number of <2000 is typically considered laminar, and >2000 is generally considered turbulent. Reynold's number can be defined as the ratio of the inertial force to viscous force, and can be represented using the following equation:

$$Reynold's\ number = \frac{pVD}{u}$$

Eq 6.02 Definition of Reynold's number

D being Hydraulic diameter (m)

V being flow rate (m/s)

p being fluid density (kg/m3)

u being viscosity of the fluid (kg/ms)

The Reynold's number of this flow system (2mm diameter tube, with the liquid assumed to have a property similar to water at 25°C) is 13.4 at slowest movement (6.7mm/s, F300 in Gcode) and 53.6 at fastest movement (26.7mm/s, F1200 in Gcode), which would predict very little turbulent mixing between fluid boundaries.

However the above analysis assumes a smooth cross section across the entire flow channel. Any disruption in the tubing, particularly changes in tube cross sectional area or other spatial rearrangements would result in a change in hydraulic diameter, and therefore increased mixing as a result of turbulence. The cumulative effect of these changes could be significant. In order to reduce dimensional change at tube-manifold and tube-block interfaces, pneumatic tube fittings are used. The stainless steel pneumatic fittings were purchased from SMC USA, series KQG2, product code KQG2S04-M5. The datasheet for this item can be found here [172]. This pneumatic connector design has the benefit of positive sealing under pressure and simple one push connection and disconnections which allow for faster maintenance and assembly. Internal diameter is 2 mm which is ideal for our application. This series of connectors is chemically resistant to most disinfectants, and resistant to autoclave temperatures.

Other potential area of turbulence include the motor pump (assuming it is of peristaltic pump design) and solenoid valve. The solenoid valve is of particular concern, as the liquid will need to pass through a flow chamber of 12mm diameter, which will significantly deform solution boundaries. However the majority of the solenoid valves on the manifold do not cause turbulence mixing of solution, since they are utilized to regulate flow from reagent source containers, and hence handle only one type of solution.

The implementation of air gaps at plug to buffer boundaries was also considered as a means of preventing mixing. This could have been implemented by the replacement of the liquid solenoid valve nearest the output of the manifold with a gas solenoid valve. As the boundary of a newly added plug is pumped pass the location of the output vent of the gas solenoid valve, gas injection could take place enabling the isolation of the plug from the buffer liquid. This was not implemented as the boundary distortion was already considered acceptable (see results below) without separation by gas segments. Gas solenoid valves are structurally different from liquid solenoid valves, and therefore the implementation of a gas solenoid valve would have required significant modification of the PTFE manifold. Gas solenoid valve design that utilize electromagnetically controlled tilting plungers and

sliding rods would also have been significantly more difficult to fabricate, and would have required the use of a 4 axis CNC milling device. Another potential concern is that the gas plug may compress and expand as a response to pump pressure, reducing the accuracy of liquid handling.

6.04d Liquid Handling Model 4 (LHM4):

In the earliest phases of liquid handling design it was assumed that any pump used in this device would likely be mono-directional. Therefore due to the cyclical nature of the SELEX process it is essential, under such an assumption, that a flowback system is implemented to enable the return of PCR product back to the affinity selection chamber. In the absence of reverse flow capable pump, a flowback loop is implemented. After the process of PCR, the second solenoid valve manifold switches from drain to loop, allowing the solution in the PCR chamber to return to the affinity selection chamber.

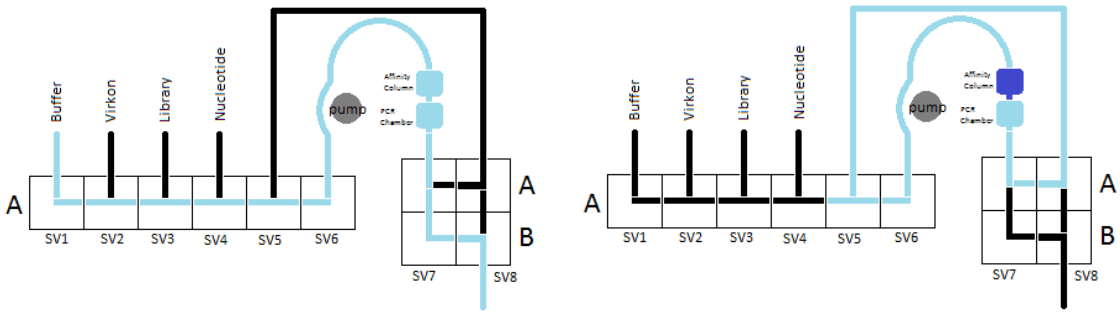

Fig 6.11 An early Liquid Handling Model (LHM1) operation showing effect of switching output of 2nd manifold on flow, which shifts from an source to drain flow system to a cyclic flow system.

From a liquid handling perspective, the most beneficial property of the WPM-e pump (this peristaltic pump will be discussed in the next section) is its ability to operate in both directions. By reversing flow, it is possible to transport amplified product from the PCR chamber back into the affinity selection chamber. This eliminates the necessity of a loop tube, and more relevantly the solution boundary deforming solenoid valve that controls it. Since the loop tube is no longer necessary, it is also no longer necessary for the peristaltic pump to be located between the manifold and the loop tube/drain junction. It is therefore possible for the peristaltic pump to be located between the last component of the flow system and the drain. This prevents deformation of solution interfaces of either the DNA library or PCR mix plugs, since neither of these solutions in this new setup has to pass through the peristaltic pump.

This enables the entire length of the flow channel after the (single solution) solenoid valve feed to have a bore diameter of 2mm, which should minimize mixing through turbulence and allow flow boundaries to be maintained.

Thus the loop solenoid valve in the old model is removed in LHM4, and a new solenoid valve is placed at the end of the block, and acts as a second drain while the peristaltic pump is operating to reverse the flow. In practice the loop manifold is replaced by a second manifold to take advantage of the reverse flow system in enabling a more direct feed to the affinity selection chamber. A reservoir tube is also added after the forward drain solenoid valve, to supply fluid to the system while the pump is acting in reverse. In practice the only type of solution in the reservoir tube which reenters the system is buffer as every step requiring reverse flow is preceded immediately by a buffer wash step.

For more details on the operational aspects of LHM4, please see the previously discussed protocol section (see page 194) and the device operation section (see page 241) of this chapter.

6.04e Liquid Handling Results

A simulated SELEX round was performed on the ASD, with the reagents being replaced by coloured dyes.

Correct liquid handling was determined by observation of liquid volume in the source reservoirs. A decrease in the correct source reservoir during the simulated steps, and absence of volume change in other reservoirs, indicates correct liquid handling has been successfully achieved. This, combined with weight measurement of the expelled liquid, which will be discussed in the next section of this chapter, enables us to determine that the correct volume of the correct liquid is being handled.

Boundary distortion were never successfully eliminated, and indeed this might not be realistically possible for mesofluidic systems flow tubes with an ID as large as 2mm. The final model of the SELEX device reduced distortions at boundaries to at most 4cm, which should be acceptable so long as this distortion is taken into consideration in the operational protocols. Assuming each distortion boundary extends equally on both sides of a liquid-liquid interface, this means 2cm of a reagent plug would be deformed, resulting in a loss of 62.8ul of reagent (3.142mm2 cross sectional area, 20mm section length). This equals to 125.7 ul of reagent loss per plug (two liquid-liquid buffer boundaries). Since plugs for DNA

library and PCR master mix are planned to be 15.2 cm long, this would equate to a loss of approximately 26.3%.

Visual observation of dye section movements through the flow channel also indicates that reagent plugs have been successfully formed. Dye molecular weight is significantly lower than those of either template or primers (by at least 1 order of magnitude in both cases) so effect of diffusion should be more pronounced in this simulation than with actual components of PCR. Free nucleotides utilized in PCR is of similar weight to the dyes, but is used in excess concentration during PCR, and therefore their loss can be considered less significant than the loss of primers and library sequences.

6.05 Flow Rate Control System

6.05a Peristaltic Pumps

A number of liquid handling pumps were considered, both made in house and commercially available. Peristaltic pumps were considered the most suitable class of pump for liquid transportation in this device. Peristaltic pumps are a form of positive displacement pump. In the vast majority of peristaltic pumps, fluid is driven by running a roller along a flexible tube against a circular outer casing. The tubes are thus occluded where the rollers have contact, and liquid is thus driven up the tube as the roller moves onward. After the roller passes a section of the tube, the tuber expands back, resulting in negative pressure which draws liquid into the tube. This peristaltic mechanism is similar to those found in biological cases such as the gastrointestinal system.

One of the inherent advantages of the peristaltic pump is the complete isolation of the tube interior surface from the mechanical components of the pump. This is a significant advantage since mechanical parts of any pump are difficult to sterilize, mainly because good sterilization techniques are incompatible with sound mechanical operation. In peristaltic pumps, the cleanliness of the exterior mechanical parts of is irrelevant since only the interior surface of the flexible tube comes in contact with reagent. The reverse is also true; in that isolation of the liquid from the mechanical components also protects the mechanical components from damage should the pumped liquid be particularly reactive. This is not likely to occur with the reagents used in the SELEX process, but broadens the option of cleaning methods that can be implemented.

Other advantages of peristaltic pumps include mechanical simplicity, and the fact the peristaltic pump blocks all liquid movement while not in operation, allowing it to act as a valve. This removes the need for a valve to regulate against liquid backflow and overflows in the main channel where the pump is present. Although there are limitations in the performance of peristaltic pumps such as maximum flow rates and pulsatility, these are not significant ones in the system described here.

6.05b Peristaltic Pump 3 (Welco WPM-E)

Attempts was made to build an in-house peristaltic pump based on parts fabricated by 3D printing, though none were able to achieve the level of precision or mechanical reliability needed for practical SELEX operation. The datasheet for the WPM-e pump can be found here [173].

In the final design, a commercially available peristaltic pump was selected for the LHS system. The Welco peristaltic pump proved to be accurate, chemically resistant and mechanically highly reliable. The device was also compact and relatively easy to assemble and disassemble.

WPM series peristaltic pumps are modular, and thus a number of options regarding structural materials and drive motor were available. WPM2-P2EA-CP variant was selected. This variant uses a Pharmed BPT for peristaltic tube material and a stepper motor as drive motor. The former was selected for its generally good chemical resistance and excellent heat resistance, which should facilitate cleaning process. Tube inner diameter was 2mm. Stepper motor was selected for accuracy, controllability and simple integration with existing software. The pump is capable of operating under 80°C, which should exceed operational requirements.

The entire device could be autoclaved in disassembled state, though this should not be necessary, as only the internal surface of the tube comes into contact with the reaction and thus needs to be sterilized. Life span of tube is >1000 hours, which is better than silicone, and the tube could be autoclaved repeatedly at 135C.

The device was tested using SELEX buffer as fluid. The mass of liquid transferred is calculated by weight change of a weighing boat.

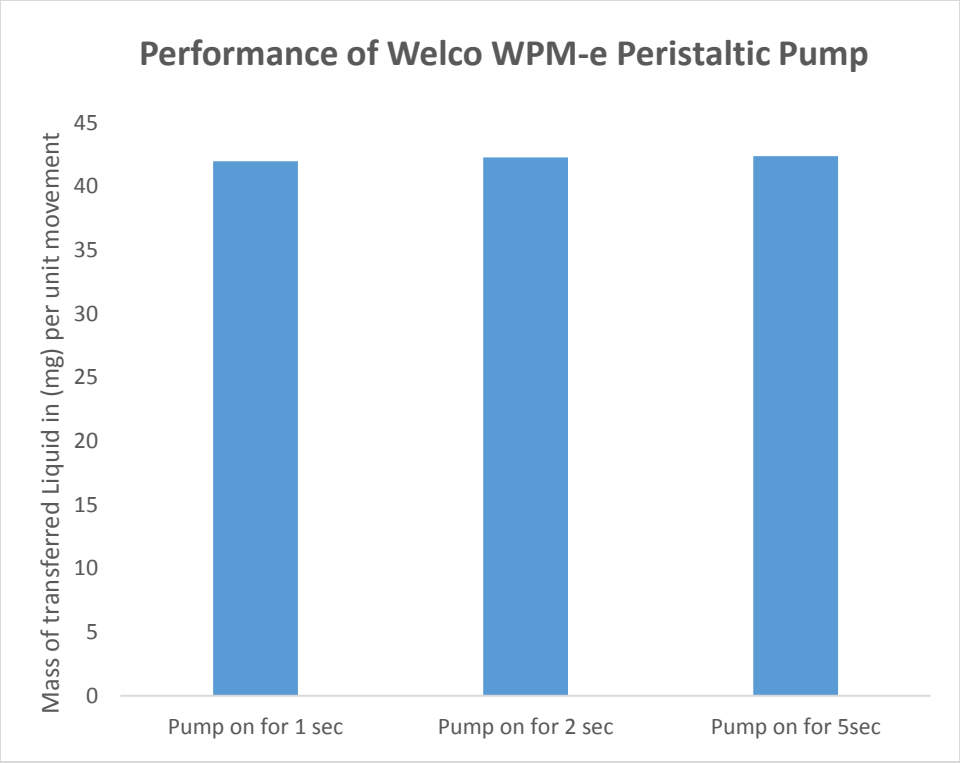

Fig 6.12 Output of Model 3 in weight of liquid transferred standardized to 2.7mm effective movement. This translates Gcode based movement commands into syringe movement, which should determine volume pumped. Volume is measured in weight due to mode of measurement (a Sartorius scale)

The results would indicate that the WPM-e pump is able to transfer liquid with a resolution sufficient for this application.

6.06 Electromagnetic Separation System (ESS)

In the final design of the ASD, Magnetic Nanoparticle (MNP) based partitioning of target bound DNA from unbound library, as well as single strand separation of affinity selected sequences from PCR product was used.

6.06a Preparation of Target MNP

Target is bound to Streptavidin Coated MNP by a commonly used, NHS-Biotin mediated, bioconjugation protocol which can be found in the methodology section (see page 77)

6.06b Streptavidin Coated MNP (SCMNP) separation non-selected amplification product

The ssDNA output library selected by affinity selection should (in theory) all bind to the target molecule. However as these sequences are only a small fraction of the input library they need to be re-amplified prior to the next selection round. The PCR amplification process generates a double stranded product with complementary sequences to the original template.

This results in the loss of effective DNA concentration, since some sequences will no longer be able to bind to target as a result of binding with complementary sequences, as well as possible introduction of non-target specific sequences with high affinity to platform.

A common method of removing these complementary sequences is through the use of biotinylated reverse primers during PCR. This results in the final amplified library containing biotinylated reverse sequences and unbiotinylated forward sequences. By incubating the amplified pool with excess streptavidin-MNP, most of the reverse sequences become bound to the MNPs and can be selectively removed from the solution. A comparison of conventional MNP separation protocol and the automated MNP separation protocol developed for this study can be found in the protocol section of this chapter (see page 194)

6.06c Design of Electromagnet

Most conventional electromagnets are composed of wire wound around an iron core. In the final design, the core is composed of multiple laminar layers of thin insulated iron sheets, derived from the “E” component of an E-I lamination. This core design acts as the equivalent of multiple individual magnet circuits, each one receiving a small portion of magnetic flux. Since eddy current flows around lines of flux, the lamination reduces eddy currents, restricting its flow to smaller, high resistance regions. Reduction of eddy currents is important in order to reduce losses by induction heating. An E shaped core was selected to increase the surface area of contract between the magnetic pad and the affinity selection chamber.

The wound wire is composed of copper, 0.5mm in diameter. Application of current through this wire results in the formation of a magnetic field, with the polarity of the central prong of the “E” being opposite to those of the flanking prongs.

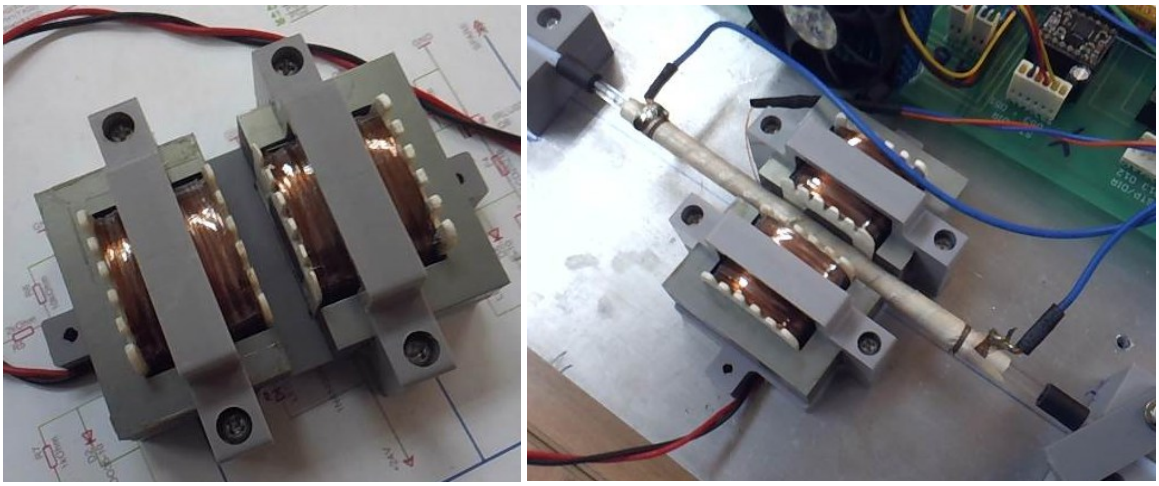

Fig 6.13 Model 3 Electromagnet. (Right) in loose state (Left) In position during operation, note affinity selection chamber location between the two magnet prongs.

The final design of MSS is composed of two of the above described magnetic cores arranged in mirror image of each other and held in place with an assembly fabricated from CNC milled PVC. The space between the cores is equal to the width of the heating tube surrounding the affinity selection chamber. This allows the magnets to be as close to affinity selection chamber as practicable, which is important since magnetic field strength drops exponentially as a function of distance.

Current flow direction is applied in the opposite direction in the two magnets, which result in complementary charges between all 3 prongs of both electromagnets. Thus main magnetic field between the two magnets run between the prongs and their complements on the other magnet, rather than between the differently changed center and flanking prongs.

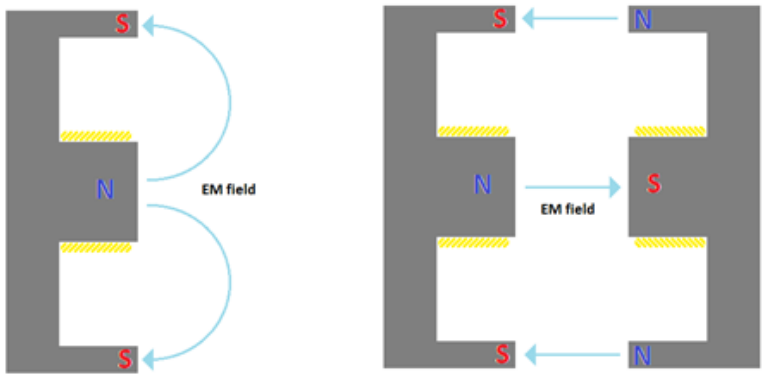

Fig 6.14 Comparison between the EM field of a system with one magnet only and a system with two complementing magnets

6.06d Results for ESS

A pilot simulation of the SELEX operation was conducted in order to determine the performance of the ESS. The MNP retention protocol is identical to those of the final SELEX operational protocol, but with the wash length extended by 100%. Flow rate during wash is 42 ul/s (13.4mm/s liquid movement along flow tube, or F600 in Gcode terms).

Perhaps the easiest method of quantifying MNP mass in solution is through observation of turbidity, the more particles in solution the greater the obstruction of light. A UV/Vis spectrophotometer in scan mode could be used as turbidity meter. A literature review did not reveal any previous study describing the quantification of MNP using UV/Vis spectrophotometry which could be applied to this application, and reference regarding quantification of MNP by UV/Vis spectrophotometry does not exist in the MNP manufacturer's handbook.

Since no reference sample is available, 3 known concentrations of MNP were used as baseline for comparison, these being 100%, 30.3% and 15.2% of the concentration of the MNP in the reservoir (and 33%, 10% and 5% of the stock MNP solution). Results from MNP retainment from a previous model of ESS and from a hand placed strong magnet (80mm long) is also included for comparison. The UV/Vis spectrophotometry results of a full concentration of the above samples were not able to distinguish between the higher concentrations results, and so all samples were diluted down by a factor of 1/3.

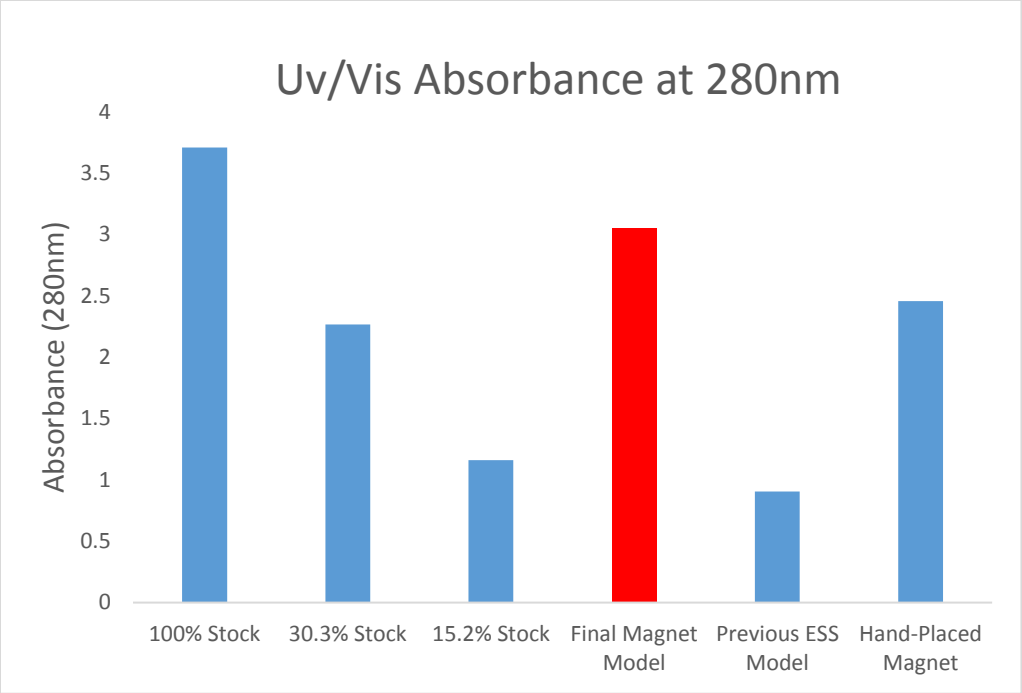

Fig 6.15 UV/Vis Spectrograph comparing concentration of MNP isolated using different protocols and known concentrations, all samples were diluted down by a factor of 1/3.

The UV/Vis results would indicate that the final model of ESS is capable of retaining at least 30% of the MNP concentration of the input reservoir. The reservoir concentration of MNP is 0.33mg/ml, and therefore retained concentration of MNP is 0.1mg/ml. Since target load is 400 pmole per mg of MNP (based on manufacturer specifications [174]), this equates to target mass of 1.26 pmole per 10mm section of 2mm ID affinity selection chamber. The estimated effective length of the affinity selection chamber is 120 mm, therefore total target mass is expected to be at least 15.1 pmole.

Expected oligonucleotide load is at least 500 pmole per mg of MNP based on manufacturer's specifications [174]), which equates to 18.9 pmole per 120 mm of flow tube length. This is considerably below the capacity needed to bind the same volume of 0.4 uM reverse biotinylated sequences present in the PCR product solution (both unreacted primers and amplified sequences), which would require a binding capacity of 151 pmole. However it should be noted that these figures are based on worst case assumptions, with total MNP retainment of 30% (which the results above would indicate that the final ESS exceeds). It should also be noted that the total binding capacity per mg of MNP is 2.5 nmole and that, due to the shortness of sequence used in this study more oligonucleotide could be bound per mg of MNP than 500 pmole.

6.06e Results of MNP mediated ss Separation

The product of MNP separation can pose a challenge to the quality control, as they are similar in appearance to the non-specific large amplicons discussed in the Temperature Control System section of this chapter (see page 205), typically appearing as multiple distinct bands of different sizes on the agarose gel.

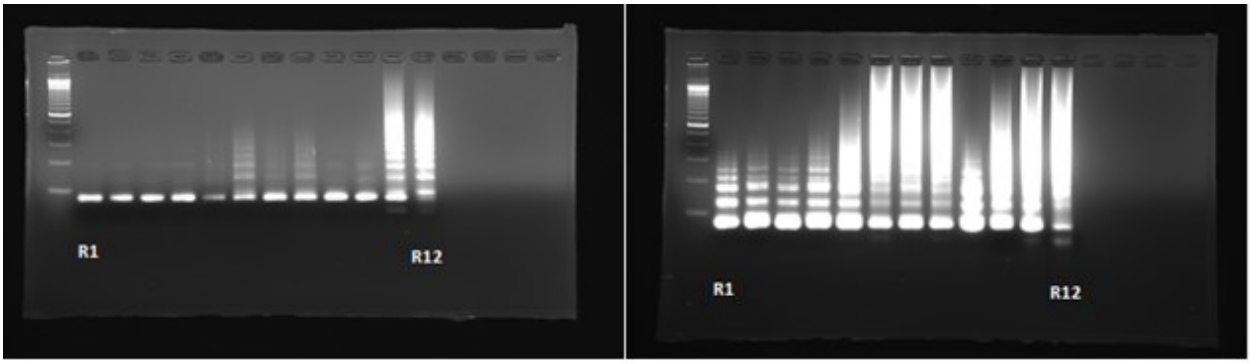

Fig 6.16 A comparison of gel electrophoresis results of series 1 from archive samples, with ladder in right most well, followed by rounds in ascending order (R1 left most, R12 right most) (left) immediately after PCR and (right) after MNP separation. Note that the presence of large non-specific amplicons that have started to accumulate by round 11.

It is hypothesized that the cause of this appearance is the formation of secondary structures by the ssDNA product of single strand separation. While the primers of the Trilink library have been designed specifically to have no complementarity to each other, the presence of the 30bp random means that sequence to sequence affinity is possible. These secondary structure travel down the agarose gel at a slower rate, since these aggregates have combined molecular weight greater than the single stranded single sequences, resulting in appearance of multiple bands. A comparison between the post PCR and post SCMNP based ss separation products (both generated manually for archival and feedstock generation purposes), could be found below (see Fig 6.18).

This analysis is supported by the results of Lambda nuclease digested product, which shows very similar results when analyzed using agarose gel. While MNP and Lambda based single strand separation are very different, the product of both processes are similar (single stranded sequences, though biotinylated sequences are retained in lambda cut, while MNP separation retains non-biotinylated sequences). Since Lambda digest is a heatless process in the absence of PCR solution (unlike the automated series 8 SELEX

MNP separation process, which is done in the presence of both), the formation of non-specific large amplicons during the lambda digest process is impossible and thus the appearance of multiple bands can only be the result of ssDNA aggregation as a result of secondary structure formation.

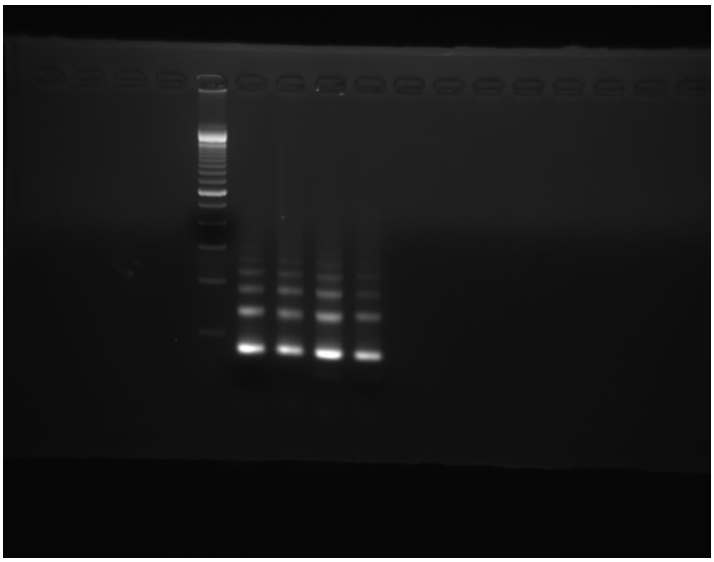

Fig 6.17 PCR product after cleaving by Lambda nuclease. Note similarity between the band patterns to those of ss MNP separation, a process with analogous end results.

Because the automated SELEX protocol includes automated SCMNP based single strand separation (and therefore delivers the SELEX product in an ss separated state), this imposes a significant challenge to quality control since it prevents the presence of large non-specific amplicons from being observed directly by gel electrophoresis of the automated SELEX product (which appears as multiple bands regardless of the presence of large non-specific amplicons). It is impossible to extract the product of automated PCR (where the presence of large non-specific amplicons could be easily observed on agarose gel) and return it for single stand separation due to the volume of the solenoid valve chamber (see section 6.10 of this chapter, page 241).

The solution for this is to observe the product of PCR performed using the single strand separation product as template. Secondary structures formed from short sequences are denatured in the melting step of PCR, resulting in the breakdown of these aggregates. The component short sequences receive complementary sequences with greater thermal stability than the secondary structures, and thus secondary structure do not reform after the PCR process. This results in a single distinct band. Non-specific large amplicons contain primers binding regions, and the whole sequence is amplfied by the PCR process, resulting PCR product which display multiple bands of varying sizes on the agarose gel.

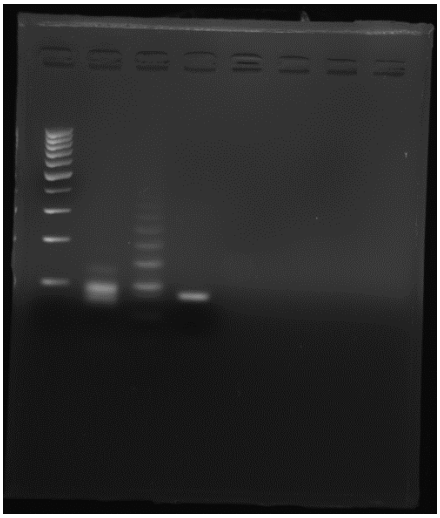

Fig 6.18 A comparison between gel electrophoresis of (ss separated) extracted product and PCR product. Left to Right 1) 100bp ladder 2) ASD product extracted immediately after PCR 3) ASD product, extracted after manual MNP ss separation 4) Sample (3) used as template for 12 cycles of manual PCR

6.07 Electronics

6.07a Arduino

Arduino is a low cost open-source single-board microcontroller. The Arduino hardware is effectively composed of an eight bit Atmel microcontroller (the exact chip varies depending on board) along with its necessary infrastructure needed in order to allow it to function (such as a 16MHz clock and 5V regulator), and facilitate communication with other devices (such as blank pins used to communicate with actuators and sensors and a USB port for communication with a PC).

The Arduino board variant selected was the Arduino Mega, which contains an Atmel Atmega1280 8 bit microcontroller. The datasheet for this device can be found here [175], and for the microcontroller here [176]. ArduinoMega board has a total of 39 standard digital pins, 15 PWM digital pins, and 16 analogue pins, this exceeds the requirement of the SELEX device, which require 14, 2 and 2 of each respectively.

The 5V control circuit Arduino board is powered directly by the USB cable. The system has a maximum current output of 40mA per I/O pin, and a voltage of 5V. This necessitates the use of an amplifier, which mimics the communication signal from the I/O pin of the Arduino board, but with much greater amplitude.

6.07b Design of Amplifier Circuit

Both electromechanical relays and solid state transistors were considered for use as amplifiers for the remaining actuators. MOSFETs were selected due to lower cost, smaller size and compatibility with PWM based temperature control system.

IRLU 024 MOSFETs (datasheet can be found here [177]) are used for all amplifier circuits connected to solenoid valves and electromagnets. The gate pin of the IRLU 024 is connected to the blank digital pin assigned to this actuator on the Arduino. A 2kOhm resistor is placed between the MOSFET gate and the blank pin as a current limiter. MOSFET ground pin and signal is wired to ground through a 10 kOhm resistor. Tyco Electronics RXEF025 Polyswitch [178] is added as a precaution to prevent over current from damaging the system. This is particularly important during prototyping stage while the circuit was constructed on breadboard, and loose wiring was common. A Vishay 1N4148 [179] flyback diode is present to protect system from voltage spikes as a result of inductive load (all actuators in this system has a coil magnetic component with the exception of the temperature control system).

The LED and its current limiter does not play a role in the SELEX machine operation, but are primarily present to allow inspection and testing of circuits without the actuator being connected. Additionally the solenoid valve housing and the manifold completely enclosed the valve mechanism, thus the only method of determining solenoid valve on/off state is by observing the LED for the pin associated with this solenoid valve.

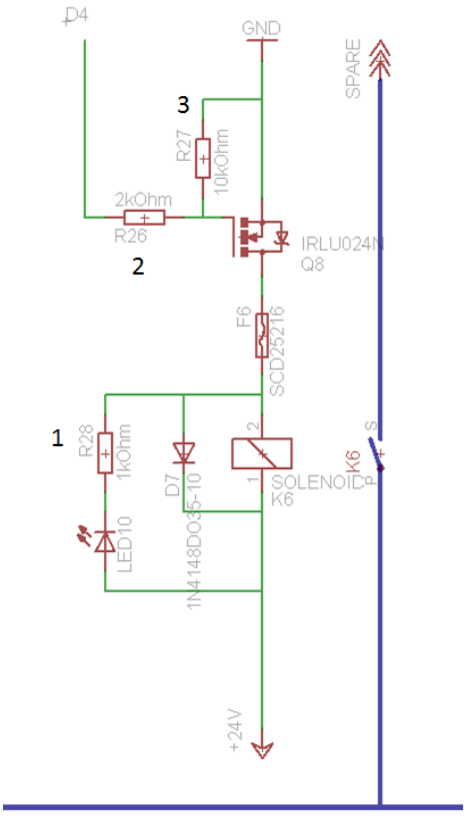

Fig 6.19 Design for amplifier component of circuit, designed on Eagle CAD.

All MOSFET amplifiers on the circuits are wired in this fashion using the same components, allowing them to be interchangeable. This has the added benefit of increasing flexibility in case of future modifications. The only exception are the two MOSFETs controlling the heating tube for the temperature control system, which utilizes the more powerful International Rectifier IRF640n [180] MOSFET with an increased power rating to fulfill the requirements of the nichrome wire heater. This MOSFET was observed to heat up quickly during temperature ramps, and so a heatsink-fan cooler assembly was attached to the temperature control MOSFET to enhance heat dissipation.

Stepper driver used to control the LHS is an A4988 Pololu [181] type device, another holdover commonly used in basic 3D printer setups. As mentioned in the LHS section, Stepper motor is a brushless DC motor that divides a full rotation into a number of equal steps. Each step is generally performed sequentially at high speed, giving the appearance of smooth motion, in the same way a PWM digital signal has the

appearance of an analogue signal. The quantitative mode of movement allows the position of the motor to be determined without the use of a feedback sensor, based on number of steps moved.

In practice stepper motors are controlled by 2 signals, one either in a long 0/1 state signal determining direction of movement, the other pulsed as a short signal with each 1 resulting in a movement step. This signal is generated by the microcontroller as a 5V signal. This signal is not powerful enough to drive the mechanical motor, and thus a stepper motor driver (such as Pololu) is used to amplify this control signal, as well as provide fractional steps, which smooths out the motion of the stepper motor, reducing vibration and jerkiness.

6.07c Migration to Printed Circuit Board (PCB)

It was decided relatively early into the development of the ASD to migrate the electronics of the automated SELEX device onto PCB once electronics design becomes finalised. This was primarily done to decrease the total area of the circuit board and the number of failures due to loose connections as the complexity of the device increased with development. The PCB was wholly designed by the author using Cadsoft Eagle CAD software[182]. Microcontroller board and the PCB circuitry is connected to each other in a shield format.

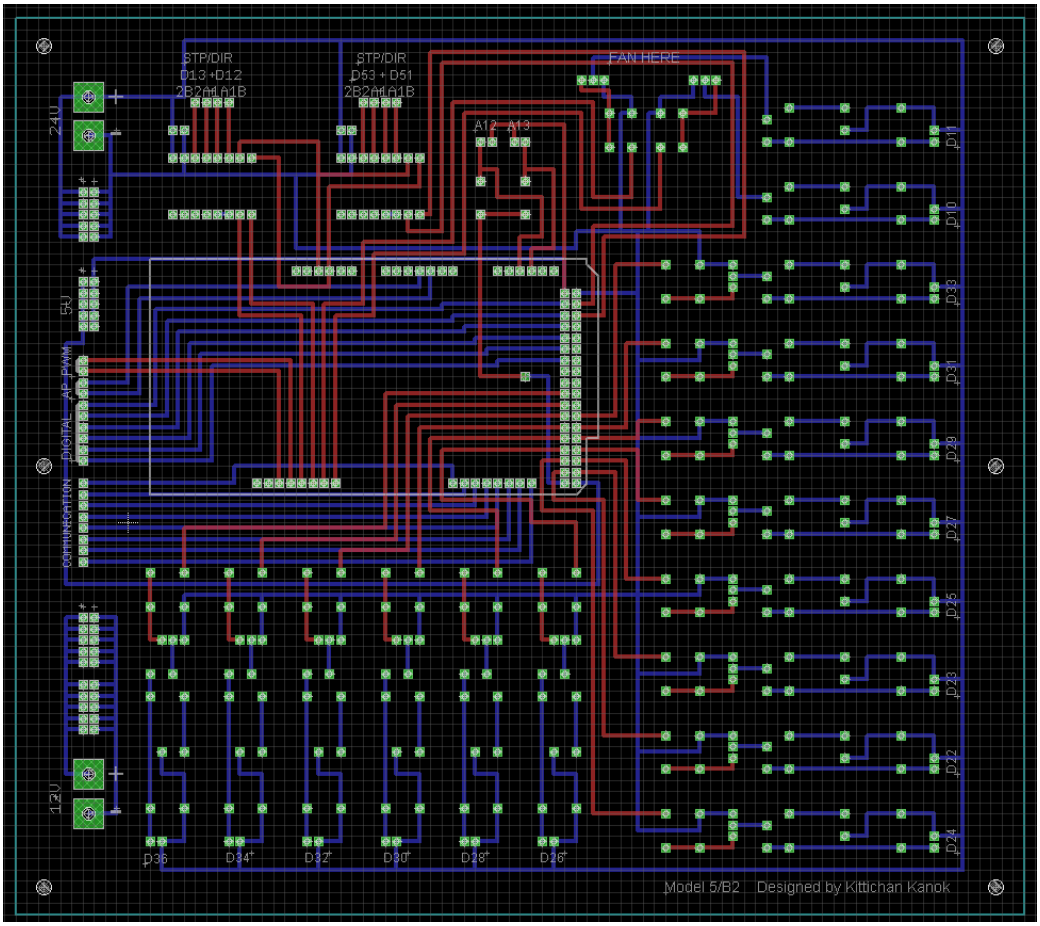

Fig 6.20 PCB design for SELEX device control circuit. Red) Top Layer, Blue) Bottom Layer, Cyan) Milled Layer, White) Ink Annotation, Green) Copper Pads

Unlike the breadboard, the PCB cannot be easily upgraded. Thus special care was taken to increase the numbers of redundant outputs in anticipation for future use. Two extra redundant solenoid valve control circuits were added beyond the number needed for all valves in the original circuit design. Two Pololu steppers were also integrated (one needed by original design). 6 digital, 2 analogue and 2 PWM connectors were extended on the Arduino shield for easy access in case of future needs. 12V auxiliary system power is kept separate from the remaining circuitry hardwired in an always on state, these are used by peripheral systems such as cooling fans.

The PCB was fabricated by KAT Intertech Co.,Ltd. Migration to a PCB could be considered a considerable improvement. While no statistics were taken, failure rate decreased significantly after migration to PCB (no known failures related to electronics hardware took place). The only noticed flaw in the PCB design is that the circuit for the two cooled MOSFETs of the temperature control system are duplicated in mirror image to each other. This would result in the two MOSFET facing opposite directions when

assembled, preventing use of the same heatsink. This problem was easily resolved by abrading the PCB connection to one of the MOSFET, and reconnecting by wire soldering.

6.08 Software

The software of the SELEX device can be categorized into 3 main elements, the SELEX device-side sprinter firmware, PC-side Printrun software, and the Gcode instruction which supplies commands to the device. The relationship between this triad can be summarized as the Gcode providing specific instructions on how the specific task is to be carried out, the PC-based software providing a means for which this instruction could be communicated to the SELEX device in a way that is comprehensible to the firmware, and the firmware being the means by which the instruction is coordinated and communicated to the correct effector, enabling a correct response to be formed.

6.08a Sprinter Firmware

Sprinter is an open source 3rd party firmware commonly used in Reprap 3D printers. The firmware represents the non-volatile instruction sets of the device, installed within the flash memory of the Arduino device, and cannot be changed without complete re-programming. In a sense the firmware provides a basic set of functions to the device, providing an environment in which the more volatile software could function. The unmodified sprinter firmware can be downloaded here [183].

Sprinter firmware was chosen because it is a well proven software which is known for highly stability. It has existing infrastructure for PC interaction via USB, pre-existing control coding for motor and temperature control, and pre-existing coding for direct Gcode control of blank pins. The presence of SD card reading infrastructure in sprinter software raises the possibility in future times of building a platform capable of operating without a PC (by allowing the device to directly read Gcode from SD device), as well as communication pins needed for integration of direct input and display device to enable this. Sprinter is also relatively simple compared to similar 3D printer firmwares, allowing it to be easily modified.

The sprinter firmware was used in a largely unmodified state. The only major modifications made to the Sprinter firmware were the integration of the improved PID described in the temperature control

section of this chapter (see page 205) by the author using detailed instruction available on both the PID designer's website and the Arduino website's reference page, as well as considerable assistance form the Arduino community in general.

Some minor modifications to improve the accuracy of the temperature readout by calibration of thermistor table values. Some pins were also reassigned in order to allow for easier assembly on breadboard and IC board.

6.08b Printrun

Printrun was utilized without any modification from its original published form [184].

6.08c Gcode

Gcode, the colloquial abbreviation of G programming language, is a commonly used numerical control programming language primarily used in computer controlled machining and other computer aided manufacturing. Gcodes are basically a list of sequential instructions for commanding a computerised machine to perform a series of sequential actions. For example, a AutoCAD generated .dxf file containing 3D model for one of the Solenoid Array parts is converted by ArtCAM to Gcode, which guides a cutting head through a tool path removing unwanted parts in a CNC milling machine, or a solidwork generated .stl file containing a 3D model for components of the Syringe pump is sliced by Slic3r to a Gcode, which results in the layered fabrication of the machine part by a 3D printer.

As such most of the Gcodes deal with aspects of computer controlled milling and are not relevant to the SELEX operation. Less than a dozen Gcodes are utilized for the control of the SELEX devices:

G4: Dwell, this causes the device to idle for a specified period of time. Example G4 S5 causes the device to idle for 5s.

G1: Linear movement between two points. The program moves between two points specified via interpolated points between the two points, resulting in a linear movement via fastest route (ie a straight line). The device automatically calculates the number of steps needed by the stepper motor to achieve this. Rounds per second of motor rotation determines speed of movement, though for obvious

reasons number of rotation remains the same for all speeds. Direction of movement depends on the wiring of the stepper motor. Example G1 Y800 F1200, assuming we start at Y = 0, will induce a 80 cm movement at the rate of 20mm/sec.

G92: Set coordinates to. In computer assisted manufacturing this sets the current position of the machine head to the coordinates specified. For this SELEX device it is invariably used as a means of resetting Y axis value to 0, resetting the movement. This prevents accumulation of Y value and makes the Gcode presentationally easier to understand and more amenable to later modification.

M42: Switch blank pin on and off. This is used to switch the value of a I/O pin controlling a solenoid valve or the electromagnet on or off.

M104/M140: Set temperature. Sets temperature for either the Affinity Chamber or the PCR Chamber of the device. Adjustment of temperature to fit this figure is otherwise automatic. Example M140 S90 sets the temperature of chamber controlled by Pin D08 to 90°C.

6.08d Key Software Tasks for SELEX operation

There are a number of tasks the SELEX device needs to be able to execute in order to perform a SELEX round.

Liquid Handling

As mentioned in the FRCS section of this chapter (see page 212), the liquid flow rate control from this system is controlled by a peristaltic pump, which is driven by a stepper motor. A stepper motor is the standard axis regulation component of a CNC milling/3D printer device also, as distances moved by the stepper motor can be very exactly controlled. While peristaltic pump's operational unit for SELEX operation is flow rate, the stepping motors unit of action in Gcode is distance moved. Direction of movement is regulated by controlled opening and closing of solenoid valves. Control is achieved by the following script:

M42 P[Input Port] S255

G4 S2

G92 Y0

G1 Y[Volume of Flow in theoretical distance] F1200

G4 S[Time needed for Flow]

M42 P[Input Port] S0

The first line instructs switches on the O/I pin controlling the input port solenoid valve to high, opening the port. S255 simply means signal to high.

The second line is a 2s wait to allow port to open (theoretical open time is 100ms).

The third line resets the Y axis to 0

Fourth line instructs the stepper to move theoretical machine tool to theoretical Y coordinate, result is peristaltic pump induced flow proportional to new Y axis value.

Fifth line holds signaling in wait till step four is completely carried out. Wait time = (theoretical distance/movement speed) + margin for error.

Sixth line closes input port. S0 switches I/O pin to low.

Output port is always the 1st Drain (output from peristaltic pump) with the exception of the step reversing flow, at which point the opened solenoid valve is always the reverse Drain (this is the solenoid valve at the opposite end of the flow path to the peristaltic pump), source reservoir in such case is from the reserve coil attached to the peristaltic pump. Y movement in this case is completely analogous to positive movement, but with a negative value.

Temperature Control

Temperature is controlled by heating block. As mentioned in the temperature control section of this chapter, temperature is regulated through feedback mechanism by the PID component of the firmware, Gcode simply sets the desired temperature of the heating chamber. The following script is used:

M[M104 or M140] S[Desired temp]

G4 S[Time of heating]

Line 1 sets heating temperature

Line 2 sets heating time by holds signaling in idle. A good rule of thumb is the desired heating period plus (ΔT/3) seconds for heating.

Two important practical issues need to be emphasized here. 1) The power supply is not designed to operate both heaters at once at full power (this never happens in SELEX operation, it was noticed that the signal for heating is stuttered even at the initial ramp) 2) This system does not automatically reset temperature to 25°C once heating is complete. Thus all heating steps must necessarily be followed by M[M104 or M140] S25.

The most important heating step for the SELEX process is the temperature cycling needed for the process of PCR. For the process of PCR the following script is used.

M104 S90

G4 S140

X [M104 S90

G4 S60

M104 S57

G4 S65

M104 S72

G4 S55

M104 S25

The first 2 lines of the script is a 120s pre heating step, followed by Thermal cycles of 30s melting at 90°C, 30s annealing at 57°C, and 30s extension at 72°C represented by the area in parenthesis. A delay of 30, 35 and 25s are added to the melting, annealing and extending steps respectively to allow heating unit to reach the set temperatures (these numbers are reached based on empirical observation). The last line returns the heater to room t3emperature.

Magnetic Separator control

The electromagnetic precipitator is used to separate MNP from solution. The EM precipitator are controlled in exactly the same way as the solenoid valves, both being on/off electromagnets. The following script is used:

M42 P[Magnet Pin] S255

M42 P[Magnet Pin] S0

The first line switches magnet on

The second line switches magnet off

In practice this would only result in the MNP in the immediate region nearest to the electromagnet to be attracted to the magnet. In order to ensure a significant part of the MNP in the flow tube is attracted to the magnet, the system is pulsed forward and backwards gently several times.

X[

M42 P[BUFFER] S255

G4 S1

G92 Y0

G1 Y15 F1200

G4 S1

M42 P[BUFFER] S0

M42 P[REVERSE] S255

G4 S2

G92 Y0

G1 Y-30 F1200

G4 S2

M42 P[REVERSE] S0

]

It should be noted that during MNP precipitation, it is recommended that a decreased speed of movement is used in order to optimize MNP deposition by decreasing hydrodynamic force.

6.09 Minimizing contamination and decontamination

The importance of avoiding contamination in SELEX cannot be overemphasized. While good technique is essential in obtaining consistent results in any molecular biology application, it is particularly important in cascading processes such as SELEX, where products of earlier selection rounds are used in subsequent rounds of selection.

The interior flow path of the final design of automated SELEX device is composed of EPDM rubber, PTFE, Borosilicate glass and stainless steel. These material are compatible with a wide range of chemical cleaning methods (applied by pumping through flow channels in the same manner as reagents), as well as high temperature high pressure steam cleaning up to 120°C (either by flooding the interior flow channels with high pressure steam or by autoclaving the entire flow path, including solenoid valve manifolds).

The final full cleaning protocol is composed of firstly of disconnecting the reverse flow reservoir. The flow tube is then purged with MilliQ water (>100ml per input reservoir), followed by purging with steam (>15 sec per input reservoir), followed by purging with Virkon (>20ml per input reservoir), followed by purging with sterile buffer (>100ml per input reservoir). Subsequent to each step, the cleaning was applied in reverse direction with a reservoir connected to the output of the peristaltic pump, with the flow being ejected via the reverse drain. Steam cleaning requires the disconnection of the peristaltic pump. The reverse flow tube is cleaned by autoclaving, and reconnected after the final sterile buffer purge.

6.10 Device Operation

Although the product of selection could be sent through another round of SELEX automatically; for the purposes of evaluating the performance of the instrument it was decided to extract the sample after each round. This served to provide both an evaluation and reserve sample (should the instrument malfunction subsequently). Once extract the sample cannot be returned directly to the automated

system. This is because the internal volume of the affinity selection chamber (and therefore the volume of the extracted plug) is 395 ul (assuming a plug length of 126mm). The solenoid valve chamber on the other hand has an internal dead volume of >700ul when open which means a minimum feed volume to produce a 400ul plug is 1.1ml.

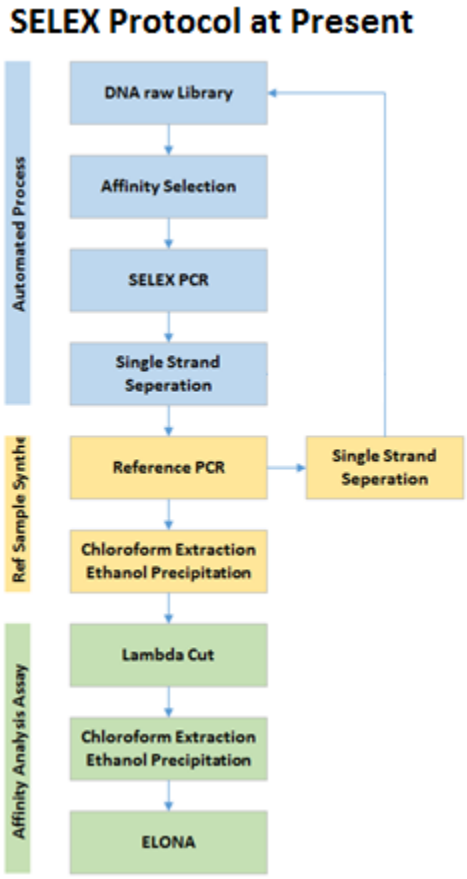

Fig 6.21 Overview of the protocol used in the final device operation

The library must therefore be amplified and the single strand separation performed manually and returned to the system via a solenoid valve (a 3ml volume in the reservoir is recommended). Concentration of the returned DNA is kept as close as feasible to the concentration of the extracted SELEX product. Thus while the returned library will be of different volume to the extracted sample, it should be of similar composition.

As mentioned at the start of this section extraction of the product is necessary in order that quality control steps can be performed subsequent to every round of selection, so that data obtained could be used to further optimize the device and failed SELEX rounds could be identified. The incremental nature

of the development of this device also necessitates the synthesis of an archive sample, for use in pilot tests or in case an applied upgrade proves to be counterproductive.

With future development, it is hoped that the device will be capable of performing multiple SELEX rounds in a consecutive manner, with reference sample generation and affinity assay being performed manually only occasionally between multiple automated rounds.

A pre-selection round is carried out prior to the first round of selection in order to remove sequences with affinity for the MNP. No investigation of the product of this round was carried out, and the product was moved to PCR chamber for storage while affinity selection chamber was purged and replaced with target enriched MNP. The pre-selected library was then subsequently used in the first round of Selection. This round "0" and the first round of selection are performed back to back in a manner similar to consecutive SELEX operations. All subsequent rounds of selection follow the protocol described in the protocol section of this chapter (see page 194).

6.10a Quantification of Extracted DNA concentration and Quality Control

The concentration of DNA product of SELEX operation in the extracted samples cannot be directly quantified, since the mass of DNA in such sample is too dilute to be measured by the nanodrop device or display visible bands on agarose gel. However the concentration of the extracted sample could be determined after phenol/chloroform extraction and ethanol precipitation.

Quality control was performed as described in the MSS section of this chapter (see page 222).

6.10b ELONA determination of selected sequences affinity to target

Material preparation for the ELONA process was performed manually. PCR was used to generate a pool of biotinylated forward (selected) sequence, using purified reference sample as template. The double stranded sequences were then cut with Lambda nuclease, which digests 5'-phosphorylated double stranded DNA in the 5' to 3' direction. Activity against single-stranded and non-phosphorylated sequences is negligible by comparison. Thus the biotinylated forward sequence and already single strand separated sequences are unaffected by lambda nuclease activity.

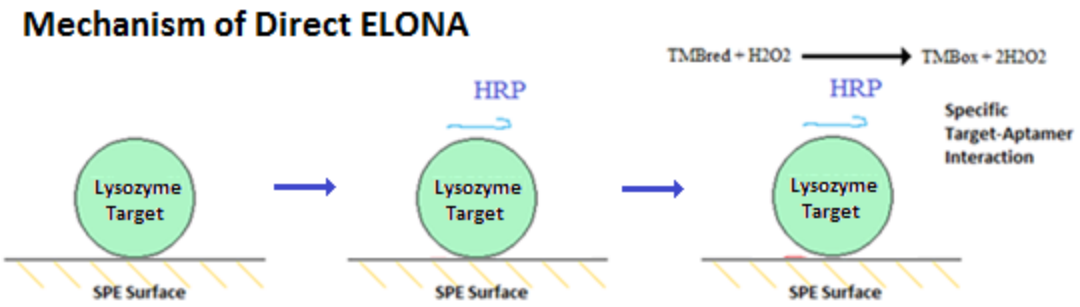

Fig 6.22 Mechanism of Direct ELONA

The ELONA protocol used in this study can be found in the methodology section (see section 2.02e of chapter 2, page 74)

6.10c ELONA Results for first series of SELEX rounds conducted

Twelve rounds of SELEX were carried out in the first series, of which the first eight was used in ELONA assay. The extracted concentration and quality control data for these can be found in the Appendix J (page 319).

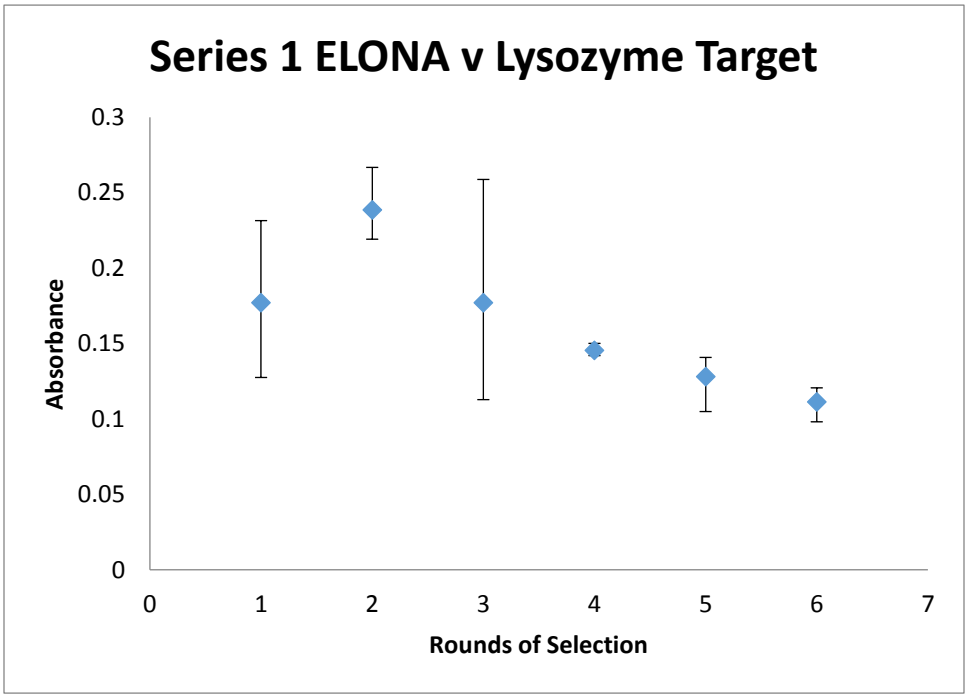

Fig 6.23 Direct ELONA results for first series of SELEX rounds, performed against Lysozyme target

The results show no significant correlation between round of selection and average sequence affinity to target molecule. This could only lead to the conclusion that automated SELEX protocol was not successful in generating a final library with a high affinity to target analyte.

As a response to the failure of the series 1, an attempt was made to determine the most likely cause of failure of the SELEX device, so that an attempt could be made to enhance the chance of success of future cycles. It was determined that, due to time constraints, major hardware improvements to the SELEX device was no longer a feasible option at this point. Thus improvements must be limited to protocol, minor hardware, and pre-operation preparation changes. Improvements undertaken are described below.

Software/Protocol based improvement are as follows:

Implement decreased feed rate during periods in which MNP is to be retained in affinity selection chamber by magnetization. This is to prevent loss of MNP material to hydrodynamic pressure.

Implement agitation during incubation period as forward/backward pulses. This prevents settling of MNP during incubation. This improvement may result in a minor increase in liquid border distortion, but this trade off was considered acceptable.

During the separation process the temperature of the affinity selection chamber was kept in an on state throughout separation including backflow to PCR chamber, rather than being switched off before back flow is implemented. The purpose is to prevent possible reformation of target-aptamer hybrids during cooling. Since the reverse flow leads to the heat resistant manifold, and PCR chamber, there is no chance of thermal damage to hardware.

Increased buffer wash period on most buffer washes.

Preparative improvements are as follows:

Preparation of DNA library and SELEX product to use glass vessels exclusively whenever possible. This is to decrease loss of material as a result of adsorption to container surfaces. PTFE based container was also considered but rejected as not likely to provide improvement over borosilicate glass vessels used.

Buffer preparation no longer to be autoclaved due to possible contamination from shared autoclave device. Vacuum filtration to replace autoclave as means of disinfection.

New lysozyme stock was ordered and stored at -20°C instead of 0°C

Hardware based improvements are as follows:

Redirection of heating tube cooling fan downwards away from storage vessels for reagents. This should decrease possibility of airborne contaminant entry into reagent vessel.

Improved U shaped reagent bottle plug inlet tube to decrease entry of airborne contaminant to reagent storage. This replaces original tin foil cap.

6.10d ELONA Results for second series of SELEX rounds conducted

Eight rounds of SELEX were carried out in the second series, incorporating improvements suggested as feedback from series 1 ELONA results (see above), all of which were used in ELONA assay. The extracted concentration and quality control data for these can be found in the Appendix J (page 319).

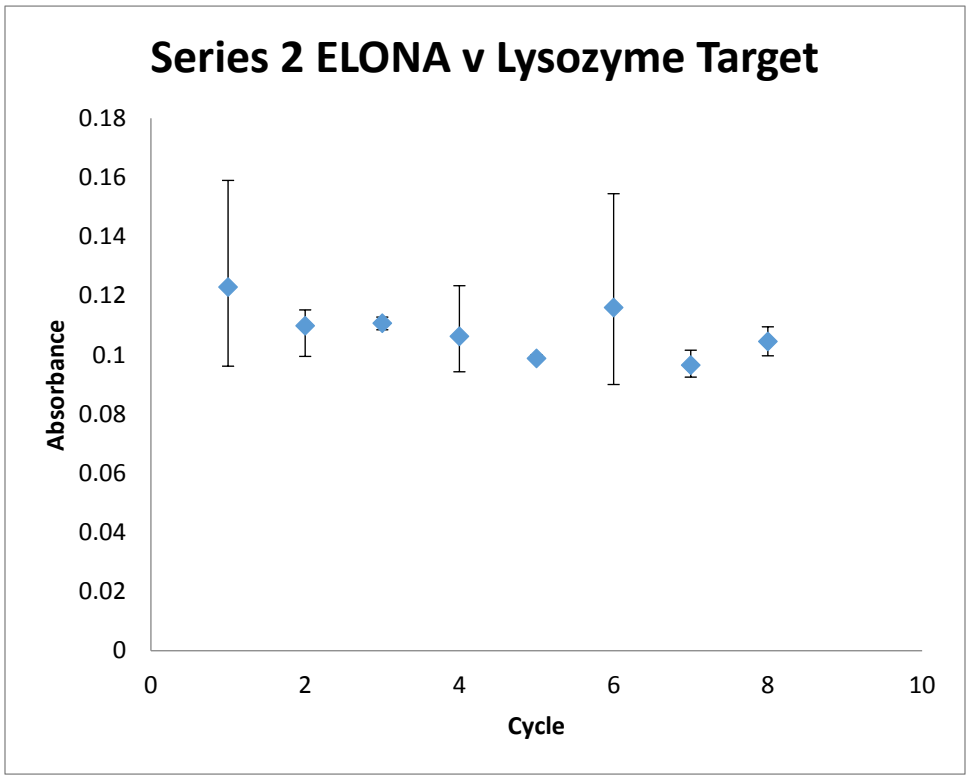

Fig 6.24 Direct ELONA results for second series of SELEX rounds, performed against Lysozyme target

Again, the results show no significant correlation between round of selection and average sequence affinity to target molecule. This could only lead to the conclusion that the improved operation protocol was not successful in generating a final library with a high affinity to target analyte, and that the improvements implemented the series of SELEX rounds has largely failed.

6.10e Conclusion of ELONA results

The ELONA results above would indicate that the ASM was not able to successfully enrich lysozyme binding sequence from the starting library.

6.11 Potential Causes of Failure of SELEX Protocol

Based on the results that have been obtained so far, it is possible to rule out a number of factors as potential causes in the failure of the SELEX device.

It is unlikely that the PCR amplification protocol of the device is the cause of failed SELEX operation. This is because Gel Electrophoresis of SELEX product extracted after PCR amplification (but before MNP separation) show a single distinct band of correct MW when observed by agarose gel electrophoresis. Post-Selection but pre-amplification mass analysed by gel electrophoresis show no visible bands at that MW. Deterioration of PCR Master Mix is not suspected to be the cause of failure of the SELEX operation for the same reason.

Nuclease contamination is unlikely to be the cause of failure since sufficiently high DNA mass of correct length was observed post-amplification.

Liquid handling failure is unlikely to be the cause of failed SELEX operation since the presence of amplified mass of DNA suggest that PCR mastermix related plug (the longest step in the liquid handling process) has been successfully handled).

Failure to retain MNP is unlikely to be the cause of failure of the SELEX operation, since the UV/Vis spectrograph of MNP mass retained after wash indicates at least 30% of MNP mass is retained (see section 6.06 of this chapter, page 222), which is above minimal threshold needed for successful SELEX. Sedimentation of MNP in reservoir and tubes is also unlikely to be cause of failure since visual inspection

reveals no sedimentation within the flow system. MNP reservoirs are agitated manually prior to MNP feeds (automated agitation has not yet been implemented by the latest mode).

Thus having determined the components which are operating correctly, it is possible to narrow down the likely causes of failure of the SELEX device. At present there is a number of reasons for the failure of the automated SELEX process, the most likely of which are listed below, along with potential solutions:

Perhaps the most likely cause of failure of the SELEX operation is the retention of non-specific sequences retained in system as a result of target-platform interaction. In other word the sequence amplified during the amplification stage of the SELEX operation is not the result of target-aptamer interaction but a sequence retained as a result of its affinity to a component of the SELEX platform. PTFE, stainless steel, and borosilicate glass are relatively unadsorptive materials. Since these material make up >95% of the path length in all models tested, the risk of adsorption of most of the platform is relatively low. The greatest weakness by far of the device is at the glass/PTFE tube joints, which are made of vulcanised rubber sleeves. In theory this sleeve should not be exposed to the operational solution flow at all. In practice gap between glass and PTFE tube result in a gap between the tubes, resulting in both minor liquid retainment and exposure of potentially adsorptive material.

Based on this analysis, the solution to non-specific selection would be the replacement of all glass-PTFE EPDM joints with compression joints made out of PTFE. Negative side effect of this is that the joint will be impossible to disassemble, as pressure needed would break glass tube and distort the cross section of PTFE tube. It is also likely that the compression joint would increase gap at junction, increasing liquid retainment and distortion of flow boundary. Another potential solution is to increase the number of rounds and stringency of the pre-selection operation, which is designed to remove non-specific platform binders.

Based on the UV/Vis spectrophotometry results, it is possible that the electromagnet does not retain sufficient MNP for total removal of PCR generated non-selected complementary sequences. This is discussed in the MSS section of this chapter (see page 222). As of the present time no solution to this problem has yet been determined.

Insufficient heat during the separation stage could result in the failure of the separation process, resulting in the nucleotide remaining attached to the target-MNP. This would result in loss of the

selected library along with the target-MNP when the latter is purged via the drain. A solution to this would be to increase separation temperature, perhaps from 80°C to 90°C.

Another potential cause of failure is loss of initial DNA library mass in reservoir as a result of non-specific adsorption to reservoir vessel (disposable syringes are made of polypropylene). This could be solved by simply fabricate future reservoir vessels out of milled PTFE.

6.12 Concluding Remarks

The automated SELEX device was unsuccessful in its intended objective in its present form. None of the operational series of SELEX rounds have succeeded in selecting a library with measurably increased affinity to the target molecule.

It is impossible at present to determine conclusively whether mesofluidic device could potentially be successful in isolating nucleotides with high affinity to target with further development. The device design was developed (including all design, fabrication and testing) within a 15 month period. Thus very little optimization has been conducted using feedback from real tests. Time constraints also mean that no major modifications to the design philosophy has been considered at all, with all improvements based on feedback being limited to software, minor hardware, and pre-operation preparation changes.

There are a number of future improvements which can be suggested for the device. The most obvious short term improvements are noted in section 6.11 of this chapter (see page 247). Many of the suggestions made there can be performed with minimal effort, if given the time to do so.

It needs to be remembered that the final objective of the ASM is to perform multiple consecutive rounds of SELEX without human intervention. This may necessitate the addition of components not present in the final developed ASM, such as reagent coolers, input air decontaminators, and MNP solution mixers. These could be easily implemented (the first two have already been developed, but never integrated) respectively by the use of a Peltier's element connected to a heat sink and aluminium block, combining the air intake tube of the reservoirs to a heating block, and either implementation of a motor spun magnet or simply by integrating a commercial magnetic stirrer.

Despite the failure of the integrated device, the subsystems are able to adequately perform their specified functions, based on their component results. A number of parties have already expressed

interest in the PTFE solenoid valve manifold. The total cost of production of a single ASD is less than USD500 (GBP340, Bloomberg 180315), and the total developmental cost of this device did not exceed USD1300 (GBP886, Bloomberg 180315), which can be considered relatively low for an automated SELEX device.

Chapter 7: Concluding Remarks and Future Works

The scope of the study undertaken for this thesis is divided into three sections.

The first section of this thesis describes the design and development of an amperometric conformation change aptasensors for Kanamycin and Tetracycline, the former having a “signal off” and the latter a “signal on” output signal. Both sensors have reproducible signal trends, though variation in signal amplitude for both sensors were significant. Testing of the sensor in environmental sample matrix buffers showed no change in signal trend compared to those performed under clean buffer conditions. Further enhancement of the sensor by gel encapsulation has shown that it is possible to prevent signal loss from extended exposure to high nuclease concentrations.

The Kanamycin and Tetracycline aptasensor were combined and migrated to an automated, multichannel format, which was able to detect the presence of both target molecules with minimal human intervention.

This mode of sensing could be improved by the integration of additional conformation change aptasensor into the multichannel array. These sensors should target analytes whose detection would be beneficial in the environment investigated, such as valuable secondary metabolites for microbial product discovery, or toxic contaminants for agricultural regulation.

Another potential area for future works is to test this sensor format in other environments where antibiotic detection could be useful, such as bioreactor monitoring for example. Alternatively, the sensor could be tested against a more diverse range of soil and agricultural effluence samples.

While the gold disc electrode is useful for prototype sensor testing due to its simplicity, it is not amenable to scaling up for commercial scale production. Techniques such as gold sputtering and automated bioreceptor molecule deposition may not only improve rate of production and individual sensor cost, but also improve uniformity and consistency in the electrode fabrication process, resulting in a more uniform electrode batch signal amplitude.

Using multiple large GDEs in a multichannel array also necessitates a large electrochemical cell, which results in wastage of reagents. It may be beneficial in future works to integrate multiple biosensors into microelectrode arrays.

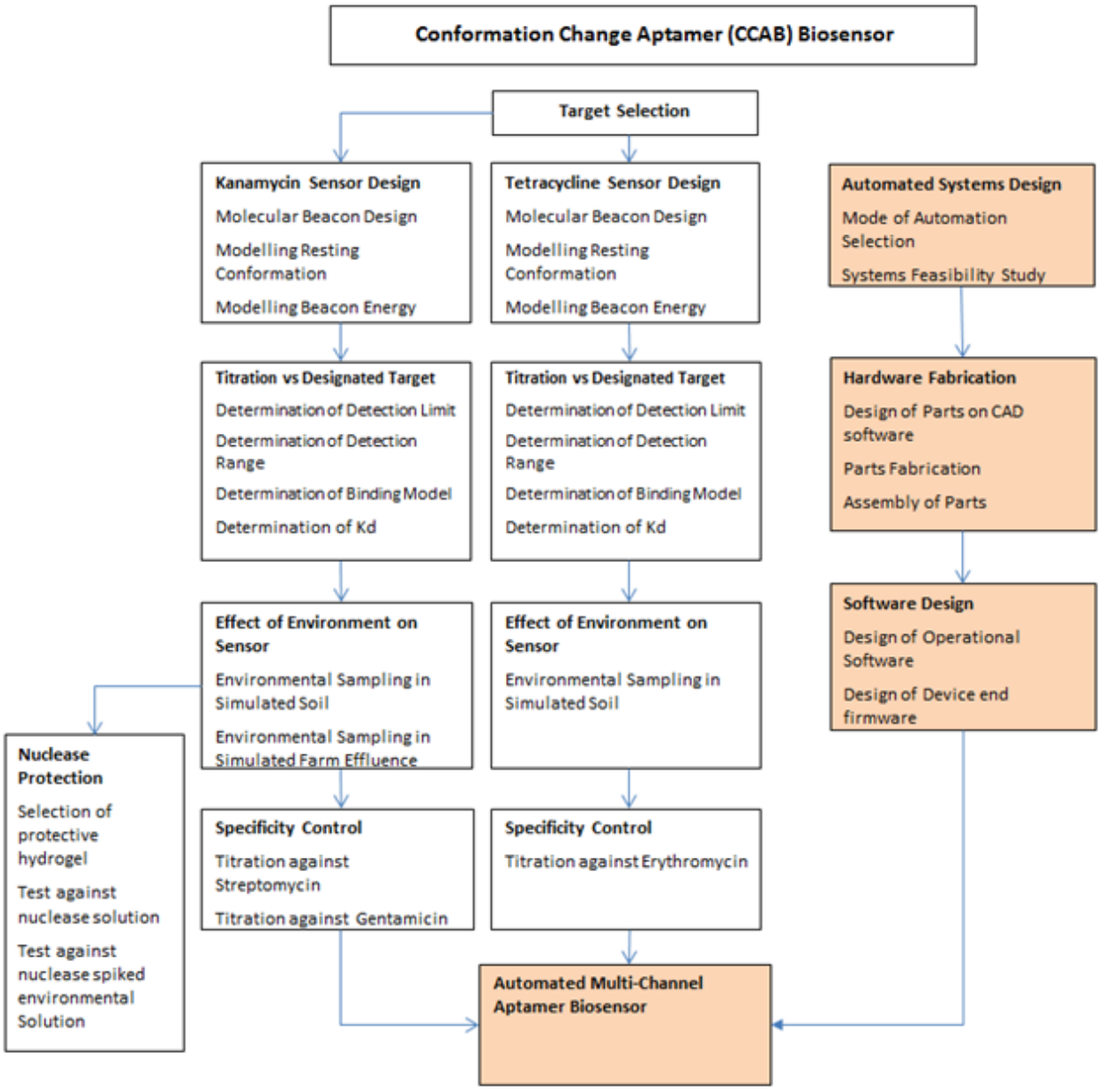

Fig 7.01 Summary of studies conducted on CC Aptasensor. Studies performed in chapter 3 in white boxes, studies conducted in chapter 4 in orange boxes.

The second area of this thesis describes the development of an amperometric biosensor based on Enzyme-Linked Oligonucleotide Assay (ELONA) technology. Sensing formats based on both direct and indirect ELONA were developed, though only the indirect ELONA based design displayed reproducible signal within the concentration ranged used in this study. This sensor has a reproducible signal trend,

with a significantly greater signal amplitude than the CCA desgn. However this sensor is also more complex than the CCA design, and relies on known spatial interaction between the TBA and HD22 aptamers and the thrombin target.

Future works should take one of two directions. The first would be to test the sensor in its most likely target environment (simulated by animal serum perhaps). The second would be to automate the IAELAB format, which should reduce the effect some of this sensor's greatest weaknesses (complexity and potential for human error).

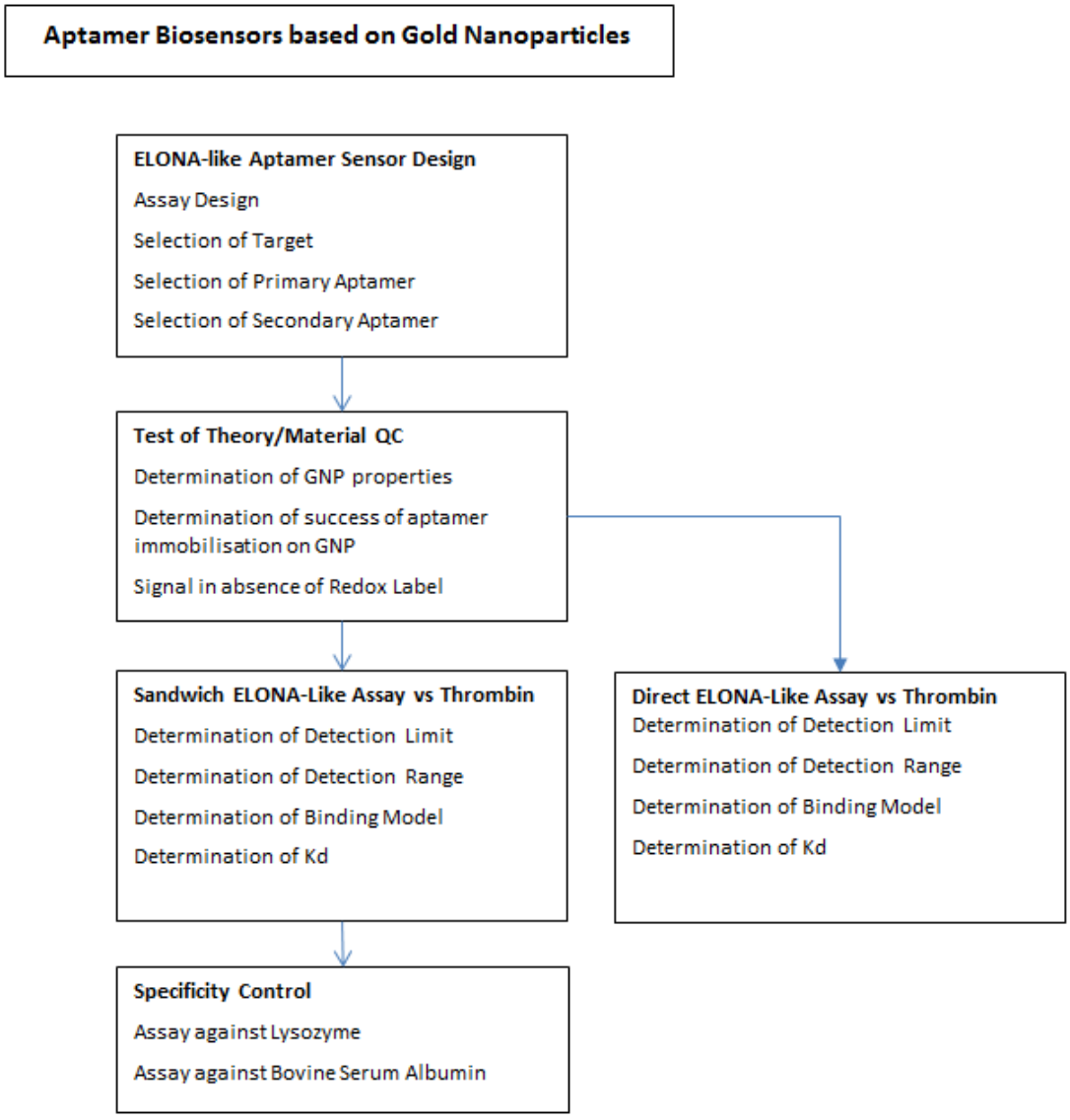

Fig 7.02 Summary of studies conducted on Configuration Change Aptasensor.

The third area of this thesis was not yet complete by the time of conclusion of this study, and describes an attempt to develop an automated SELEX device based on mesofluidic flow channels. It was hoped that mesofluidic flow channels would retain both the advantages of the conventional SELEX protocols (large library and sequence variation), while also gaining the advantages of microfluidic SELEX (reduced contamination risk and less reagent wastage). The components deemed necessary for the SELEX operation (such as thermal cycler, liquid handling, and electromagnetic separation), as well as electronics and software infrastructure necessary for device operation, were designed and fabricated. These components individually performed to designed specifications in wet tests, though no nucleic acid with high affinity to target has yet to be successfully isolated.

The most obvious areas of improvements which can be implemented for this device could be found in section 6.11 of chapter 6(see page 247).

At present the ASD is performed in single round operations. The final objective of the ASD is to perform multiple consecutive rounds of SELEX without human intervention. The addition of components not present in the final developed ASD such as reagent coolers, input air decontaminators, and MNP solution mixers will be necessary to achieve this. These components could be easily implemented (the first two have already been developed, but never integrated) respectively by the use of a Peltier element connected to a heat sink and aluminium block, combining the air intake tube of the reservoirs to a heating block, and either implementation of a motor spun magnet or simply by integrating a commercial magnetic stirrer.

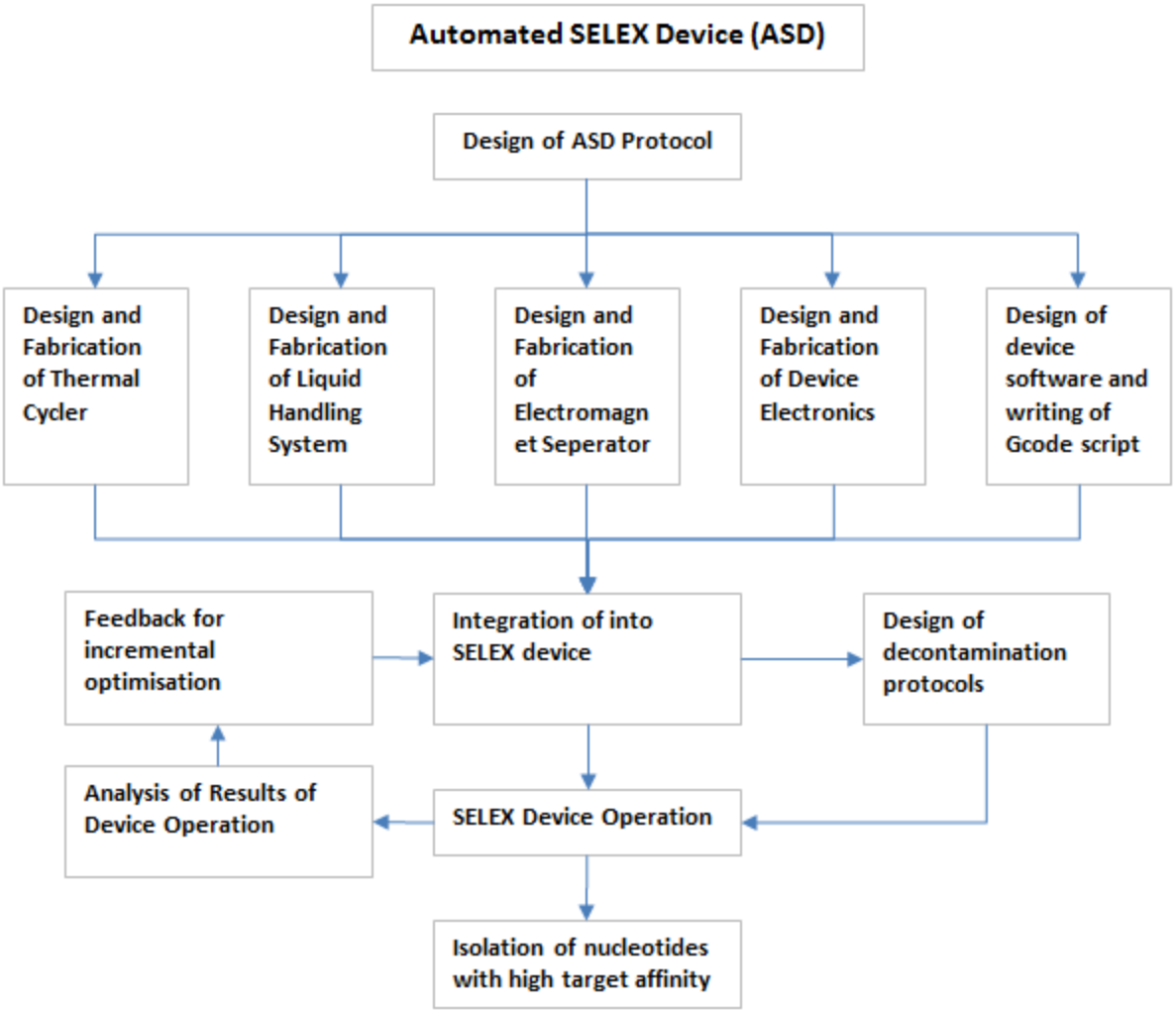

Fig 7.03 Summary of studies conducted on the automated SELEX device

References

[1] J Cooper and A Cass, *Biosensors (Practical Approach)*, 2nd edition, Chapter 2, p19

[2] Rogers K, *Principles of affinity-based biosensors*, Mol Biotechnol. 2000, V14(2), p109

[3] Bruls D et al, *Rapid integrated biosensor for multiplexed immunoassays based on actuated magnetic nanoparticles*, Lab Chip. 2009, V9(24), p3504

[4] Cass A et al *Ferrocene-mediated enzyme electrode for amperometric determination of glucose*, Anal. Chem., 1984, V56(4), p667

[5] Mihai J et al, *Label-free detection of lysozyme in wines using an aptamer based biosensor and SPR detection*, Sens Actuators B Chem. 2015, V206, p198

[6] Bausells J*, Piezoresistive cantilevers for nanomechanical sensing,* Microelectron Eng. 201, V145, p9

[7] Yan Z et al, *A label-free immunosensor for detecting common acute lymphoblastic leukemia antigen (CD10) based on gold nanoparticles by quartz crystal microbalance*, Sens Actuators B Chem 2015, V210, p248

[8] Mairal T, *Aptamers, p molecular tools for analytical applications, Anal Bioanal Chem*. 2008, V390(4), p989-1007

[9] ZIbupoto Z et al, *Development of a disposable potentiometric antibody immobilized ZnO nanotubes based sensor for the detection of C-reactive protein*, Sens Actuators B Chem. 2012, V166, p809

[10] Omidfar K et al, *New analytical applications of gold nanoparticles as label in antibody based sensors*, Biosens Bioelectron. 2013, V43, p336

[11] Cordeiro C et al, *In vivo continuous and simultaneous monitoring of brain energy substrates with a multiplex amperometric enzyme-based biosensor device*, Biosens Bioelectron 2015, V67, p 677

[12] Syshchyk O et al, *Enzyme biosensor systems based on porous silicon photoluminescence for detection of glucose, urea and heavy metals*, Bio sensors and Bioelectron. 2015, V66, p89

[13] Baker B et al, *An electronic, aptamer-based small-molecule sensor for the rapid, label-free detection of cocaine in adulterated samples and biological fluids*, J Am Chem Soc. 2006, V128(10), p3138

[14] Bouchet-Spinelli A et al, *Oligosaccharide biosensor for direct monitoring of enzymatic activities using QCM-D, Biosensors and Bioelectronics*, 2013, V49, p290

[15] Bhand S et al, *Fructose-selective calorimetric biosensor in flow injection analysis*, Anal Chim Acta. 2010, V668(1), p13

[16] Ballesta-Claver J, *Electrochemiluminescent disposable cholesterol biosensor based on avidin–biotin assembling with the electroformed luminescent conducting polymer poly(luminol-biotinylated pyrrole)*, Anal Chim Acta 2012, V 754, p91

[17] Miyawaki A et al, *Lighting up cells, p labelling proteins with fluorophores*, Nat Cell Biol. 2003 Sep, VSuppl, p1

[18] Raymo F, *Photoactivatable Fluorophores*, ISRN Phys Chem, V 2012, p15

[19] Grieshaber D et al, *Electrochemical Biosensors - Sensor Principles and Architectures*, Sensors (Basel). 2008, V8(3), p1400

[20] Ronkainen N, *Electrochemical biosensors*, Chem. Soc. Rev V39, p 1747

[21] Ellington A and Szostak J, *In vitro selection of RNA molecules that bind specific ligands*, Nature 1990, V346, p818

[22] Tuerk C and Gold L, *Systematic evolution of ligands by exponential enrichment, p RNA ligands to bacteriophage T4 DNA polymerase*, Science 1990 Aug, V249(4968), p505

[23] Ellington A and Szostak J, *Selection in vitro of single-stranded DNA molecules that fold into specific ligand-binding structures*, Nature 1992, V355, p850

[24] Stojanovic M et al, *Aptamer-based folding fluorescent sensor for cocaine*, J Am Chem Soc. 2001, V123(21), p4928

[25] Yang Q, Goldstein I, Mei H, Engelke D, *DNA ligands that bind tightly and selectively to cellobiose*, Proc Natl Acad Sci U S A. 1998, V95(10), p5462

[26] Lozupone C et al, *Selection of the simplest RNA that binds isoleucine*, RNA. 2003, V9(11), p1315

[27] Vater A et al, *Short bioactive Spiegelmers to migraine-associated calcitonin gene-related peptide rapidly identified by a novel approach*, p Tailored-SELEX, Nucleic Acids Res. 2003, V 31(21), p e130

[28] Kim M et al, *RNA aptamers that bind the nucleocapsid protein contain pseudoknots*, Mol Cells. 2003, V16(3), p413

[29] Gopinath S et al, *An efficient RNA aptamer against Human Influenza B Virus Hemagglutinin*, J Biochem 2006, p139(5), p827

[30] Bruno G et al, *In vitro selection of DNA aptamers to anthrax spores with electrochemiluminescence detection*, Biosens Bioelectron 1999, V14(5), p457

[31] Nestler E and Hyman S, *Neuropsychopharmacology: The Fifth Generation of Progress*, Chapter 14 Regulation of Gene Expression, p217

[32] Alberts B et al, *Molecular Biology of the Cell*, Chapter 10 Control of Gene Expression, p551

[33] Lee S and Oh M, *A synthetic suicide riboswitch for the high-throughput screening of metabolite production in* Saccharomyces cerevisiae, Metab Eng, 2015, V28, p 143

[34] Nudler E and Mironov A, *The riboswitch control of bacterial metabolism*, Trend Biochem Sci. 2004, V29(1), p11

[35] Ruigrok et al, *Characterization of Aptamer-Protein Complexes by X-ray Crystallography and Alternative Approaches*, Int. J. Mol. Sci. 2012, V13(8), p10537

[36] Jayasena S, *Aptamers: an emerging class of molecules that rival antibodies in diagnostics*, Clin Chem. 1999, V45(9), p1628

[37] Cho E et al, *Applications of Aptamers as Sensors*, Annu Rev Analy Chem. 2009, V2, p241

[38] Muyldermans S, Nanobodies: *Natural Single-Domain Antibodies*, Annu Rev Biochem. 2013, V82, p775

[39] Stryer, *Biochemistry, 4th ed*, Chapter 16, page 418

[40] Jones F, *The Effect of Heat on Antibodies*, J Experim Med. 1927, V36(2), p291

[41] Manning M et al, *Stability of Protein Pharmaceuticals: An Update*, Pharmaceut Res. 2010, V27(4), p544

[42] Famm K et al, *Thermodynamically Stable Aggregation-Resistant Antibody Domains through Directed Evolution*, J Mol Biol. 2008, V376(4), p926

[43] Gong R et al, *Engineered human antibody constant domains with increased stability*, J Biol Chem. 2009, V284(21), p14203

[44] Hagihara Y et al, *Stabilization of an immunoglobulin fold domain by an engineered disulfide bond at the buried hydrophobic region*, J Biol Chem, 2007, V282(50), p36489

[45] Saerens D et al, *Disulfide bond introduction for general stabilization of immunoglobulin heavy-chain variable domains*, J Mol Biol. 2008, V377(2), p478

[46] Maynard J and Georgiou G, *Antibody Engineering*, Annu Rev Biomed Eng Vol. 2, p339

[47] Schirrmann T et al, *Production systems for recombinant antibodies*, Front Biosci. 2008, V13, p4576

[48] Goodchild J, *Conjugates of oligonucleotides and modified oligonucleotides, p a review of their synthesis and properties*, Bioconjugate Chem., 1990, 1 (3), p165

[49] Ho S et al, *Potent antisense oligonucleotides to the human multidrug resistance-1 mRNA are rationally selected by mapping RNA-accessible sites with oligonucleotide libraries*, Nucleic Acids Res. 1996, V 24(10), p1901

[50] Eckert T and Kunkel T, *High fidelity DNA synthesis by the Thermus aquaticus DNA polymerase*, Nucleic Acids Res. 1990, V18(13), p3739

[51] Bianchini M et al, *Specific oligobodies against ERK-2 that recognize both the native and the denatured state of the protein*, J Immunolog Meth. 2001, V252(1), p191

[52] Schneider D et al, *Selective enrichment of RNA species for tight binding to Escherichia coli rho factor*, FASEB J. 1993, V7(1), p201

[53] Mie M et al, *Selection of DNA aptamers with affinity for pro-gastrin-releasing peptide (proGRP), a tumor marker for small cell lung cancer*, Appl Biochem Biotechnol. 2013 Jan, V169(1), p250-5

[54] Tombelli S et al, *Aptamer-based biosensors for the detection of HIV-1 Tat protein*, Bioelectrochem, 2005, V 67(2), p135

[55] Lupold S et al, *Identification and characterization of nuclease-stabilized RNA molecules that bind human prostate cancer cells via the prostate-specific membrane antigen*. Cancer Res. 2002, V62(14), p4029-33.

[56] Kikuchi K et al, RNA *aptamers targeted to domain II of hepatitis C virus IRES that bind to its apical loop region*. J Biochem. 2003, V133(3), p263

[57] Murphy M et al, *An improved method for the in vitro evolution of aptamers and applications in protein detection and purification*. Nucleic Acids Res. 2003, V31(18), p110

[58] Mendonsa S and Bowser M, *In vitro selection of high-affinity DNA ligands for human IgE using capillary electrophoresis*. Anal Chem. 2004, V76(18), p5387

[59] Mosing R et al, *Capillary electrophoresis-SELEX selection of aptamers with affinity for HIV-1 reverse transcriptase*. Anal Chem. 2005, V77(19), p6107

[60] Mallikaratchy P et al, *Selection of DNA ligands for protein kinase C-delta*. Chem Commun (Camb). 2006, V(30), p3229

[61] Tang J et al, *The DNA aptamers that specifically recognize ricin toxin are selected by two in vitro selection methods*. Electrophoresis. 2006, V27(7), p1303

[62] Tsai R and Reed R, *Identification of DNA recognition sequences and protein interaction domains of the multiple-Zn-finger protein Roaz*. Mol Cell Biol. 1998, V18(11), p6447

[63] Ngubane et al, *Selection of RNA aptamers against the M. tuberculosis EsxG protein using surface plasmon resonance-based SELEX*. Biochem Biophys Res Comm. 2014, V449(1), p114

[64] Le T et al, *Aptamer-based biosensors for the rapid visual detection of flu viruses*. Chem. Commun., 2014, V50, p15533

[65] Yang X et al, *Immunofluorescence assay and flow-cytometry selection of bead-bound aptamers*. Nucleic Acids Res. 2003, V31(10), p54.

[66] Stoltenburg R et al, *FluMag-SELEX as an advantageous method for DNA aptamer selection*. Anal Bioanal Chem. 2005, V383(1), p83

[67] Bridonneau P et al, *Site-directed selection of oligonucleotide antagonists by competitive elution*. Antisense Nucleic Acid Drug Dev. 1999, V9(1), p1

[68] Paul A et al, *Streptavidin-coated magnetic beads for DNA strand separation implicate a multitude of problems during cell-SELEX*. Oligonucleotides. 2009, V19(3), p243

[69] Avci-Adali M et al, *Upgrading SELEX technology by using lambda exonuclease digestion for single-stranded DNA generation*. Molecules. 2009, V15(1), p1

[70] Cox J and Ellington A, *Automated selection of anti-Protein aptamers*, Bioorgan Med Chem, 2001, V9(10), p2525

[71] Cox J et al, *Automated RNA selection*. Biotechnol Prog. 1998, V14(6), p845.

[72] Hybarger G et al, *A microfluidic SELEX prototype*. Anal Bioanal Chem. 2006, V384(1), p191

[73] Wang J, *Analytical Electrochemistry, 2nd Edition*, Chapter 1: Fundimental Concepts, p3

[74] Numnuam A et al, *Aptamer-based potentiometric measurements of proteins using ion-selective microelectrodes*. Anal. Chem. 2008, V80, p707

[75] Polsky R et al, *Nucleic acid-functionalized Pt nanoparticles: catalytic labels for the amplified electrochemical detection of biomolecules*. Anal. Chem. 2006, V78, p2268

[76] Zuo X et al, *A target-responsive electrochemical aptamer switch (TREAS) for reagentless detection of nanomolar ATP*. J. Am. Chem. Soc. 2007, V129, p1042

[77] Lu Y et al, *Aptamer-based electrochemical sensors with aptamer-complimentary DNA oligonucleotides as probe*. Anal. Chem. 2008, V80, p1883

[78] Xiao Y et al, *Label-free electronic detection of thrombin in blood serum by using an aptamer-based sensor*. Angew. Chem. Int. Ed. 2005, V44, p5456

[79] Lai R et al, *Aptamer-based electrochemical detection of picomolar platelet-derived growth factor directly in blood serum*. Anal. Chem. 2007, V79, p229

[80] Rodriguez M et al, *Aptamer biosensor for label-free impedance spectroscopy detection of proteins on recognition-induced switching of the surface charge*. Chem. Commun. 2005, p4267–4269

[81] Li J et al, *Drug discovery: practices, processes, and perspectives*, Chapter 3, page 64

[82] EPA, PREPARATION OF SOIL SAMPLING PROTOCOLS: SAMPLING TECHNIQUES AND STRATEGIES,

Retrieved 160315: http://www.epa.gov/OUST/cat/mason.pdf

[83] Peirson S and Butler J, *RNA extraction from mammalian tissues*. Methods Mol Biol. 2007, V362, p315

[84] Rushizky G et al, *S1 nuclease hydrolysis of single-stranded nucleic acids with partial double-stranded configuration*. Biochemistry. 1975, V14(19), p4221

[85] Manica D et al, *Characterization of Electrode Fouling and Surface Regeneration for a Platinum Electrode on an Electrophoresis Microchip*. Anal. Chem. 2003, V75(17), p4572

[86] da Silva I et al, *Strategies to avoid electrode fouling for nimesulide detection using unmodified electrodes*. Anal. Methods, 2013, V5, p3546

[87] Kraatz H et al, *Ferrocenoyl Amino Acids, p A Synthetic and Structural Study*. Inorg Chem. 1997, V36(11), p2400

[88] EZ-Link Sulfo-NHS-SS-Biotin Datasheet, last accessed 180315:

https://tools.lifetechnologies.com/content/sfs/manuals/MAN0011183_EZ_SulfoNHS_SS_Biotin_UG.pdf

[89] Dynabead C1 Datasheet, last accessed 180315:

https://tools.lifetechnologies.com/content/sfs/manuals/dynabeads_myone_savC1_man.pdf

[90] Frens G, *Particle size and sol stability in metal colloids*. Colloid & Polymer Science, 1972, V250, p736–741

[91] C Niemeyer, *Bioconjugation Protocols, Strategies and Methods*, Chapter 22, p295

[92] Tyagi S and Kramer F, *Molecular beacons: probes that fluoresce upon hybridization*. Nat Biotechnol. 1996, V14(3), p303

[93] Miao X et al, *Electrochemical molecular beacon biosensor for sequence-specific recognition of double-stranded DNA*. Biosens Bioelectron. 2014, V59, p54

[94] Nasef H et al, *Electrochemical molecular beacon DNA biosensor for the detection and discrimination of the DF508 cystic fibrosis mutation*. J Electroanal Chem. 2011, V662(2), p322

[95] Zhuang J et al, *Binding-induced internal-displacement of inverted aptamer beacon, p Toward a novel electrochemical detection platform*. Electrochem Commun. 2014, V47, p25

[96] Liao Y et al, *Electrochemiluminescence quenching via capture of ferrocene-labeled ligand-bound aptamer molecular beacon for ultrasensitive detection of thrombin*, Sens Actuators B Chem, 2011, V158(1), p393

[97] Dougherty T and Pucci M, *Antibiotic Discovery and Development*, Chapter 2, Page 59

[98] Graham J et al, Growth *Promoting Antibiotics in Food Animal Production: An Economic Analysis*, Public Health Rep. 2007, V122(1), p79

[99] FDA, 2011 SUMMARY REPORT On Antimicrobials Sold or Distributed for Use in Food-Producing Animals, Retrieved 160315:
http://www.fda.gov/downloads/ForIndustry/UserFees/AnimalDrugUserFeeActADUFA/UCM338170.pdf

[100] FDA, CPG Sec. 615.200 Proper Drug Use and Residue Avoidance by Non-Veterinarians

FDA, Retrieved 160315:
http://www.fda.gov/ICECI/ComplianceManuals/CompliancePolicyGuidanceManual/ucm074660.htm

[101] FDA, Guidance for Industry, Evaluating the Safety of Antimicrobial New Animal Drugs with Regard to Their Microbiological Effects on Bacteria of Human Health Concern, Retrieved 160315:

http://www.fda.gov/downloads/AnimalVeterinary/GuidanceComplianceEnforcement/GuidanceforIndustry/ucm052519.pdf

[102] Song K et al, *Gold nanoparticle-based colorimetric detection of kanamycin using a DNA aptamer*. Anal Biochem. 2011, V415(2), p17

[103] mFold Model Location, last accessed 170315:

http://mfold.rna.albany.edu/?q=mfold

[104] Zuker M, *Mfold web server for nucleic acid folding and hybridization prediction*, Nucleic Acids Res, 2003, V31(13), p3406

[105] OligoAnalyser Model Location, last accessed 170315

https://www.idtdna.com/calc/analyzer

[106] H Meislich et al, *Theory and Problems of Organic Chemistry*, Chapter 3, p26

[107] Beyer D et al, *New class of bacterial phenylalanyl-tRNA synthetase inhibitors with high potency and broad-spectrum activity*. Antimicrob Agents Chemother. 2004, V48(2), p525

[108] Lu J et al, *Synthesis, structure and biological activity of cobalt(II) and copper(II) complexes of valine-derived schiff bases*. J Inorgan Biochem. 2006, V100(11), p1888

[109] Nirenberg M et al, *RNA codewords and protein synthesis, VII. On the general nature of the RNA code*. Proc Natl Acad Sci U S A. 1965, V 53(5), p 1161

[110] Wallis C et al, *Concentration of Viruses from Water by Membrance Chromatography*. Ann Rev of Microbiol Vol. 33, p 413

[111] Mahmood T and Yang P, *Western blot: technique, theory, and trouble shooting.* N Am J Med Sci. 2012, V4(9), p429

[112] Parker J et al, *Crystal structure of a PIWI protein suggests mechanisms for siRNA recognition and slicer activity*, The EMBO Journal, 2004, V23, p4727

[113] Shaw K et al, *Molecular genetics of aminoglycoside resistance genes and familial relationships of the aminoglycoside-modifying enzymes*. Microbiol Rev. 1993, V57(1), p138

[114] Cameron F et al, *Nucleotide sequence of the AAD(2'') aminoglycoside adenylyltransferase determinant aadB. Evolutionary relationship of this region with those surrounding aadA in R538-1 and dhfrII in R388*. Nucleic Acids Res. 1986, V14(21), p8625

[115] Tenover F et al, *Detection of two different kanamycin resistance genes in naturally occurring isolates of* Campylobacter jejuni *and* Campylobacter coli. Antimicrob Agents Chemother. 1988, V32(8), p 1170

[116] Stellwagen J and Stellwagen N, *Internal Structure of the Agarose Gel Matrix*. J. Phys. Chem. 1995, V99(12), pp 4247

[117] Pernodet N et al, *Pore size of agarose gels by atomic force microscopy*. Electrophoresis. 1997, V18(1), p55

[118] Vogt V, *Purification and further properties of single-strand-specific nuclease from Aspergillus oryzae*. Eur J Biochem. 1973, V33(1), p192

[119] Pubchem Compound Database, last accessed 220716

https://pubchem.ncbi.nlm.nih.gov/

[120] Niazi J et al, *Single-stranded DNA aptamers specific for antibiotics tetracyclines*. Bioorg Med Chem. 2008, V16(15), p7245

[121] Le T et al, *Determination of minimal sequence for binding of an aptamer. A comparison of truncation and hybridization inhibition methods*. RSC Adv. 2014, V4, p47227

[122] Chen H and Gold L, *Selection of high-affinity RNA ligands to reverse transcriptase, p inhibition of cDNA synthesis and RNase H activity.* Biochemistry, 1994, V33, p8746

[123] Jellinek D et al, *Inhibition of receptor binding by high-affinity RNA ligands to vascular endothelial growth factor*. Biochemistry, 1994, V33, p10450

[124] Ouellet E et al, *A simple method for eliminating fixed-region interference of aptamer binding during SELEX*. Biotechnology and Bioengineering, 2014, V111(11), p2265

[125] GQRS Model Location, last accessed 170315:

http://bioinformatics.ramapo.edu/GQRS/

[126] Kikin O et al, *QGRS Mapper, p a web-based server for predicting G-quadruplexes in nucleotide sequences*. Nucleic Acids Res. 2006, V34, p676

[127] Takahashi N et al, *The effects of tetracycline, minocycline, doxycycline and ofloxacin on Prevotella intermedia biofilm*. Oral Microbiol Immunol. 2006, V21(6), p366

[128] Zhang et al*, Fast determination of the tetracyclines in milk samples by the aptamer biosensor*, Analyst. 2010, V135(10), p2706

[129] Dong et al, *Real-time and label-free detection of chloramphenicol residues with specific molecular interaction*, J Microsc. 2009, V234(3), p255-61

[130] Kim et al, *Specific detection of oxytetracycline using DNA aptamer-immobilized interdigitated array electrode chip*, Anal Chim Acta. 2009, V23(2), p250

[131] Guo et al, *Aptamer Biosensor for Antibiotic Residues Detection in Food Analysis, Sensors & Transducers*, V156(9), p368

[132] González-Fernández et al, *Monovalent labeling system improves the sensitivity of aptamer-based inhibition assays for small molecule detection*, Sensors and Actuators B: Chemical, V182, p668

[133] Wochner et al, *A DNA aptamer with high affinity and specificity for therapeutic anthracyclines*, Anal Biochem. 2008 V373(1), p34

[134] Nikolaus et al, *DNA-Aptamers Binding Aminoglycoside Antibiotics*, Sensors (Basel), 2014, V14(2), p3737

[135] Azzouzi S et al, *A novel amperometric biosensor based on gold nanoparticles anchored on reduced graphene oxide for sensitive detection of l-lactate tumor biomarker*. Biosens Bioelectron. 2015, V69, p280

[136] Kowalczyk A et al, *A dual DNA biosensor based on two redox couples with a hydrogel sensing platform functionalized with carboxyl groups and gold nanoparticles*. Sens Acurtors B Chem. 2015, V208, p220

[137] Shi J et al, *A fluorescence resonance energy transfer (FRET) biosensor based on graphene quantum dots (GQDs) and gold nanoparticles (AuNPs) for the detection of mecA gene sequence of* Staphylococcus aureus. Biosens Bioelectron. 2015, V67, p595

[138] Luo X et al, *A novel glucose ENFET based on the special reactivity of MnO2 nanoparticles*. Biosens Bioelectron. 2004, V9(10), p1295

[139] Rurack K et al, *The Supramolecular Chemistry of Organic-Inorganic Hybrid Materials*. Electrochemistry Communications, V2, p722

[140] Mody V et al, *Introduction to metallic nanoparticles*. J Pharm Bioallied Sci. 2010, V2(4), p282

[141] Sau T et al, *Properties and applications of colloidal nonspherical noble metal nanoparticles*. Adv Mater. 2010, V22(16), p1805

[142] Luo X et al, *Application of Nanoparticles in Electrochemical Sensors and Biosensors*. Biosens Electroanaly. 2006, V18(4), p319

[143] Brust M et al, *Synthesis of thiol-derivatised gold nanoparticles in a two-phase Liquid–Liquid system*. J Chem Soc Chem Comm, 1994, V7, p801

[144] Callaghan M et al, *An investigation of the impedance properties of gold nanoparticles*. Journal of Physics: Conference Series V224 Number 1

[145]Pingarrón J et al, *Gold nanoparticle-based electrochemical biosensors*, Electrochimica Acta. 2008, V53(19), p5848

[146] Sonny Mark, *Bioconjugation Protocols, Strategies and Methods*, Chapter 22, page 296

[147] Lequin R, *Enzyme immunoassay (EIA)/enzyme-linked immunosorbent assay (ELISA)*. Clin Chem. 2005, V51(12), p2415

[148] Drolet D et al, *An enzyme-linked oligonucleotide assay*. Nat Biotechnol. 1996, V14(8), p1021

[149] Bock L et al, *Selection of single-stranded DNA molecules that bind and inhibit human thrombin*. Nature. 1992, V355(6360), p564

[150] Tasset D et al, *Oligonucleotide inhibitors of human thrombin that bind distinct epitopes*. J Mol Biol. 1997, V272(5), p688

[151] Li W et al, *A novel nucleotide-based thrombin inhibitor inhibits clot-bound thrombin and reduces arterial platelet thrombus formation*. Blood. 1994, V83(3), p677

[152] Sun C et al, *A label-free and high sensitive aptamer biosensor based on hyperbranched polyester microspheres for thrombin detection*, Anal Chim Acta, 2014, V850, p33

[153] Krauss R et al, *Duplex-quadruplex motifs in a peculiar structural organization cooperatively contribute to thrombin binding of a DNA aptamer*. Acta Crystallogr D Biol Crystallogr. 2013, V69(Pt 12), p2403

[154] Krauss I et al, *High-resolution structures of two complexes between thrombin and thrombin-binding aptamer shed light on the role of cations in the aptamer inhibitory activity.* Nucleic Acids Res. 2012, V40(16), p8119

[155] Hasegawa H et al, *Improvement of Aptamer Affinity by Dimerization*, Sensors (Basel). 2008 Feb, V8(2), p1090

[156] Rezwan K et al, *Lysozyme and bovine serum albumin adsorption on uncoated silica and AlOOH-coated silica particles: the influence of positively and negatively charged oxide surface coatings*, Biomaterials. 2005, V26(21), p4351

[157] Haiss W et al, *Determination of size and concentration of gold nanoparticles from UV-vis spectra*. Anal Chem. 2007, V79(11), p4215

[158] Jianwei J et al, *Molecular Aptamer Beacons for Real-Time Protein Recognition*. Biochem Biophys Res Comm. 2002, V292(1), p31

[159] Liu et al, Amplified Fluorescence Aptamer-Based Sensors Using Exonuclease III for the Regeneration of the Analyte, Chemistry, V18(8), p2165

[160] Xiao et al, Label-Free Electronic Detection of Thrombin in Blood Serum by Using an Aptamer-Based Sensor, V117(34), p5592

[161] Li et al, G-quadruplex-based DNAzyme for facile colorimetric detection of thrombin, Chem. Commun., 2008, V31, p3654

[162] Zhang et al, Bifunctional colorimetric oligonucleotide probe based on a G-quadruplex DNAzyme molecular beacon, Anal. Chem., 2011, V83, p8871

[163] Mir et al, Different strategies to develop an electrochemical thrombin aptasensor, Electrochem. Commun., 2006, V8, p505

[164] Zheng et al, Label-free fluorescent detection of ions, proteins, and small molecules using structure-switching aptamers, SYBR Gold, and exonuclease, Anal. Chem., 2012, V84, p3554

[165] Adkins J et al, *Toward a human blood serum proteome, p analysis by multidimensional separation coupled with mass spectrometry*. Mol Cell Proteomics. 2002, V1(12), p947

[166] NXFT15XH103FA2B100 Thermistor Datasheet. Last Retrieved (180315) from:

http://www.mouser.com/ds/2/281/r44e-3685.pdf

[167] Brett Beauregard's 3rd Party, Open-Source, PID. Last Retrieved (180315) from:

http://brettbeauregard.com/blog/tag/pid/

[168] APPLICATION NOTE ProFlex™ 96-Well PCR System Thermal Cycler Datasheet. Last Retrieved (220716) from:

https://www.thermofisher.com/content/dam/LifeTech/global/life-sciences/PCR/pdfs/ProFlexvs9700C1000MasterCyclerPro_AppNote.pdf

[169] Solenoid Valve Datasheet. Last Retrieved (180315) from:

http://roundstar.en.made-in-china.com/product/oXVJezIxJmhl/China-RSC-2-RO-Machine-Solenoid-Valve.html

[170] Teflon PTFE Properties Handbook, Dupont. Retrieved (180315) from:

http://www.rjchase.com/ptfe_handbook.pdf

[171] Lee C et al, *Microfluidic Mixing: A Review*. Int J Mol Sci. 2011, V12(5), p3263

[172] SMC Stainless Steel 316 Fittings Datasheet. Retrieved (180315) from:

http://www.smcusa.com/media/23010/nas50-33a-kqg2.pdf

[173] Welco WPM-E Datasheet. Retrieved (180315) from:

http://www.welco.net/dcms_media/other/WPX1_selectguid.pdf

[174] Dynabead C1 Product Handbook. Retrieved (180315) from:

https://tools.lifetechnologies.com/content/sfs/manuals/dynabeads_myone_savC1_man.pdf

[175] Arduino Mega 1280, 8bit Handbook. Retrieved (180315) from:

http://www.arduino.cc/en/Main/arduinoBoardMega

[176] Atmel 1280, 8bit Datasheet. Retrieved (180315) from:

http://www.atmel.com/Images/Atmel-2549-8-bit-AVR-Microcontroller-ATmega640-1280-1281-2560-2561_datasheet.pdf

[177] IRLU024N MOSFET datasheet. Retrieved (180315) from:

http://www.irf.com/product-info/datasheets/data/irlr024n.pdf

[178] RXEF025 Polyswitch Datasheet. Retrieved (180315) from:

http://pdf1.alldatasheet.com/datasheet-pdf/view/346676/MACOM/RXEF025.html

[179] N4148 Diode Datasheet. Retrieved (180315) from:

http://www.vishay.com/docs/81857/1n4148.pdf

[180] IRF640N MOSFET Datasheet. Retrieved (180315) from:

http://www.irf.com/product-info/datasheets/data/irf640n.pdf

[181] Pololu Stepper Motor Controller Datasheet. Retrieved (180315) from:

https://www.pololu.com/file/0J450/A4988.pdf

[182] Eagle Cad Download Location, last accessed 180315:

http://www.cadsoftusa.com/

[183] Sprinter Download Location, last accessed 180315:

https://github.com/kliment/Sprinter

[184] Pronterface Download Location, last accessed 180315:

https://github.com/kliment/Printrun

Appendix A: Replicate Results of SWV of kanamycin fcn-aptamer biosensor's response to kanamycin titration vs Ag/AgCl, performed in clean buffer.

Replicate 5 of this series of titration can be found in the main body of the text.

Target Concentration (nM)	130714	280714	120814	140814	150814	260914 EI1	221214 EI1	221214 EI2	231214
0	0.0226	0.0720	0.0727	0.0838	0.0689	0.0464	0.0379	0.0372	0.0453
75	0.0224	0.0718	0.0752	0.0792	0.0759	0.0386	0.0332	0.0311	0.0346
150	0.0153	0.0635	0.0621	0.0619	0.0520	0.0278	0.0243	0.0238	0.0291
300	0.0108	0.0540	0.0508	0.0527	0.0419	0.0181	0.0166	0.0169	0.0139
600	0.0050	0.0373	0.0390	0.0409	0.0358	0.0086	0.0081	0.0082	0.0064
1200	0.0010	0.0301	0.0246	0.0309	0.0269	0.0062	0.0058	0.0036	0.0027
2400	0.0000	0.0210	0.0134	0.0241	0.0202	0.0040	0.0000	0.0000	0.0026
4800	0.0002	0.0156	0.0117	0.0113	0.0133	0.0088	0.0000	0.0000	0.0000
Best-fit values									
Bmax	-0.0349	-0.0775	-0.1028	-0.0650	-0.0620	-0.0585	-0.0463	-0.0474	-0.0550
Kd	479.9000	736.3000	955.9000	314.6000	379.6000	291.3000	331.7000	366.8000	248.9000
NS	0.0000	0.0000	0.0000	0.0000	0.0000	0.0000	0.0000	0.0000	0.0000
Background	0.0241	0.0752	0.0762	0.0860	0.0739	0.0476	0.0391	0.0378	0.0463
Goodness of Fit									
Degrees of Freedom	4.0000	4.0000	4.0000	4.0000	4.0000	4.0000	4.0000	4.0000	4.0000
R square	0.9796	0.9876	0.9879	0.9888	0.9391	0.9916	0.9898	0.9977	0.9846
Absolute Sum of Squares	0.0000	0.0000	0.0001	0.0001	0.0002	0.0000	0.0000	0.0000	0.0000
Sy.x	0.0018	0.0033	0.0037	0.0036	0.0073	0.0019	0.0020	0.0009	0.0028

Table A.1 Summary of kanamycin fcn-aptamer biosensor's response to kanamycin titration vs Ag/AgCl, performed in clean buffer.

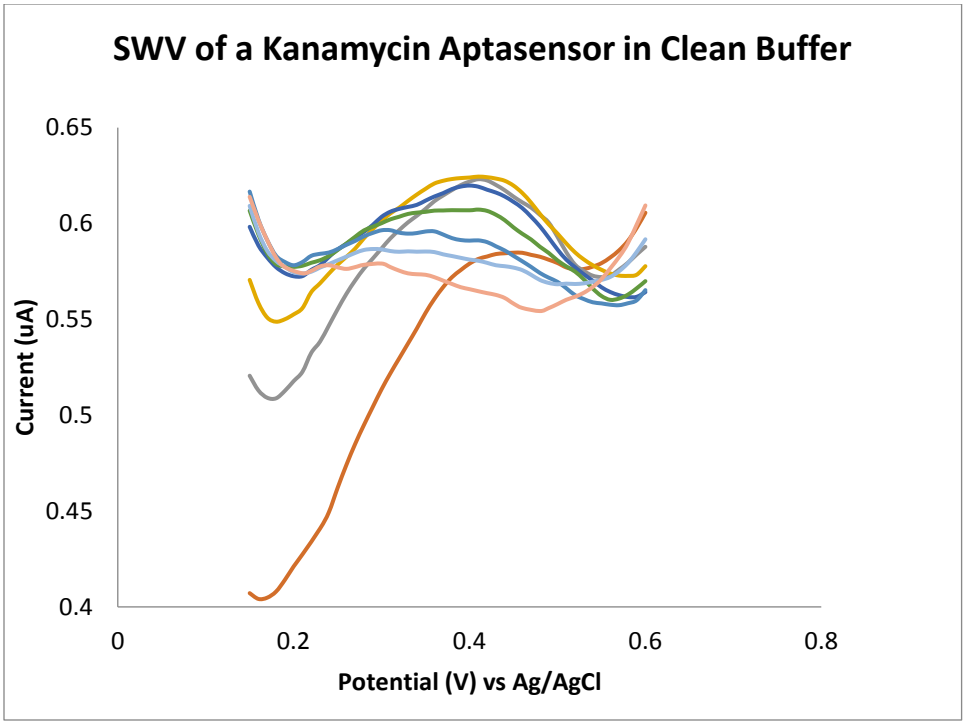

Fig A.1 SWV of kanamycin fcn-aptamer biosensor's response to kanamycin titration vs Ag/AgCl, performed in clean buffer, replicate 1 130714

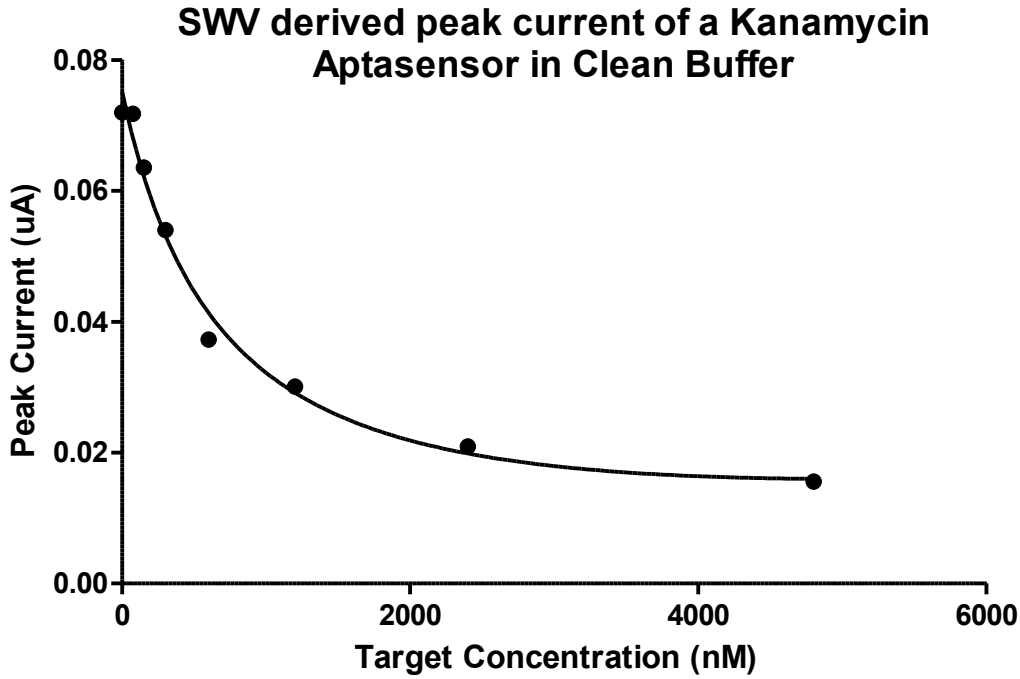

Fig A.2 SWV derived peak current response of kanamycin Fcn-aptamer biosensor to kanamycin titration vs Ag/AgCl, performed in clean buffer, replicate 1 130714

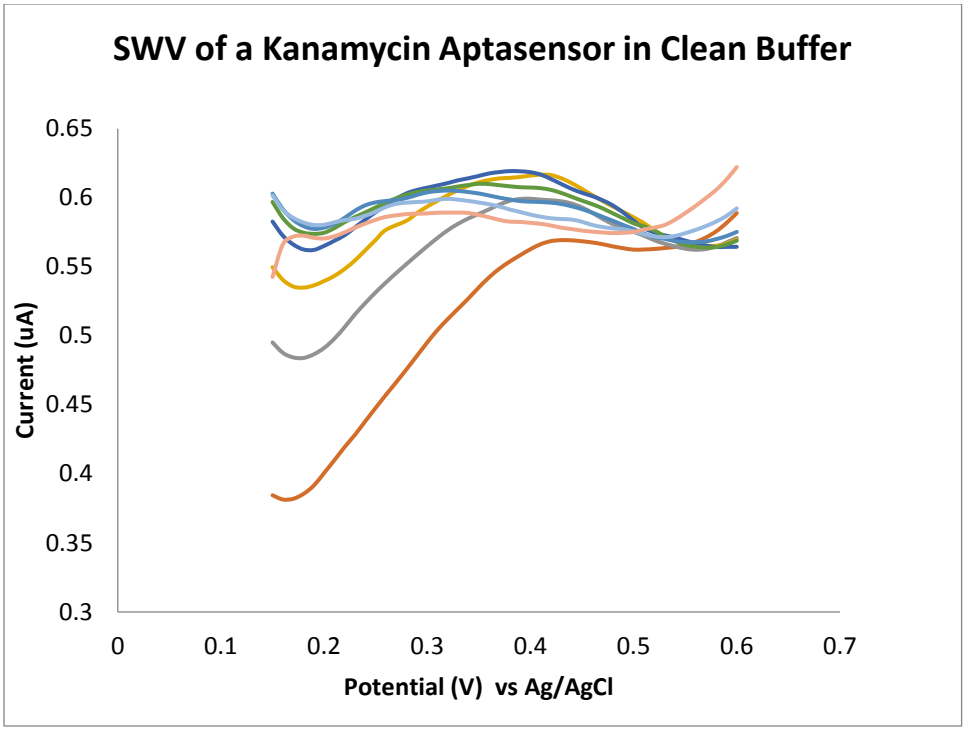

Fig A.3 SWV of kanamycin fcn-aptamer biosensor's response to kanamycin titration vs Ag/AgCl, performed in clean buffer, replicate 2 280714

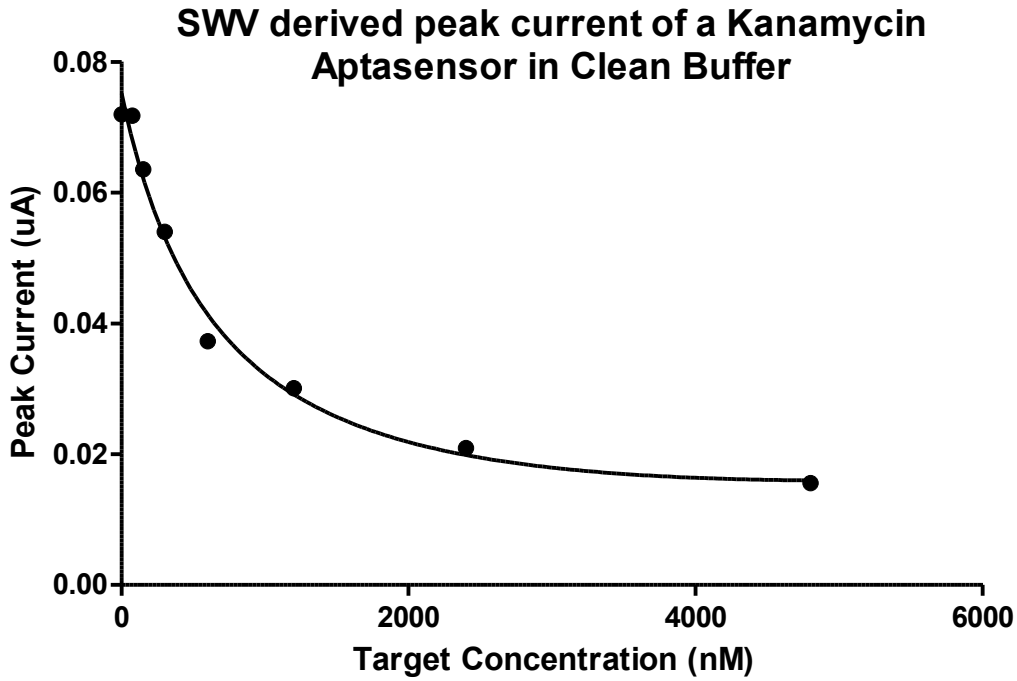

Fig A.4 SWV derived peak current response of kanamycin Fcn-aptamer biosensor to kanamycin titration vs Ag/AgCl, performed in clean buffer, replicate 2 280714

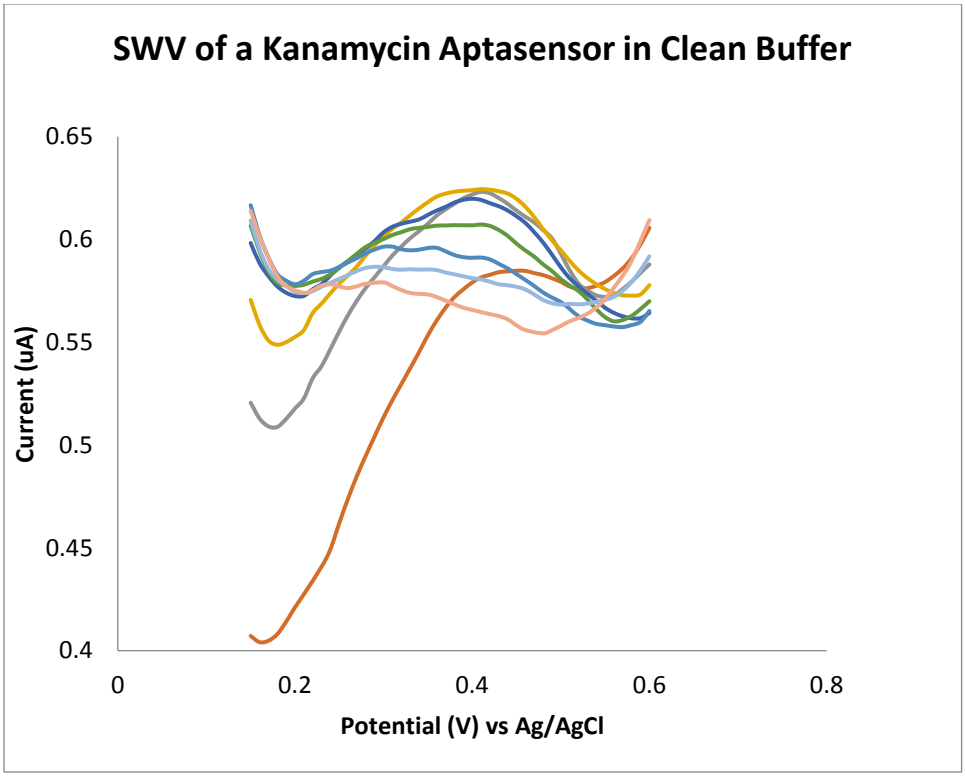

Fig A.5 SWV of kanamycin fcn-aptamer biosensor's response to kanamycin titration vs Ag/AgCl, performed in clean buffer, replicate 3 120814

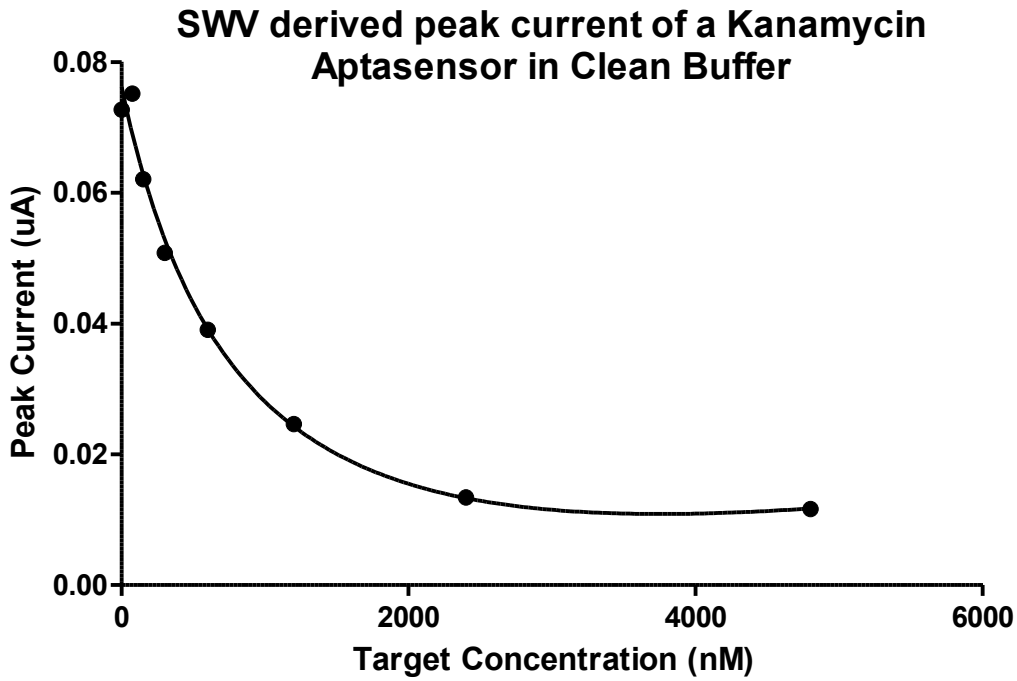

Fig A.6 SWV derived peak current response of kanamycin Fcn-aptamer biosensor to kanamycin titration vs Ag/AgCl, performed in clean buffer, replicate 3 120814

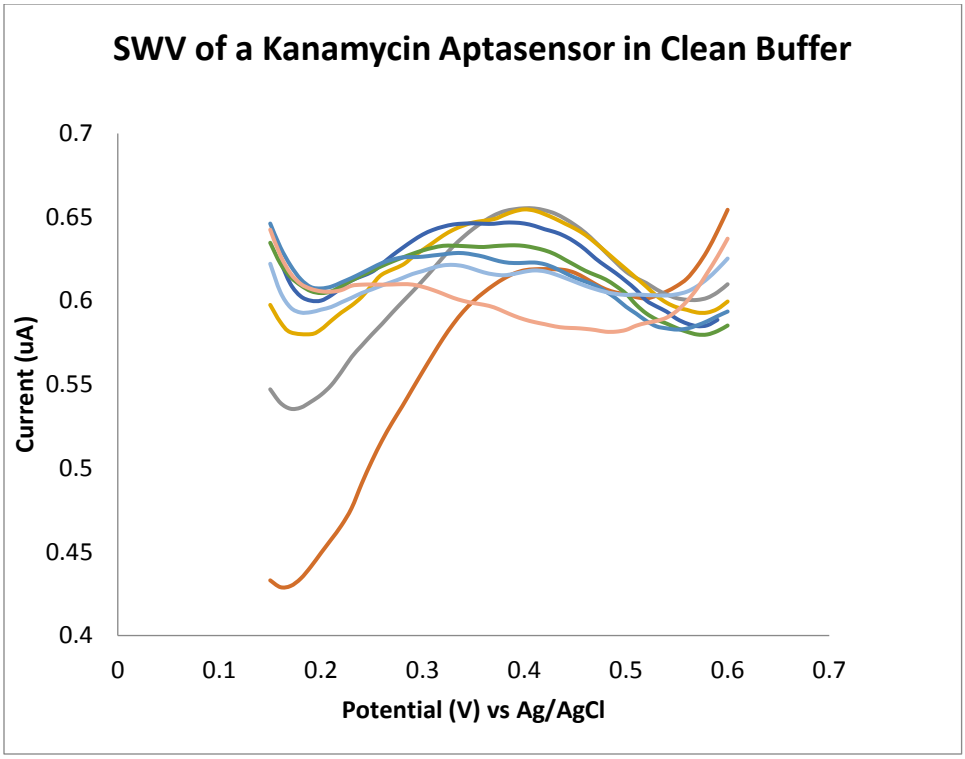

Fig A.7 SWV of kanamycin fcn-aptamer biosensor's response to kanamycin titration vs Ag/AgCl, performed in clean buffer, replicate 4 140814

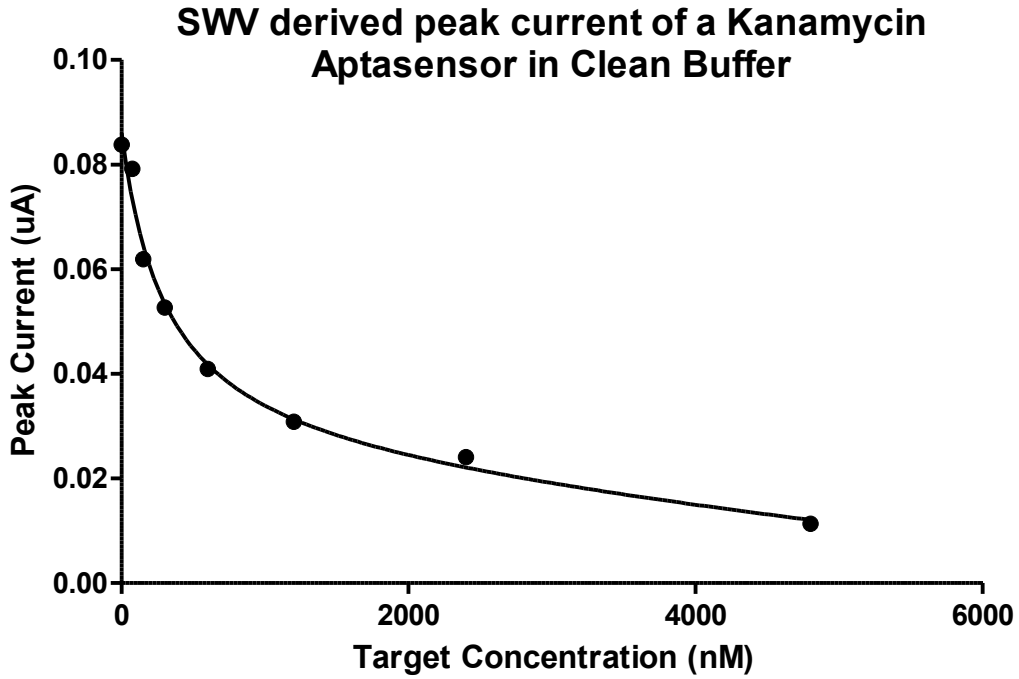

Fig A.8 SWV derived peak current response of kanamycin Fcn-aptamer biosensor to kanamycin titration vs Ag/AgCl, performed in clean buffer, replicate 4 140814

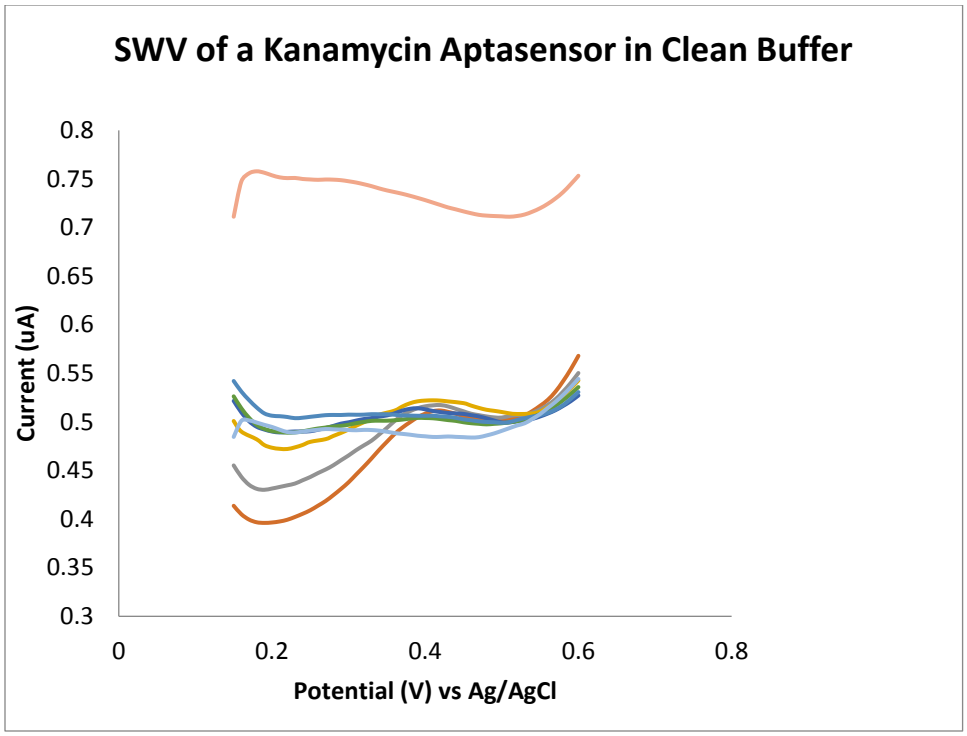

Fig A.9 SWV of kanamycin fcn-aptamer biosensor's response to kanamycin titration vs Ag/AgCl, performed in clean buffer, replicate 6 260914

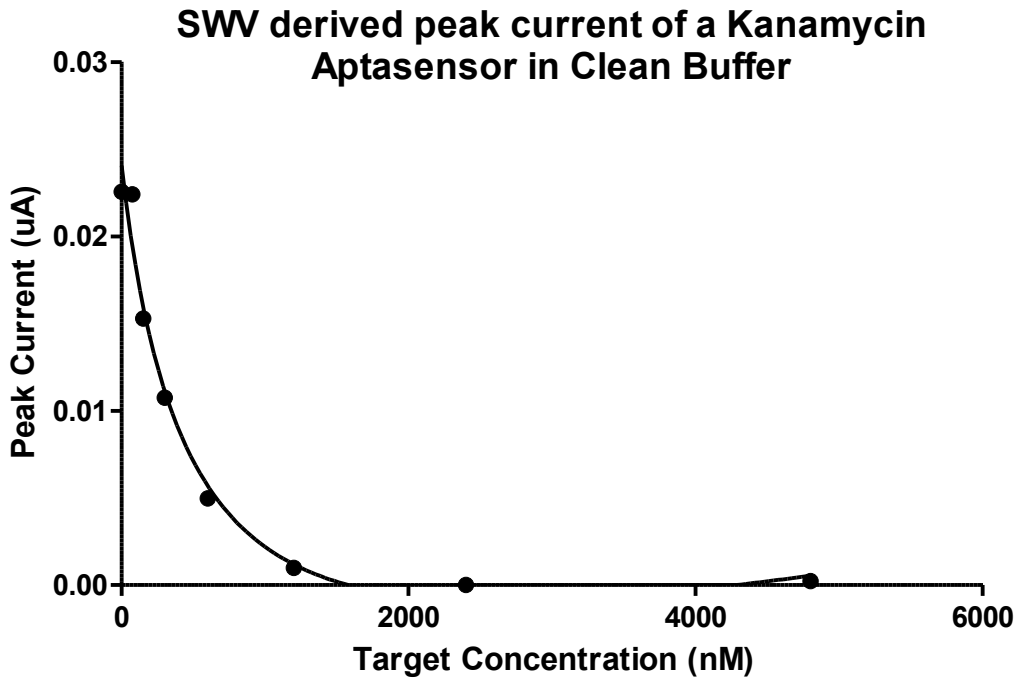

Fig A.10 SWV derived peak current response of kanamycin Fcn-aptamer biosensor to kanamycin titration vs Ag/AgCl, performed in clean buffer, replicate 6 260914

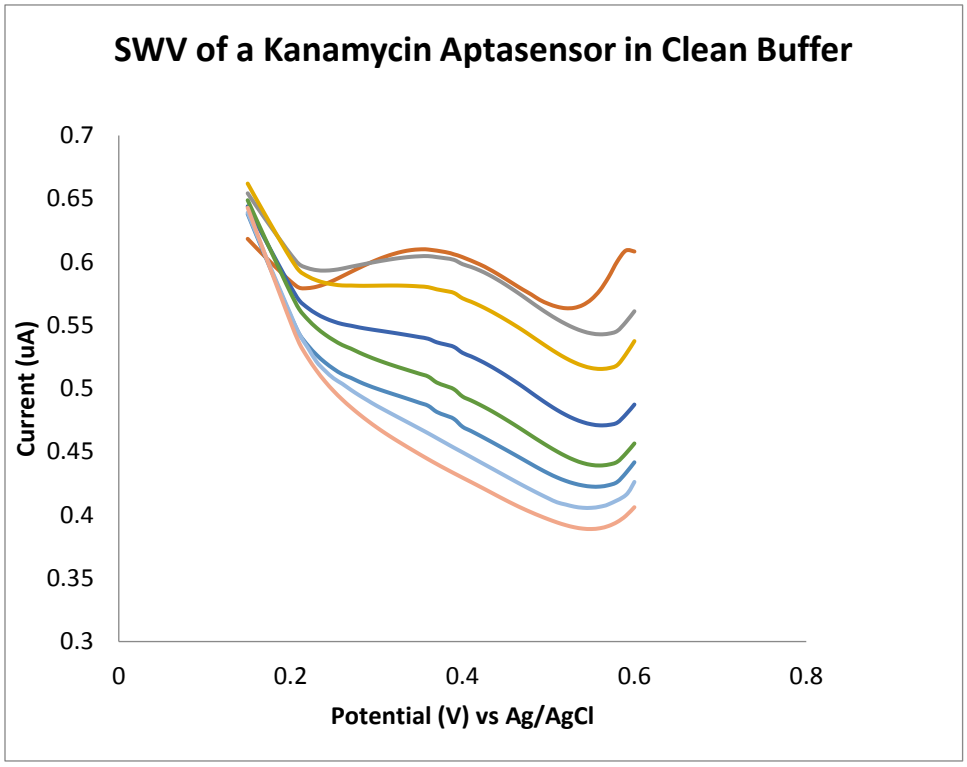

Fig A.11 SWV of kanamycin fcn-aptamer biosensor's response to kanamycin titration vs Ag/AgCl, performed in clean buffer, replicate 7 221214El1

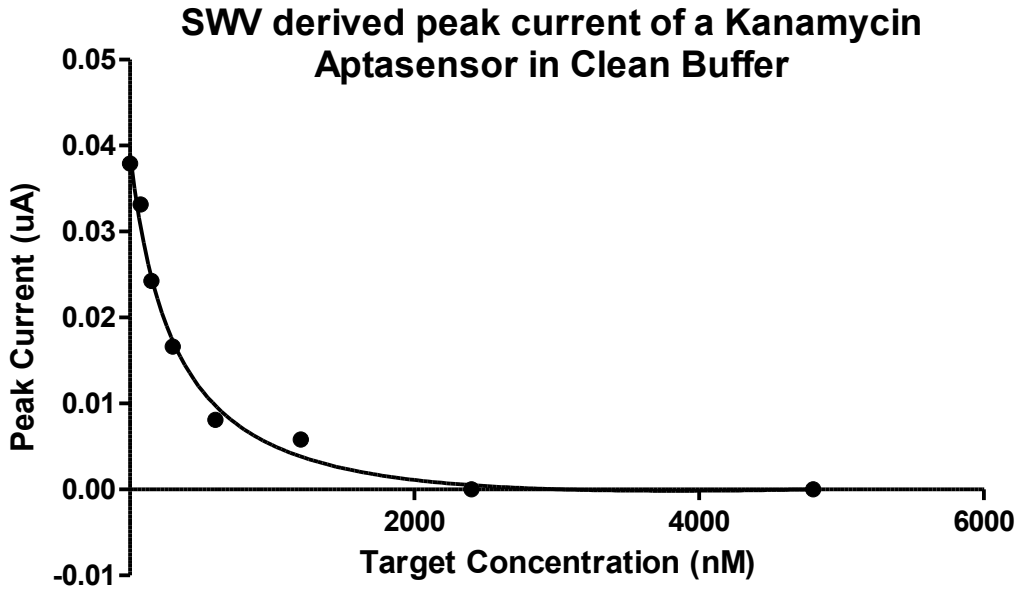

Fig A.12 SWV derived peak current response of kanamycin Fcn-aptamer biosensor to kanamycin titration vs Ag/AgCl, performed in clean buffer, replicate 7 221214El1

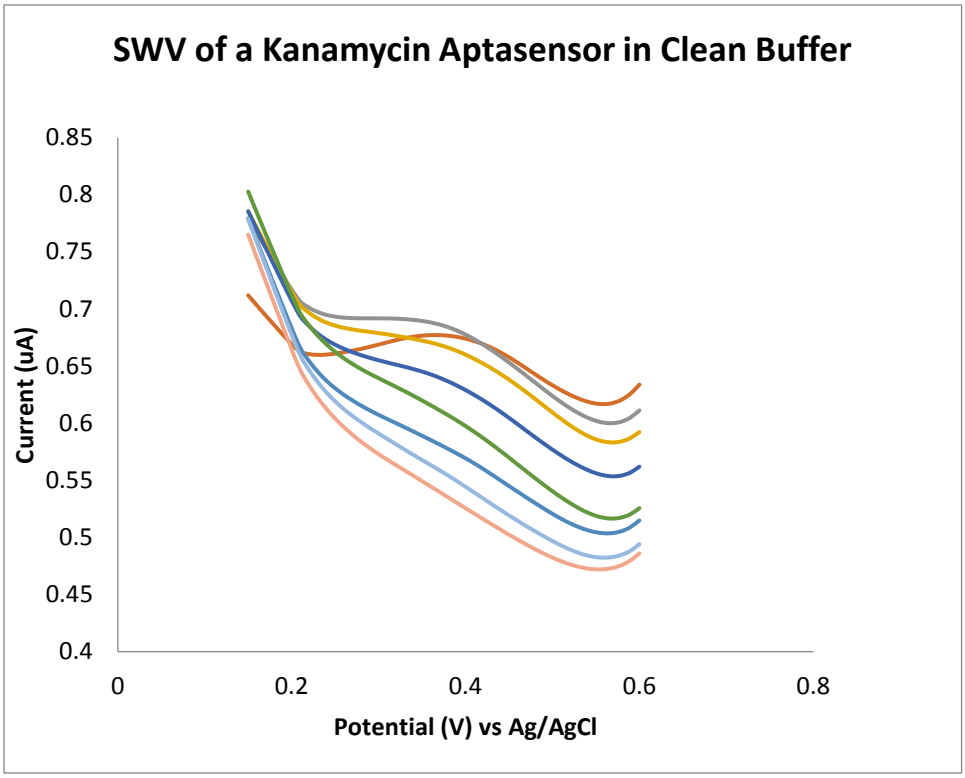

Fig A.13 SWV of kanamycin fcn-aptamer biosensor's response to kanamycin titration vs Ag/AgCl, performed in clean buffer, replicate 8 221214El2

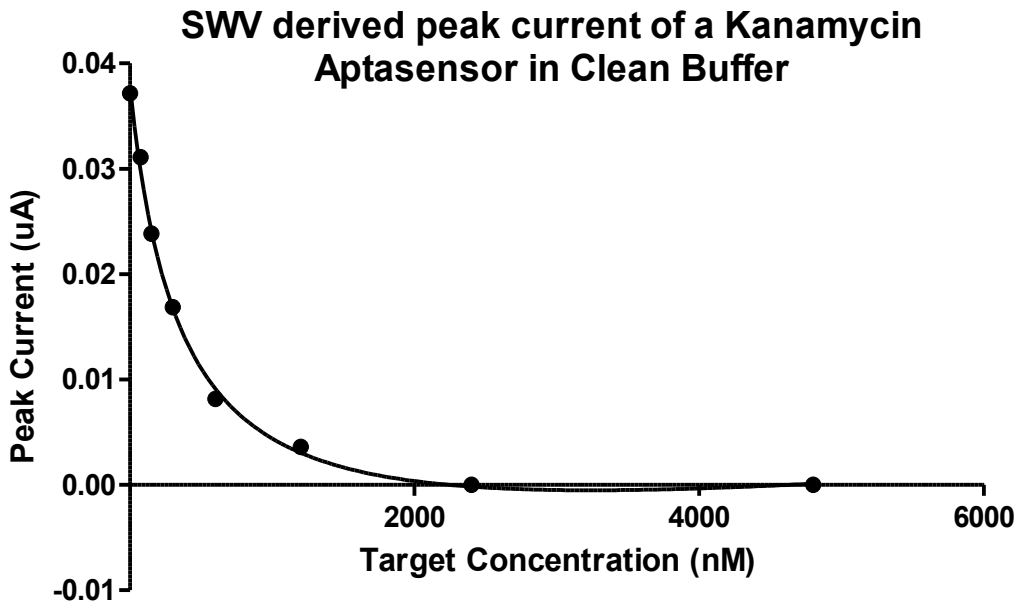

Fig A.14 SWV derived peak current response of kanamycin Fcn-aptamer biosensor to kanamycin titration vs Ag/AgCl, performed in clean buffer, replicate 8 221214El2

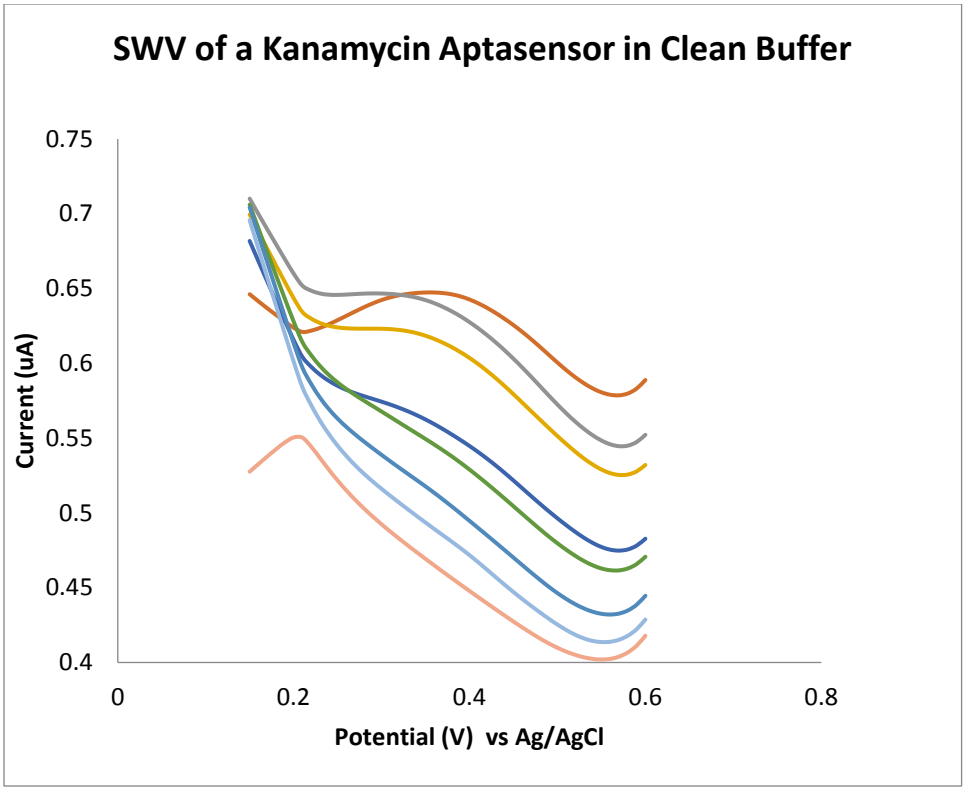

Fig A.15 SWV of kanamycin fcn-aptamer biosensor's response to kanamycin titration vs Ag/AgCl, performed in clean buffer, replicate 9 231214

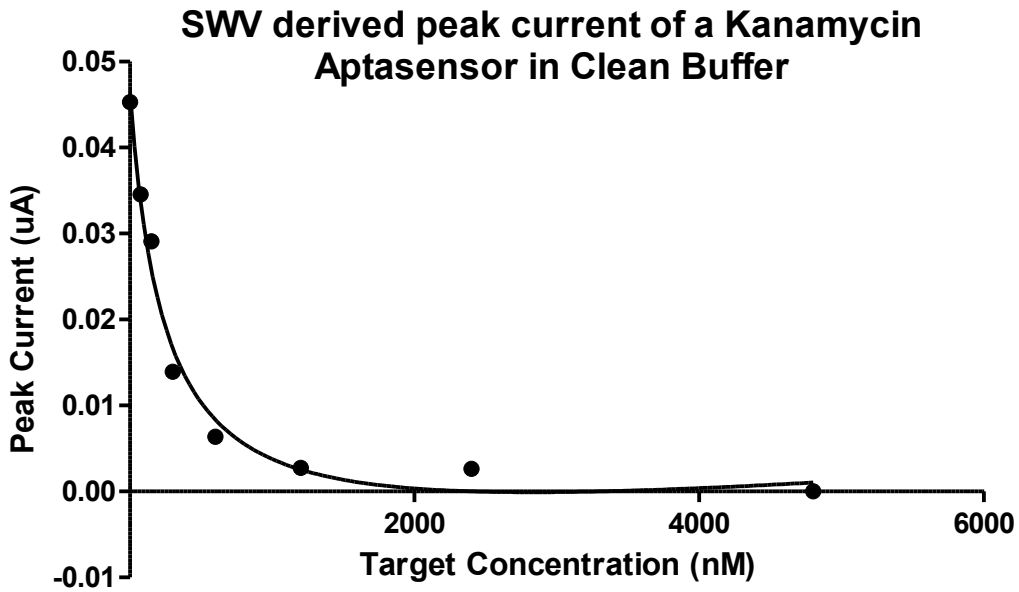

Fig A.16 SWV derived peak current response of kanamycin Fcn-aptamer biosensor to kanamycin titration vs Ag/AgCl, performed in clean buffer, replicate 9 231214

Appendix B: Replicate Results of SWV of kanamycin fcn-aptamer biosensor's response to kanamycin titration vs Ag/AgCl, performed in environmental matrix

Replicate 1 the soil environment, replicate 1 of the soil sample with 2h incubation and replicate 2 of the faecal sample titration can be found in the main body of the text.

	Soil Environment			Soil Env, 2h incubation		Faecal Environment		
Target Concentration (nM)	010914 E1	010914 E2	040914 E2	241014 El1	241014 El2	040914 E3	040914 E4	220914 E2
0	0.0257	0.0236	0.0161	0.0298	0.0400	0.0088	0.0123	0.0590
75	0.0237	0.0142	0.0119	0.0283	0.0377	0.0134	0.0101	0.0595
150	0.0183	0.0086	0.0114	0.0227	0.0290	0.0123	0.0110	0.0551
300	0.0100	0.0021	0.0087	0.0192	0.0227	0.0082	0.0074	0.0503
600	0.0051	0.0035	0.0064	0.0121	0.0183	0.0081	0.0055	0.0447
1200	0.0003	0.0000	0.0000	0.0107	0.0148	0.0049	0.0017	0.0381
2400	0.0000	0.0000	0.0017	0.0066	0.0054	0.0009	0.0000	0.0339
4800	0.0000	0.0000	0.0000	0.0049	0.0071	0.0000	0.0000	0.0284
Best-fit values								
Bmax	-0.03877	-0.02633	-0.02051	-0.02913	-0.03973	~ -7.751	-0.02421	-0.03616
Kd	421.9	108	538.7	429.3	423.7	~ 92543	1238	818
NS	1.85E-06	4.39E-07	6.64E-07	1.99E-07	4.3E-07	~ 7.722e-005	1.48E-06	-2.1E-07
Background	0.02719	0.02382	0.01554	0.03078	0.04082	0.01152	0.01221	0.06049
Goodness of Fit								
Degrees of Freedom	4	4	4	4	4	4	4	4
R square	0.984	0.9788	0.9603	0.9858	0.9747	0.8924	0.9837	0.9916
Absolute Sum of Squares	1.31E-05	1.08E-05	1.01E-05	9.19E-06	0.00003	1.78E-05	2.84E-06	8.14E-06
Sy.x	0.001811	0.001644	0.001591	0.001516	0.002739	0.002109	0.000843	0.001426

Table B.1 Summary of kanamycin fcn-aptamer biosensor's response to kanamycin titration vs Ag/AgCl, performed in environmental matrix

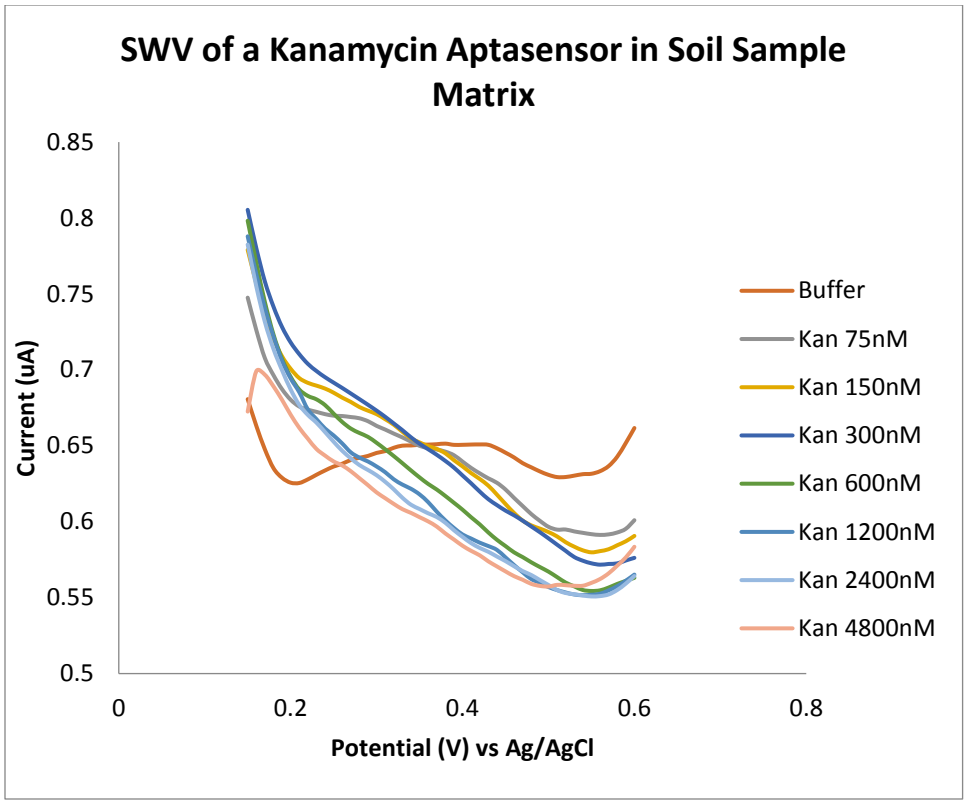

Fig B.1 SWV of kanamycin fcn-aptamer biosensor's response to kanamycin titration vs Ag/AgCl, performed in soil sample matrix, replicate 2 010914El2

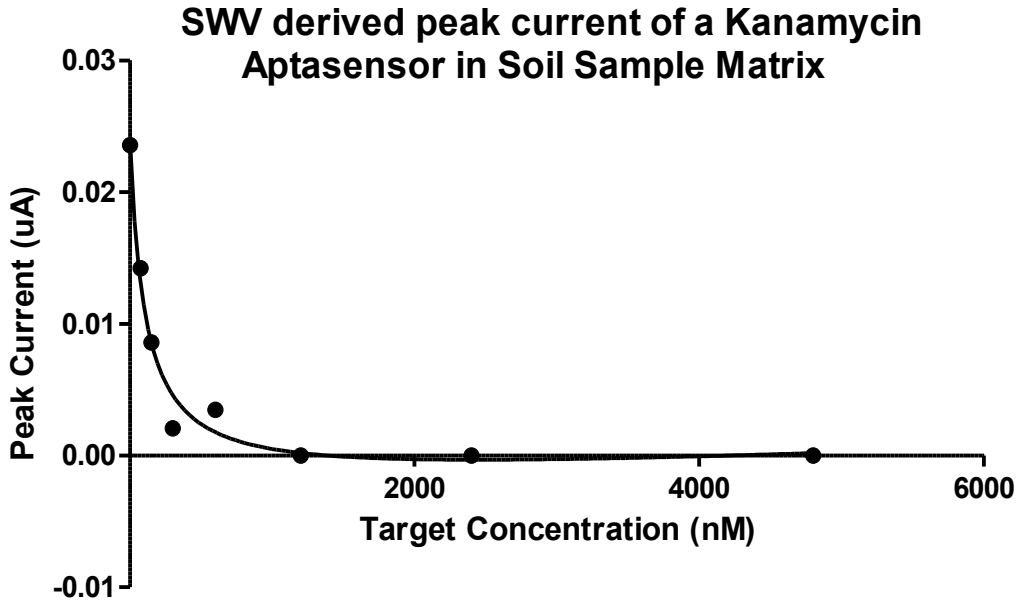

Fig B.2 SWV derived peak current response of kanamycin Fcn-aptamer biosensor to kanamycin titration vs Ag/AgCl, performed in soil sample matrix, replicate 2 010914El2

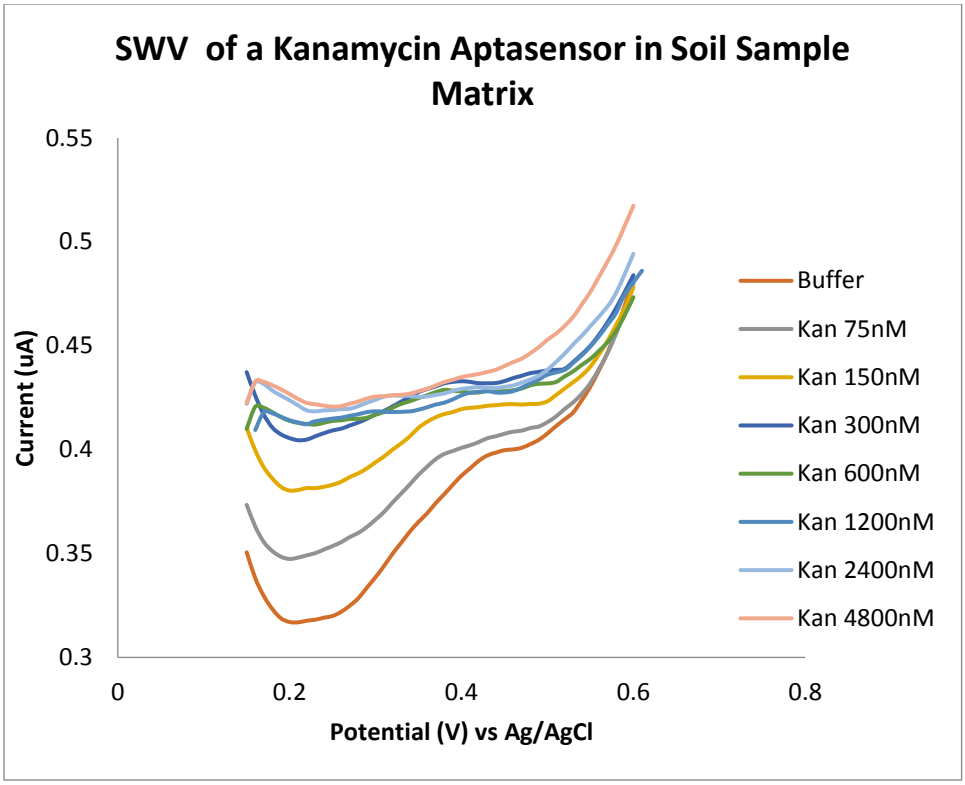

Fig B.3 SWV of kanamycin fcn-aptamer biosensor's response to kanamycin titration vs Ag/AgCl, performed in soil sample matrix, replicate 3 040914El2

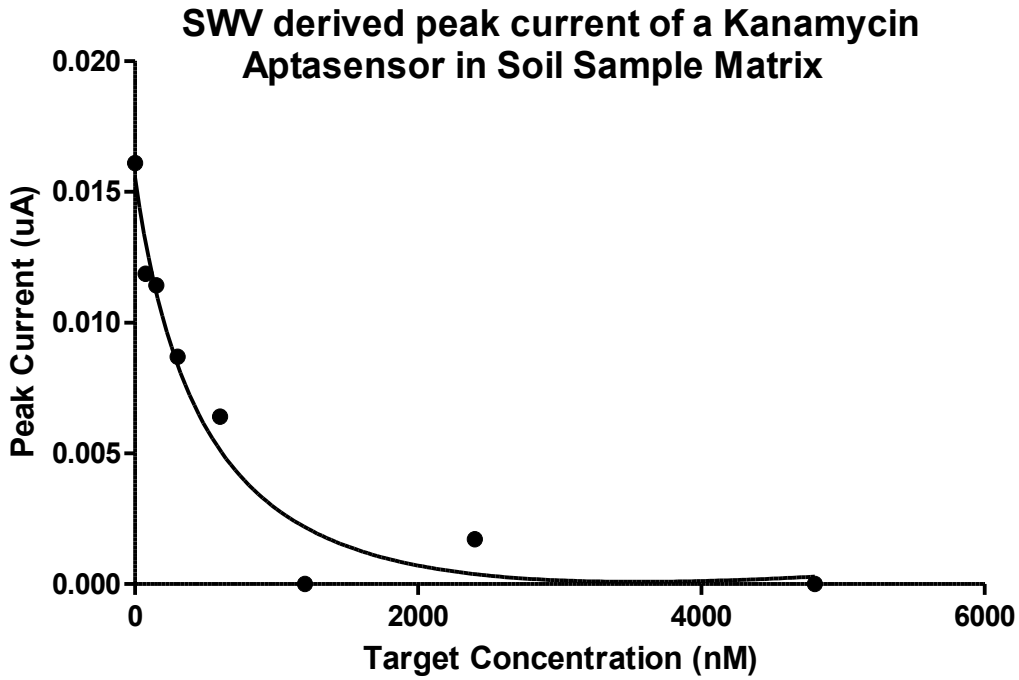

Fig B.4 SWV derived peak current response of kanamycin Fcn-aptamer biosensor to kanamycin titration vs Ag/AgCl, performed in soil sample matrix, replicate 3 040914El2

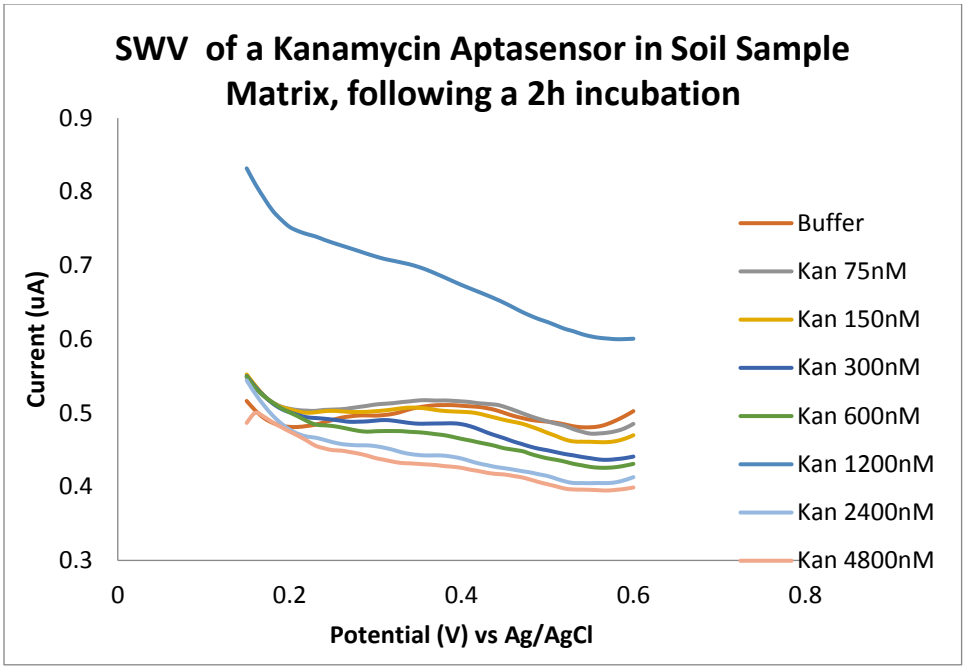

Fig B.5 SWV of kanamycin fcn-aptamer biosensor's response to kanamycin titration vs Ag/AgCl, performed in soil sample matrix following a 2h incubation, replicate 2 241014El2

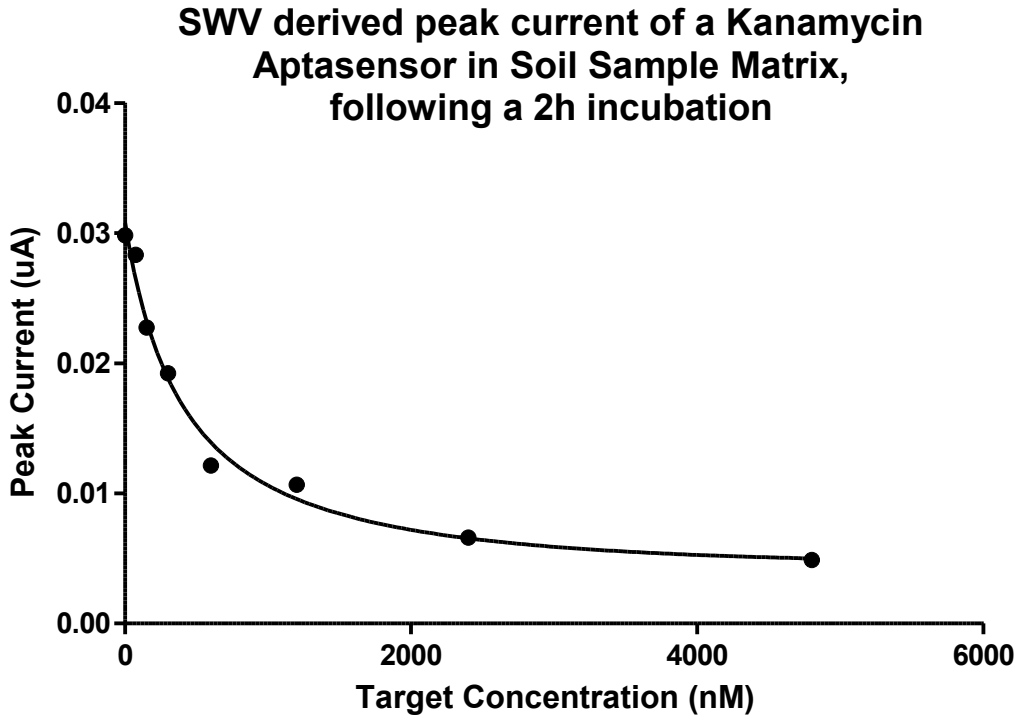

Fig B.6 SWV derived peak current response of kanamycin Fcn-aptamer biosensor to kanamycin titration vs Ag/AgCl, performed in soil sample matrix following a 2h incubation, replicate 2 241014El2

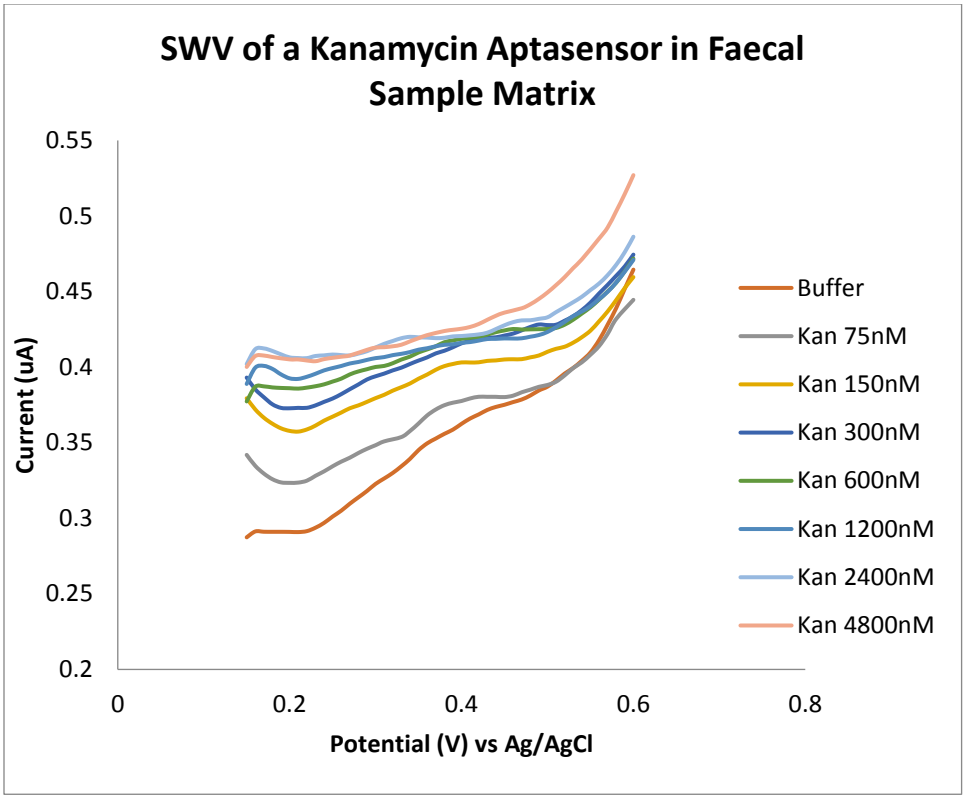

Fig B.7 SWV of kanamycin fcn-aptamer biosensor's response to kanamycin titration vs Ag/AgCl, performedin faecal sample matrix, replicate 1 040914El3

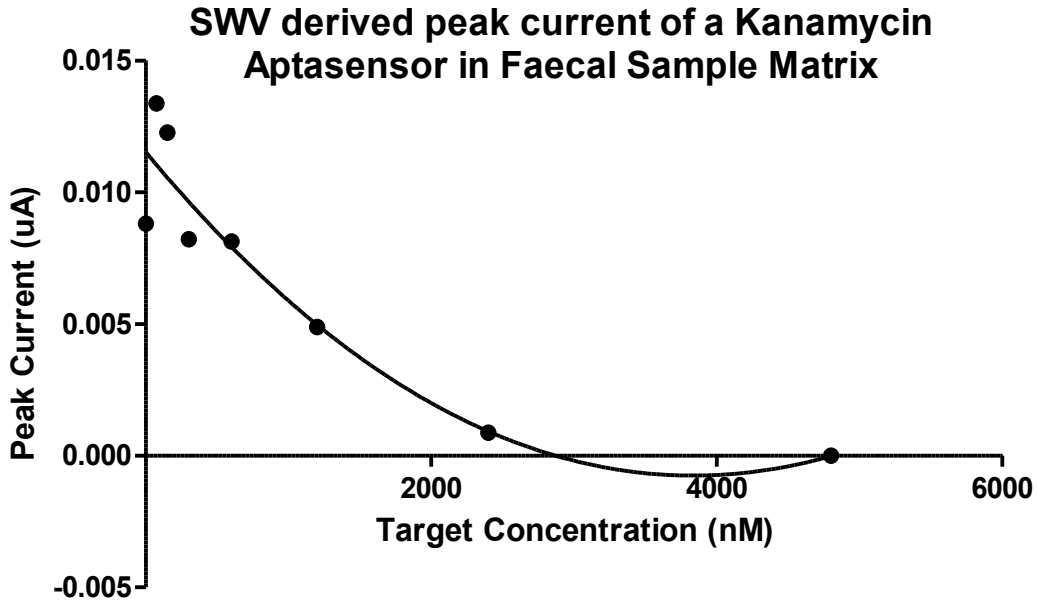

Fig B.8 SWV derived peak current response of kanamycin Fcn-aptamer biosensor to kanamycin titration vs Ag/AgCl, performed in faecal sample matrix, replicate 1 040914El3

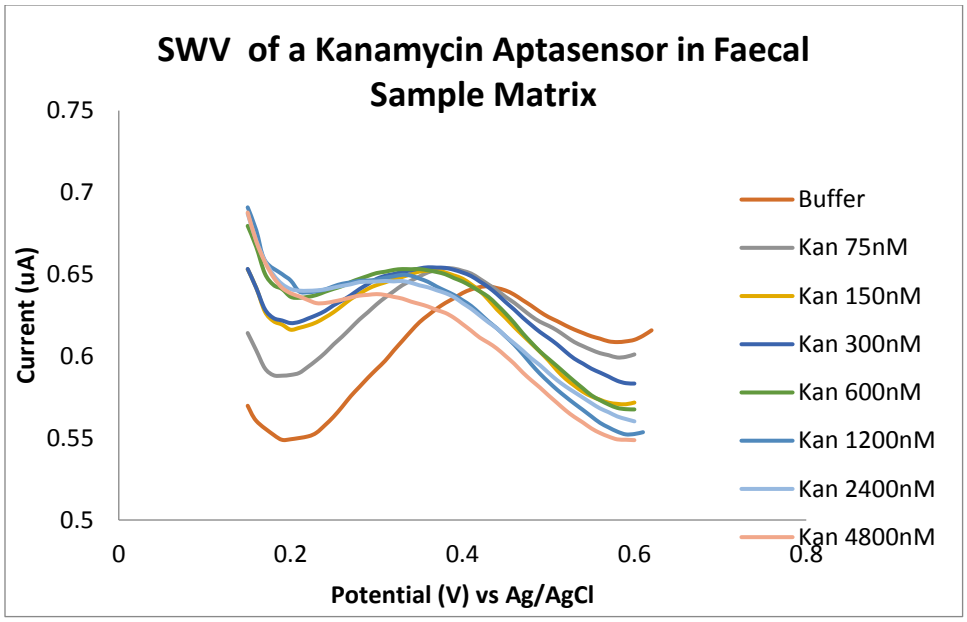

Fig B.9 SWV of kanamycin fcn-aptamer biosensor's response to kanamycin titration vs Ag/AgCl, performedin faecal sample matrix, replicate 2 040914El4

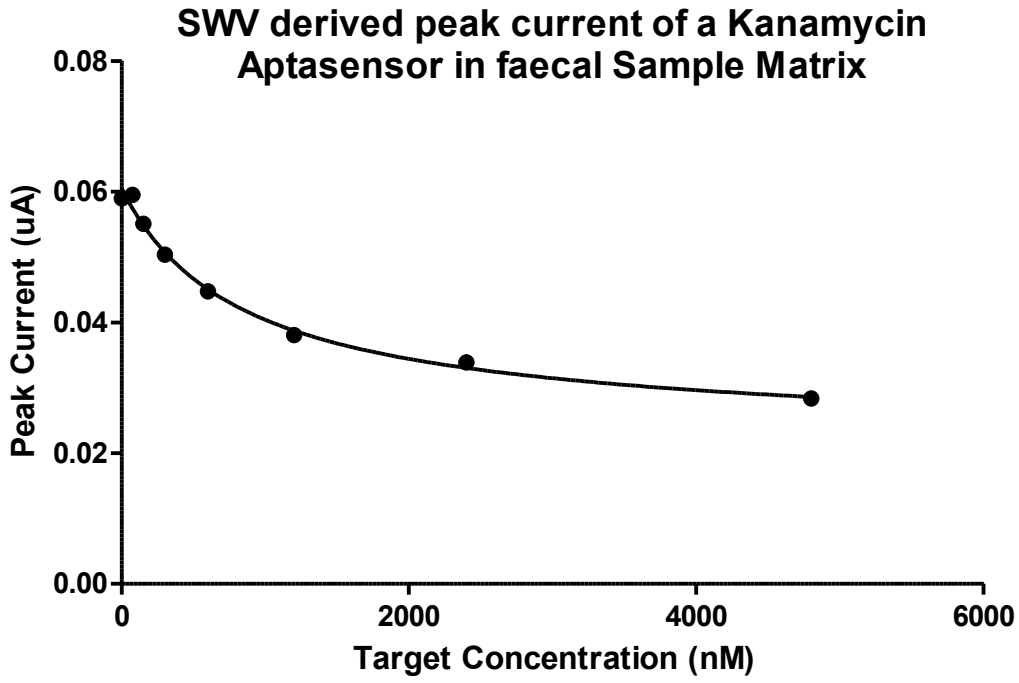

Fig B.10 SWV derived peak current response of kanamycin Fcn-aptamer biosensor to kanamycin titration vs Ag/AgCl, performed in faecal sample matrix, replicate 2 040914El4

Appendix C: Replicate Results of SWV of gel encapsulated and unprotected kanamycin fcn-aptamer biosensor's response to kanamycin titration vs Ag/AgCl, performed in clean buffer following 2h incubation in nuclease solution.

	Gel Encoated				Unprotected			
Target Concentration (nM)	171214 El1 Gel	171214 El2 Gel	191214 El1 Gel	191214 El2 Gel	171214 El1 no Gel	171214 El2 no Gel	191214 El1 no Gel	191214 El2 no Gel
0	0.0705	0.0512	0.0838	0.0689	0.0192	0.0235	0.0292	0.0230
75	0.0594	0.0463	0.0792	0.0759	0.0234	0.0248	0.0253	0.0193
150	0.0513	0.0395	0.0619	0.0520	0.0211	0.0243	0.0208	0.0156
300	0.0352	0.0311	0.0527	0.0419	0.0188	0.0185	0.0146	0.0118
600	0.0257	0.0233	0.0409	0.0358	0.0131	0.0150	0.0087	0.0087
1200	0.0168	0.0145	0.0309	0.0269	0.0116	0.0110	0.0052	0.0070
2400	0.0098	0.0099	0.0241	0.0202	0.0084	0.0086	0.0030	0.0028
4800	0.0052	0.0083	0.0113	0.0133	0.0094	0.0078	0.0027	0.0015
Best-fit values								
Bmax	-0.07028	-0.05545	-0.06496	-0.06203	0.000585	-0.0331	-0.03472	-0.02012
Kd	328.5	519.8	314.6	379.6	-68.35	1241	388.2	258.4
NS	-4.1E-08	1.38E-06	-2.7E-06	-5.4E-07	-2.3E-06	1.86E-06	1.08E-06	-6E-07
Background	0.07139	0.05183	0.08603	0.07392	0.01701	0.02537	0.02987	0.02323
Goodness of Fit								
Degrees of Freedom	4	4	4	4	4	4	4	4
R square	0.9967	0.9983	0.9888	0.9391	0.7279	0.9664	0.9966	0.9939
Absolute Sum of Squares	1.35E-05	3.19E-06	5.28E-05	0.000216	6.21E-05	1.18E-05	2.61E-06	2.53E-06
Sy.x	0.00184	0.000893	0.003633	0.00734	0.003939	0.001721	0.000808	0.000795

Table C.1 Summary of gel encapsulated and unprotected kanamycin fcn-aptamer biosensor's response to kanamycin titration vs Ag/AgCl, performed in clean buffer following 2h incubation in nuclease solution.

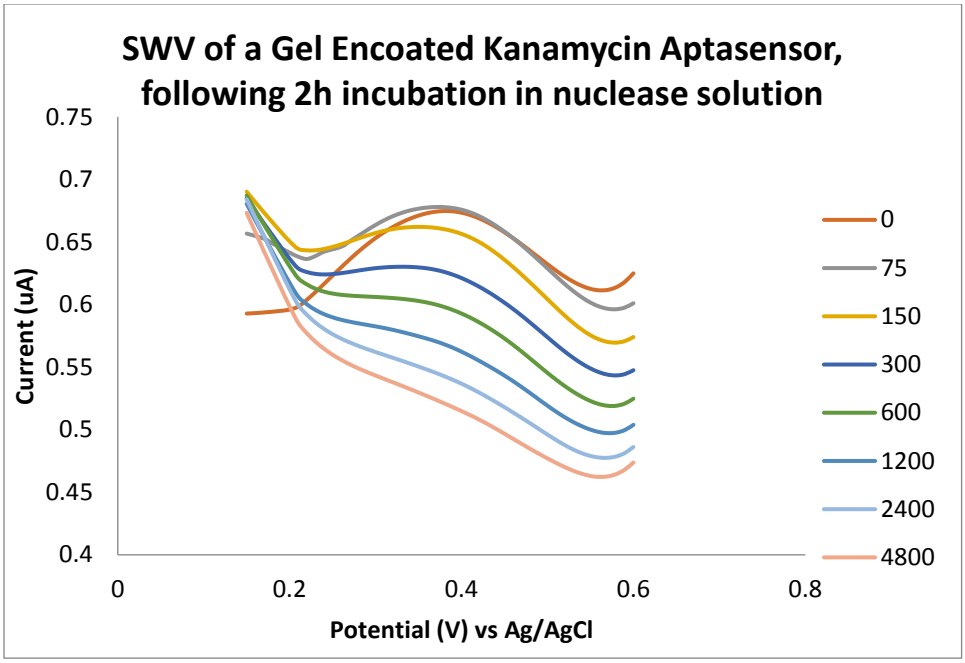

Fig C.1 SWV of gel encoated kanamycin fcn-aptamer biosensor's response to kanamycin titration vs Ag/AgCl, performed in clean buffer following 2h incubation in nuclease solution, replicate 1 171214El1

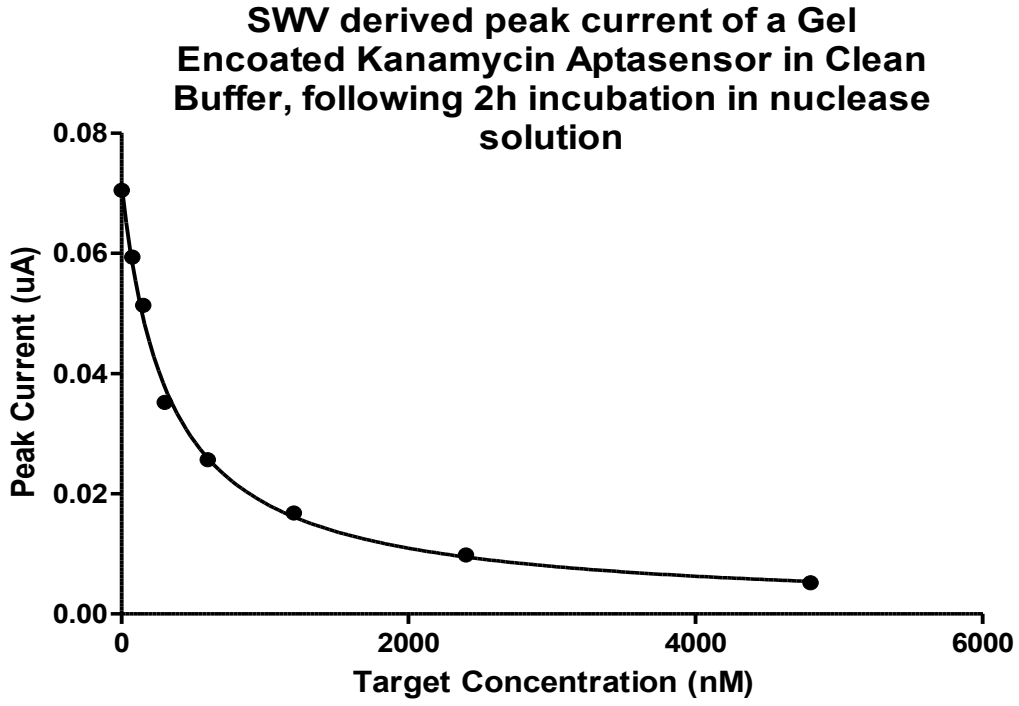

Fig C.2 SWV derived peak current response of gel-encoated kanamycin Fcn-aptamer biosensor to kanamycin titration vs Ag/AgCl, performed in clean buffer following 2h incubation in nuclease solution replicate 1 171214El1

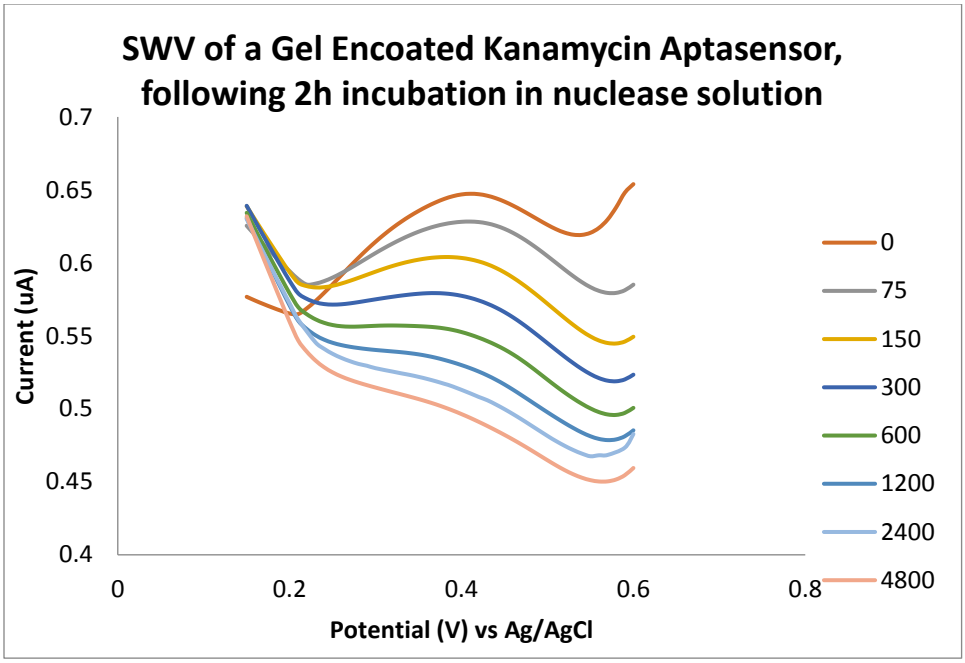

Fig C.3 SWV of gel encoated kanamycin fcn-aptamer biosensor's response to kanamycin titration vs Ag/AgCl, performed in clean buffer following 2h incubation in nuclease solution, replicate 2 171214El2

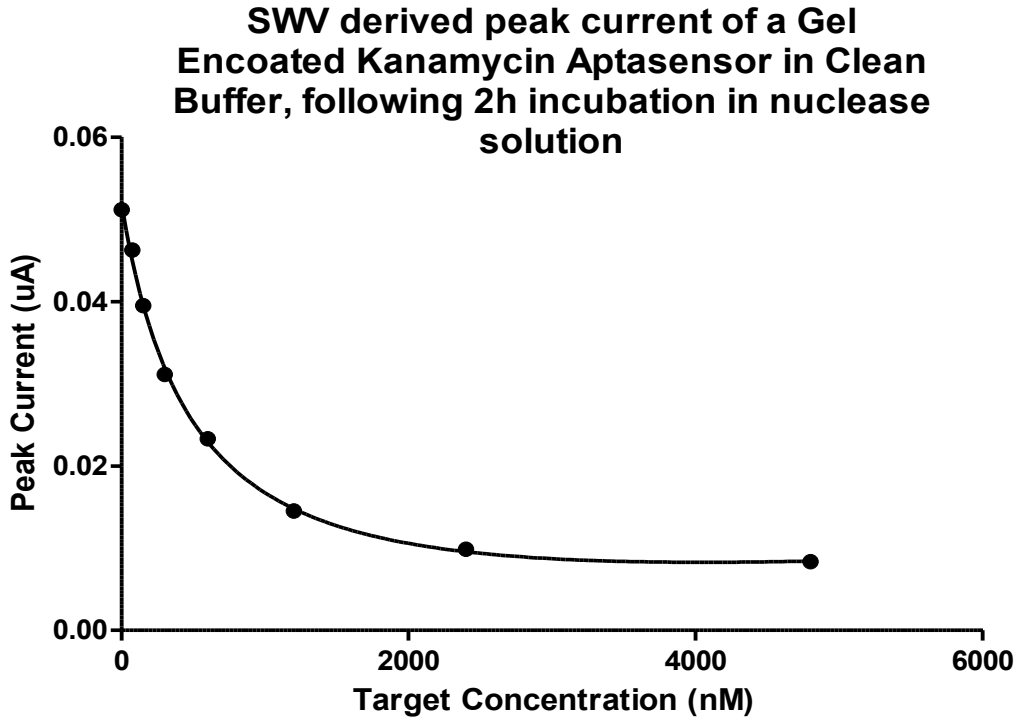

Fig C.4 SWV derived peak current response of gel-encoated kanamycin Fcn-aptamer biosensor to kanamycin titration vs Ag/AgCl, performed in clean buffer following 2h incubation in nuclease solution replicate 2 171214El2

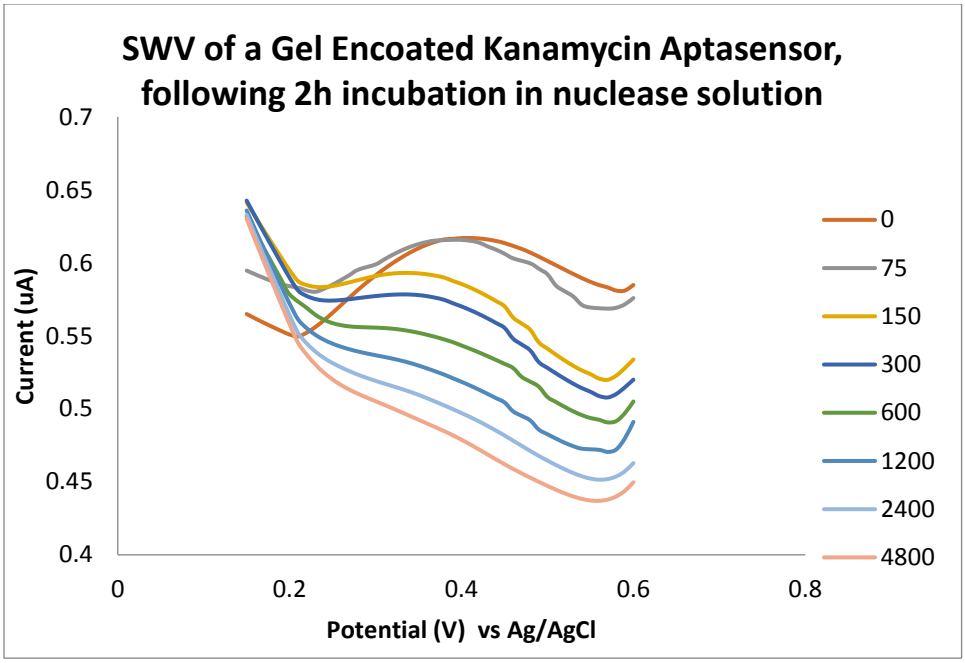

Fig C.5 SWV of gel encoated kanamycin fcn-aptamer biosensor's response to kanamycin titration vs Ag/AgCl, performed in clean buffer following 2h incubation in nuclease solution, replicate 3 191214El1

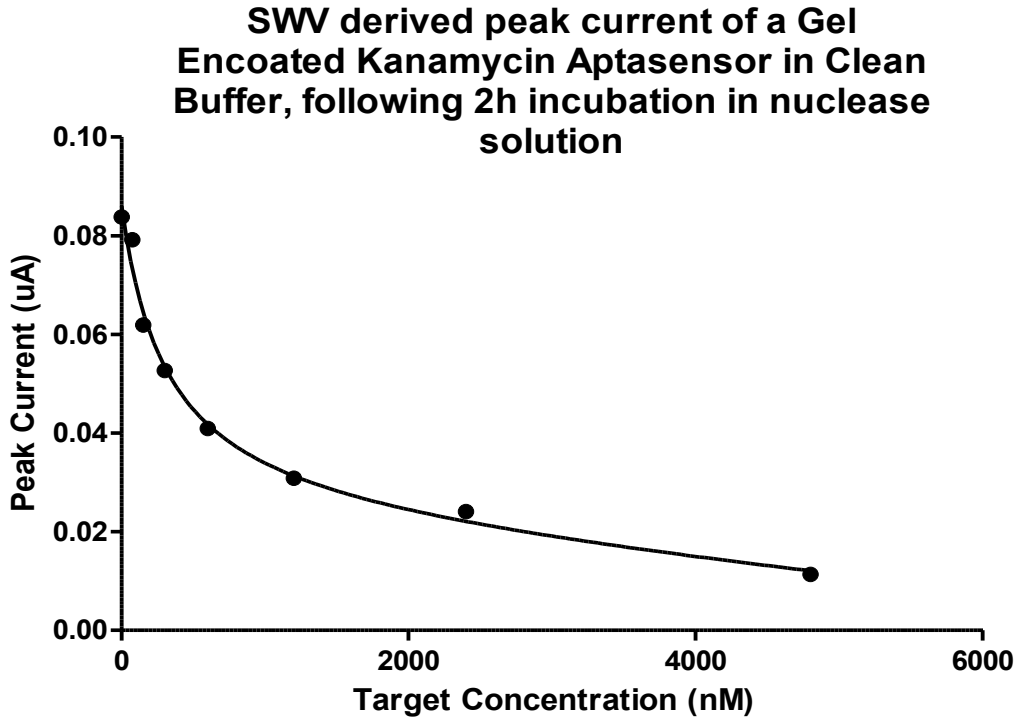

Fig C.6 SWV derived peak current response of gel-encoated kanamycin Fcn-aptamer biosensor to kanamycin titration vs Ag/AgCl, performed in clean buffer following 2h incubation in nuclease solution replicate 3 191214El1

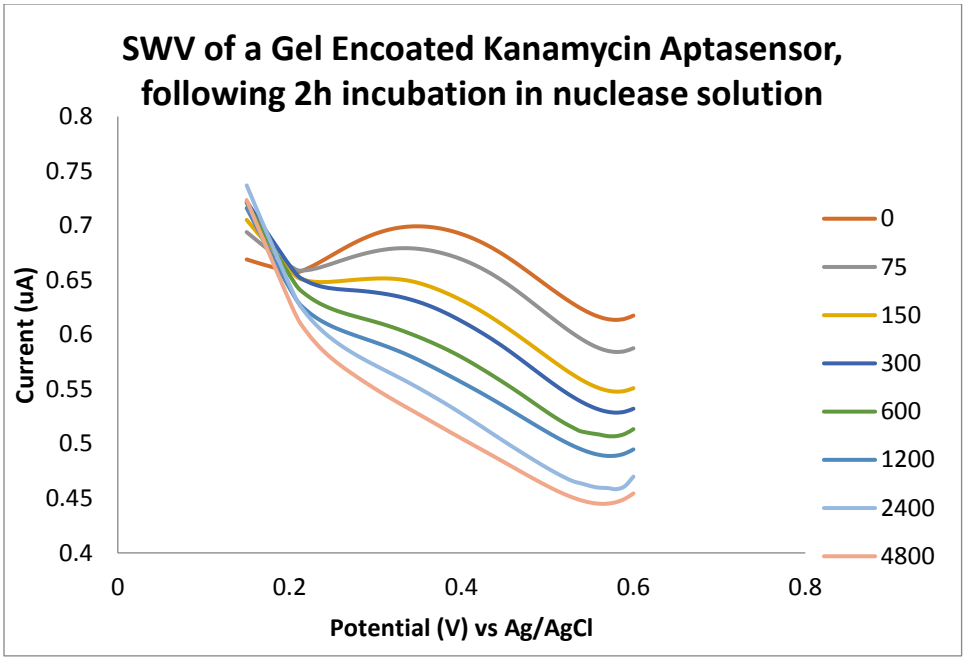

Fig C.7 SWV of gel encoated kanamycin fcn-aptamer biosensor's response to kanamycin titration vs Ag/AgCl, performed in clean buffer following 2h incubation in nuclease solution, replicate 4 191214El2

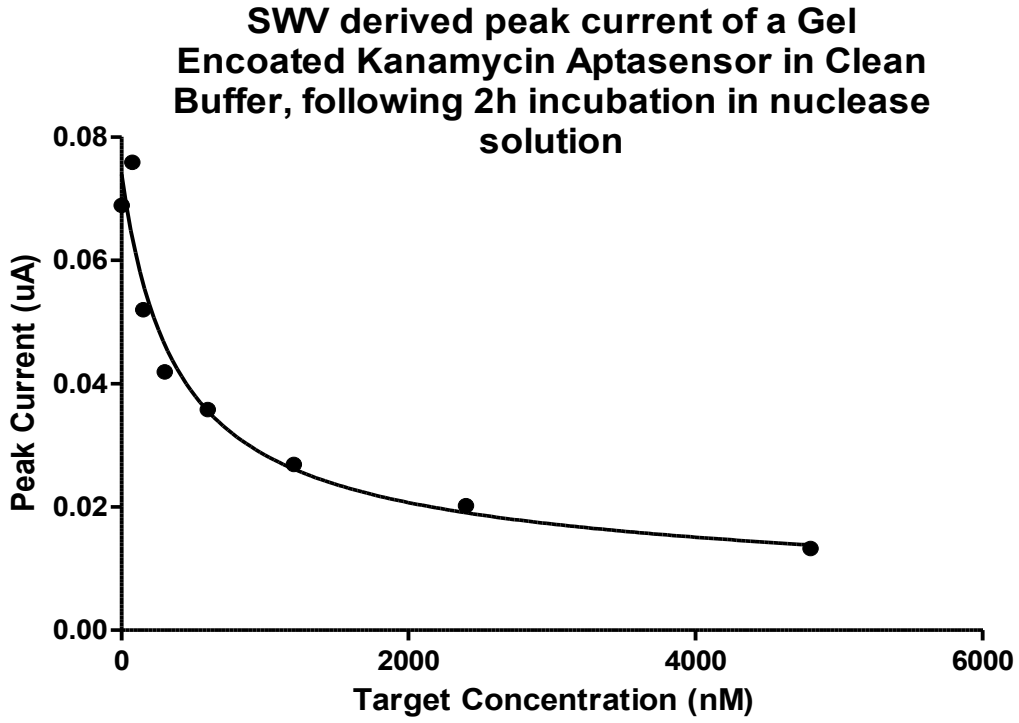

Fig C.8 SWV derived peak current response of gel-encoated kanamycin Fcn-aptamer biosensor to kanamycin titration vs Ag/AgCl, performed in clean buffer following 2h incubation in nuclease solution replicate 4 191214El2

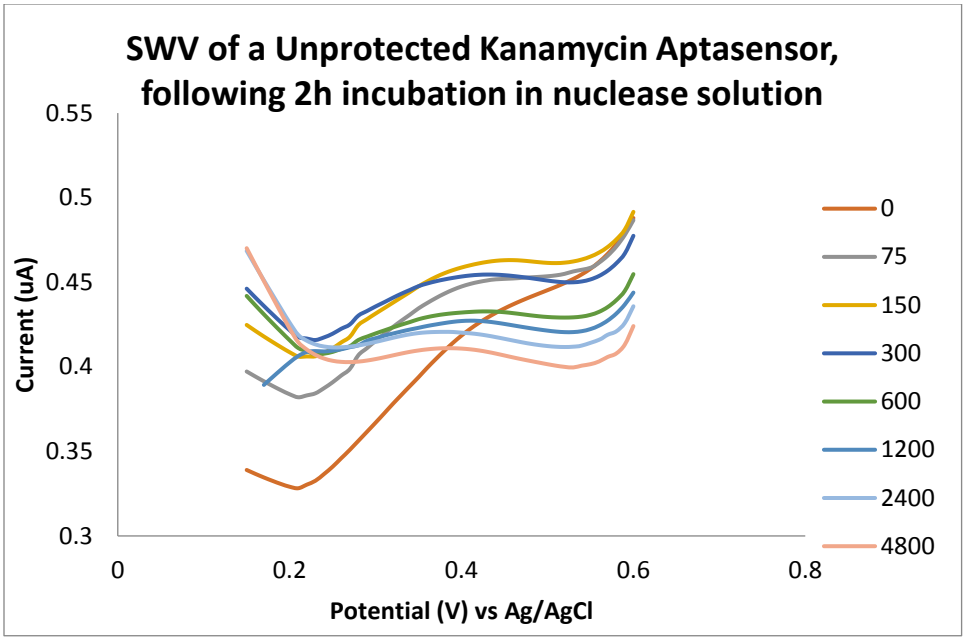

Fig C.9 SWV of unprotected kanamycin fcn-aptamer biosensor's response to kanamycin titration vs Ag/AgCl, performed in clean buffer following 2h incubation in nuclease solution, replicate 1 171214El3

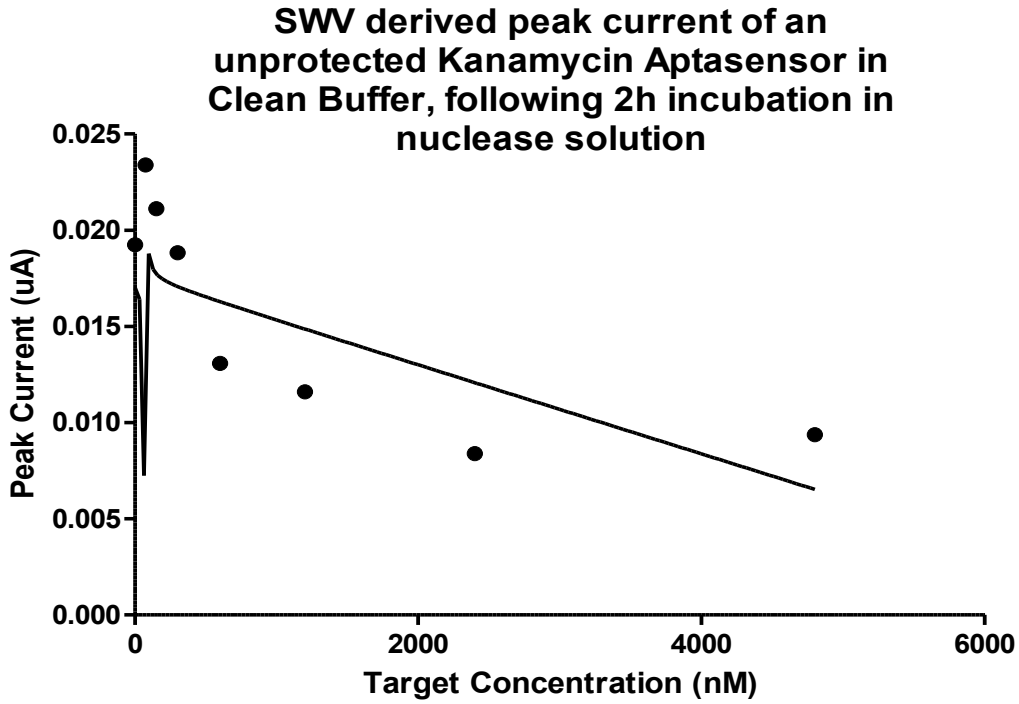

Fig C.10 SWV derived peak current response of unprotected kanamycin Fcn-aptamer biosensor to kanamycin titration vs Ag/AgCl, performed in clean buffer following 2h incubation in nuclease solution replicate 1 171214El3

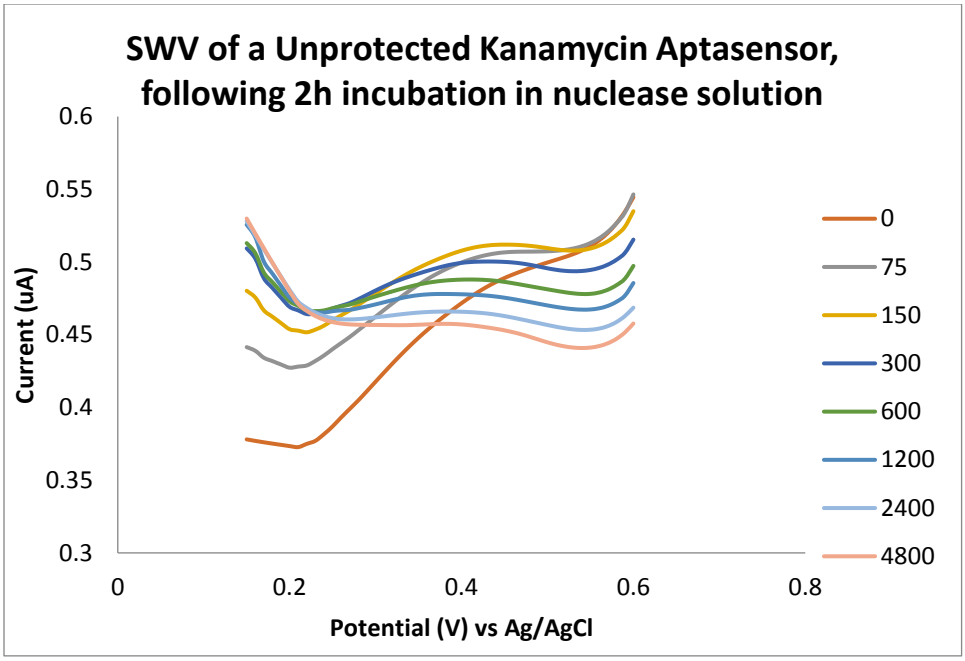

Fig C.11 SWV of unprotected kanamycin fcn-aptamer biosensor's response to kanamycin titration vs Ag/AgCl, performed in clean buffer following 2h incubation in nuclease solution, replicate 2 171214El4

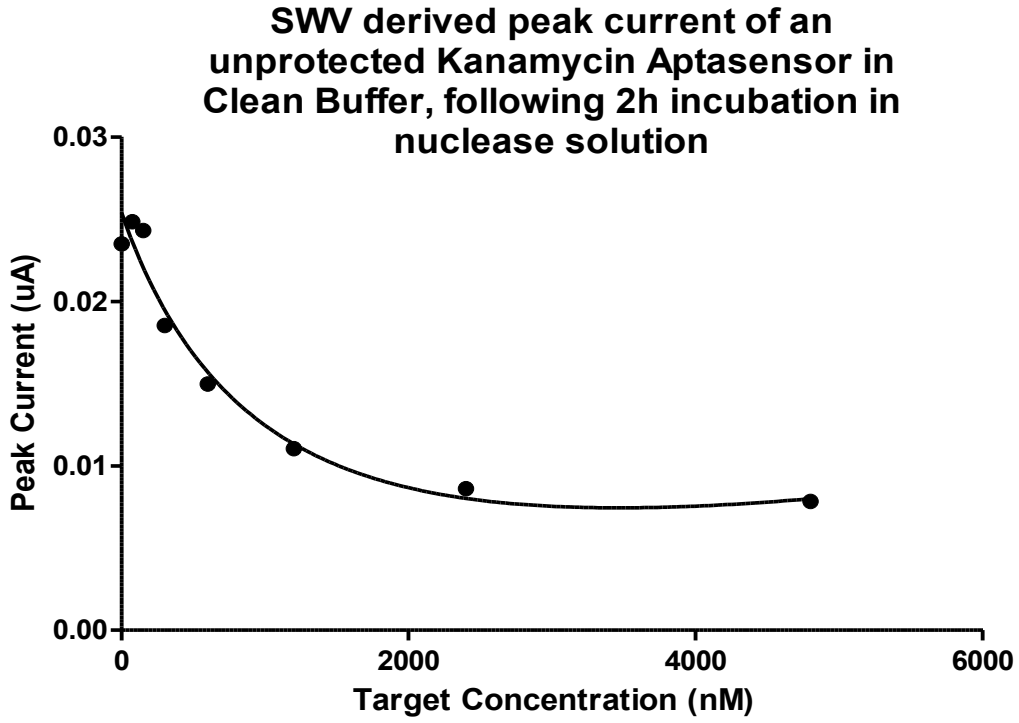

Fig C.12 SWV derived peak current response of unprotected kanamycin Fcn-aptamer biosensor to kanamycin titration vs Ag/AgCl, performed in clean buffer following 2h incubation in nuclease solution replicate 2 171214El4

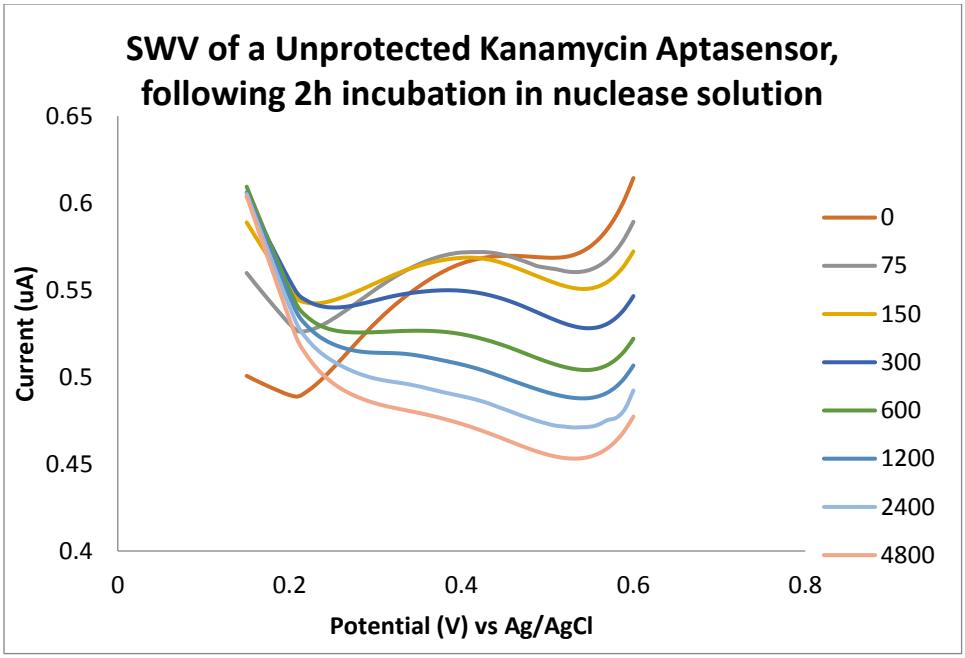

Fig C.13 SWV of unprotected kanamycin fcn-aptamer biosensor's response to kanamycin titration vs Ag/AgCl, performed in clean buffer following 2h incubation in nuclease solution, replicate 3 191214El3

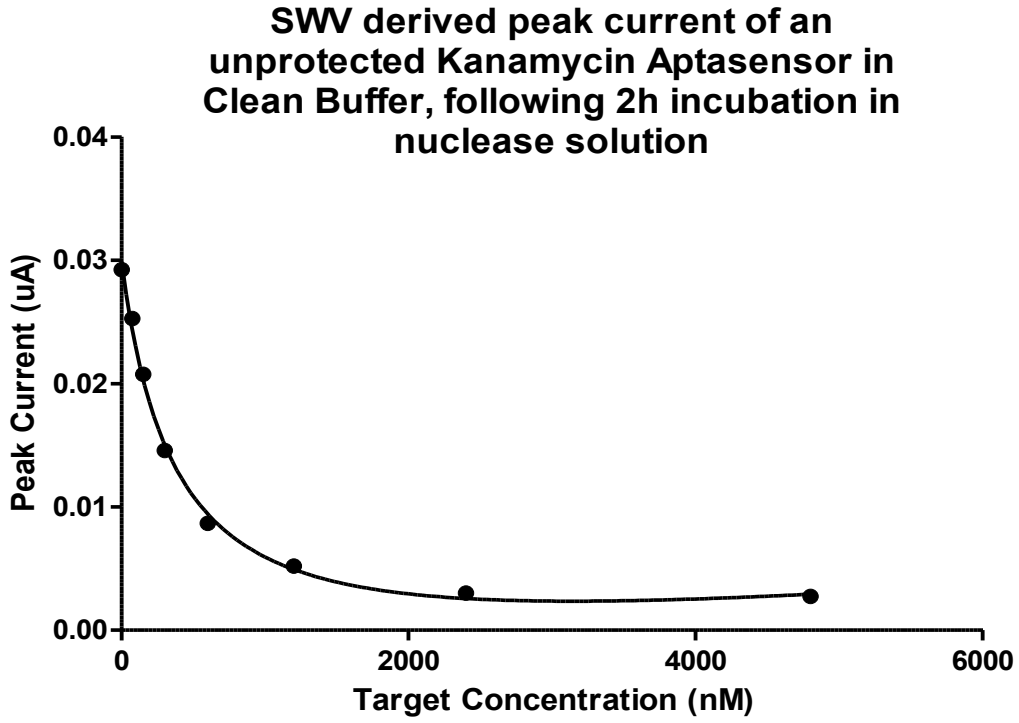

Fig C.14 SWV derived peak current response of unprotected kanamycin Fcn-aptamer biosensor to kanamycin titration vs Ag/AgCl, performed in clean buffer following 2h incubation in nuclease solution replicate 3 191214El3

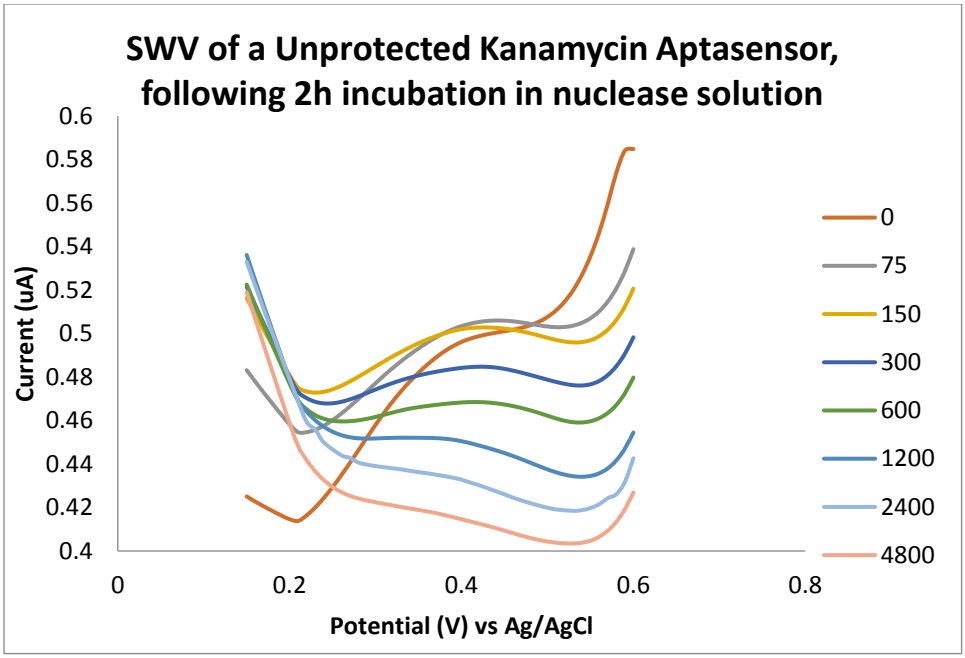

Fig C.15 SWV of unprotected kanamycin fcn-aptamer biosensor's response to kanamycin titration vs Ag/AgCl, performed in clean buffer following 2h incubation in nuclease solution, replicate 4 191214El4

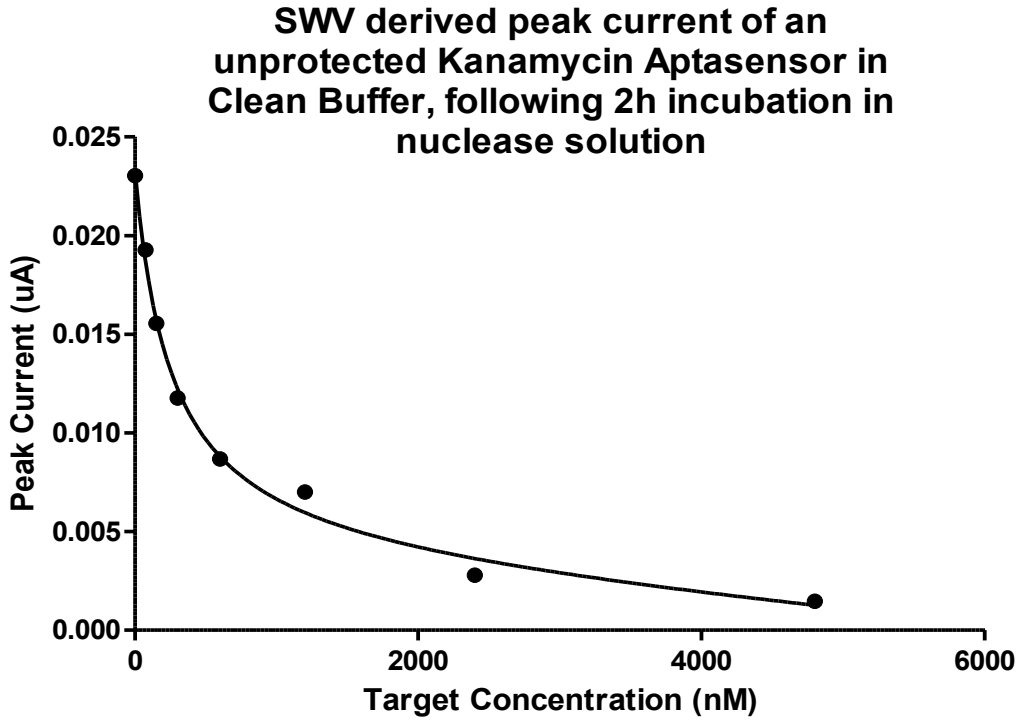

Fig C.16 SWV derived peak current response of unprotected kanamycin Fcn-aptamer biosensor to kanamycin titration vs Ag/AgCl, performed in clean buffer following 2h incubation in nuclease solution replicate 4 191214El4

Appendix D: Replicate Results of SWV of kanamycin fcn-aptamer biosensor's response to negative control titration vs Ag/AgCl

Replicate 1 the Streptomycin and replicate 1 of the Gentamicin titration can be found in the main body of the text.

Target Concentration (nM)	0608 E1	0608 E2	1208 El1
0	0.058609	0.048495	0.062134
75	0.055837	0.075639	0.066327
300	0.057481	0.07534	0.067331
1200	0.054075	0.069305	0.064964
4800	0.053971	0.065464	0.059709
9600	0.057078	0.054443	0.061515

Target Concentration (nM)	2409El1	2409El2
0	0.011525	0.034892
75	0.014261	0.031072
150	0.016936	0.034686
300	0.015058	0.034791
1000	0.014408	0.034256

Table D.1 Summary of kanamycin fcn-aptamer biosensor's response to negative control titration vs Ag/AgCl

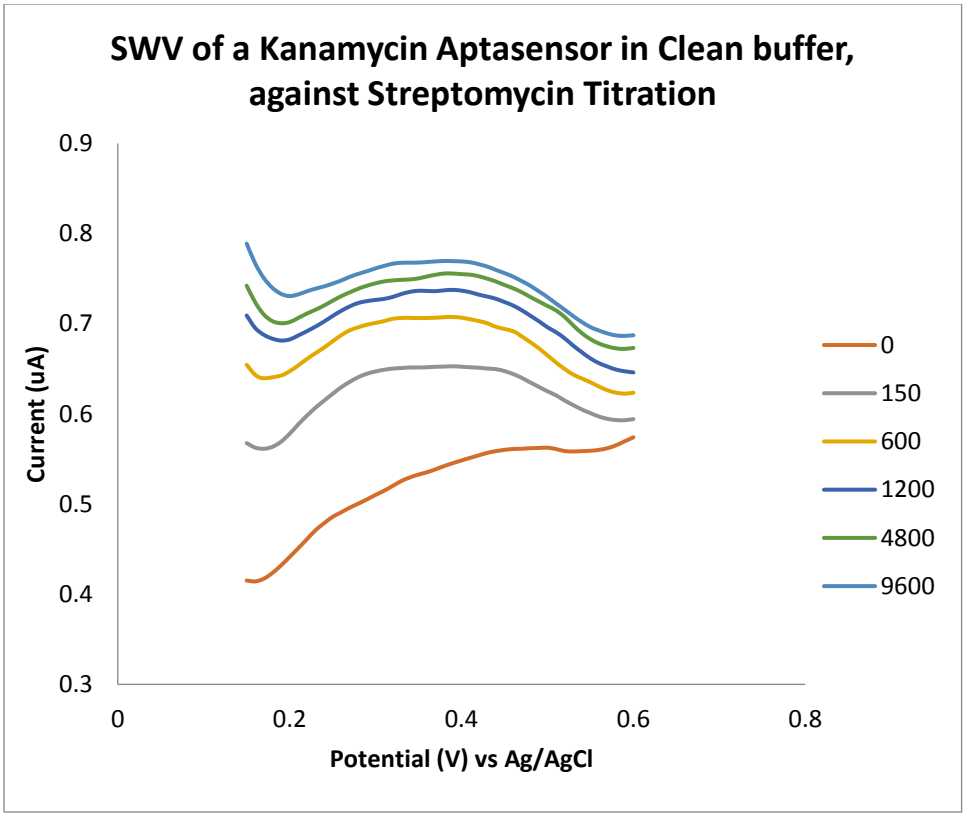

Fig D.1 SWV of kanamycin fcn-aptamer biosensor's response to Streptomycin titration vs Ag/AgCl, replicate 2 060814El2

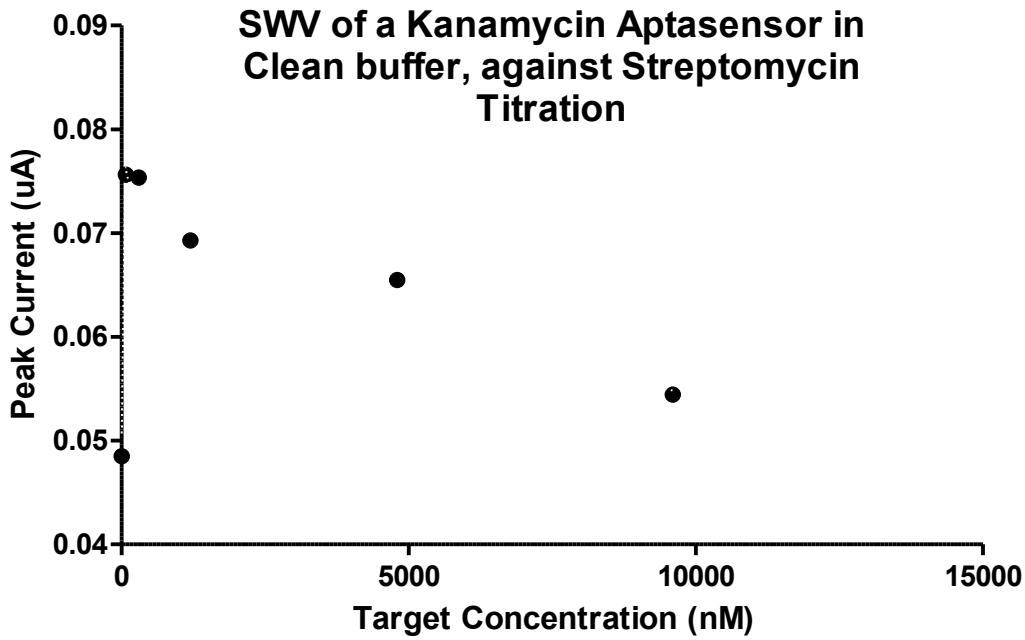

Fig D.2 SWV derived peak current response of kanamycin Fcn-aptamer biosensor to Streptomycin titration vs Ag/AgCl, replicate 2 060814El2

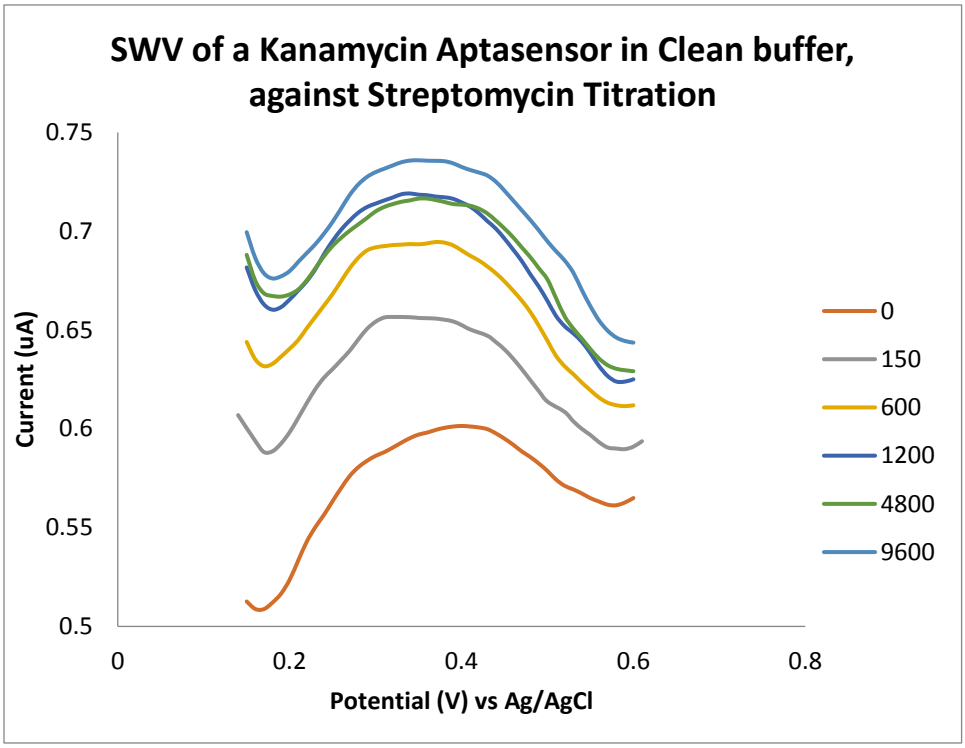

Fig D.3 SWV of kanamycin fcn-aptamer biosensor's response to Streptomycin titration vs Ag/AgCl, replicate 2 120814El1

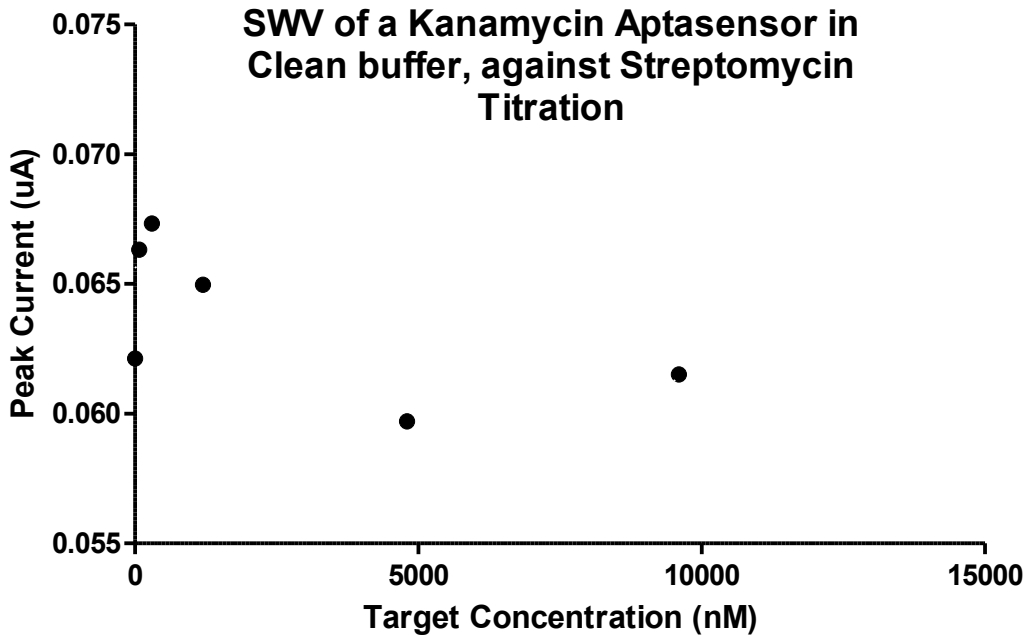

Fig D.4 SWV derived peak current response of kanamycin Fcn-aptamer biosensor to Streptomycin titration vs Ag/AgCl, replicate 2 120814El1

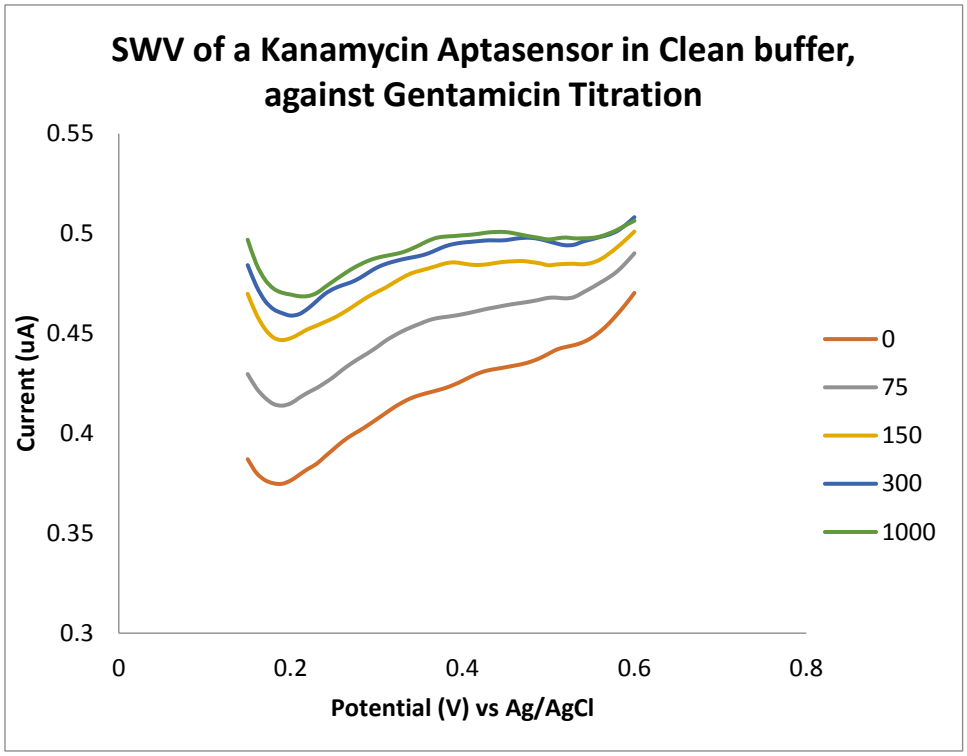

Fig D.5 SWV of kanamycin fcn-aptamer biosensor's response to Gentamicin titration vs Ag/AgCl, replicate 2 120814El1

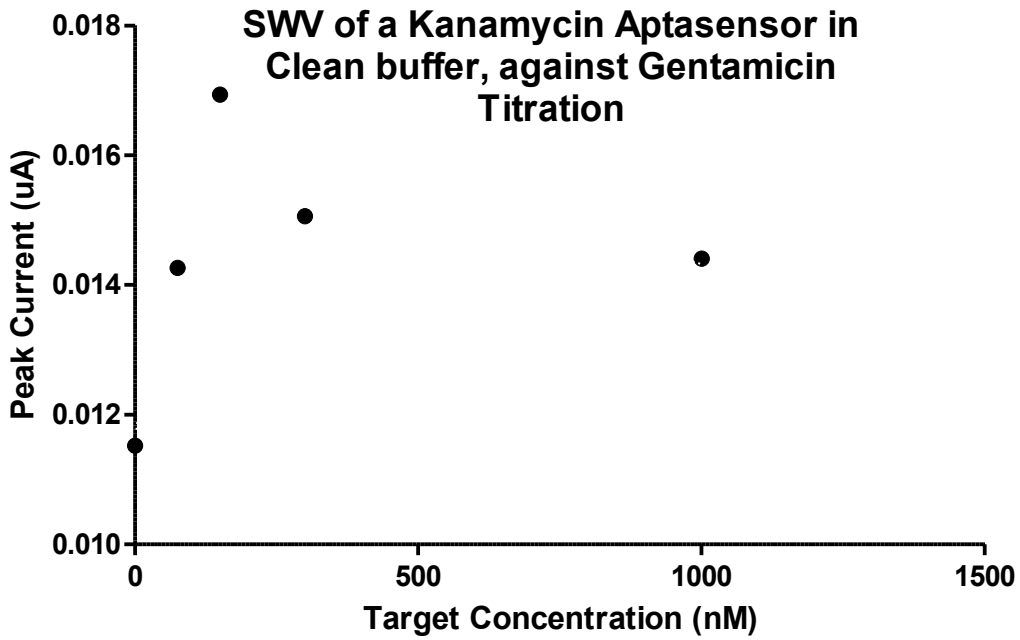

Fig D.6 SWV derived peak current response of kanamycin Fcn-aptamer biosensor to Gentamicin titration vs Ag/AgCl, replicate 2 120814El1

Appendix E: Replicate Results of SWV of tetracycline fcn-aptamer biosensor's response to tetracycline titration vs Ag/AgCl, performed in clean buffer.

Replicate 2 of this series of titration can be found in the main body of the text.

Target Concentration (nM)	180714 E2	300714	040814 E1	040814 E2	050814
0	0.007178	0.021718	0.041409	0.063193	0.053365
4	0.013424	0.044194	0.063381	0.104269	0.081326
8	0.011966	0.05468	0.080107	0.116517	0.091782
16	0.019599	0.059445	0.086778	0.125778	0.096692
32	0.023717	0.065976	0.092279	0.129973	0.10313
64	0.024779	0.06368	0.095375	0.127436	0.107315
128	0.028908	0.060644	0.097772	0.137467	0.113035
Best-fit values					
Bmax	0.02284	0.05335	0.06212	0.06946	0.05237
Kd	16.89	5.053	5.721	2.553	3.404
NS	8.53E-06	-9.9E-05	-2.4E-05	3.58E-05	6.78E-05
Background	0.007345	0.02164	0.04093	0.06306	0.05333
Goodness of Fit					
Degrees of Freedom	3	3	3	3	3
R square	0.9613	0.9956	0.9916	0.991	0.9989
Absolute Sum of Squares	1.44E-05	6.33E-06	2.11E-05	3.43E-05	2.61E-06
Sy.x	0.002192	0.001452	0.002651	0.003382	0.000933

Table E.1 Summary of tetracycline fcn-aptamer biosensor's response to tetracycline titration vs Ag/AgCl, performed in clean buffer.

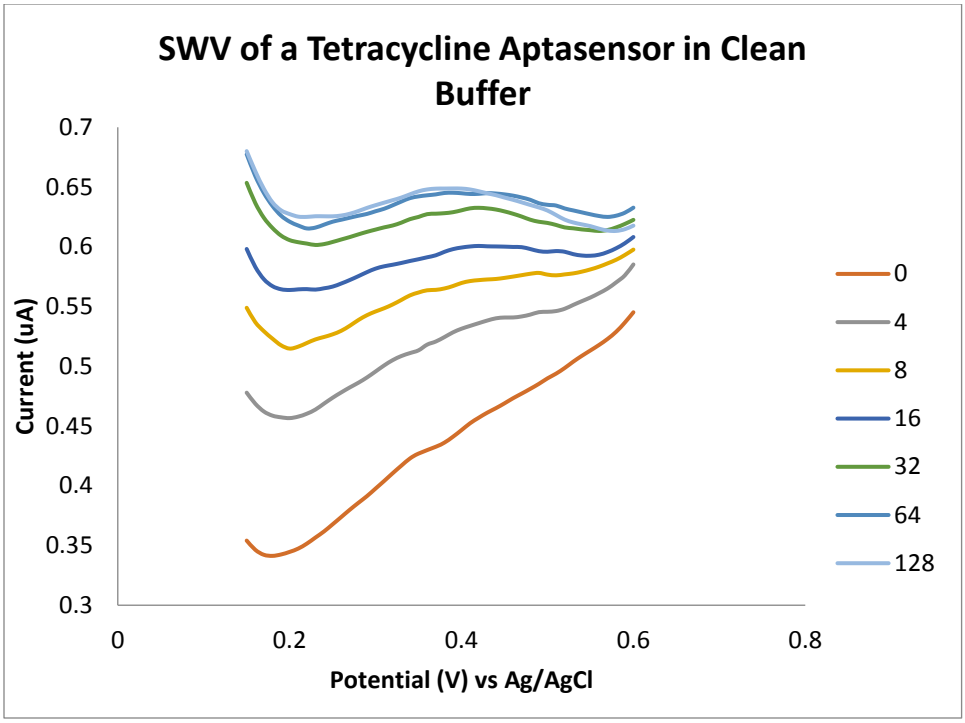

Fig E.1 SWV of tetracycline fcn-aptamer biosensor's response to tetracycline titration vs Ag/AgCl, performed in clean buffer, replicate 1 180714El2

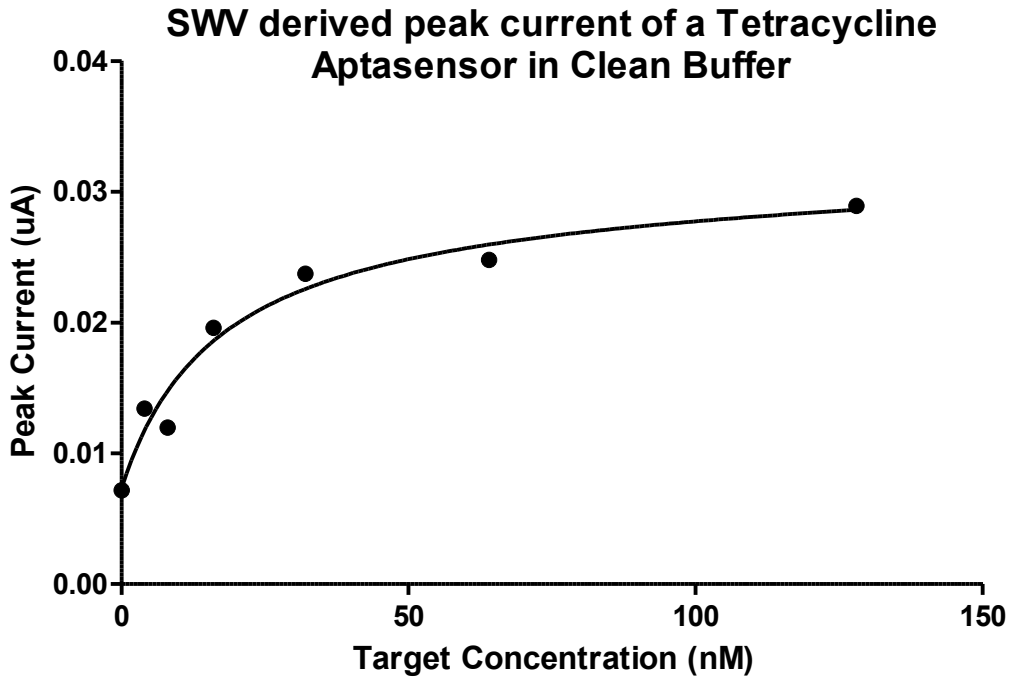

Fig E.2 SWV derived peak current response of tetracycline Fcn-aptamer biosensor to tetracycline titration vs Ag/AgCl, performed in clean buffer, replicate 1 180714El2

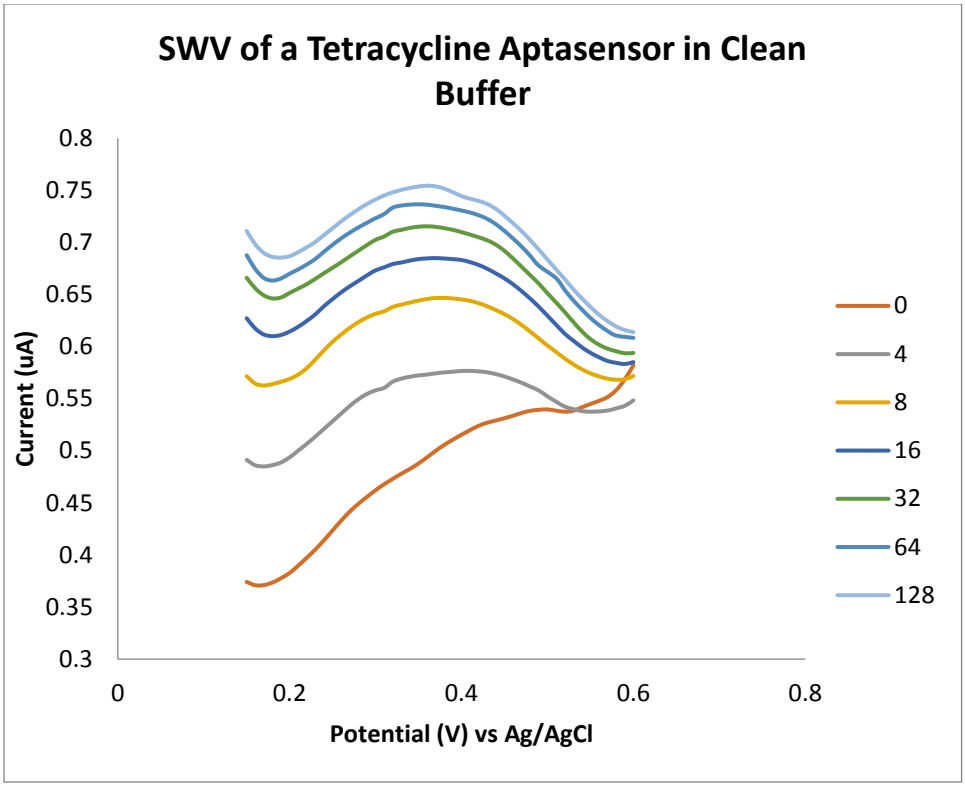

Fig E.3 SWV of tetracycline fcn-aptamer biosensor's response to tetracycline titration vs Ag/AgCl, performed in clean buffer, replicate 3 040814El1

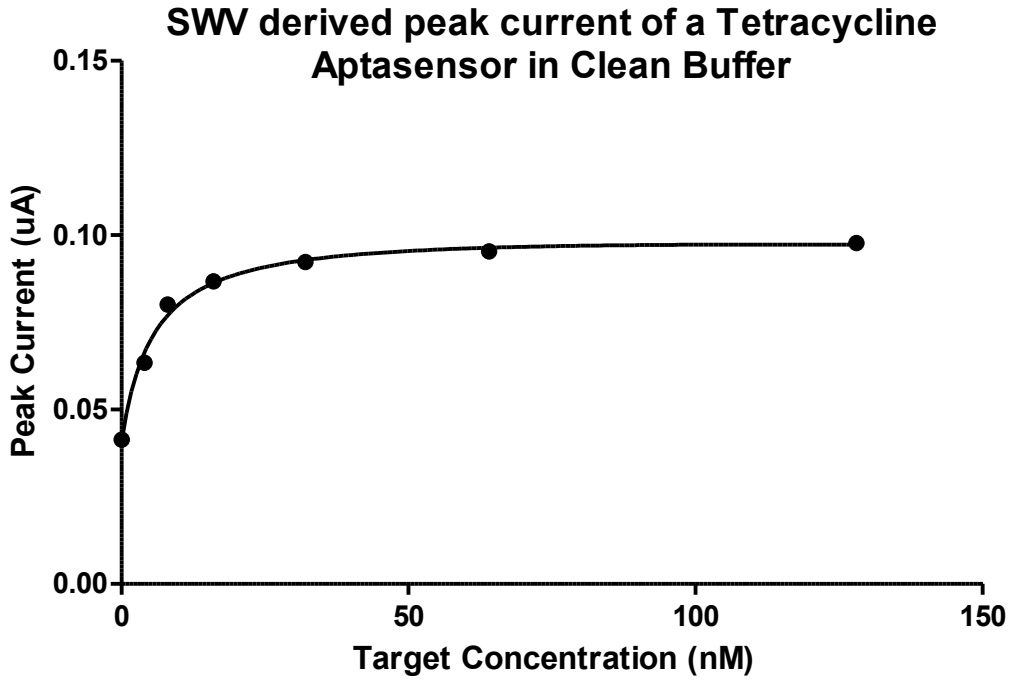

Fig E.4 SWV derived peak current response of tetracycline Fcn-aptamer biosensor to tetracycline titration vs Ag/AgCl, performed in clean buffer, replicate 3 040814El1

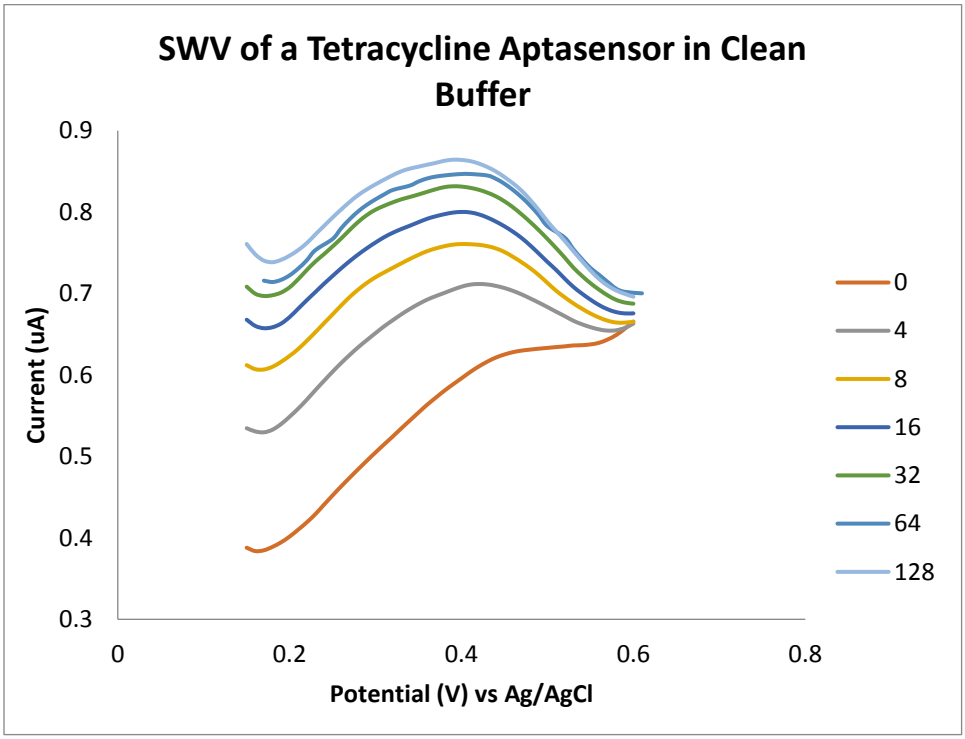

Fig E.5 SWV of tetracycline fcn-aptamer biosensor's response to tetracycline titration vs Ag/AgCl, performed in clean buffer, replicate 4 040814El2

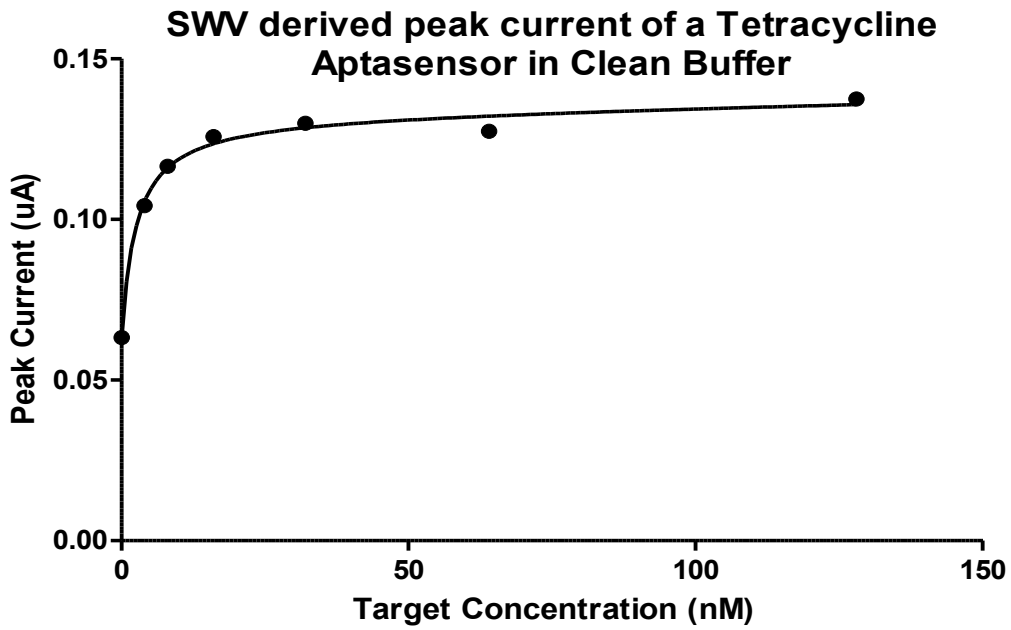

Fig E.6 SWV derived peak current response of tetracycline Fcn-aptamer biosensor to tetracycline titration vs Ag/AgCl, performed in clean buffer, replicate 4 040814El2

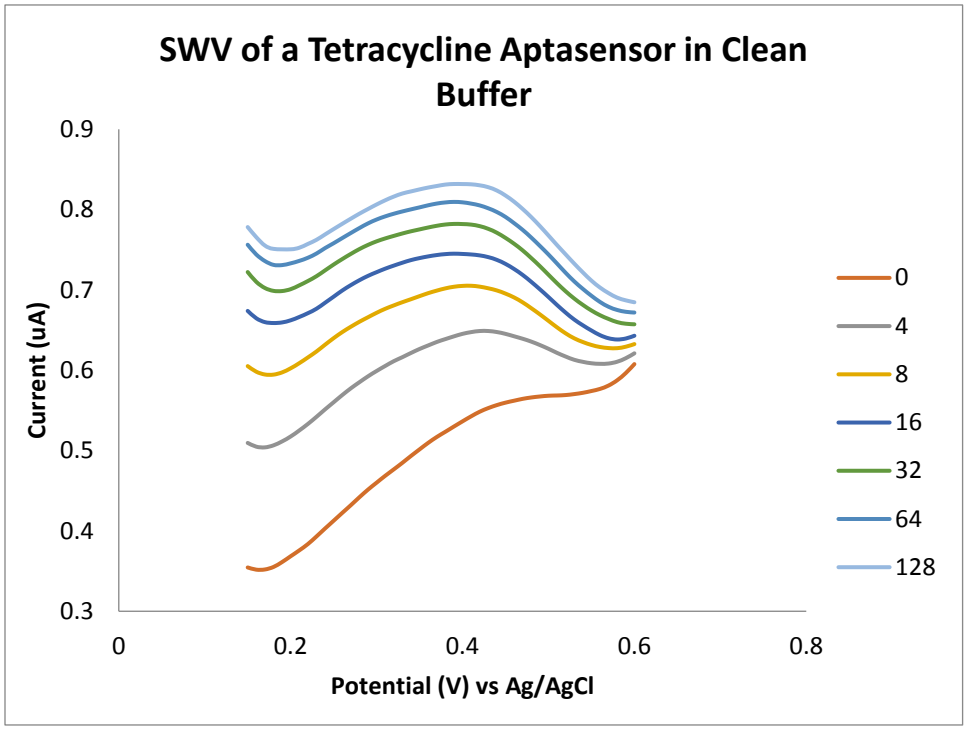

Fig E.7 SWV of tetracycline fcn-aptamer biosensor's response to tetracycline titration vs Ag/AgCl, performed in clean buffer, replicate 5 050814

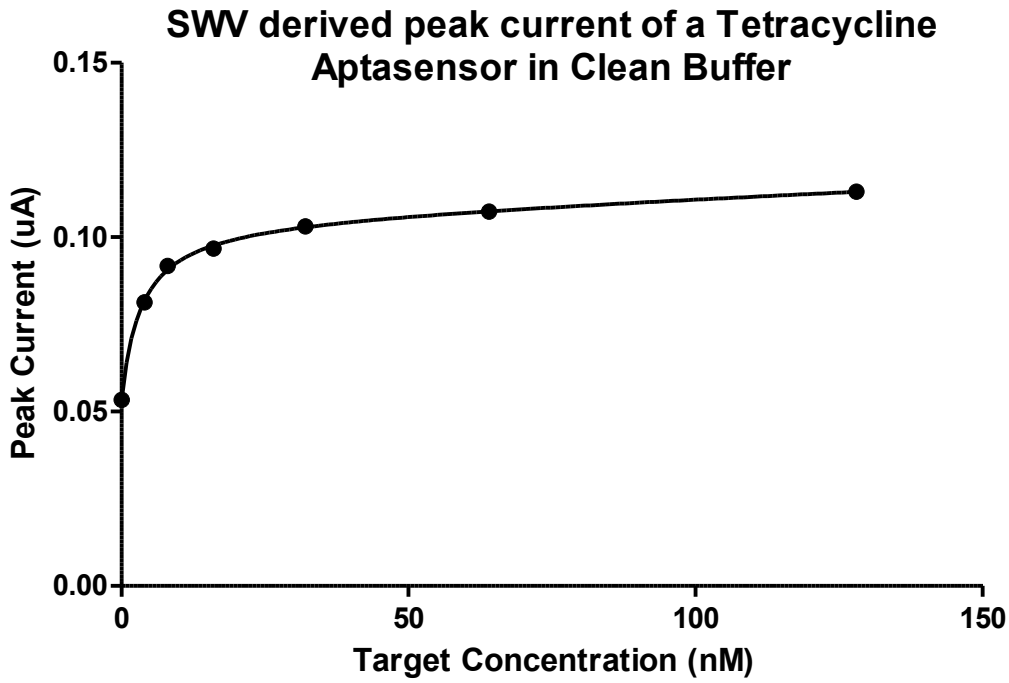

Fig E.8 SWV derived peak current response of tetracycline Fcn-aptamer biosensor to tetracycline titration vs Ag/AgCl, performed in clean buffer, replicate 5 050814

Appendix F: Replicate Results of SWV of tetracycline fcn-aptamer biosensor's response to tetracycline titration vs Ag/AgCl, performed in soil sample matrix.

Replicate 4 of this series of titration can be found in the main body of the text.

Target Concentration (nM)	3107 EI1	3107 EI2	1109 EI1	1109 EI2
0	0.073005	0.08922	0.091762	0.079315
4	0.087003	0.11574	0.112105	0.103628
8	0.087117	0.149825	0.123423	0.112893
16	0.090669	0.160661	0.127574	0.12365
32	0.094324	0.166797	0.132966	0.130682
64	0.089485	0.165029	0.137831	0.138354
128	0.086557	0.158061	0.13978	0.135245
Best-fit values				
Bmax	0.02354	0.1098	0.04758	0.0675
Kd	3.389	7.407	4.852	7.788
NS	-7.6E-05	-0.00027	1.93E-05	-5.8E-05
Background	0.07313	0.08736	0.09165	0.07967
Goodness of Fit				
Degrees of Freedom	3	3	3	3
R square	0.9513	0.9687	0.9959	0.9963
Absolute Sum of Squares	1.31E-05	0.000165	7.01E-06	9.62E-06
Sy.x	0.00209	0.007418	0.001528	0.001791

Table F.1 Summary of tetracycline fcn-aptamer biosensor's response to tetracycline titration vs Ag/AgCl, performed in soil sample matrix.

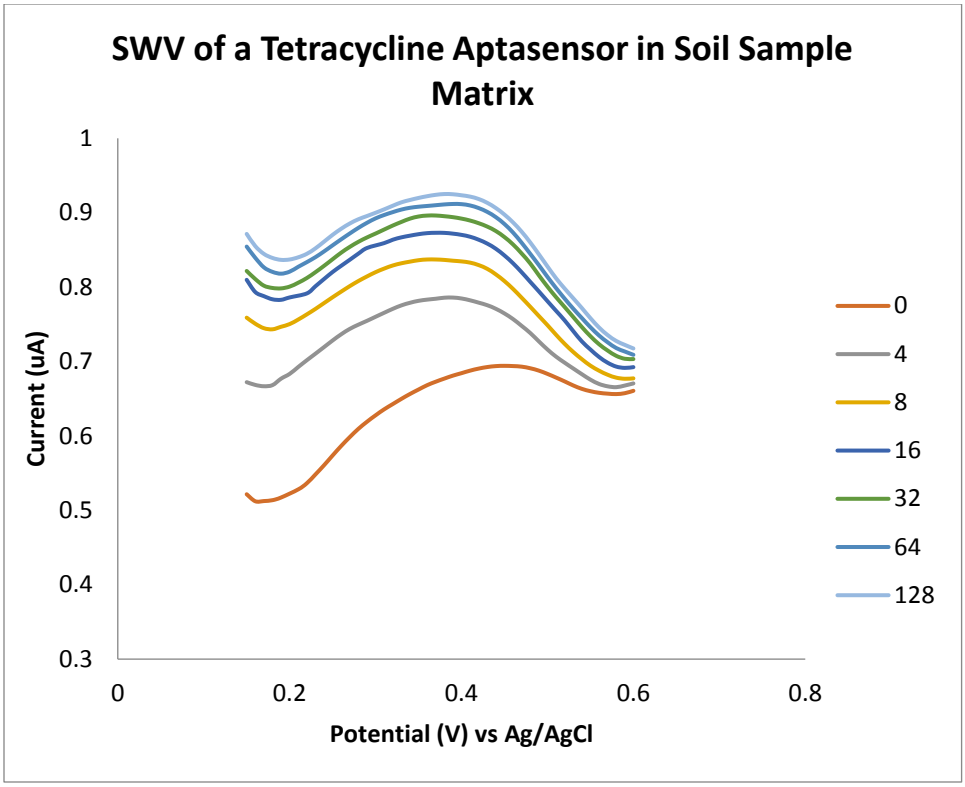

Fig F.1 SWV of tetracycline fcn-aptamer biosensor's response to tetracycline titration vs Ag/AgCl, performed in soil sample matrix, replicate 1 310714El1

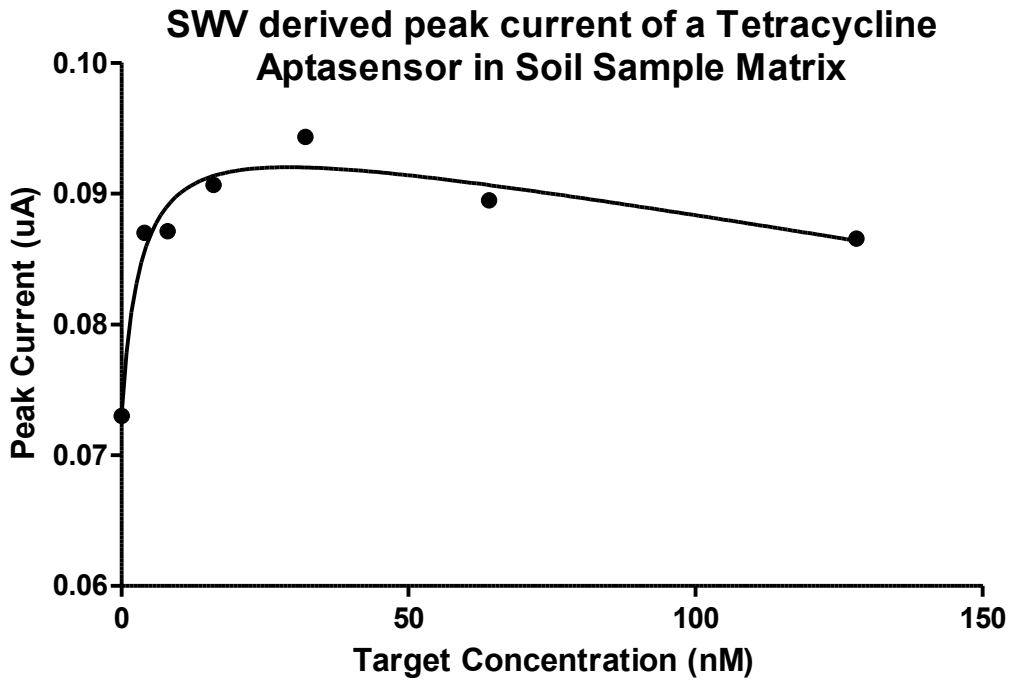

Fig F.2 SWV derived peak current response of tetracycline Fcn-aptamer biosensor to tetracycline titration vs Ag/AgCl, performed in soil sample matrix, replicate 1 310714El1

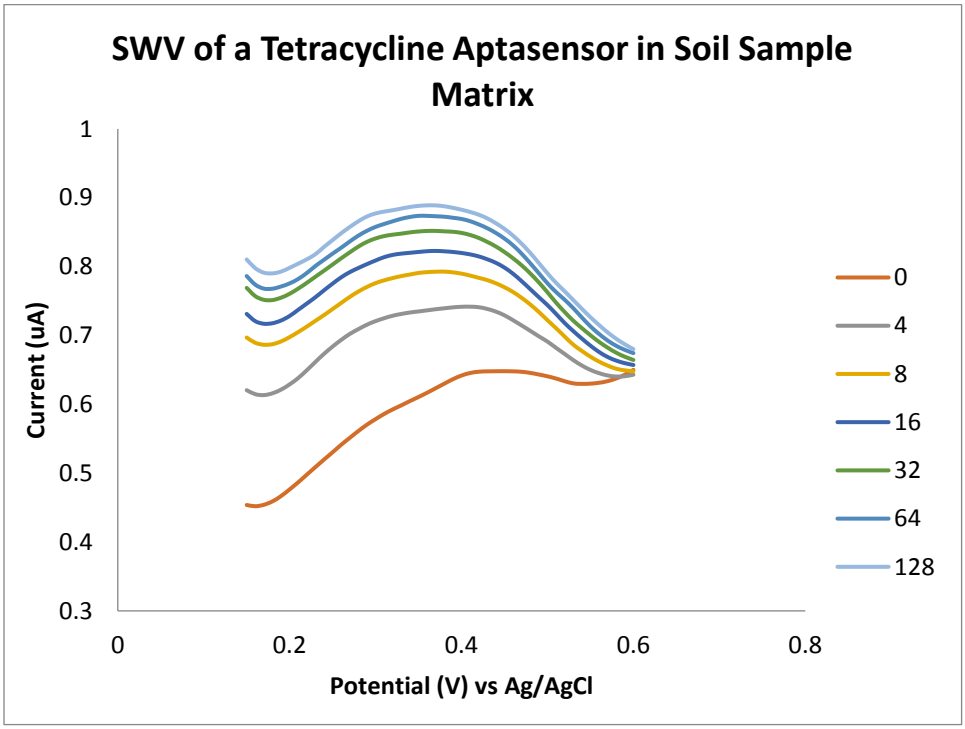

Fig F.3 SWV of tetracycline fcn-aptamer biosensor's response to tetracycline titration vs Ag/AgCl, performed in soil sample matrix, replicate 2 310714El2

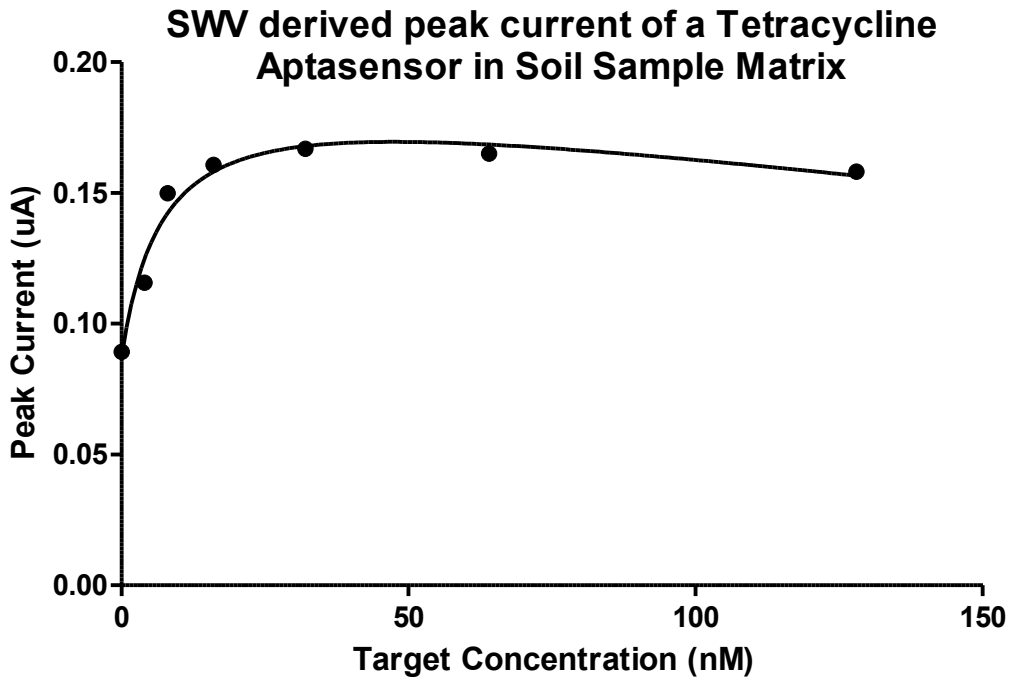

Fig F.4 SWV derived peak current response of tetracycline Fcn-aptamer biosensor to tetracycline titration vs Ag/AgCl, performed in soil sample matrix, replicate 2 310714El2

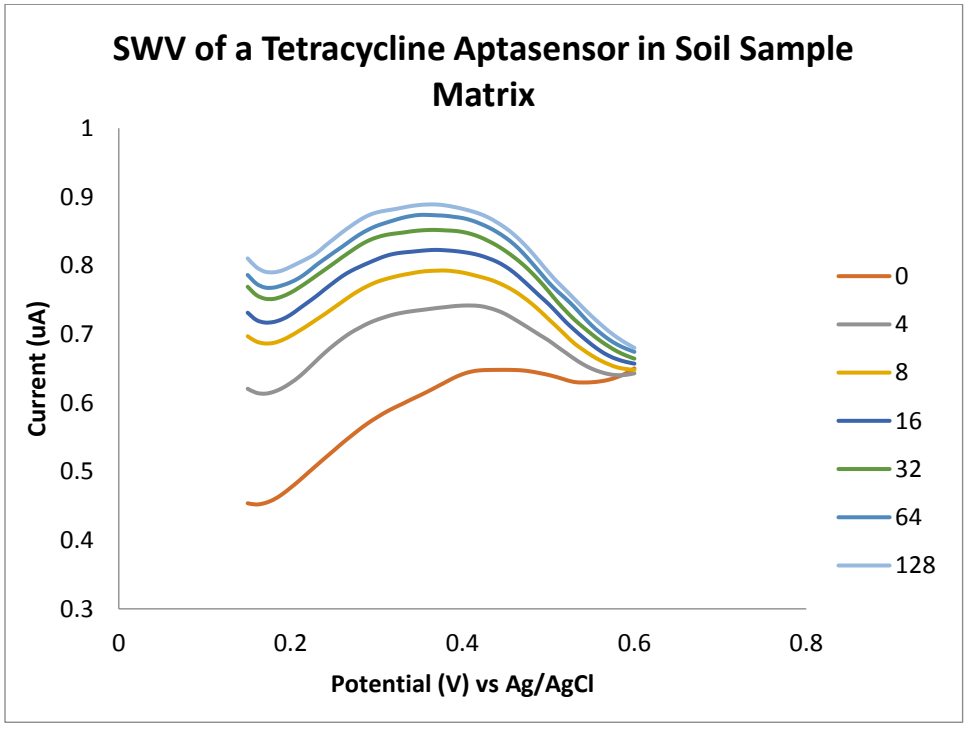

Fig F.5 SWV of tetracycline fcn-aptamer biosensor's response to tetracycline titration vs Ag/AgCl, performed in soil sample matrix, replicate 3 110914El1

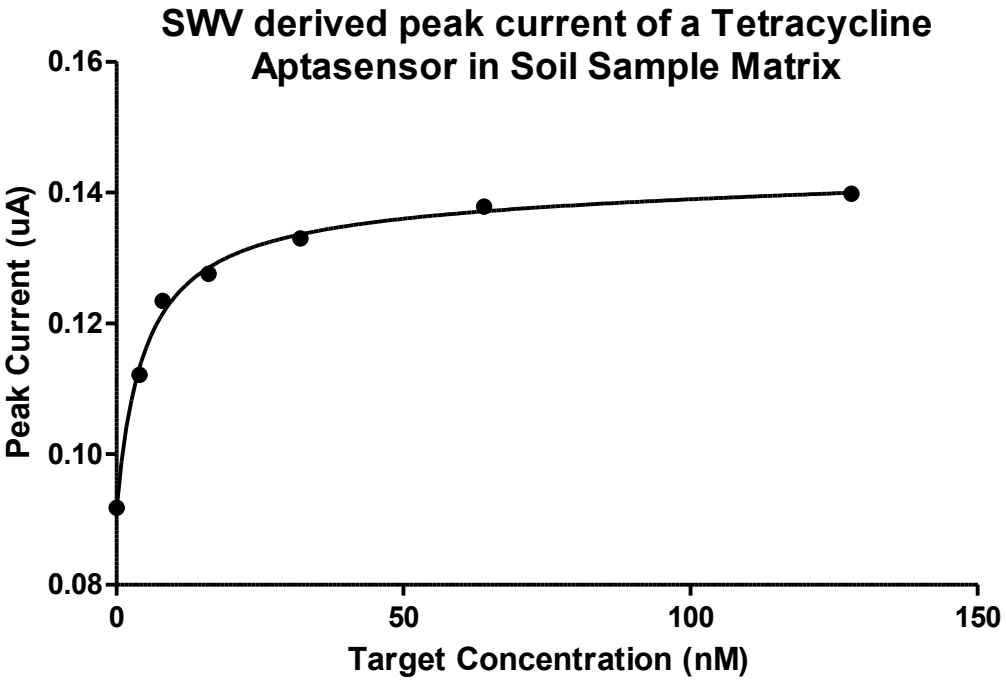

Fig F.6 SWV derived peak current response of tetracycline Fcn-aptamer biosensor to tetracycline titration vs Ag/AgCl, performed in soil sample matrix, replicate 3 110914El1

Appendix G: Replicate Results of SWV of tetracycline fcn-aptamer biosensor's response to erythromycin negative control titration vs Ag/AgCl

Replicate 2 of the erythromycin titration can be found in the main body of the text.

Target Concentration (nM)	061014 EI3	061014 EI4	161014 EI3
0	0.073005	0.08922	0.091762
8	0.087003	0.11574	0.112105
32	0.087117	0.149825	0.123423
128	0.090669	0.160661	0.127574
512	0.094324	0.166797	0.132966
1024	0.089485	0.165029	0.137831

Table G.1 Summary of tetracycline fcn-aptamer biosensor's response to erythromycin negative control titration vs Ag/AgCl

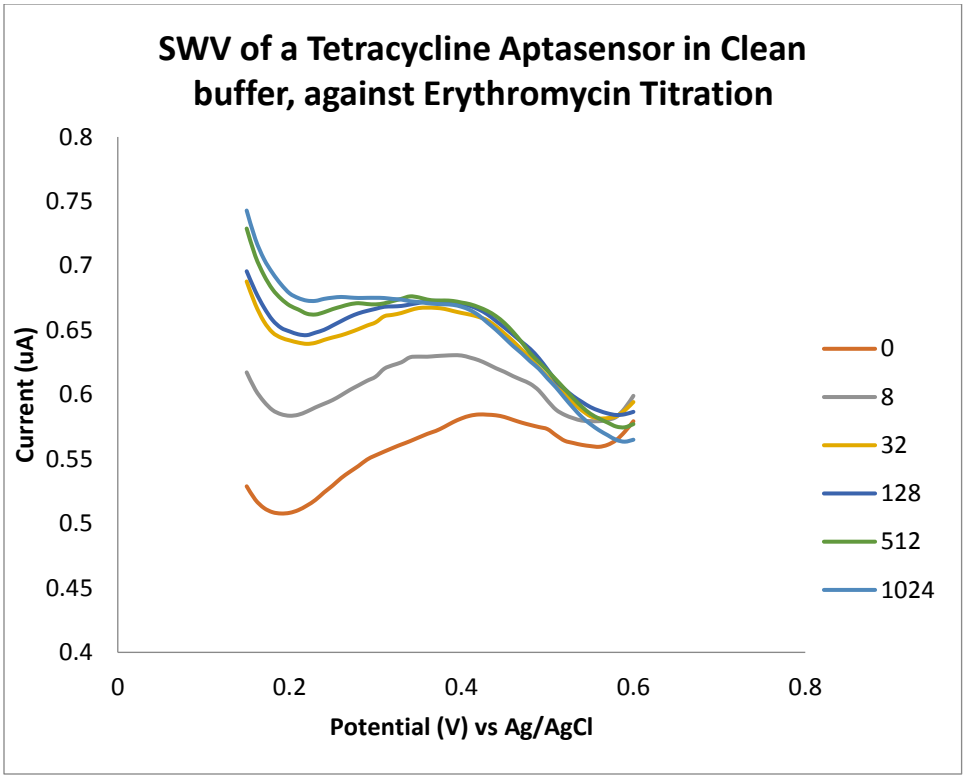

Fig G.1 SWV of tetracycline fcn-aptamer biosensor's response to erythromycin titration vs Ag/AgCl, performed in clean buffer, replicate 1 061014El3

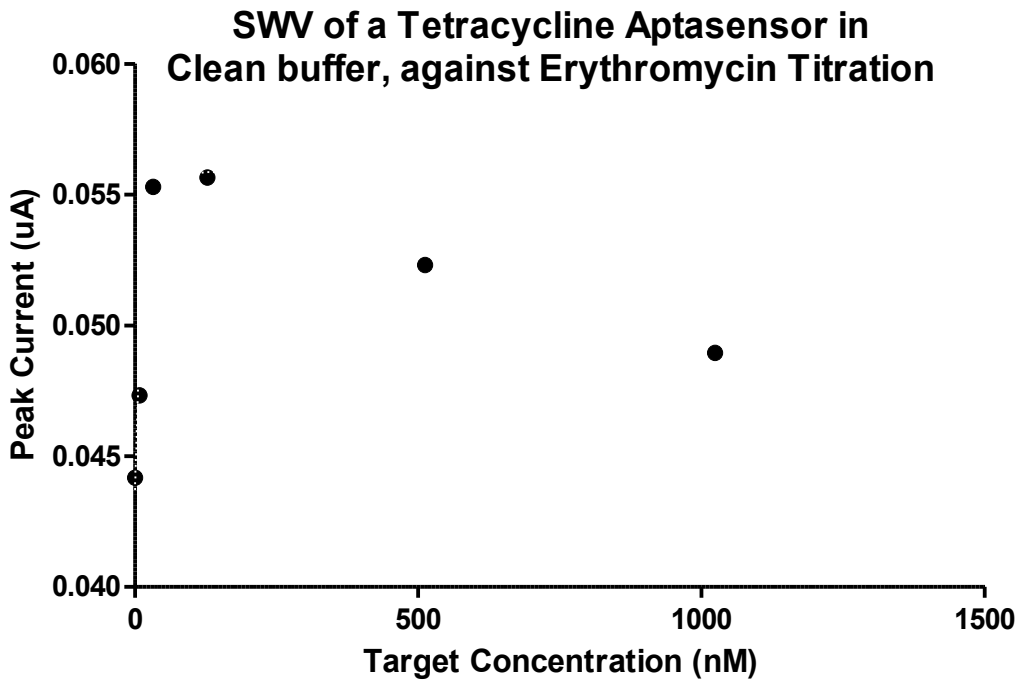

Fig G.2 SWV derived peak current response of tetracycline Fcn-aptamer biosensor to erythromycin titration vs Ag/AgCl, performed in clean buffer, replicate 1 061014El3

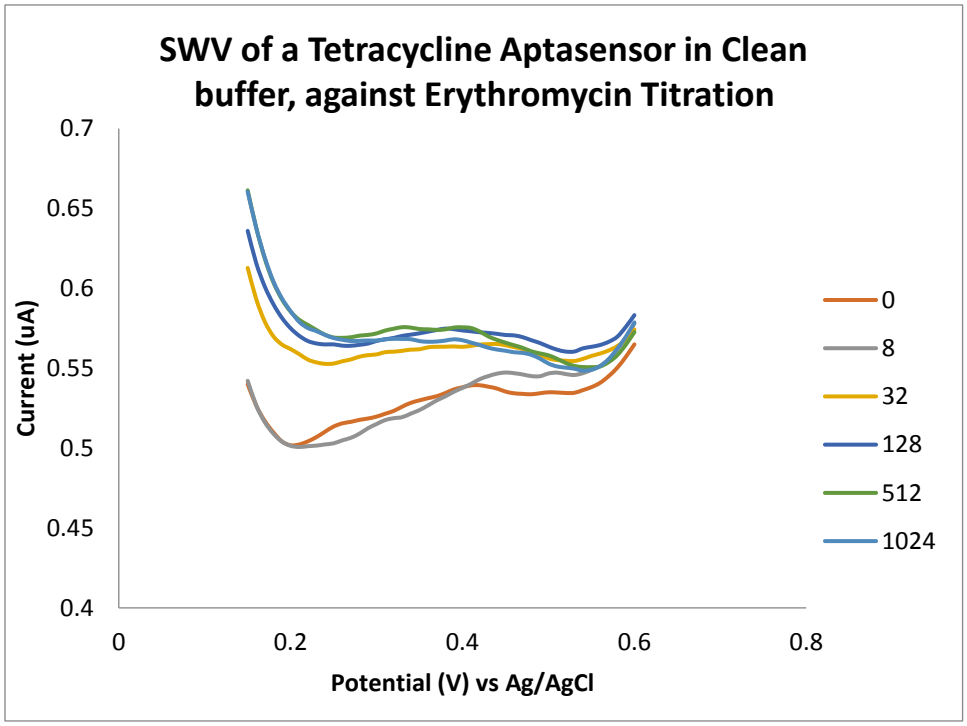

Fig G.3 SWV of tetracycline fcn-aptamer biosensor's response to erythromycin titration vs Ag/AgCl, performed in clean buffer, replicate 3 161014El3

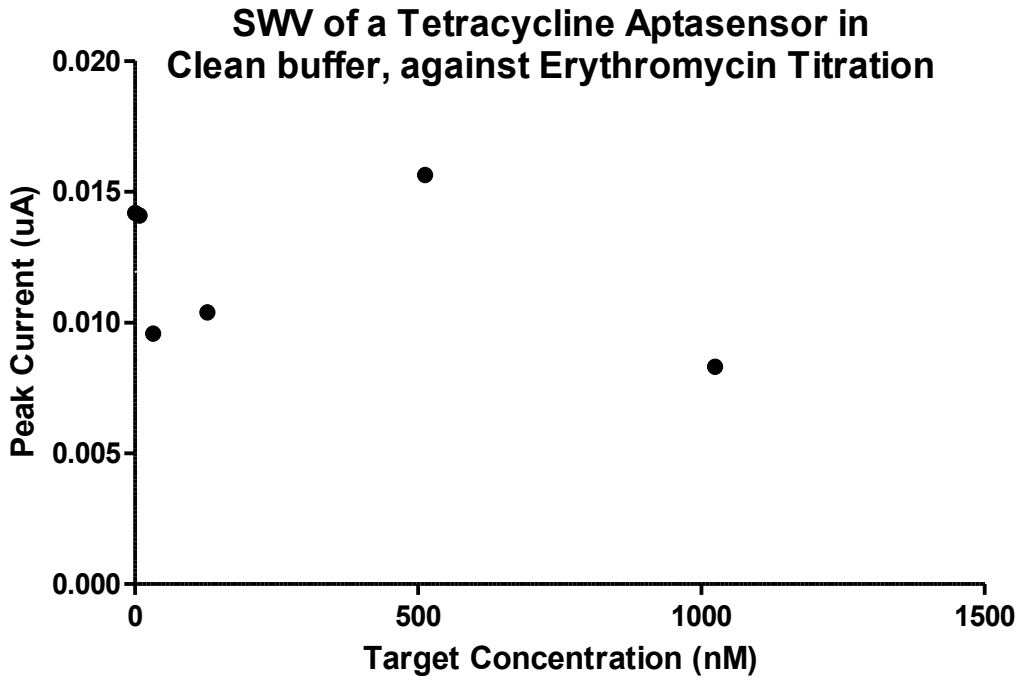

Fig G.4 SWV derived peak current response of tetracycline Fcn-aptamer biosensor to erythromycin titration vs Ag/AgCl, performed in clean buffer, replicate 3 161014El3

Appendix H: Replicate Results of SWV of automated kanamycin and tetracycline fcn-aptamer biosensor's response to multi-target titration vs Ag/AgCl, performed in clean buffer in multi target assay

Test 5 and 8 can be found in the main body of the text.

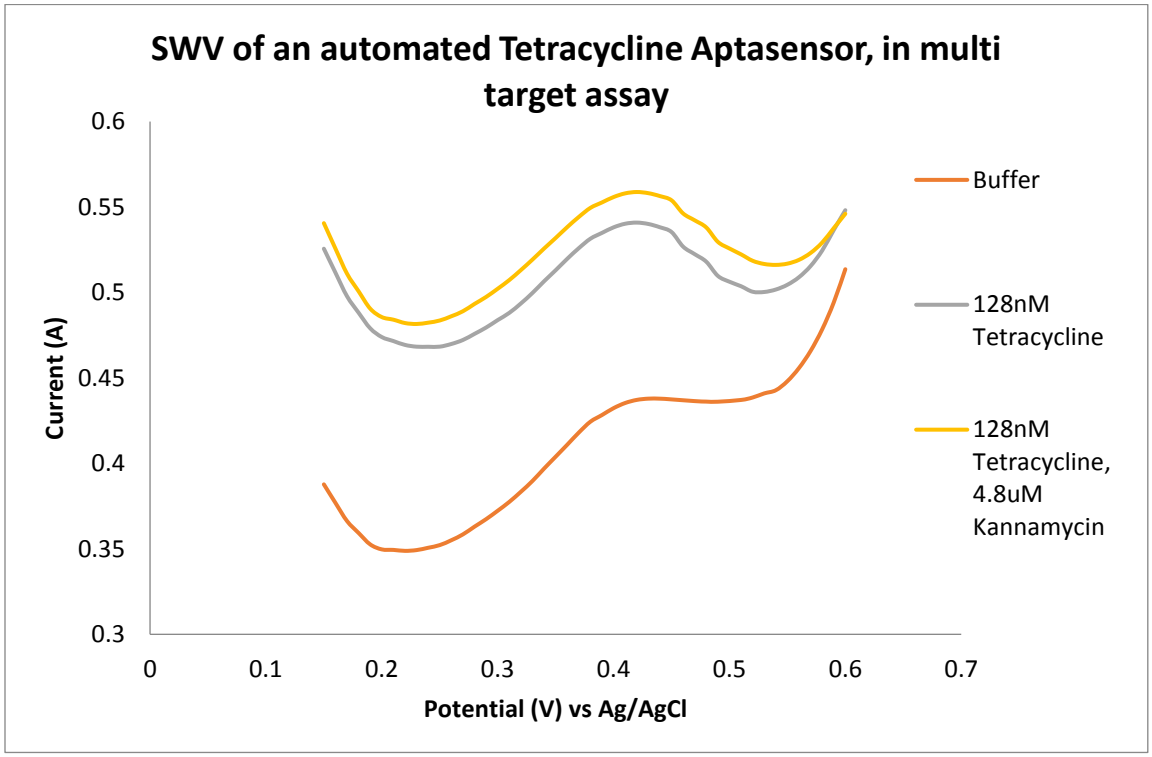

Fig H.1 SWV of an automated Tetracycline Aptasensor, in multi target assay, replicate 1 (Test 3) 281014ElT2

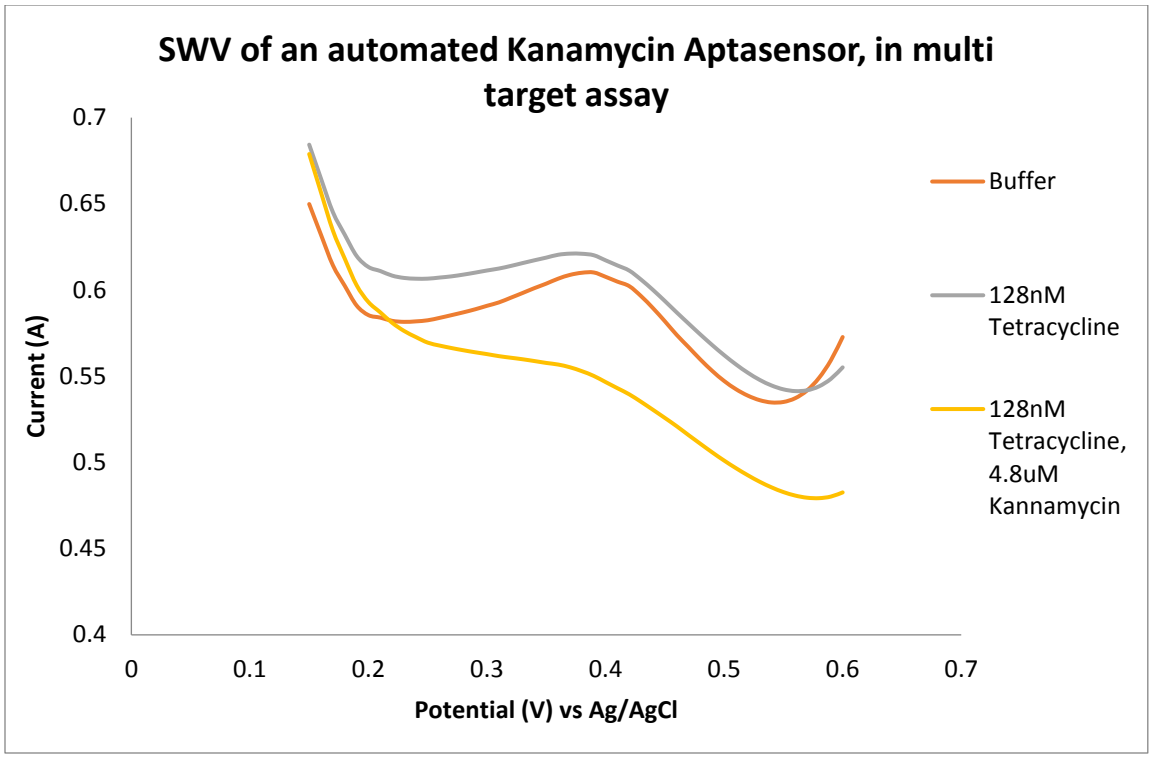

Fig H.2 SWV of an automated Kanamycin Aptasensor, in multi target assay, replicate 1 (Test 3) 281014ElK2

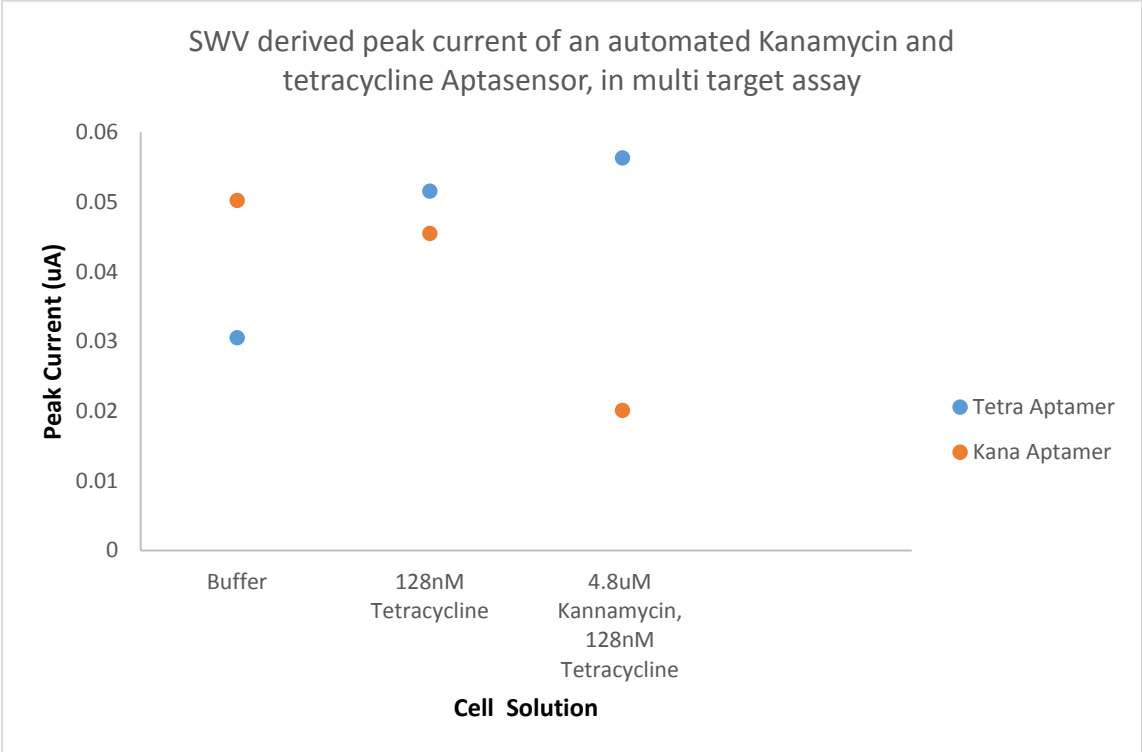

Fig H.3 SWV derived peak current of an automated Kanamycin and tetracycline Aptasensor, in multi target assay, replicate 1 (Test 3)

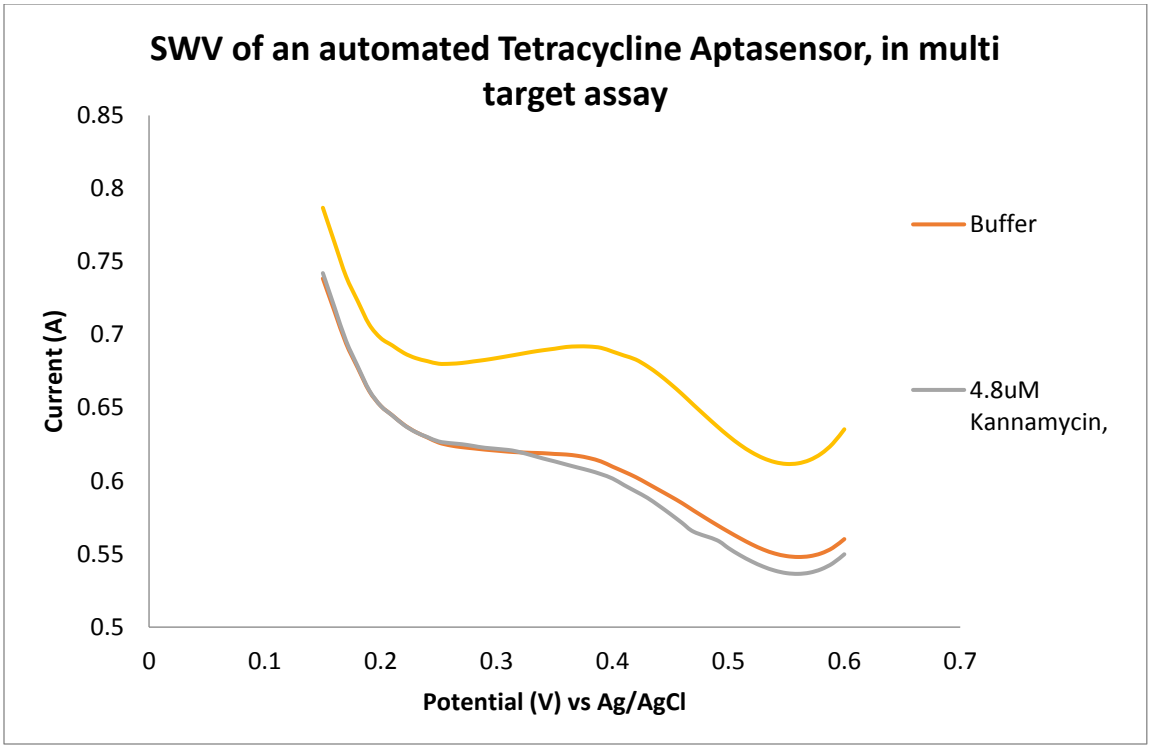

Fig H.4 SWV of an automated Tetracycline Aptasensor, in multi target assay, replicate 3 (Test 8) 281014ElK2

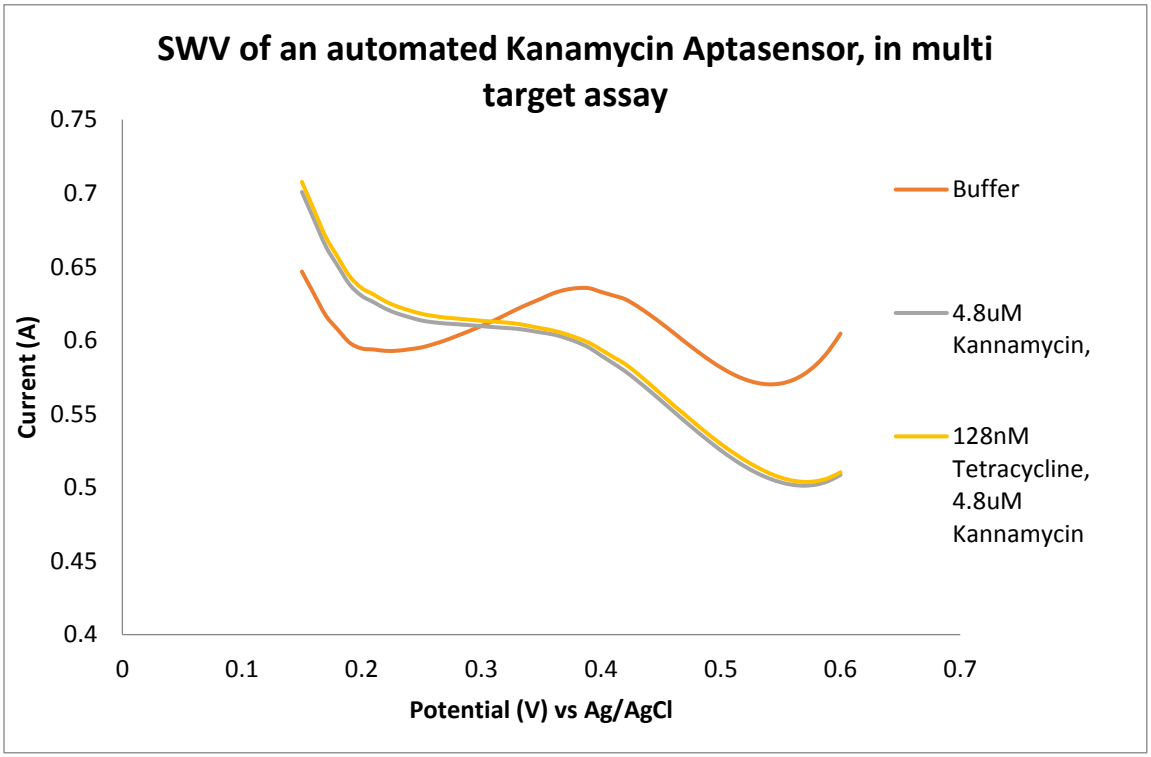

Fig H.5 SWV of an automated Kanamycin Aptasensor, in multi target assay, replicate 3 (Test 8) 061114ElK1

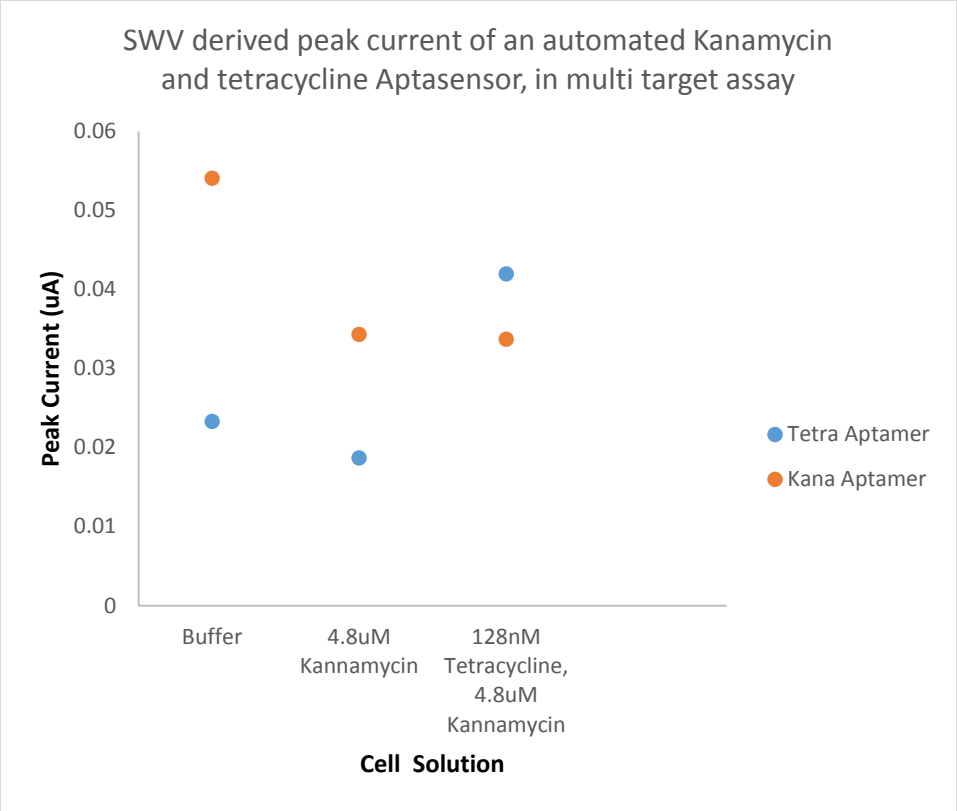

Fig H.6 SWV derived peak current of an automated Kanamycin and tetracycline Aptasensor, in multi target assay, replicate 3 (Test 8)

Appendix I: SWV of Thrombin fcn-aptamer biosensor with sandwich configuration (IAELAB)'s response to Thrombin titration vs Ag/AgCl

Replicate 3 of this series of titration can be found in the main body of the text.

Target Concentration (nM)	010514	250414	300414	140514	150514	150714
0	0.0000	0.0000	0.0000	0.0000	0.0000	0.0000
75	0.1222	0.0950	0.1481			0.2595
150	0.2062	0.2564	0.2905	0.2968	0.3867	0.3608
300	0.3901	0.5330	0.4153	0.5191	0.8125	0.5402
600	0.6801	0.4015	0.3132	0.7371	0.9319	0.8231
1200	0.8286	0.6236	0.5751	0.8117	1.1294	0.8335
2400	1.6442	0.7496	0.6719			0.8901
4800	1.1883	1.0082	0.9147	0.9013	1.0606	0.8914
Best-fit values						
Bmax	1.3400	0.5943	0.5485	1.1560	1.6160	1.1030
Kd	660.9000	168.6000	144.2000	354.5000	341.0000	266.9000
NS	0.0000	0.0001	0.0001	0.0000	-0.0001	0.0000
Background	-0.0145	-0.0235	-0.0100	-0.0092	-0.0144	-0.0006
Goodness of Fit						
Degrees of Freedom	3.0000	4.0000	3.0000	2.0000	2.0000	4.0000
R square	0.9956	0.9540	0.9946	0.9937	0.9825	0.9873
Absolute Sum of Squares	0.0049	0.0371	0.0032	0.0037	0.0169	0.0102
Sy.x	0.0403	0.0963	0.0327	0.0433	0.0920	0.0505

Table I.1 Summary of fcn-aptamer biosensor with sandwich configuration (IAELAB)'s response to Thrombin titration vs Ag/AgCl

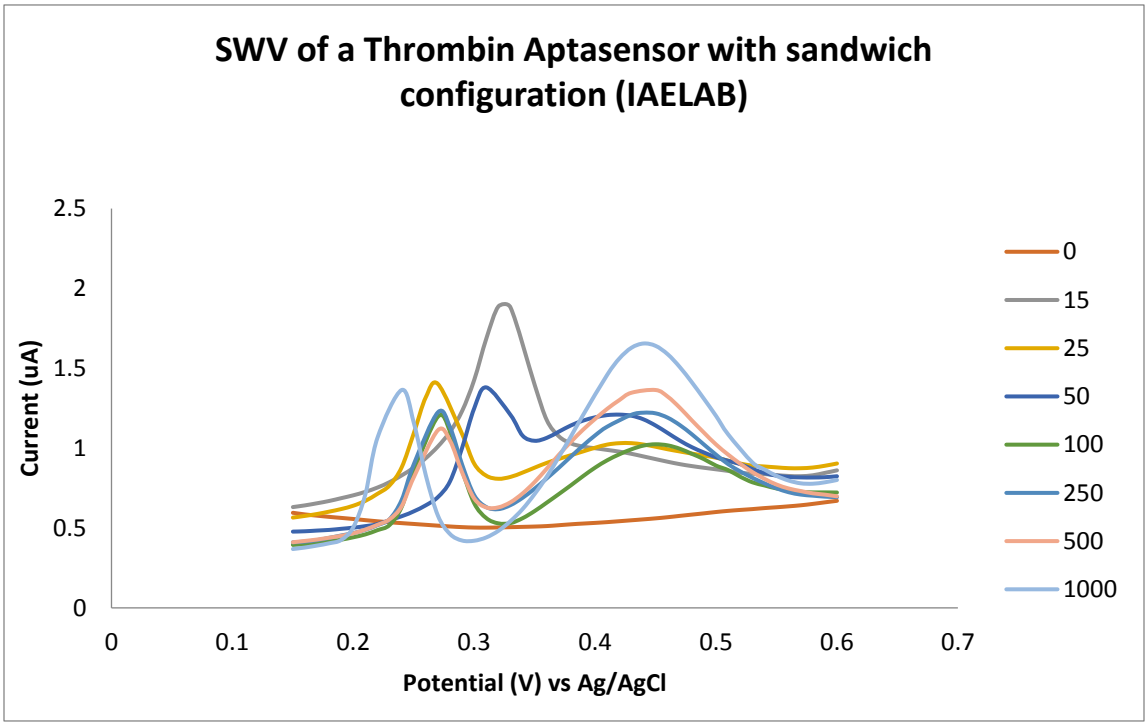

Fig I.1 SWV of Thrombin fcn-aptamer biosensor with sandwich configuration (IAELAB)'s response to Thrombin titration vs Ag/AgCl, replicate 1 250414

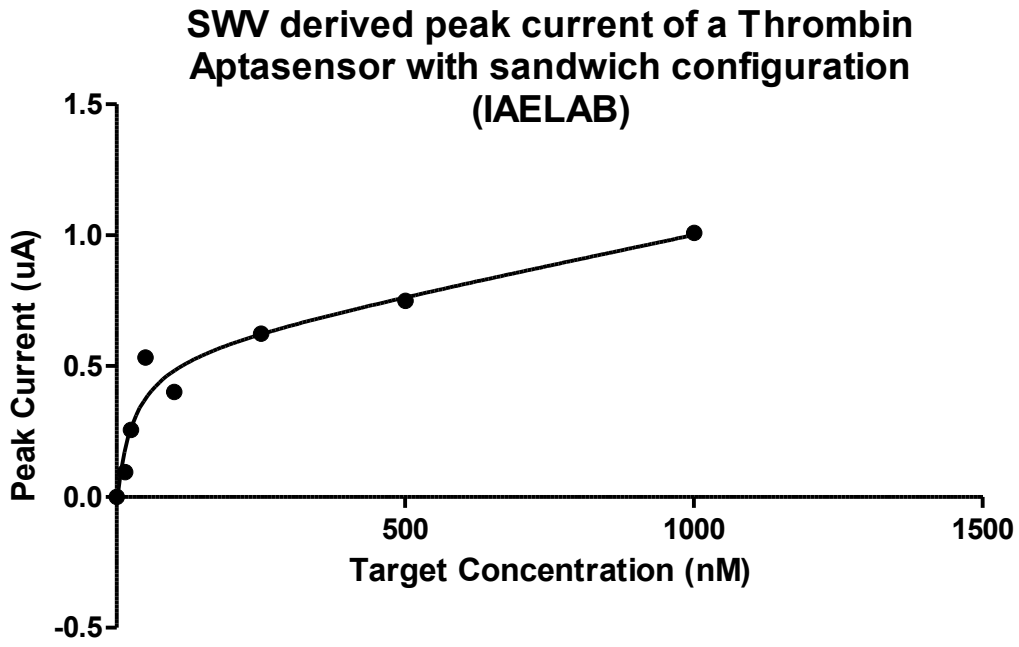

Fig I.2 SWV of Thrombin fcn-aptamer biosensor with sandwich configuration (IAELAB)'s response to Thrombin titration vs Ag/AgCl, replicate 1 250414

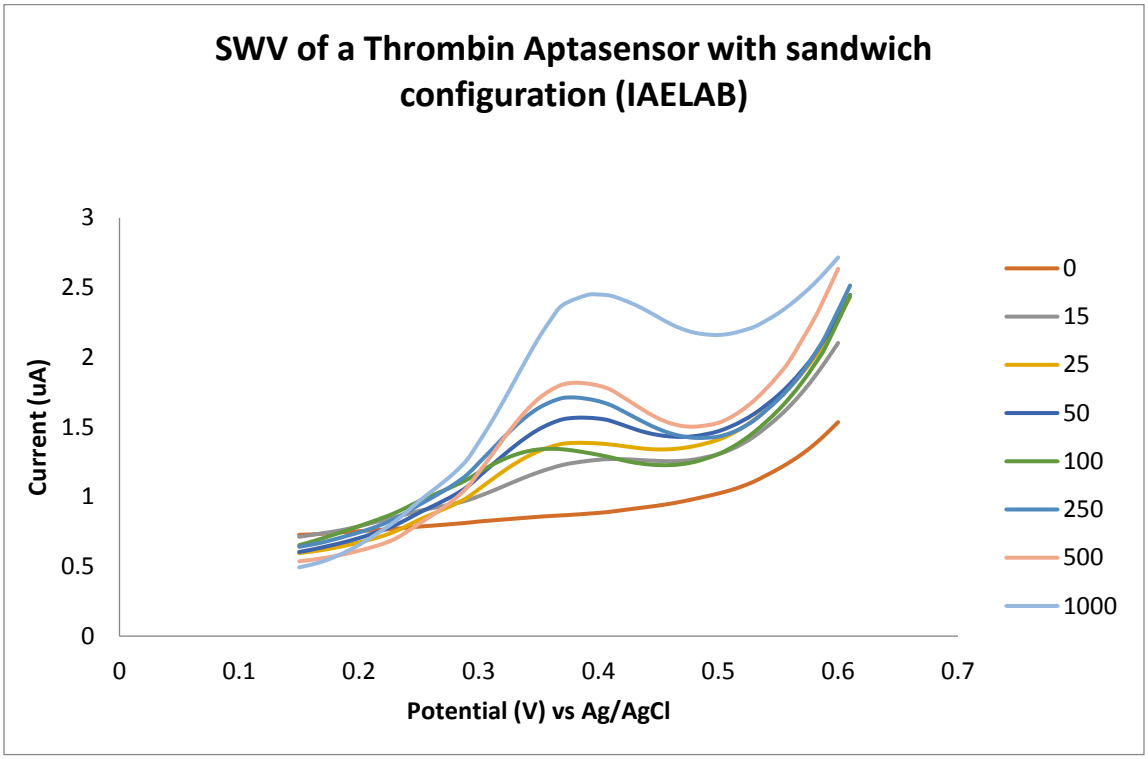

Fig I.3 SWV of Thrombin fcn-aptamer biosensor with sandwich configuration (IAELAB)'s response to Thrombin titration vs Ag/AgCl, replicate 2 300514

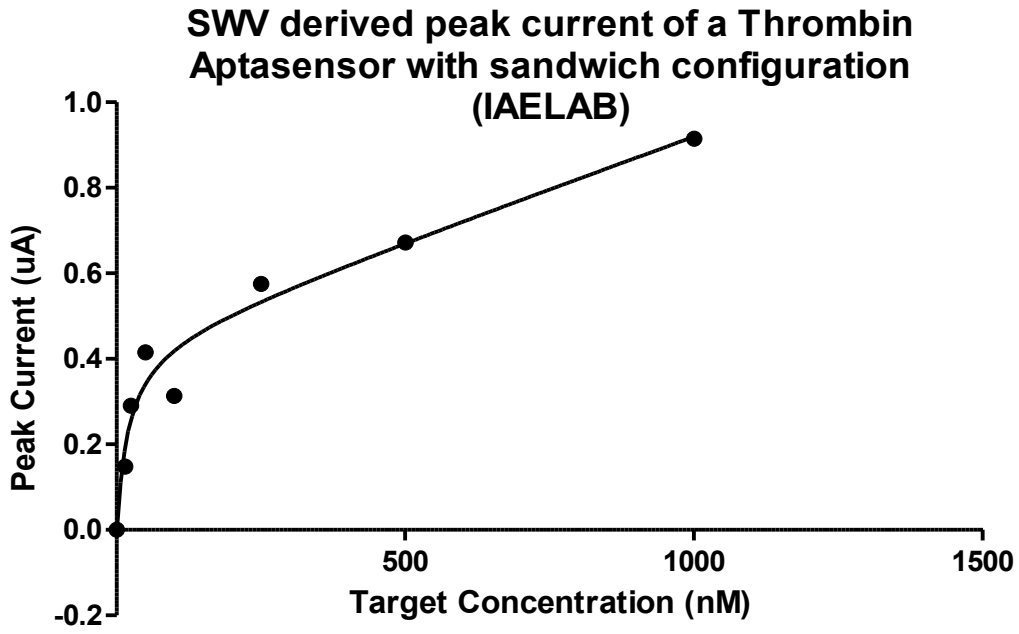

Fig I.4 SWV derived peak current response of Thrombin Fcn-aptamer biosensor to Thrombin titration vs Ag/AgCl, replicate 2 300514

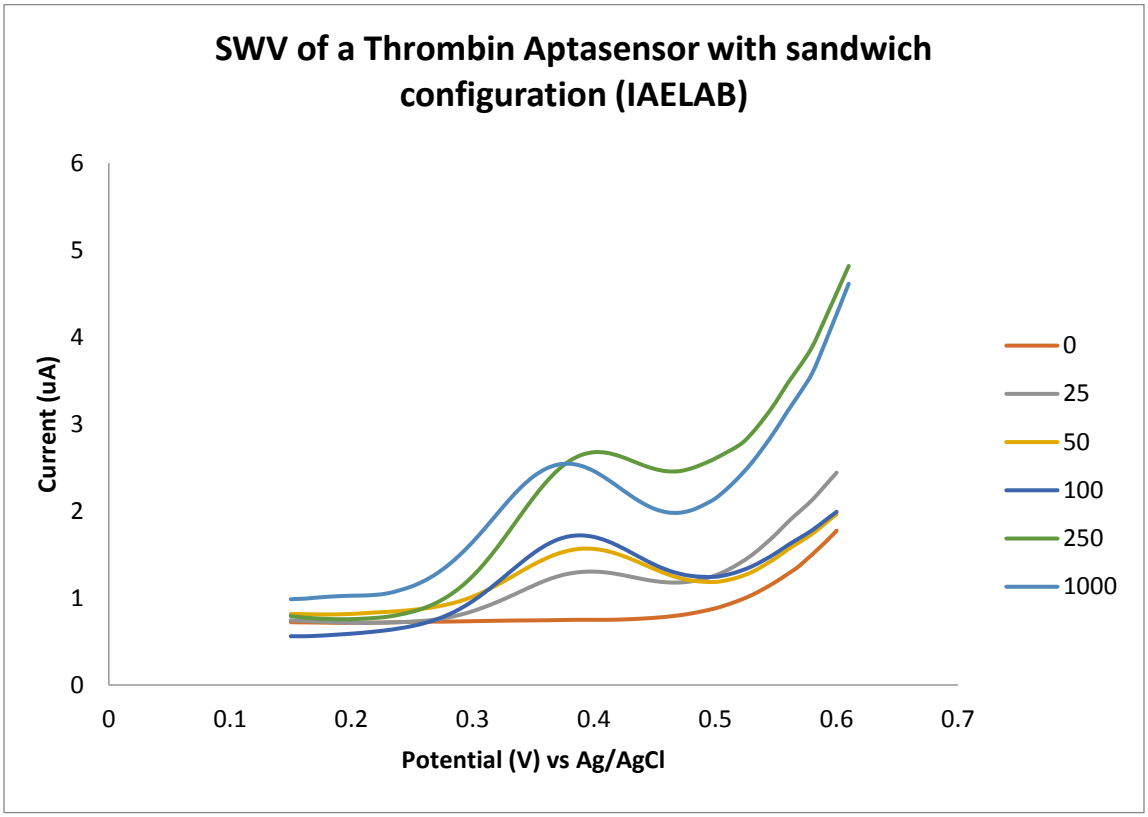

Fig I.5 SWV of Thrombin fcn-aptamer biosensor with sandwich configuration (IAELAB)'s response to Thrombin titration vs Ag/AgCl, replicate 4 140514

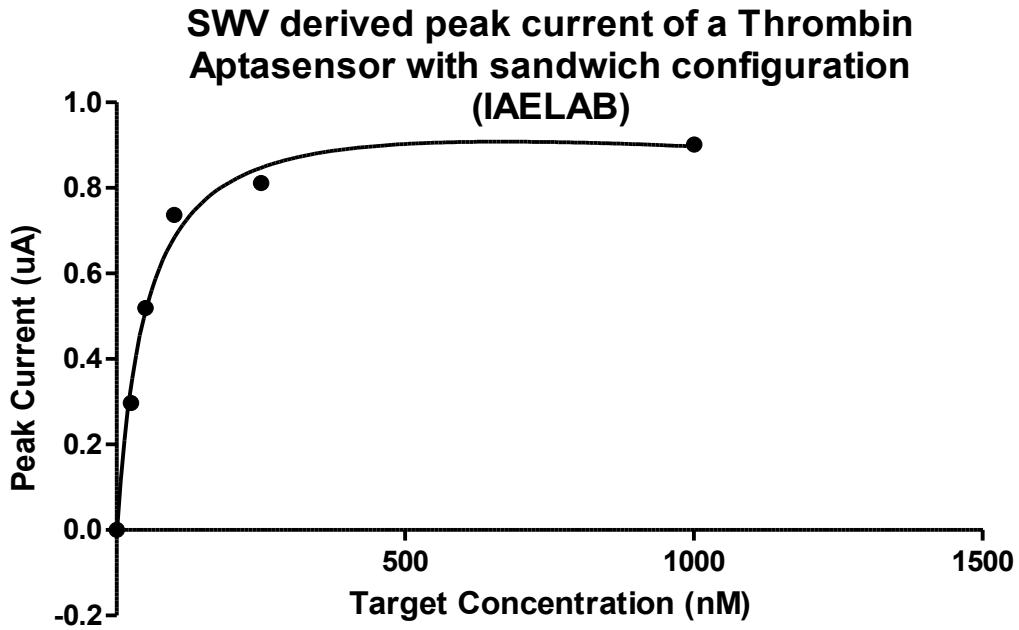

Fig I.6 SWV derived peak current response of Thrombin Fcn-aptamer biosensor to Thrombin titration vs Ag/AgCl, replicate 4 140514

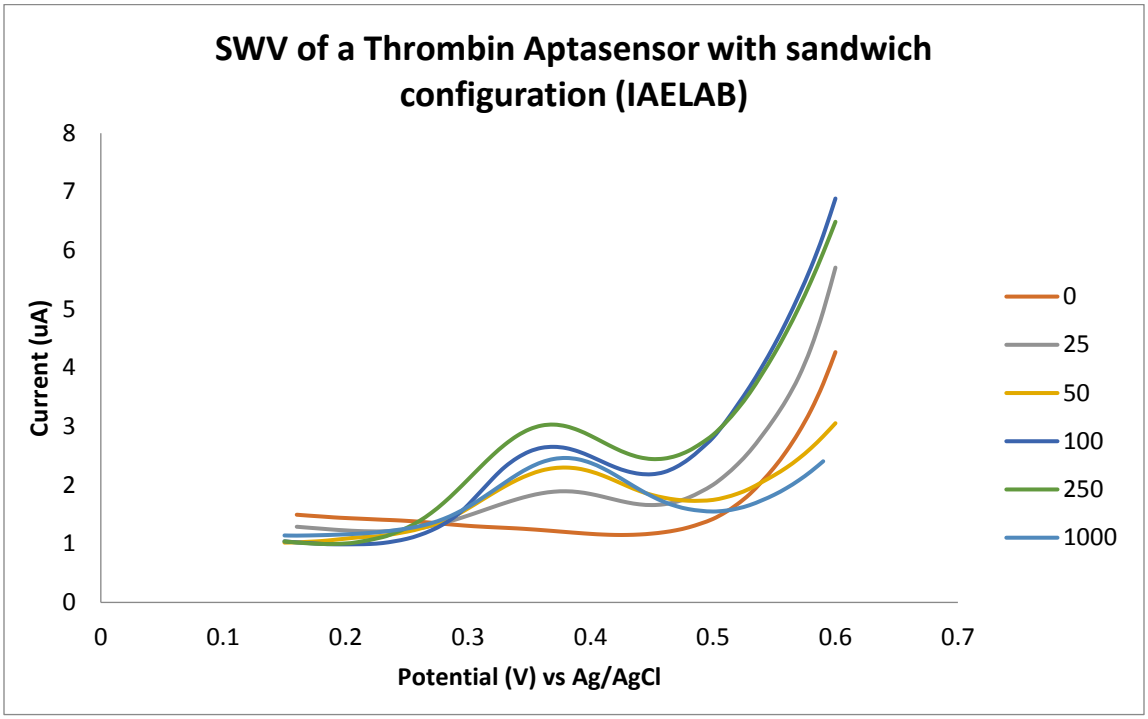

Fig I.7 SWV of Thrombin fcn-aptamer biosensor with sandwich configuration (IAELAB)'s response to Thrombin titration vs Ag/AgCl, replicate 5 150514

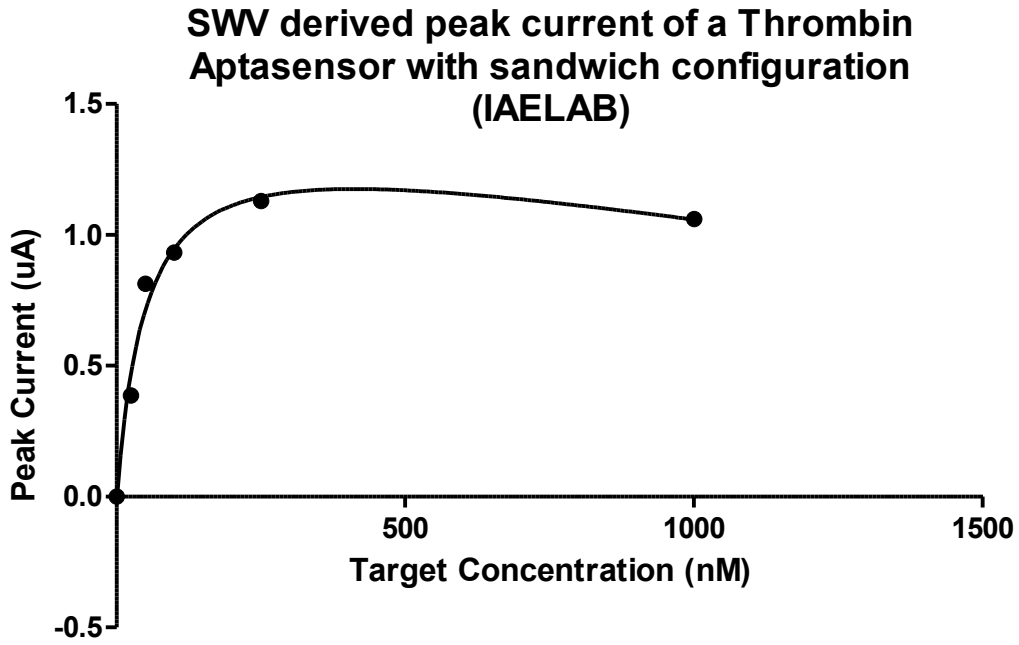

Fig I.8 SWV derived peak current response of Thrombin Fcn-aptamer biosensor to Thrombin titration vs Ag/AgCl, replicate 5 150514

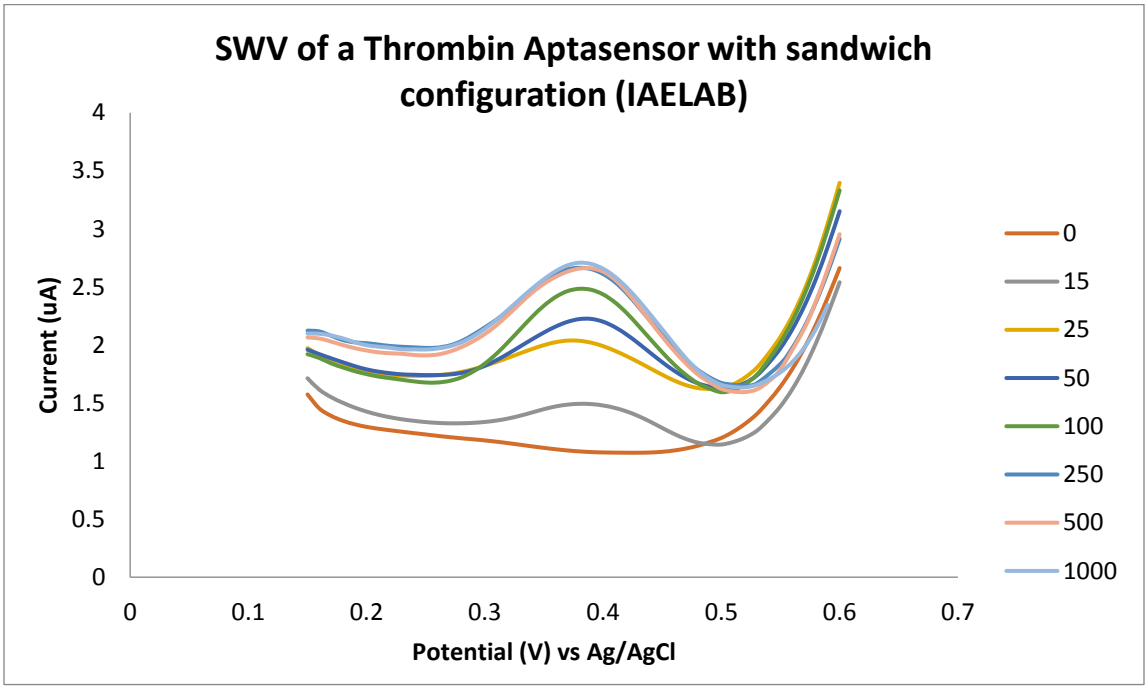

Fig I.9 SWV of Thrombin fcn-aptamer biosensor with sandwich configuration (IAELAB)'s response to Thrombin titration vs Ag/AgCl, replicate 6

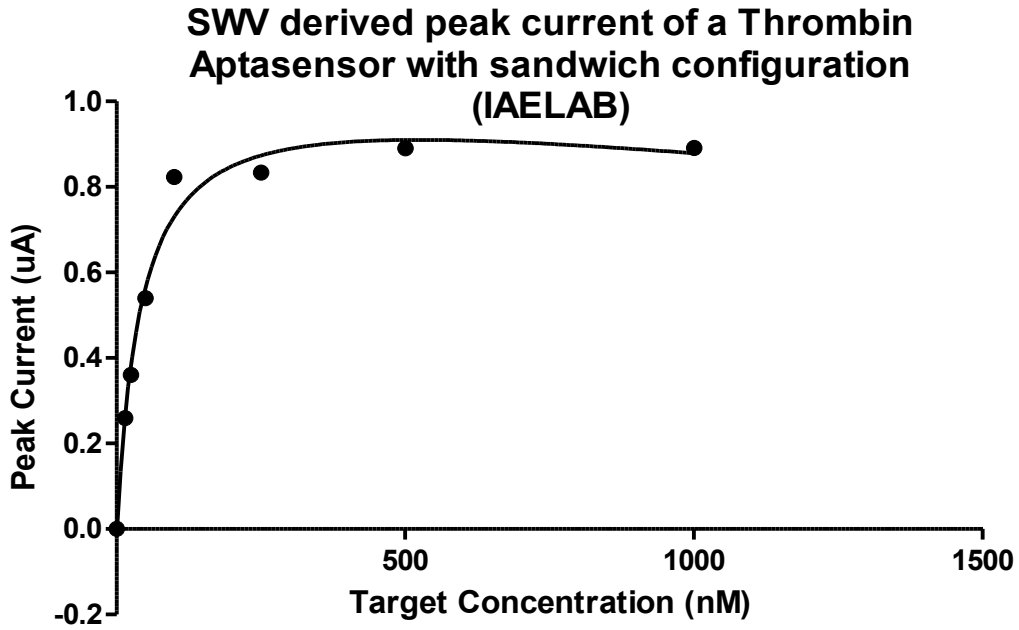

Fig I.10 SWV derived peak current response of Thrombin Fcn-aptamer biosensor to Thrombin titration vs Ag/AgCl, replicate 6

Appendix J: SWV of Thrombin fcn-aptamer biosensor with direct adsorption configuration (IAELAB)'s response to Thrombin titration vs Ag/AgCl

Replicate 2 and 4 of this series of titration can be found in the main body of the text.

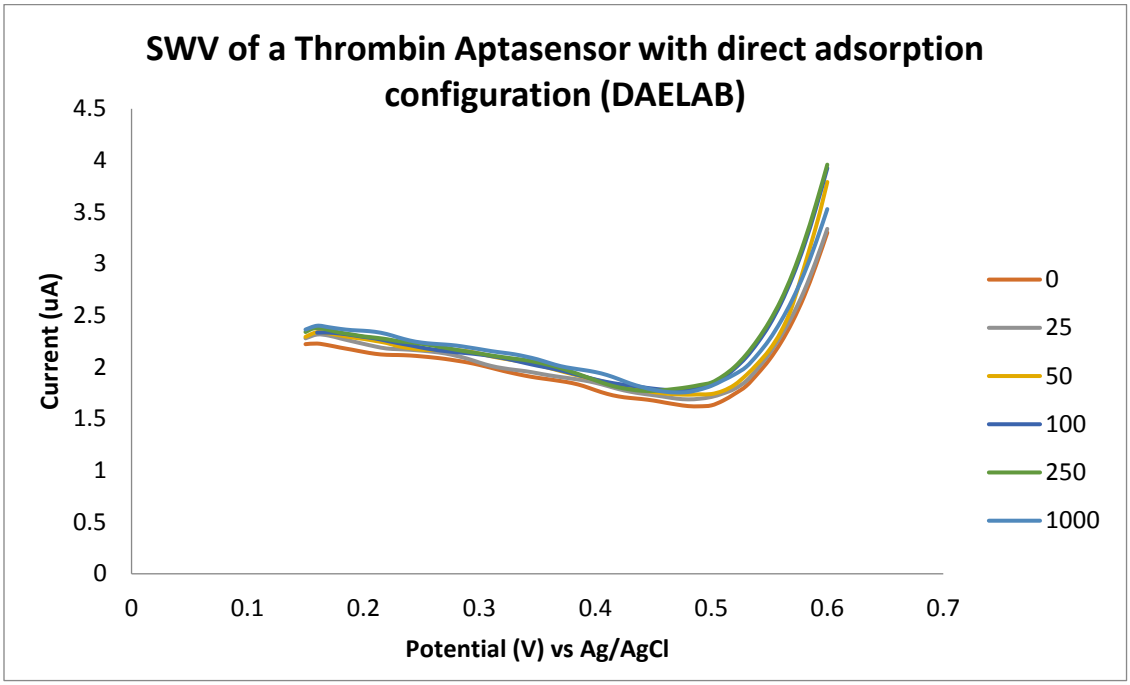

Fig J.1 SWV of Thrombin fcn-aptamer biosensor with direct adsorption configuration (DAELAB)'s response to Thrombin titration vs Ag/AgCl, replicate 1

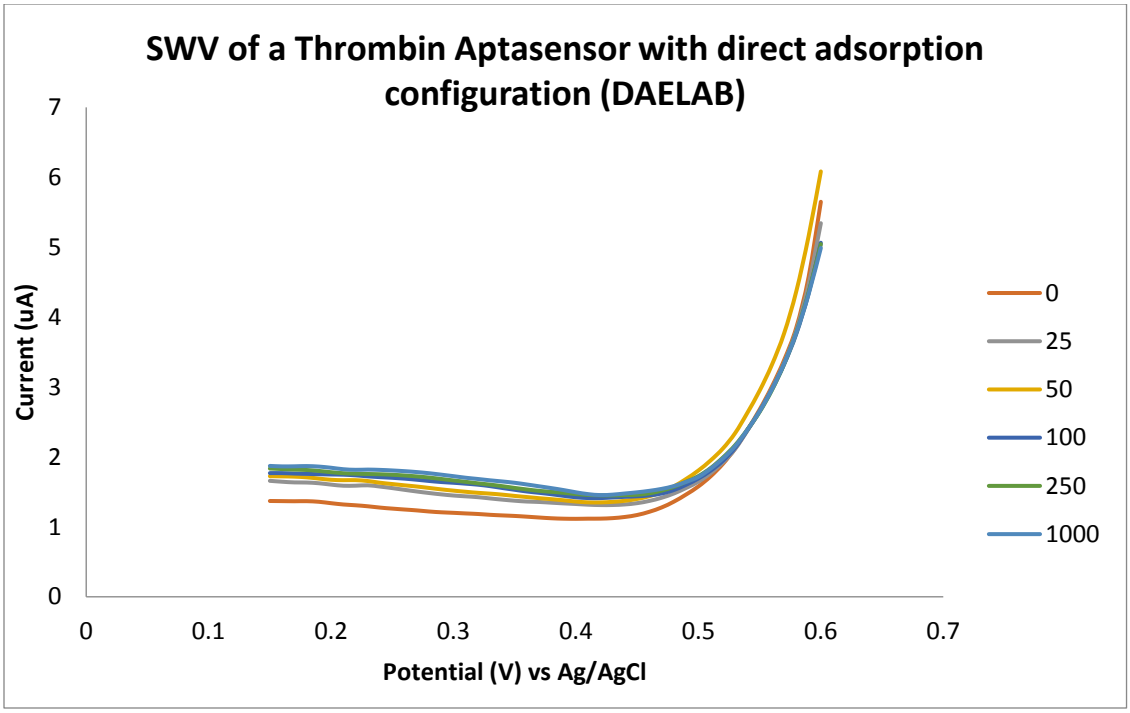

Fig J.1 SWV of Thrombin fcn-aptamer biosensor with direct adsorption configuration (DAELAB)'s response to Thrombin titration vs Ag/AgCl, replicate 3

Appendix K: SWV of unferrocenated Thrombin aptamer's response to thrombin titration and Thrombin fcn-aptamer biosensor with sandwich configuration (DAELAB)'s response to Negative Controls vs Ag/AgCl

Replicate 2 of unferrocenated aptamer titration, 2 of Lysozyme titration and 1 of BSA titration can be found in the main body of the text.

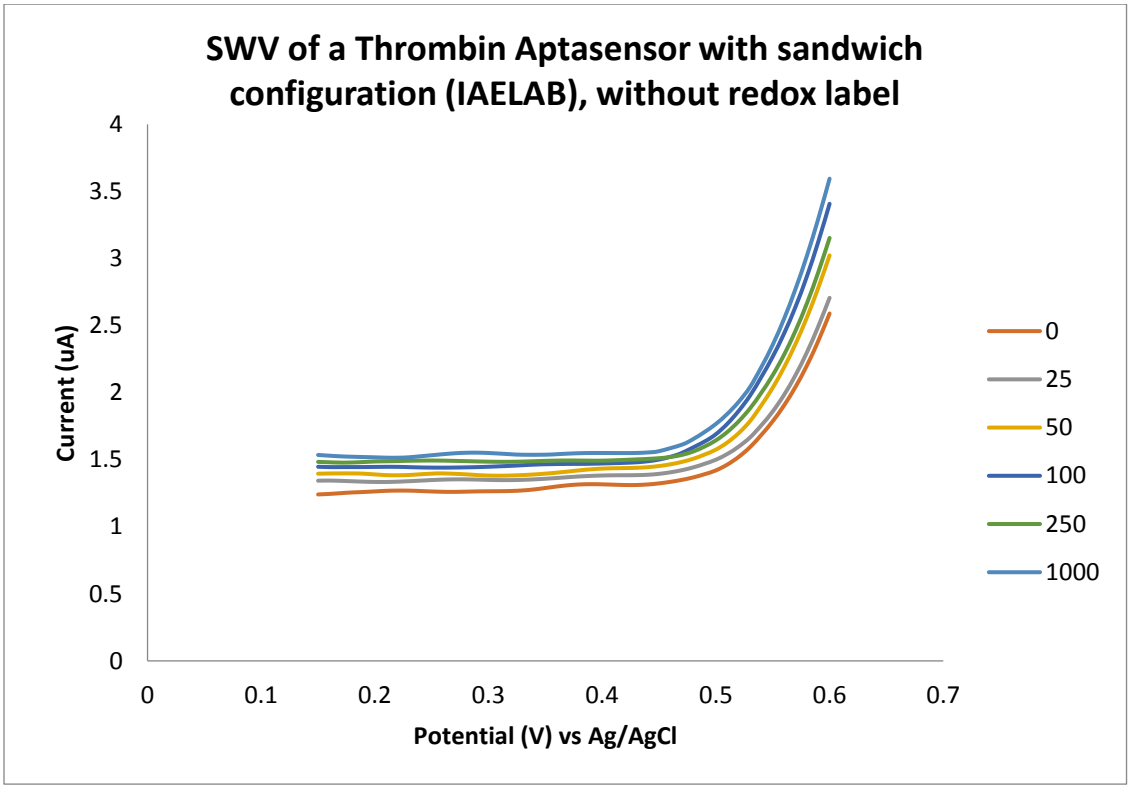

Fig K.1 SWV of unferrocenated Thrombin aptamer with sandwich configuration (IAELAB)'s response to Thrombin titration vs Ag/AgCl, replicate 1

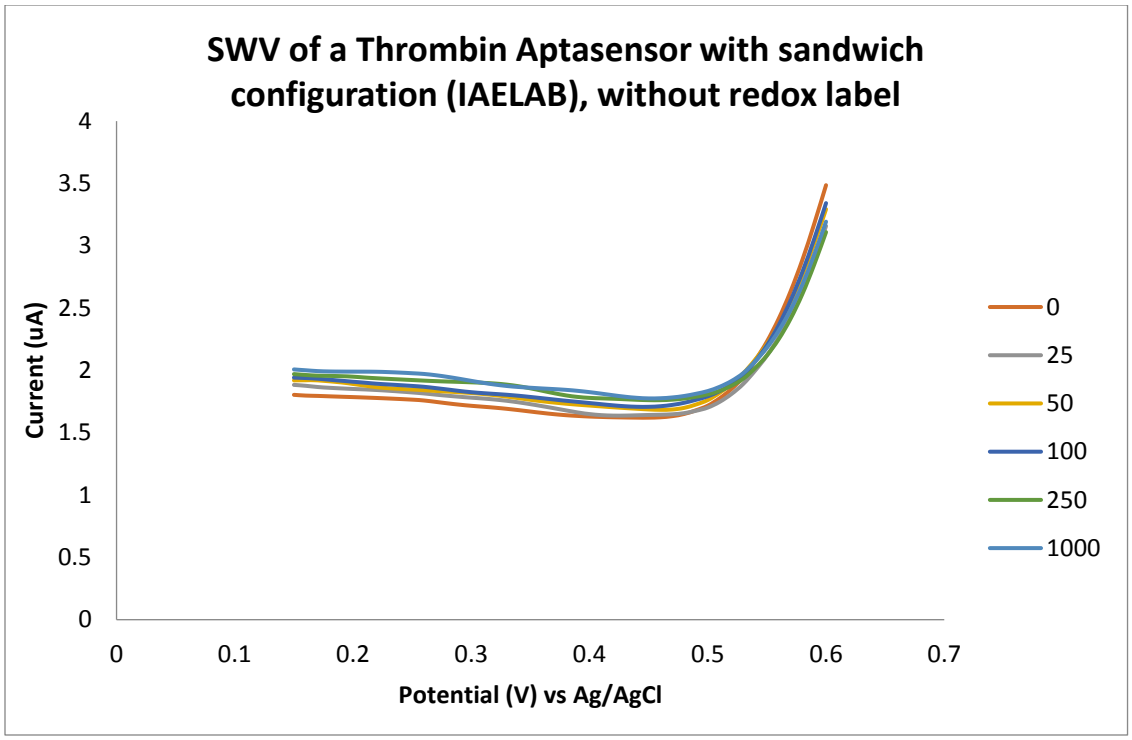

Fig K.2 SWV of unferrocenated Thrombin aptamer with sandwich configuration (IAELAB)'s response to Thrombin titration vs Ag/AgCl, replicate 3

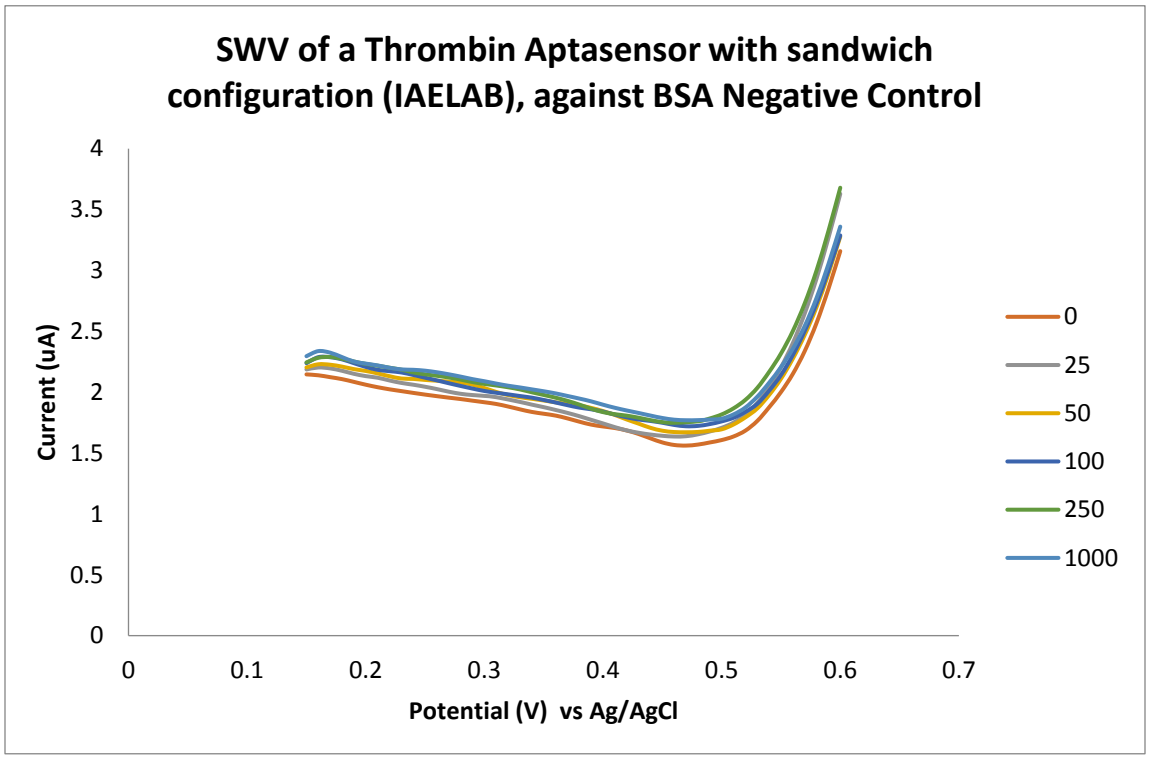

Fig K.3 SWV derived peak current response of Thrombin Fcn-aptamer biosensor to BSA titration vs Ag/AgCl, replicate 1

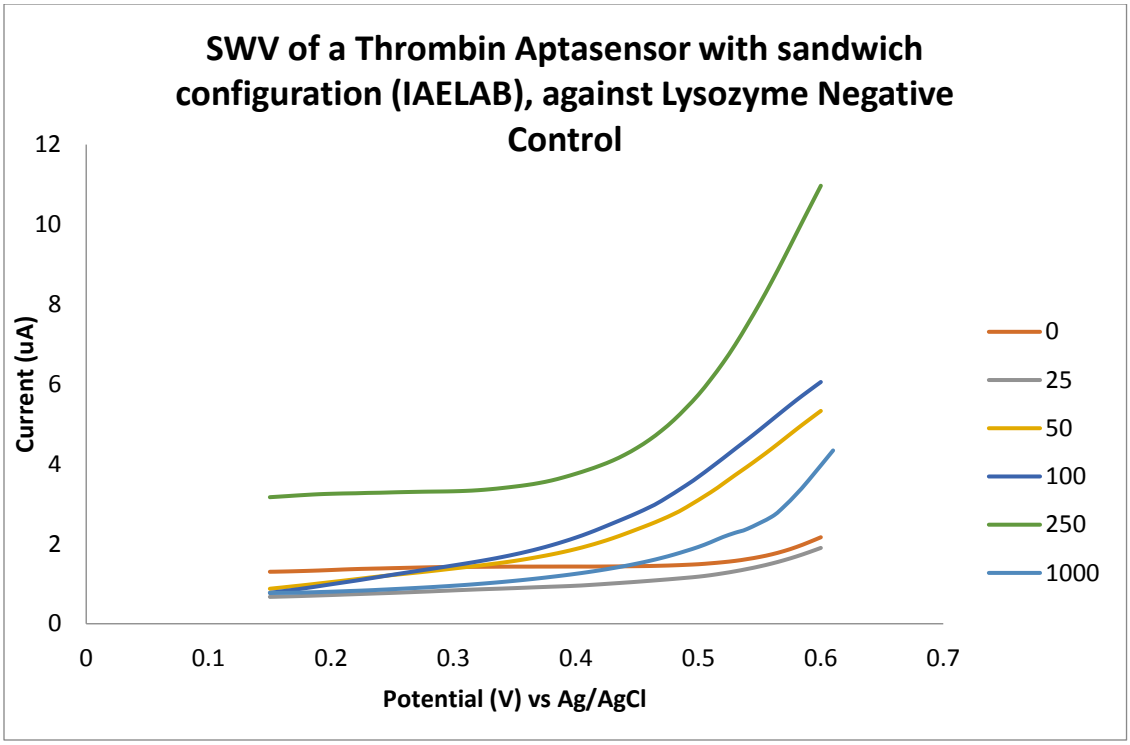

Fig K.4 SWV derived peak current response of Thrombin Fcn-aptamer biosensor to Lysozyme titration vs Ag/AgCl, replicate 2

Appendix L: Quantification of Extracted DNA concentration and observation of gel electrophoresis of PCR product formed using extracted DNA as template for quality control purposes.

Concentrations of DNA product of SELEX operation, determined after phenol/chloroform extraction and ethanol precipitation. It should be noted that the purification process typically results in the loss of 20-35% of the DNA mass.

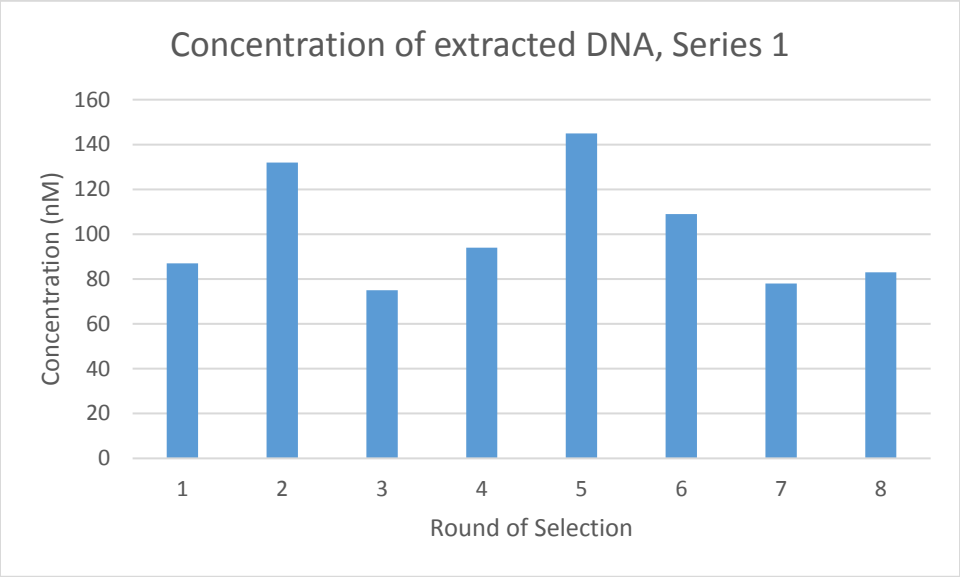

Fig L 1 Concentration of DNA extracted after Series 1 of ASD operation

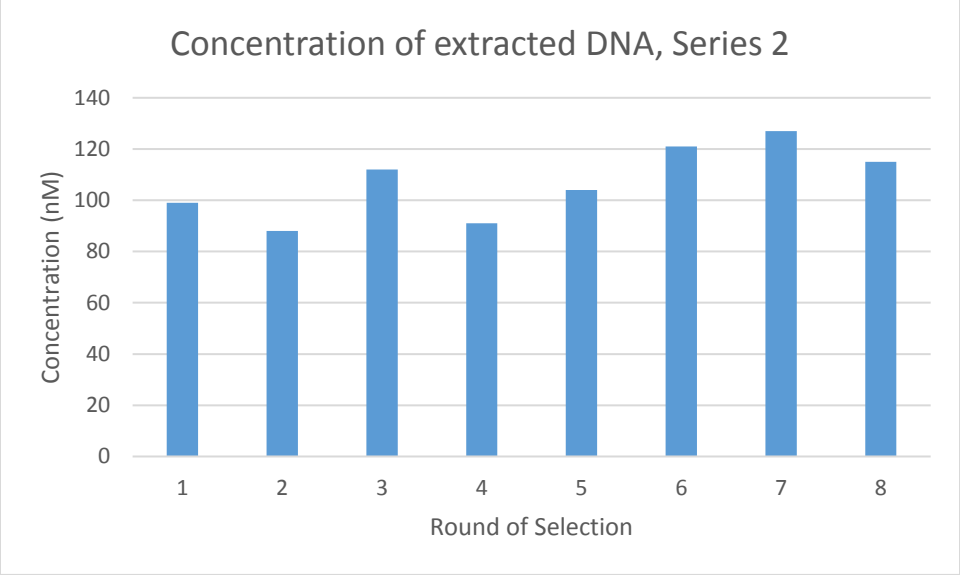

Fig L 2 Concentration of DNA extracted after Series 2 of ASD operation

Gel electrophoresis results of archival/QC PCR performed on extracted DNA product of series 1 and 2 operations.

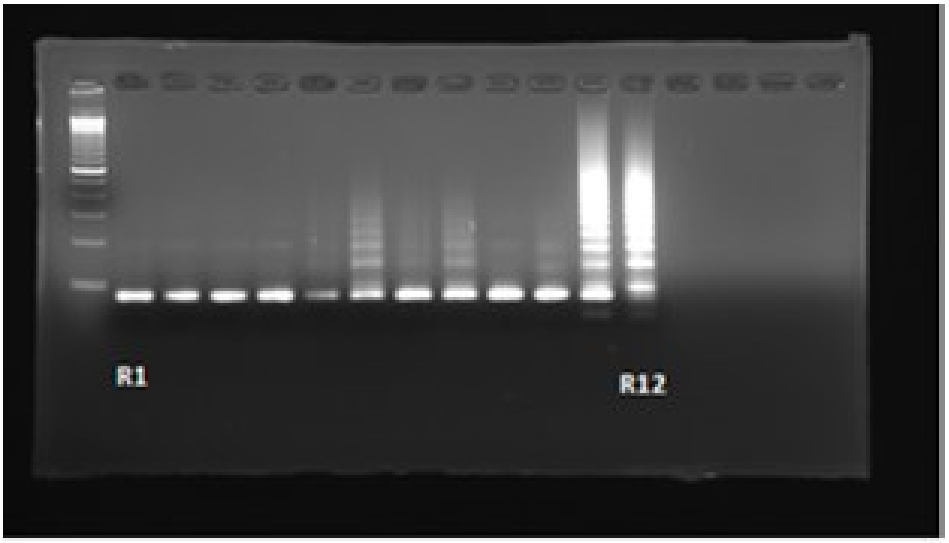

Fig L 3 Gel Electrophoresis of PCR product of DNA extracted from Series 1 operation.

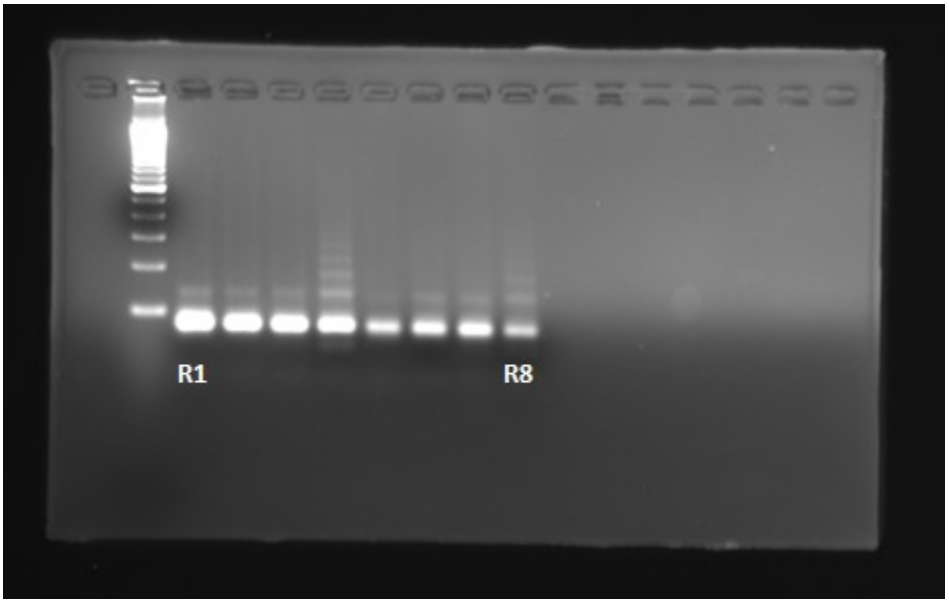

Fig L 4 Gel Electrophoresis of PCR product of DNA extracted from Series 2 operation.